WORK HARDENING OF CALCIUM FLUORIDE

Thesis submitted in Supplication

for the Degree of Doctor

of Philosophy

by

ANTHONY GLYN EVANS

B.Sc (Eng) (London 1964)

Department of Physical Metallurgy,

Imperial College,

University of London.

September, 1967

Abstract

The work hardening of calcium fluoride is investigated in some detail. The stress-strain characteristics are established for primary and secondary slip in the temperature range where a thermal stress component is involved. On the primary system there are five distinct work hardening stages (these are not all apparent at a specific temperature); there is a small yield region followed by a linear region of rapid work hardening, followed, in turn, by a typical three stage hardening curve. On the secondary system the curves are parabolic at all temperatures.

The athermal and thermal components of the applied stress are distinguished and the origins of these components tentatively identified.

The approach to the identification of the thermal component involves firstly a theoretical consideration of dislocation structures followed by experimental investigations of the rate of movement of dislocations; both individual dislocations, through etch pitting, and large numbers of dislocations, through macroscopic thermal deformation characteristics, are studied. These reveal that the movement of the edge dislocations probably controls the deformation on the primary system and this is associated in some way with regions of high local charge on the edge dislocations. The experimental activation parameters indicate that the most likely rate controlling mechanisms are either the interaction of the edge dislocation with isolated charged point defects or the migration of defects with the dislocation.

The thermal component of secondary deformation is possibly provided by a Peierls mechanism.

The identification of the origin of the athermal stress in primary slip is approached by studying etch pits, slip lines, birefringence and latent hardening. The investigations indicate that stage I hardening is adequately explained by deriving the athermal stress from interactions between the elastic stress fields of dislocations, held up at impenetrable obstacles; these are created through the interaction of dislocations moving on intersecting slip planes. Stage II hardening is possibly associated with the interaction of dislocations with dislocation dipoles (or loops) formed in large quantities during this stage.

LIST OF CONTENTS

CHAPTER 3

THE MOTION OF INDIVIDUAL DISLOCATIONS

CHAPTER 4

STRESS STRAIN CHARACTERISTICS

CHAPTER 5

IDENTIFICATION OF THE THERMAL STRESS COMPONENT

CHAPTER 6

THE ORIGIN OF THE ATHERMAL STRESS

Part I

Dislocation Densities

CHAPTER 1

General Introduction

1. Introduction

A preliminary investigation of the plastic deformation of calcium fluoride has been conducted by Roy (1962). The investigation was primarily concerned with identifying the glide elements of this structure and with measuring yield stresses at various temperatures and strain rates. The results are summarised in fig.1.1 showing that plastic deformation is first observed above room temperature on a $\{100\}\langle 110\rangle$ system whilst a secondary system $\{110\}\langle 1\bar{1}0\rangle$ operates above 200°C.

Subsequently, Groves and Kelly (1963) have analysed the geometry of these slip systems, showing that the former yields three independent systems and the latter two. Thus, if the Von Mises criterion is valid, polycrystals of calcium fluoride can only deform plastically at temperatures above which the primary and secondary slip systems can operate simultaneously at stresses lower than the grain boundary fracture stress. So a study of the plasticity of high purity polycrystals of calcium fluoride should reflect the validity of the criterion. A brief investigation was conducted using fully dense polycrystals obtained from Kodak, Inc, Rochester, New York and the results reported by Evans, Roy and Pratt (1966). It is concluded that the criterion satisfactorily explains the observed deformation characteristics, but a more detailed investigation can only be conducted when adequate information is available on the following characteristics:-

1. The work hardening on the primary and secondary slip systems.
2. The mechanism of grain boundary fracture.

All subsequent work has been principally concerned with an investigation of the first topic. This requires firstly that the thermal and athermal contributions to the flow stress should be distinguished and secondly that the origins of these stresses should be identified. The mechanisms providing the thermal stress are most conveniently investigated using macroscopic thermal activation methods, so considerable effort is devoted to estimating the validity of the underlying theory in the case of calcium fluoride.

The overall investigation is approached in the following manner.

1. A theoretical study of dislocation configurations and interactions to elucidate the probable origins of the stress components.
2. A direct investigation of the velocity of individual dislocations. This has two distinct objectives.
   (a) To find the relative velocity of edge and screw dislocations. The slowest moving component is evidently rate controlling, so all mechanisms proposed must apply exclusively to this component.
   (b) To find values of the activation parameters. As shown in Chapter 5 these values are used to test the validity of the method of thermal activation, when applied to calcium fluoride.
3. To establish the stress-strain characteristics of these crystals in compression and tension. Roy has already conducted a brief study at widely dispersed temperatures, so this investigation is relatively comprehensive within the temperature range where flow contains a thermally activated component i.e. below 250°C.

4. A comprehensive study of thermally activated dislocation motion. This should enable the relative magnitudes of the thermal and athermal stress components to be distinguished and perhaps the origin of the short range stress to be identified.

5. To study etch pit densities and latent hardening effects. This should give some indication of the origin of the long range stress.

6. A small number of additional experiments are conducted on very high purity and yttrium doped single crystals to attempt to clarify certain ambiguous points arising from the previous work.

There is not a great deal of information available concerning the plastic properties of calcium fluoride, so it is considered expedient to summarise briefly all previous work that might be directly or indirectly associated with this investigation.

2. Previous Work

2.1 Plastic Properties

The only significant studies of plastic properties are the compression studies of Roy, Phillips Jnr.(1961) and Urovskaya and Goverskov (1966), the dislocation decoration experiments of Bontinck and Dekeyser (1956) and the etch pit studies of Phillips Jnr. These are looked at in turn.

Phillips compressed crystals along ⟨111⟩ and observed plastic deformation above 400°C only. This contrasts with the results of Roy; the discrepancies have been discussed by the latter. His etching work, conducted on specimens deformed at 600°C, showed that the etch pit density varied almost linearly

with strain. The conclusions reached in this work are:-

(a) The flow stress varies with temperature according to the relationship. $\tau = \tau_0 e^{K/T}$

(b) The rate of work hardening decreased almost linearly with temperature.

The Russian workers performed compression tests along $[110]$ using natural fluoride and synthetic doped crystals (containing Sm^{2+}, Sm^{3+} and Nd). The natural crystals deformed plastically above 200°C whilst the doped crystals deformed above 300°C only, all at stresses well in excess of those observed by Roy.

Unfortunately, neither study provides any really useful information for the investigation in hand.

Bontinck and Dekeyser decorated dislocations at high temperatures and were able to draw certain conclusions about the planes and directions of the stable dislocation networks.

The types of junction observed are as follows:-

1. Irregular networks situated mostly on $\{111\}$
2. Dislocation walls at 60°C; These are situated on $\{110\}$ in $\langle 112 \rangle$.
3. Dislocation walls at 90°C; the directions are $[10\bar{1}]$ and $[1\bar{2}1]$, the latter are again associated with $\{110\}$, whilst the former probably appear at the intersection of $\{121\}$.

The walls are only identified in impure crystals and decoration is conducted at temperatures where slip can occur equally readily on the primary and secondary systems; so the junctions are presumably formed by the interactions of dislocations moving on these systems. The importance of these observations is discussed in the following chapter.

Since the rate controlling process is frequently related either to the formation of or the interaction with point defects, the information available on point defects is also considered briefly, especially those features peculiar to this structure.

2.2 Point Defects

2.2.1 Intrinsic Defects

There are four possible forms (Koch and Wagner, 1937)

(i) Frenkel Defect (cation frenkel pair) - Ca^{++} vacancy and Ca^{++} interstitial.

(ii) Anti-frenkel defect (anion frenkel pair)-F^- vacancy and F^- interstitial.

(iii) Schottky trio (Schottky vacancy trio) - Ca^{++} vacancy and two F^- vacancies.

(iv) Anti-Schottky trio (Schottky interstitial trio)- Ca^{++} interstitial and two F^- interstitials.

The formation energies of these defects have been determined theoretically by Franklin (1964 a,b) and shown in table 1. Ure (1957) determined the formation energy of the anion frenkel pair from conductivity data. His value of 2.8 ev agrees closely with that obtained by Franklin. When considering the formation of Schottky trios a lattice energy term of about 26 ev must be taken into consideration (Franklin, 1966 c)

TABLE 1 Formation Energies of Intrinsic Defects

Defect	Formation Energy (ev)	Defect Pair	Formation Energy (ev)
Anion Vacancy	4.4 ± 0.1	Anion frenkel	2.6 ± 0.2
Cation Vacancy	22.5 ± 0.2	Cation frenkel	6.5 ± 0.7
Anion Interstitial	-1.8 ± 0.1	Schottky trio	4.2 ± 0.9
Cation Interstitial	16.0 ± 0.5		

2.2.2 Extrinsic Defects

There have been no comprehensive studies of the effects of aliovalent impurities upon the physical properties of calcium fluoride. The quantity and state of aggregation of the impurities has a marked influence upon plastic deformation (e.g. Quin, 1967), so it is important to obtain information concerning the impurities' concentration and form. It has been shown by Caffyn (1966) and Johnston et al (1966) that impurity-vacancy dipoles exist in trivalent doped crystals but their concentrations have not been estimated. This lack of information makes it imperative that tests are conducted on very high purity crystals.

Before commencing the study outlined above, a source of high purity crystals, available in relatively large quantities, had to be located.

3. Source of Crystals

The most suitable source was Harshaw Chemical Co. An analysis of the crystals obtained has been conducted both in our laboratories and by American Spectrographic Laboratories. The results are in close agreement, table 2. Other crystals obtained from Harshaw have been analysed by various

investigators (e.g. Duke, 1964 and O'Connor and Chen,1963). The results obtained are somewhat contradictory. The analysis of Duke agrees quite closely with those listed in table 2 whilst O'Connor and Chen encounter relatively large quantities of aluminium and iron (i.e. a few 100 p.p.m). The results of the latter cannot be disregarded, so no specific conclusions regarding the impurity content are attempted here. A further problem arises because the analyses used are not suitable for a detailed investigation of the oxygen content; this, according to Franklin (1966 c), could be relatively large. Thus, an estimate of the importance of these impurities, if they exist, is required. This necessitates obtaining a small quantity of carefully grown high purity single crystals; such crystals have been kindly supplied by Prof. Caffyn. The crystals have been grown to minimise the possibility of oxygen contamination at each stage and careful analysis has not detected any monovalent or trivalent impurity in excess of a few p.p.m.

TABLE 2. Analysis of Harshaw Crystals

Impurity	Concentration (p.p.m)		
	Duke	A.S.L.	I.C.L
Mg^{++}	80	50	50
Al^{3+}	15	10	10
Si^{3+}	5	N.D	< 1
K^{+}	< 0.5	N.D	N.D
Mn^{2+}	< 1	N.D	N.D
Fe^{3+}	< 1	< 1	< 1
Ca^{2+}	10	10	10
Y^{3+}	10	N.D	5
Sr^{2+}	100	30	50
Ba^{2+}	< 1	N.D	< 1

N.D. Not Detected

A.S.L. American Spectrographic Laboratories

I.C.L. Imperial College Laboratories.

It is noted here that surface contamination of the specimens (oxidation, hydrolysis) does not occur at temperatures below 350°C. So tests at temperatures below this can be conducted in air.

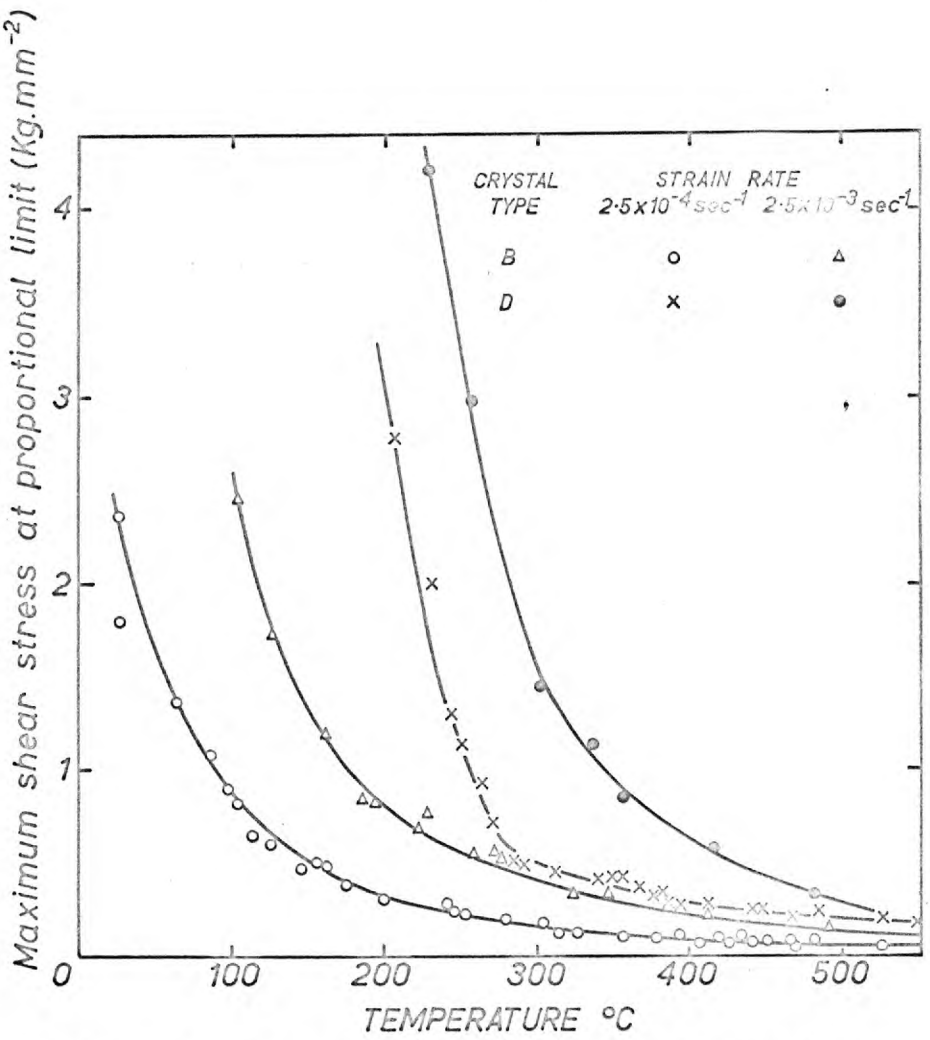

Fig. 1.1. Temperature dependence of the critical resolved shear stress

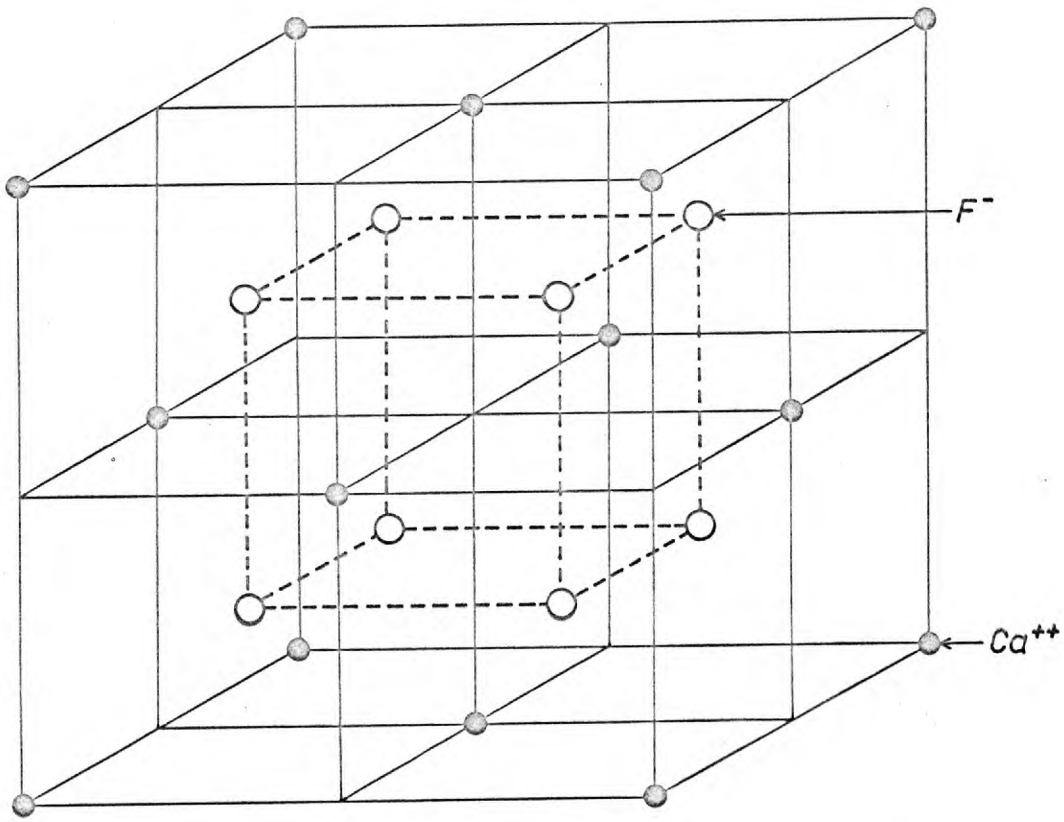

Fig. 1.2. The CaF_2 structure

CHAPTER 2

Dislocations in Calcium Fluoride

1. Introduction

In high purity single crystals, deformed at relatively low temperatures, the rate of movement of the dislocations is controlled either by the intrinsic resistance of the lattice or/and by the interactions and intersections of these dislocations with other dislocations introduced during the deformation.

Before any experimental investigations of the plastic deformation of calcium fluoride are conducted, certain theoretical aspects of dislocation structure, interactions and intersections are studied in an attempt to elucidate some of the processes likely to control the deformation. The purely geometrical aspects, peculiar to calcium fluoride are considered whilst the more general features are examined later. Where possible, the mechanisms considered are treated semi-quantitatively to enable the most unfavourable to be eliminated immediately, thereby allowing the remainder to be considered in some detail.

Dislocations on both primary and secondary slip systems are considered. Roy has already shown that unit dislocations do not dissociate into partial dislocations, so only the unit dislocations need be considered.

2. Dislocation Structures

2.1 Primary System $\{100\}\langle 011\rangle$

2.1.1 Ionic Configurations

The configurations of ions comprising both edge and screw dislocations are considered in detail. It is hoped that these will assist in understanding the formation and motion of the dislocations and enable the associated energies to be estimated. Where simple two dimensional representations are inadequate, ball models of the dislocation cores are constructed.

2.1.1.a Edge Dislocation

Amelinckx (1958) and Roy have presented a two dimensional model of this dislocation; their configuration is shown in fig. 2.1. There are two additional half planes, one ending in a row of calcium ions spaced b(the burgers vector) apart and the other in a row of fluorine ions also spaced b apart. The ion arrangement is complex and difficult to visualise. Thus, the dislocation lies along $\langle 0\bar{1}1 \rangle$, and a given $\{100\}$ consists of rows of fluorine ions in this direction; adjacent rows are spaced $b/2$ apart and arranged as shown in fig. 2.2. The $\{100\}$ above and below this plane consist of rows of calcium ions spaced b apart but these rows are arranged differently with respect to the fluorine ion rows, for the plane above and the plane below, fig. 2.2; thus the stacking is of the type A B C B A B C B A ..... To simplify the study of this dislocation, a ball model, representing the ions and the bonds between ions within the core region, has been constructed. The model has elucidated certain unexpected features of the dislocation that have not been noted by the previous investigators.

The dislocation has three possible configurations. These are considered in turn.

i) The dislocation of Amelinckx and Roy. The ball model is shown in fig. 2.3. An examination of ions at the core reveals that the calcium ions here are not bonded by eight fluorine ions as is required for electrical neutrality; only four such ions are available for each calcium ion. So, the dislocation carries an excess positive charge, equivalent to the charge on a proton, at every distance b along its length.

ii) The second configuration is shown in fig. 2.4. When a dislocation loop is initiated at a point in a perfect lattice and the edge dislocation type (i) is obtained along one section of the loop, then the edge dislocation required along the opposite segment is that shown in fig. 2.4, with both extra half planes ending in rows of fluorine ions. The fluorine ions at the core are not bonded to four calcium ions as in the perfect lattice, only three ions are available. So the dislocation carries an excess negative charge distributed such that there is a charge, equivalent to the charge on an electron, at every distance b along its length.

The creation of edge dislocations of opposite mechanical sign is shown in fig. 2.5.

There is a third possible configuration for the dislocation. This is uncharged and might form in preference to the charged configurations (i) and (ii).

iii) The uncharged configuration is shown in fig. 2.6, it is somewhat similar to the proposed configuration for a $\{111\}\langle 110\rangle$ edge dislocation in NaCl (Brown, 1960).

When a dislocation loop is formed, each alternate calcium ion at the core of dislocation (i) could be removed and added to alternate interstitial sites, below the extra half planes, at the core of dislocation (ii); this produces two identical uncharged dislocations. So the formation of this dislocation essentially corresponds to the introduction of calcium vacancies into (i) and calcium interstitials into (ii) (or fluorine vacancies into (ii) and fluorine interstitials into (i)). The resultant dislocation can be regarded as being comprised of a series of half jogs of length $a_o/4$ (a_o is the length of the unit cell) at every distance b as shown in fig. 2.7. The jogs lie on $\{110\}$ and are equivalent to small lengths of edge dislocation of the secondary system; the movement of the dislocation requires the simultaneous movement of these half jogs along $\{110\}$.

The formation energies of these different types of dislocation are looked at in a section 2.1.2 to attempt to decide upon the most likely configuration.

2.1.1.b. Screw Dislocations

The ionic configuration of the core of this dislocation is quite straight forward and is shown schematically in fig.2.8. It is produced quite simply by the displacement of the calcium ions through certain fractional amounts of b in $\langle 1\bar{1}0 \rangle$. There are no charged ions of either sign within the core.

2.1.1.c. Mixed Dislocation

The actual ionic configuration of the dislocation depends upon its orientation relative to the burgers vector. Depending upon the form taken by the edge dislocation it will either carry a charge (negative or positive) or a half jog at certain multiples of b along its length. (The multiples being smaller the closer the orientation lies to that of the pure edge dislocation).

2.1.2 Energies of Formation

This energy generally consists of two terms, the elastic strain energy and the core energy; these are considered separately.

a. Elastic strain energy

This is associated with the elastic displacement of ions outside the core of the dislocation, the displacements extending over large distances from the core. The energy that must be supplied to produce these displacements is given by Eshelby(1949) as:

$$Ee = \frac{Kb^2}{4\pi} \ln \frac{R}{r_o} \qquad - 2.1$$

K is a constant which is given by the elastic constants of the lattice and varies from one type of dislocation to another.
R is the outer limit of the displacement, usually regarded as the spacing between dislocations.

r_o is the radius of the core of the dislocation. In ionic crystals this is usually small because of the sharp increase in the energy of the core as the width of the dislocation increases (Huntington et al, 1955).

Values of K are given by Foreman (1955) for various types of dislocation in lattices with cubic symmetry. Substitution of the elastic constants of Srinivasan (1958) into Foreman's equations gives the values of K shown in table 3.

Now values of the elastic energy may be obtained by substituting these values of K into equation 2.1, assuming appropriate values for R and r_o .

R varies from $10^5 A^\circ$--$10^3 A^\circ$ during the course of a typical deformation experiment (see Chapter 6).

r_o is likely to be within the range 3 - $8A^\circ$ (c.f. NaCl).

Thus, maximum and minimum values of this energy can be determined corresponding to the beginning and end of deformation respectively; these are shown in table 3 and correspond to the elastic energies of formation of lengths b of dislocation.

Elastic Energies of Dislocations TABLE 3

Type of Dislocation	K($\times 10^{11}$ dyne cm^{-2})	Ee max(ev)	Ee min(ev)
$\{100\}\langle 110\rangle$ Edge	5.65	18.4 ± 0.9	7.4 ± 0.3
Mixed($\theta = \pi/4$)	4.85	15.8 ± 0.8	6.4 ± 0.3
Screw	4.45	14.5 ± 0.7	5.9 ± 0.3
$\{110\}\langle 1\bar{1}0\rangle$ Edge	6.24	20.4 ± 1.0	8.2 ± 0.4

b. The core energy

This is associated with non-Hookian displacements of ions within the core region. The calculation of this energy is simplified in ionic crystals by the relatively short range character of the forces involved

i.e. electrostatic and ion core repulsion. Huntington et al have obtained values for this energy in NaCl incorporating the potentials calculated by Madelung (1918). The energy of an edge dislocation on $\{110\}\langle\bar{1}10\rangle$ as a function of core diameter is shown in fig. 2.9. The screw dislocation has a lower energy (by a factor of about 2) whilst the edge dislocation on $\{100\}\langle 110\rangle$ has a larger energy (by a factor of about 3). These energies particularly the latter, are maximum possible values, so the core energies are evidently considerably smaller than the elastic energies.

The rather unusual arrangement of ions associated with $\{100\}\langle\bar{1}10\rangle$ dislocations in calcium fluoride makes an extension of these calculations to include this dislocation extremely complex. So a rigorous calculation of this type has not been conducted.

The core energy of the screw dislocation and secondary edge dislocation (see Section 2.2.1) are not likely to differ greatly from those of equivalent dislocations in NaCl. However, the primary edge dislocation carries an extra term associated either with the presence of adjacent charges of like sign or of half jogs. Which of these configurations is likely to predominate can be ascertained from simple energy considerations. Each possibility is considered in turn.

i) Charged configuration

The electrostatic repulsive energy associated with the adjacent charges results in a formation energy in excess of that associated with any uncharged configuration . If it is assumed that no relaxation occurs it is possible to determine the magnitude of this additional energy term from simple electrostatic considerations (this will evidently be a maximum possible value). The energy required to increase the length

of the dislocation by an amount b is equivalent to the work done in bringing a charge e (the charge on an electron) from infinity up to a distance b from the end of a row of existing charges spaced b apart.

If the original dislocation is of length nb, the energy is given by:-

$$\frac{e^2}{b}\sum_{1}^{n}\frac{1}{n} \qquad -2.2$$

whilst the total repulsive energy of the dislocation is

$$\sum_{1}^{n}\frac{e^2}{b}\sum_{1}^{n}\frac{1}{n} \qquad -2.3$$

Values of the energy required to increase the length of the dislocation by an amount b, for various values of n are given in table 4.

TABLE 4 The electrostatic Repulsive Energies of the Charged Configurations

n	1	2	3	6	8	12
Repulsive energy (ev)	0.5	0.75	0.92	1.22	1.35	1.51

ii) The uncharged configuration

The energy of the configuration in fig. 2.6 is in excess of that of an unjogged dislocation through the additional displacement energy associated with these half jogs. Thus, the relative magnitudes of this energy and the repulsive energies given in table 4 will determine the actual configuration preferred. The half jog energy is difficult to calculate but is smaller, the closer the spacing between the jogs.

. . One approximation is given by the energy of the length $a_o/4$ of secondary edge dislocation; this has a minimum value of about 2.5 ev. This is undoubtedly too large, for the elastic energy of such a jogged configuration is not greatly in excess of that of an unjogged dislocation, (e.g. Crocker and Bacon, 1967),

A closer approximation is given by considering the formation of edge dislocations from the perfect lattice as in fig. 2.5. The formation of a double jog on both edge dislocations has been shown to be equivalent to the formation of a calcium vacancy in one dislocation and a calcium interstitial in the other. So the formation energy of both double jogs is given approximately by the energy of formation of the cation frenkel pair. Also the different environment of this pair should be taken into consideration i.e. an increase in energy to dissociate the pair and a reduction on association with the dislocations; in addition, the presence of existing adjacent jogs probably reduces the energy that has to be supplied. The dissociation of the pair more than cancels the term due to the proximity of the jogs; the association energy with a dislocation has been calculated in NaCl by Bassani and Thomson (1956) as 0.4 ± 0.2 ev. So the resultant energy is of the order 6.5 ± 2 ev. The electrostatic energy associated with the equivalent charged configuration is now considered. Consider firstly, replacing the double jogs by three adjacent like charges; these groups clearly alternate in sign along the dislocation. For both dislocations, a maximum total energy of 3.5 ev for each double jog replaced is obtained. So this configuration almost certainly forms in preference to the jogged configuration. The final form might be that shown in fig. 2.10 but a rigorous calculation is required to determine the exact configuration.

The magnitude of this additional term is small in comparison with the elastic energy and so makes only a small contribution to the total energy of formation of this dislocation.

It is now possible to draw certain interesting conclusions concerning primary slip in calcium fluoride.

2.1.3. Conclusions

1. When a dislocation loop expands and the movement of the screw segments requires new edge dislocation to be created at existing edge dislocation, small lengths of charged dislocation form before it is energetically more favourable for a jog to be created. Then, a further length of charged dislocation of opposite sign forms before another jog is required. The spacing between jogs depends upon temperature, the spacing between edge dislocations etc.

   It is difficult to conceive that edge dislocations of opposite sign should form in physically different parts of the lattice. It is probably more realistic to consider the formation of small lengths of dislocation, from the perfect lattice as in fig.2.5, at certain positions along the screw dislocation; these 'kinks' could then move apart to constitute the forward motion of the screw dislocation. The resultant charge might then be distributed along large lengths of mixed dislocation, with a larger number of adjacent like charges before a jog is required.

   The rate of movement of the screw dislocations might be controlled by the formation of the edge dislocation rather than its interaction with obstacles on the slip plane. Thus, the nucleation of the 'kink' described above requires an energy in excess of 0.5 ev and could be regarded as analagous to the formation of a Peierl's kink and analysed in a fashion similar to the Dornand Rajnak (1964) solution for a Peierls process.

2. The formation of lengths of screw dislocation is not likely to impede the motion of the edge dislocations. The movement of these dislocations through high purity single crystals is likely

to be controlled either by the motion of the half jogs on $\{110\}$ or by the interaction of the charged sections with other charged particles close to the slip plane.

3. Since the edge dislocation has a higher energy than the screw dislocation there will always be a tendency to minimise the length of edge dislocation. This will not significantly effect deformation, for the relative lengths of edge and screw dislocation are determined by their relative rates of motion over obstacles in the slip plane; however, it might influence the annealed structure.

2.2 Secondary System $\{110\}\langle\bar{1}10\rangle$

2.2.1 Ionic Configurations and Energies of Formation

a. Edge Dislocation

The arrangement of ions on $\{110\}$ in $\langle\bar{1}10\rangle$ is relatively simple. Alternate rows in [001] consist of calcium ions spaced b apart and fluorine ions spaced $^{b}/_{2}$ apart. Adjacent planes are then merely translated $^{a_o}/_{2}[110]$. So, the stacking is A B A B A B ..... The edge dislocation can be represented quite readily using a two dimensional diagram, fig. 2.11. The two extra half planes end in rows of calcium ions and fluorine ions respectively. Construction of this dislocation from the perfect lattice requires the removal of one calcium ion for every two fluorine ions, so the resultant configuration is uncharged. The elastic energies are calculated using the equations of Foreman and are given in table 3. The arrangement of ions on $\{110\}$ in CaF_2 is similar to the arrangement on $\{100\}$ in NaCl

(except that alternate positive ion sites in [001] are vacant), so the core energy is likely to be similar in magnitude i.e. 1 to 3 ev. Thus, the total energy of formation of edge dislocations is similar for both primary and secondary systems i.e. 20 ± 2 ev and 22 ± 2 ev respectively.

b. Screw Dislocation

This has the same burgers vector as the primary dislocation so the elastic energy is identical; the core energy is likely to be slightly larger.

2.2.2 Conclusions

As in NaCl the energies of formation of dislocations on the primary and secondary slip systems are not widely different, so it is the resistance to the movement of the dislocations on these systems that determines which slip system is likely to operate.

The movement of a dislocation on the secondary system requires the relatively close approach of the fluorine ions in the core at the mid translation distance. An argument similar to that used by Gilman (1959) to explain qualitatively the high stresses required for slip on $\{100\}\langle 110\rangle$ systems in rock salt crystals, assists in understanding slip on this system. Thus, it is only at high temperatures that the polarisation of the fluorine ions is sufficient to allow these ions to come sufficiently close to permit the dislocation to move at stresses below the fracture stress. Deformation on this system should fit a Peierls type analysis if this argument is correct.

3. Dislocation Intersections and Interactions

The total applied stress required to deform a crystal at a specific rate is dependent in part upon interactions and intersections between dislocations. The actual mechanisms are not considered in detail at this stage; the purpose of this section is to consider the geometry and energetics of the intersection process. There are two distinct effects associated with intersection that are of particular interest.

1. The intersecting dislocations might interact to form dislocation junctions. If the junctions are sessile they might act as impenetrable barriers to slip such that dislocation pile ups occur behind them, thereby contributing to the long range stress (c.f. the Lomer-Cottrell barrier in f.c.c. metals).
2. The movement of the jogs, produced on screw dislocations through intersections, generally occurs conservatively for unextended dislocations. However, if the component of applied stress in the conservative direction of motion of the jog is low it might be constrained to move non-conservatively.

These two effects are considered in turn.

3.1 Interactions

3.1.1 Inclined Slip Planes

3.1.1.1 Theoretical Considerations

Interactions between dislocations moving on $\{110\}\langle\bar{1}10\rangle$ systems with other dislocations on this system have been considered by Kear, Pratt and Taylor (1959); their conclusions can be applied

to the secondary system in CaF_2. The $\{100\}\langle 110\rangle$ system has not been considered, so is now looked at some detail.

There are three available $\{100\}$ with two $\langle 110\rangle$ in each plane as shown in fig. 2.12. Consider the interaction of dislocations moving on two of these, e.g. (100) and (010). These might combine along the line of intersection of these planes (XY) to form a junction dislocation. There are two possible interactions, depending upon the direction of the burgers vectors involved.

a. If dislocations with burgers vectors b_1 and b_3 (or b_2 and b_4) combine, the resultant dislocation has a burgers vector $\sqrt{3/2}\, a_0$ [redacted] . This reaction is represented by the equation

$$\frac{a_0}{2}[011] + \frac{a_0}{2}[10\bar{1}] \rightarrow a_0[112] \qquad - 2.4$$

This corresponds to two mixed ($\theta = \pi/4$) dislocations on the $\{100\}\langle 011\rangle$ system combining to form a mixed ($\theta = \pi/6$) dislocation on the system $\{110\}\langle 112\rangle$. The stability of this junction dislocation depends upon its energy per unit length compared with that of the constituent dislocations. This cannot be ascertained unequivocally with the information available at this stage: if the elastic energy is similar to that of a $\{110\}\langle 110\rangle$ dislocation per unit length, then, its elastic energy is also similar to that of the constituent dislocations. In addition, the close approach of the calcium ions required in creating the core region of this dislocation indicates a relatively large core energy, so its formation is unlikely. However, Bontinck and Dekeyser(1956) observe this dislocation in their decoration experiments, although it also appears to dissociate quite readily. The temperatures used for decoration are well in excess of that required for secondary slip so these

dislocations might result from interactions between secondary dislocations. The situation is nebulous but, in the absence of precise values of the energy of the junction dislocation, it cannot be stated unambiguously that the reaction represented in equation 2.4 does not occur; however, even if it does occur it will not be sufficiently stable to have a significant influence upon the deformation.

b. The combination of dislocations b_1 and b_4 (or b_2 and b_3) produces a pure edge dislocation on the $\{110\}\langle\bar{1}10\rangle$ system according to the equation.

$$\frac{a_c}{2}[011] + \frac{a_c}{2}[10\bar{1}] \rightarrow \frac{a_c}{2}[110] \qquad - 2.5$$

The sum of the elastic energies of the component dislocations is 31 ev per atom plane (for a low dislocation density), whilst that of the resultant dislocation is 21 ev per atom plane. The core energies for the mixed component dislocations and the resultant edge dislocation are both likely to be within the range 1 - 3 ev, so the above reaction appears to be favourable with a release of energy of at least 8 ev per atom plane of junction dislocation produced. Dontinck and Dekeyser observe dislocations in $\langle 110\rangle$ but these appear to lie in $\{112\}$, so again there is no direct confirmation of the calculations.

The junction dislocation is a glissile one, i.e. it belongs to the secondary slip system, but it might still block slip quite effectively (c.f. Saada, 1961). The lack of confirmation of the above calculations is partly remedied by some simple etch pit experiments.

3.1.1.2. Direct Observations of Intersections by Etch Pitting

This experiment basically looks at the intersection of dislocations moving on intersecting slip planes; The dislocations emanate from two freshly introduced sources.

If B orientation crystals (fig. 2.13) are indented on $\{111\}$, the types of dislocation produced around the indent are those shown schematically in fig. 2.14. If a tensile stress is now applied to the crystal in $[112]$, dislocations of type 1 move outwards. Conversely, if a compressive stress is applied, dislocations of type 2 move outwards from the indent.

So, after the original indentation, a tensile stress is applied to extend the arms to the extremities of the crystal. Subsequently, a further indent is introduced at point X and a specific tensile stress applied for a given length of time; this moves the dislocations away from the indent. The dislocations moving on one arm are required to intersect dislocations from the original indent. As shown in fig. 2.15, intersection occurs but the dislocations do not move as far as those on the arm where intersection is not required. So a certain small stress is required for the intersection process.

A second experiment is now conducted. After the initial indent a tensile stress is applied to extend the arms out of the crystal. However, after the second indentation a compression stress, similar in magnitude and duration to the tensile stress in the first experiment, is applied. The dislocations moving on the intersecting arm pile up against the arm from the original indent. (fig. 2.16).

The experiment is a difficult one to conduct because, for some reason the reversal of stress produces a large number of dislocations from other sources under all conditions, this tends to obscure the effect under investigation. However, it is possible to observe in fig.2.16 that the 'compressive arm' on the original indent emits dislocations during the application of the compressive stress and these dislocations move over a large distance; this confirms that the dislocations from the second indentation would have moved a large distance through the crystal if intersection of the arm from the original indent were not required to proceed.

The interpretation of the above experiments requires firstly a consideration of the burgers vectors of the dislocations involved.

Definition of the burgers vector

It has already been shown that a type 1 dislocation loop moves outwards under a tensile stress whilst type 2 dislocation loops move under a compressive stress. The ambiguous definition of a burgers vector means that either loop can be asigned the vector b^+ or b^-. However the tensile and compressive loops are required to have opposite vectors, so if the vector of loop 1 is defined arbitrarily as b^+, that of loop 2 is b^-. From the symmetry of the planes of lowest resolved shear stress with respect to the applied stress it follows that the vector of loop 1_1 is, also b^+ and that of loop 2_1, is b^-. Thus, the interaction in the first experiment is that given in equation 2.4 whilst that in the second experiment is given in equation 2.5.

Now the intersection stress is greater for an attractive than repulsive intersection (a good review of intersection is given by McLean, 1962); this arises simply because the attractive intersection requires the dissociation of the junction formed. Thus, the larger the release of energy upon creation of a junction, the larger the intersection stress. So the above experiments indicate that the reaction in equation 2.5. produces a relatively stable junction capable of effectively blocking slip whilst that in equation 2.4 is either a weakly attractive or repulsive interaction.

3.1.2. Parallel Slip Planes

On any given $\{100\}$ there are two orthogonal burgers vectors (fig. 2.12). If dislocations of both types are produced on a given slip plane they might combine according to the reaction:-

$$\frac{a_o}{2}[110] + \frac{a_o}{2}[\bar{1}10] \longrightarrow a_o[010] \qquad - 2.6$$

This constitutes the combination of an edge and screw dislocation on the primary system to form a mixed ($\theta = \pi/4$) dislocation of the type $\{100\}\langle 010\rangle$. The elastic energy of the latter is 31.9 ev/atom plane whilst that of the component dislocations is 32.9 ev/atom plane. So the stability of this dislocation depends upon the relative magnitude of the core energies. It is not possible to determine these precisely but, that of the junction dislocation is clearly larger than that of a constituent dislocations(Roy) So even if the junction forms it will not be very stable. Roy has shown that dislocations with $\langle 010\rangle$ burgers vectors move only with great difficulty, so the junction will be sessile. However, its formation is not likely to block slip

effectively since even a small pile up behind it will result in its dissociation.

3.2 Intersections

The form and orientation of the jogs produced by intersection are now considered to try to determine whether they will move conservatively or non-conservatively. The formation of jogs on both edge and screw dislocations are looked at in turn.

a. Edge Dislocation (burgers vector, b_1)

When this dislocation intersects a forest dislocation (b_3 or b_4), the jog produced has a direction and magnitude given by the component of b_3 (or b_4) normal to the slip plane containing b_1 (Read 1953). In this case, the jog is essentially a length $a_o/2$ of pure edge dislocation lying in $\{110\}$ It is thus, similar in orientation to existing half jogs but different in form so that it does not alter the existing charge distribution. The jog can glide along with the dislocation and should not impede its motion significantly.

b. Screw Dislocation (b_1)

When this intersects a forest dislocation (b_3 or b_4) the orientation of the jog is identical to that produced on the edge dislocation and for conservative motion it is required to glide along $\{110\}$. In D orientation crystals the component of the applied stress in the conservative direction of motion is zero, so the jog is constrained to move non-conservatively or remain sessile with the resultant production of point defects or dislocation dipoles.

In A orientation crystals(fig.2.17) there is a component of applied stress in the conservative direction of motion; this is $\frac{1}{2}$ of that in the non-conservative direction of motion. It is not possible to determine whether the jog is sessile or moves conservatively or non-conservatively without information upon the relative magnitudes of the stresses required for motion. The flexibility of the dislocations results in the bowing out between jogs; this often diminishes the possibility of conservative motion and encourages non-conservative motion, so the situation is rather complex.

Jogs can also be produced on screw dislocations through multiple cross glide (Orowan, 1954; Gilman and Johnston,1960) under single slip conditions. The orientation of these is similar to the intersection jogs but usually larger in magnitude and can be treated in a similar fashion. If conservative motion if unlikely,long jogs tend to produce dipoles and short jogs point defects.

The bulk density measurements of Roy (see Appendix I) show that dipoles and perhaps point defect clusters are produced during the deformation of both type A and B specimens, so jogs cannot be solely conservative, even in type A specimens.

3.3 Conclusions

1. Stable dislocation junctions can be produced through interactions of dislocations moving on orthogonal slip planes; if the burgers vectors of the constituent dislocations are suitable these form in the mixed ($\theta = \pi/4$) orientation. They are not sessile but are expected to move only at relatively large stresses.

2. The jogs produced on screw dislocations through multiple cross glide or intersection cannot move conservatively in type B specimens and probably not in type A specimens. So at least in part, they are either sessile or required to move non-conservatively.

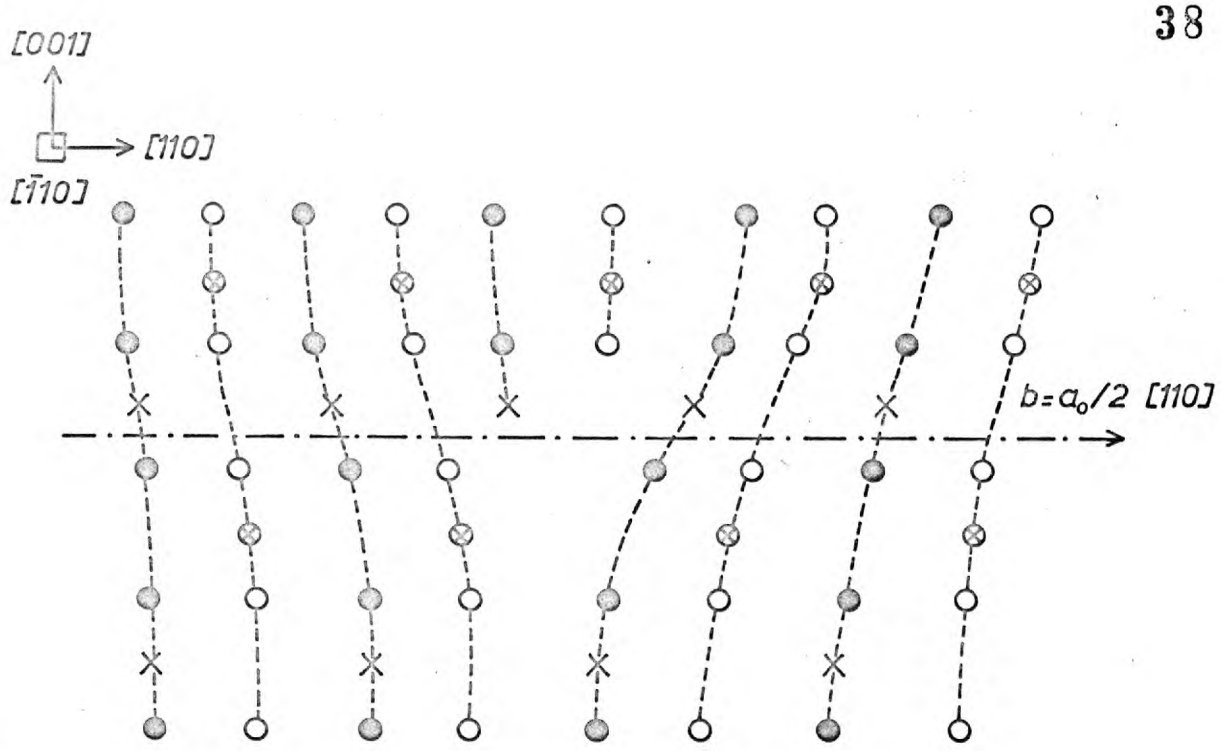

F^- ○ In plane of paper
● $a_0\sqrt{2}/4$ behind or in front of plane of paper

Ca^{++} × In plane of paper
⊗ $a_0\sqrt{2}/4$ behind or in front of plane of paper

Fig. 2.1. Edge dislocation on {100}<110> (After Amelinckx and Roy)

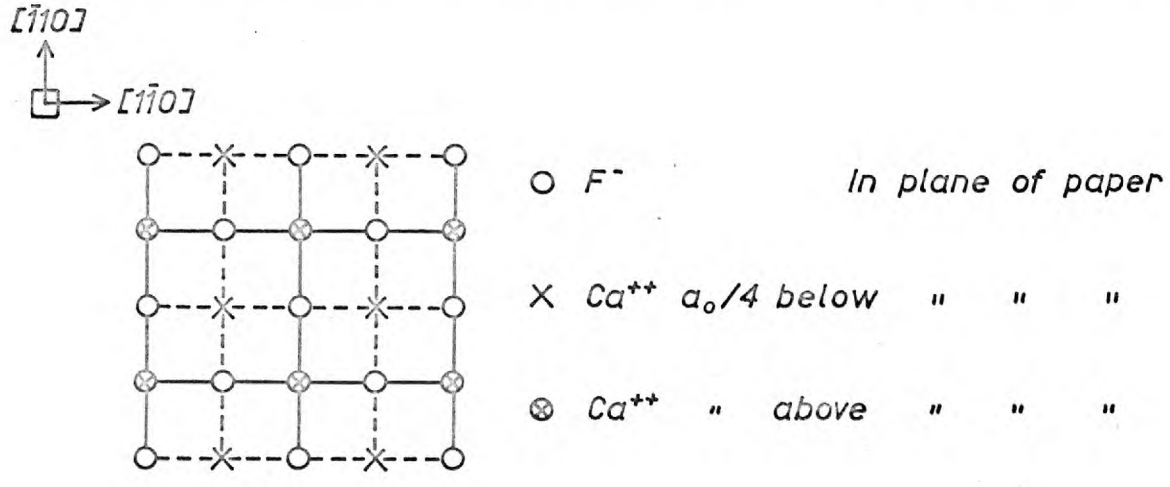

Fig. 2.2. Arrangement of ions on 3 adjacent {100}

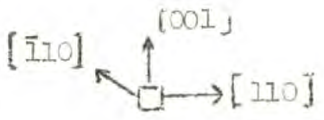

F^- - brown balls

Ca^{++} - green balls

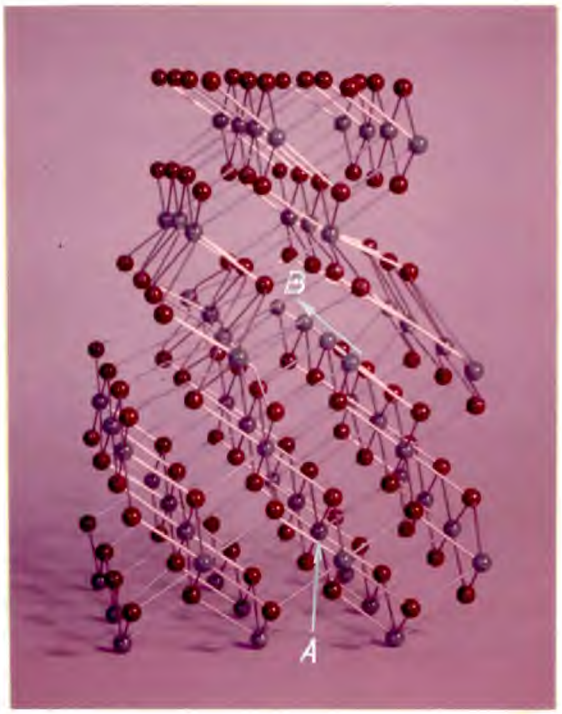

All Ca^{++} in bulk are attached to $8F^-$ ions(e.g.A)

At the core the Ca^{++} in row B are attached to $4F^-$ only, so there is a charge of e^+ at every distance b along the length.

Fig. 2.3. Positively charged configuration

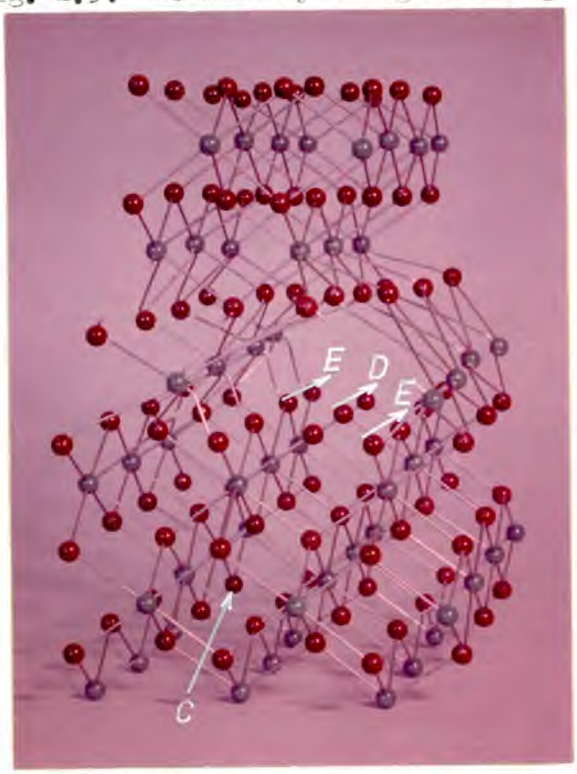

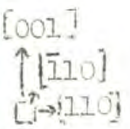

All F^- in the bulk are attached to four Ca^{++} ions (e.g. at C)

At the core F^- in row D are attached to two Ca^{++} only; F^- in rows E are attached to three Ca^{++}, so there is a charge of e^- at every distance b along the length.

Fig. 2.4. Negatively charged configuration

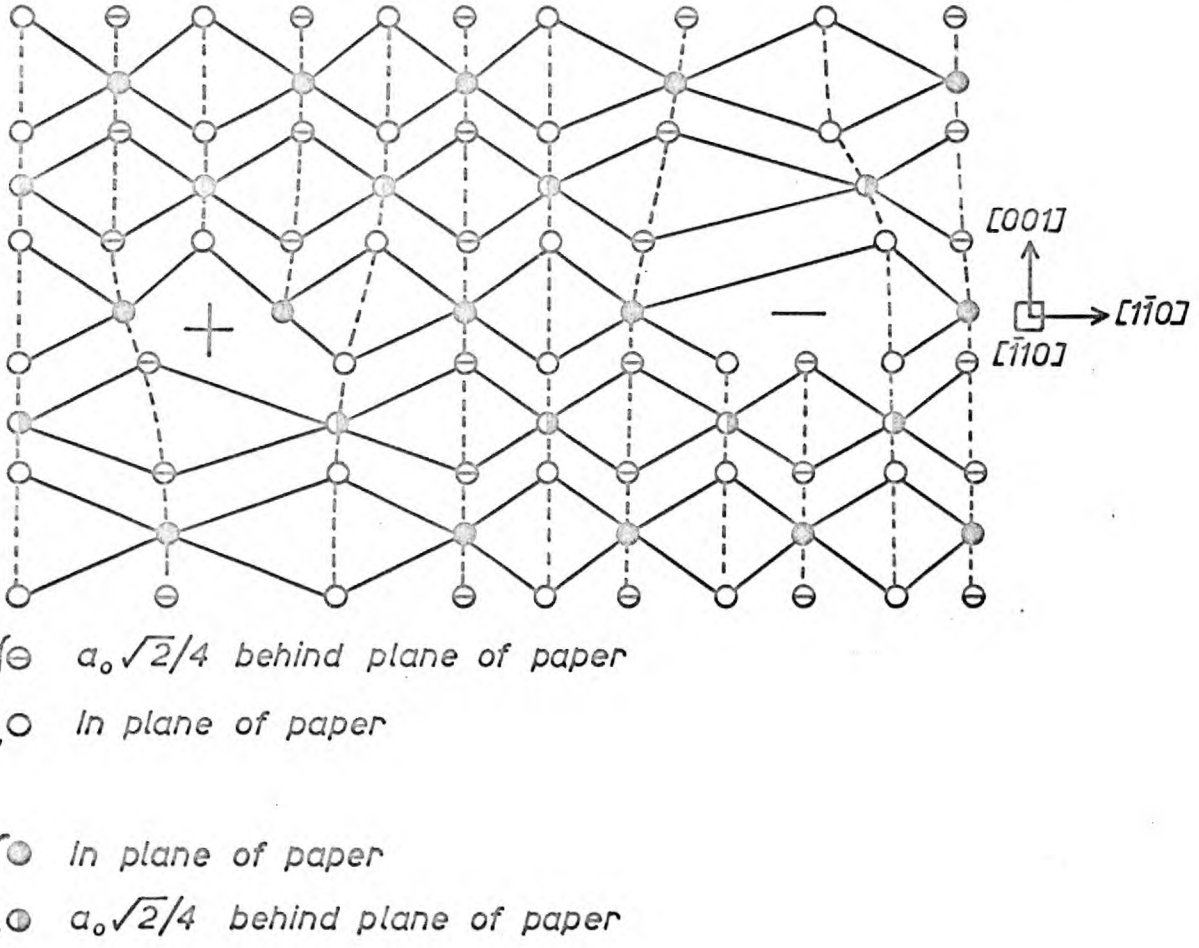

Fig.2.5Schematic formation of two edge dislocations of opposite mechanical sign from the perfect lattice.

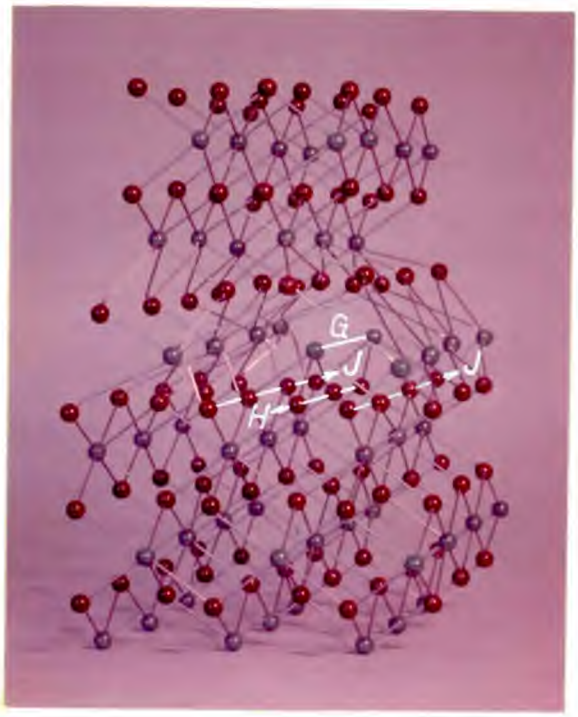

Ca^{++} in row G attached to four F^-

F^- in row H attached to three Ca^{++}

Alternate F^- in rows J attached to three Ca^{++}

So configuration is uncharged

Fig. 2.6. Uncharged configuration.

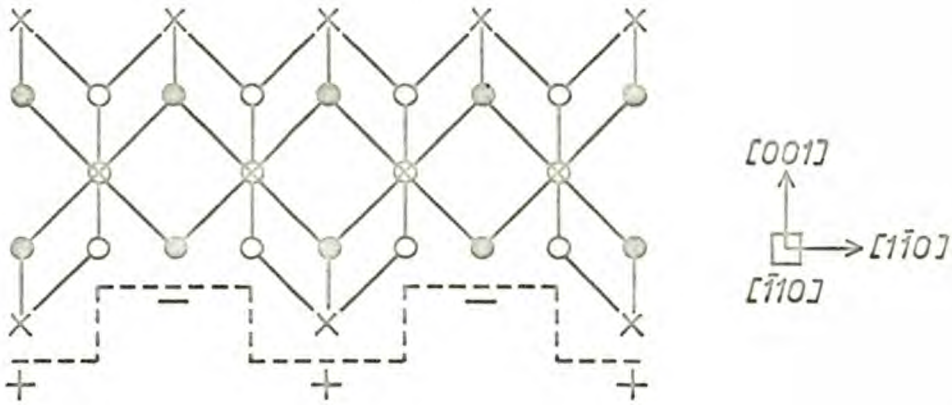

F^- ○ In plane of paper

● $a_0\sqrt{2}/4$ behind or in front of plane of paper

Ca^{++} × In plane of paper

⊗ $a_0\sqrt{2}/4$ behind or in front of plane of paper

Fig. 2.7. The extra half planes constituting the uncharged edge dislocation.

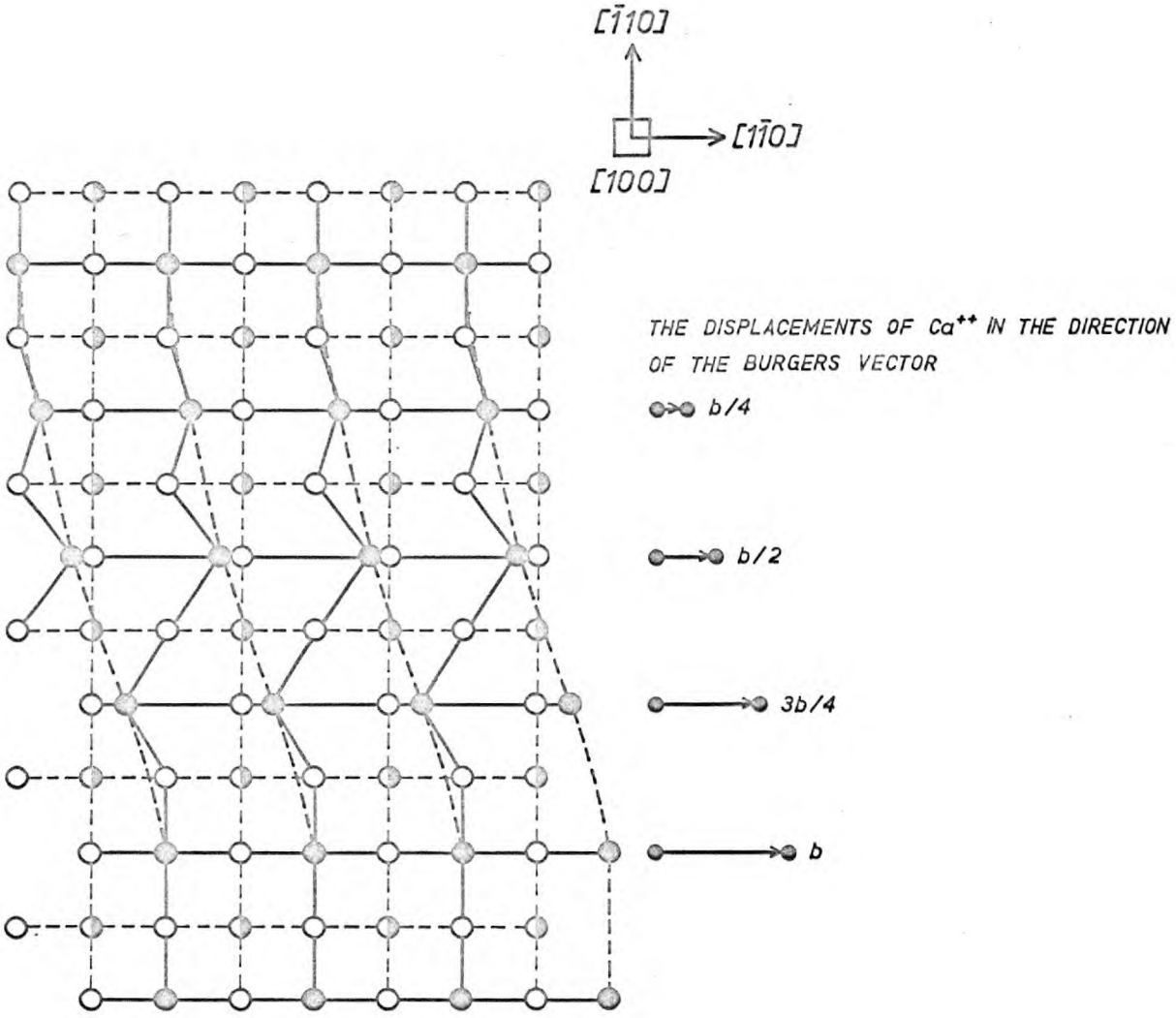

○ F^- In plane of paper

◐ Ca^{++} $a_o/4$ below plane of paper

◉ Ca^{++} $a_o/4$ .above plane of paper

Fig. 2.8. A screw dislocation on {100} <011>

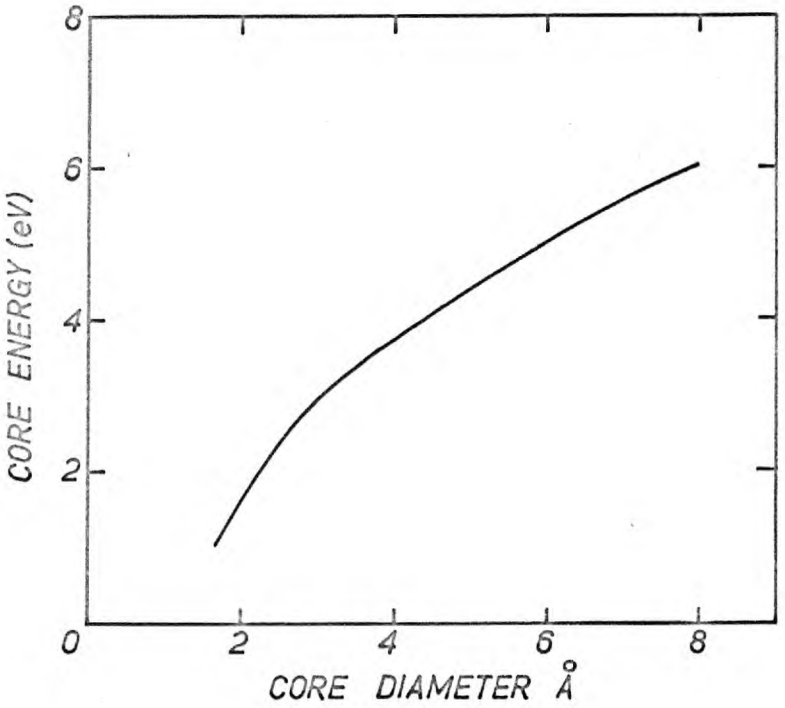

Fig. 2.9. Dislocation core energies for an edge dislocation on {110} <1$\bar{1}$0> in NaCl
(After Huntington, Dickey and Thomson, 1955)

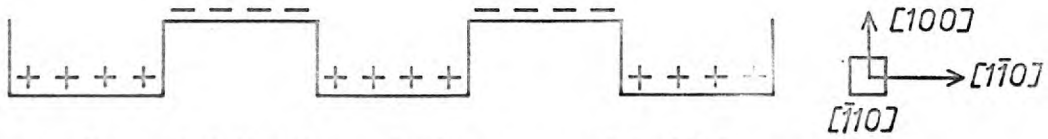

Fig. 2.10. The possible distribution of charge and half jogs along an edge dislocation on the primary system

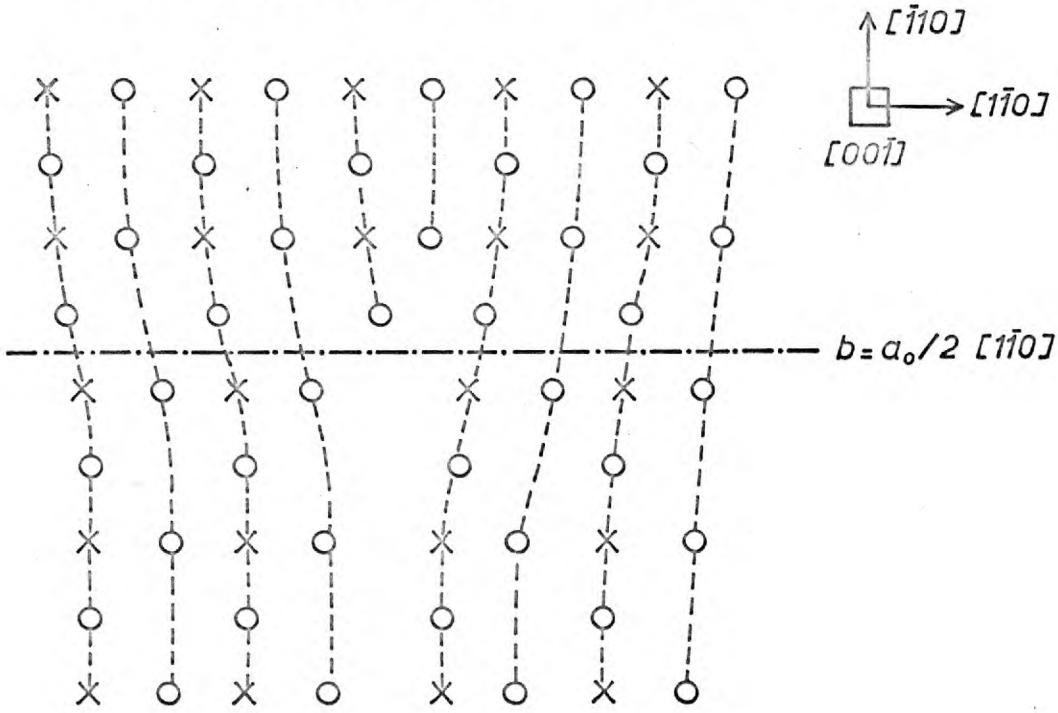

○ F^- $a_o/4$ behind plane of paper

× Ca^{++} In plane of paper

Fig. 2.11. Edge dislocation on {110} <$\bar{1}$10> (After Roy)

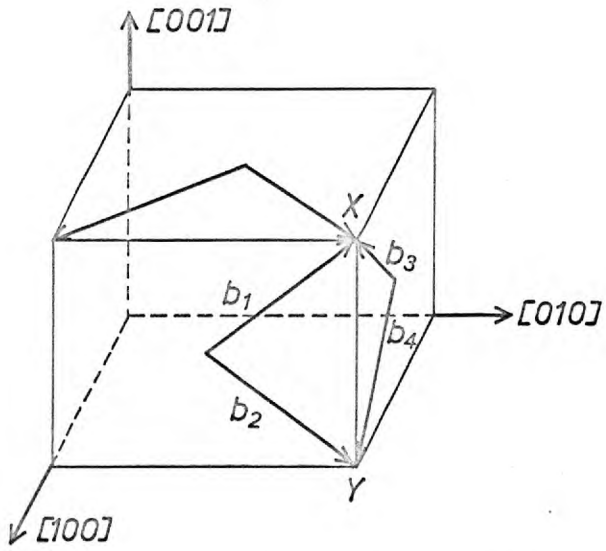

Fig 2.12. The slip vectors of the system {100} <110>

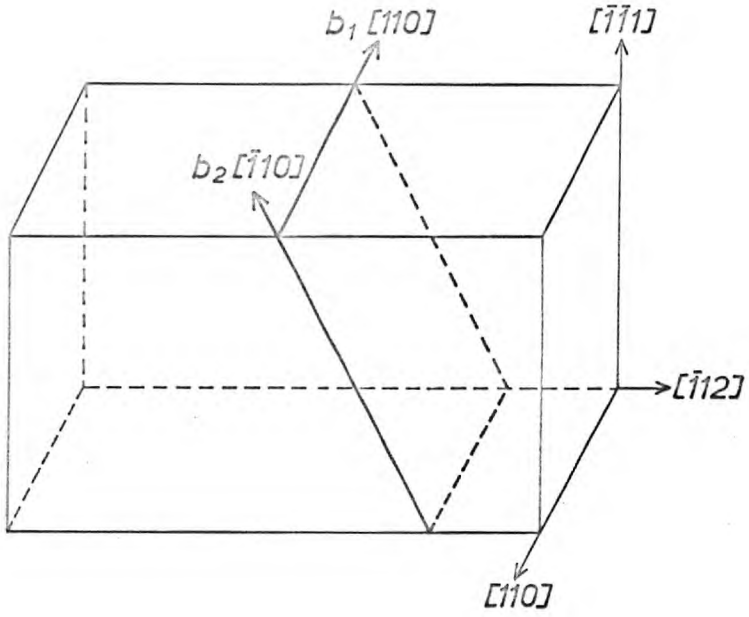

Fig. 2.13a.Type B crystal. Plane of maximum resolved stress

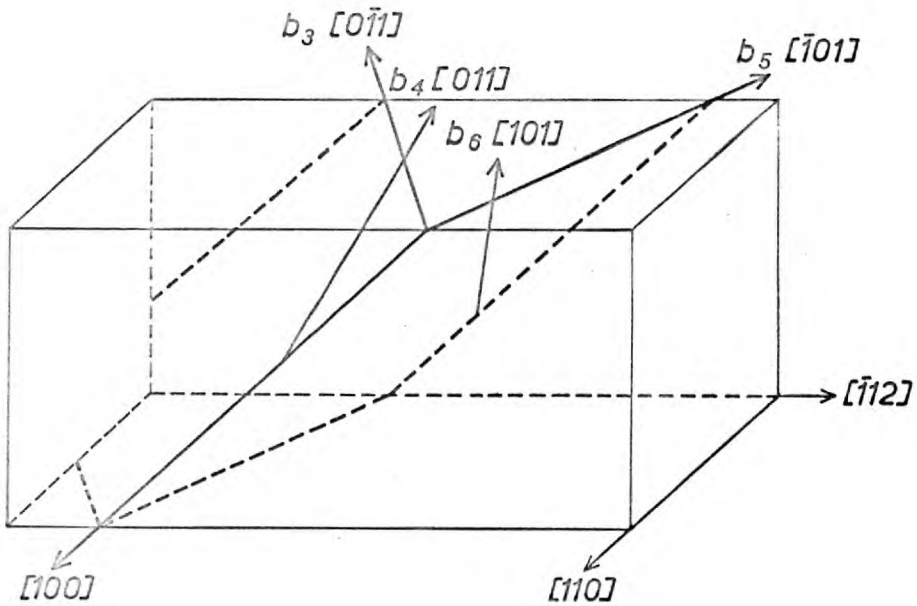

Fig. 2.13b.Type B crystal. Planes of minimum resolved stresses

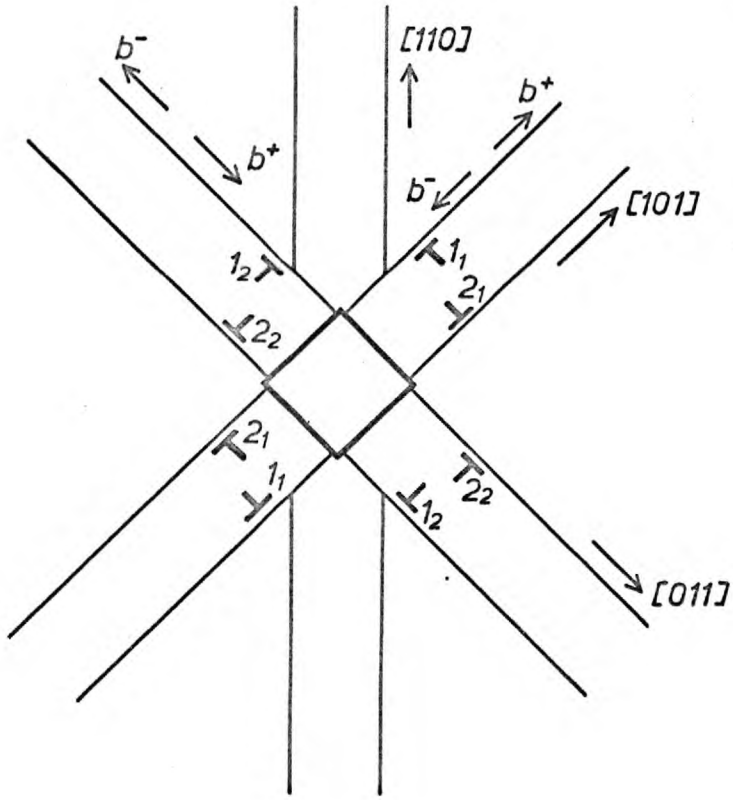

Fig. 2.14. Schematic representation of edge dislocation produced around an indent on {111}

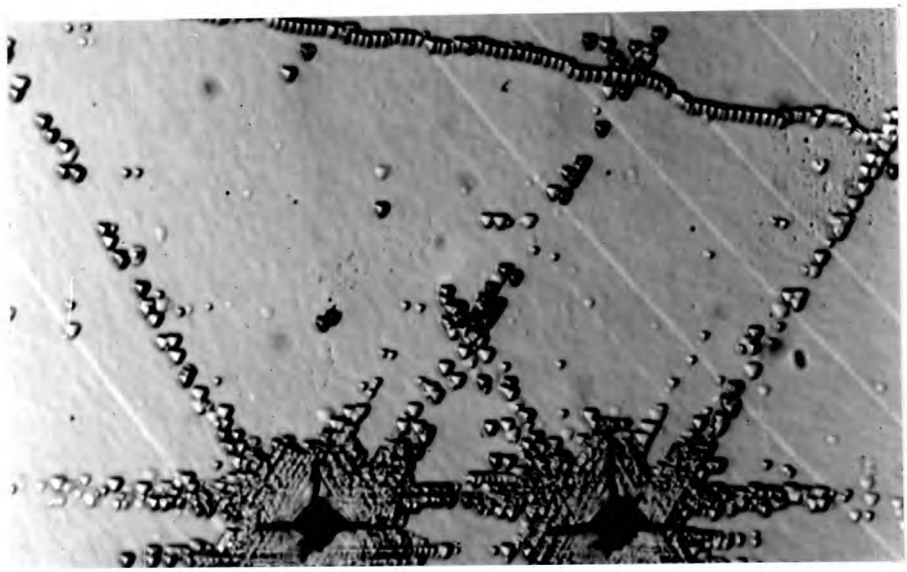

Original indent Second indent
Magnification x 150

Fig. 2.15. The intersection of dislocation arms; arms from both indents extended in tension

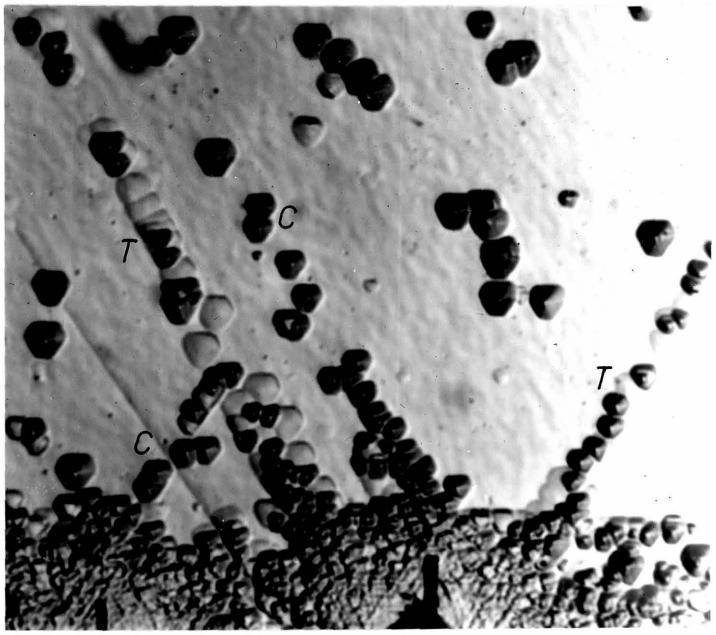

C represents compression arms.

T represents tension arms.

Second Indent Original Indent

Fig 2.16(a) x 320

Second Indent

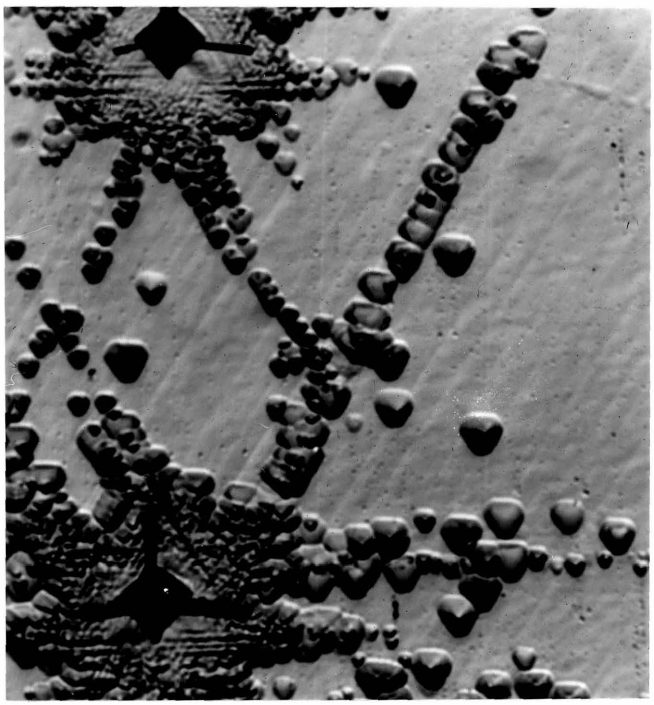

Original Indent.

The original indent here is etched before the second indent is introduced so the tension pits are larger than the compression pits. Note how the compression arms intersect and how the other compression arm is arrested at the tensile arm.

Fig 2.16 (b) x 320

The intersection of dislocation arms; the original is extended in tension and the second in compression.

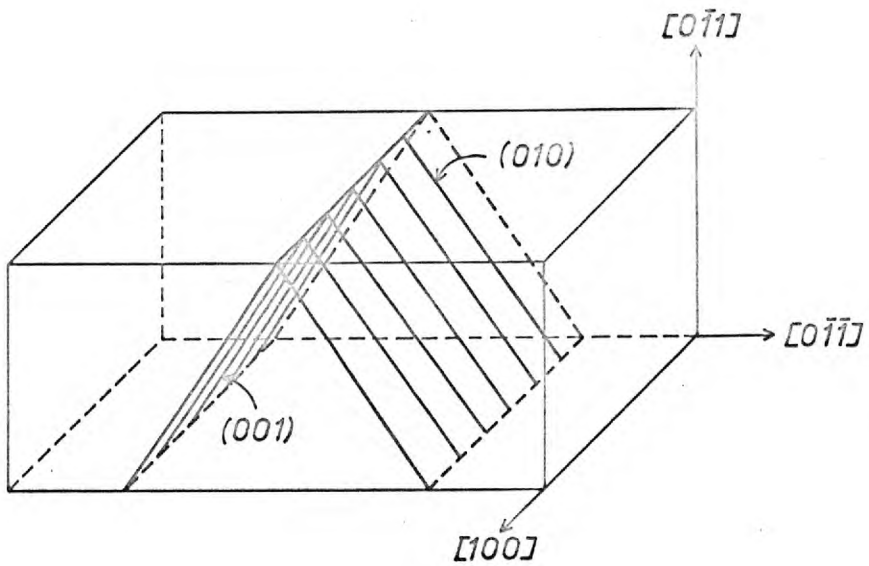

Fig. 2.17. "A" orientation crystal

CHAPTER 3

The Motion of Individual Dislocations

1. Introduction

Before conducting a comprehensive study of work hardening it is important to obtain information about the velocity of individual dislocations. The velocity and stress usually fit the empirical relationships (Li, 1967)

$$U = \left(\frac{\tau_A}{\tau_o}\right)^m_{\tau_\mu > 0} \qquad - 3.1a$$

$$\text{and } U = \left(\frac{\tau^*}{\tau_o}\right)^{m^*}_{\tau_\mu = 0} \qquad - 3.1b$$

τ_o and m^* are constants for a given temperature, whilst m may depend upon U (Michelak, 1965).

An alternative relationship has been suggested by Gilman(1962) to fit the experimental data obtained for LiF;

$$U = Uoe^{-A/\tau} \qquad - 3.2$$

Uo and A are constants for a given temperature.

Thus, the relationship applicable to calcium fluoride is to be determined; the importance of this is shown in Chapter 5.

It is also important to determine the relative velocities of edge and screw dislocations since the component with the lower velocity, for a given stress, controls the rate at which deformation proceeds.

These are the principal objectives of this investigation.

2. Theory

2.1. Introduction

The direct measurement of dislocation velocity requires the introduction of fresh dislocations into the specimen and then

the observation of the motion of these dislocations when a given stress is applied for a given time interval. The motion of the dislocations is followed by etching before and after the application of the stress.

In this investigation, crystals of type B orientation are used. Fresh dislocations can, for instance, be introduced by indentation. An indentation on $\{111\}$ produces either edge or screw dislocations in $[\bar{1}10]$ and either mixed $(\theta=\Pi/4)$ or edge in the two $[0\bar{1}1]$, fig. 2.13. If a stress is applied along $[112]$, the shear stress components, in the direction of the burgers vector and slip plane, are those given in table 5.

An indentation in $\{110\}$ produces either edge or screw dislocations along $[\bar{1}10]$ and either mixed $(\theta=\Pi/4)$ or screw along $[100]$; the associated orientation factors are also given in table 5.

TABLE 5: Schmid Factors in Type B crystals

Type of Dislocation		Orientation Factor
$\{111\}$	$\{110\}$	
Edge in $[\bar{1}10]$	Screw in $[1\bar{1}0]$	0
Screw in $[\bar{1}10]$	Edge in $[1\bar{1}0]$	0.47
Edge in $[0\bar{1}1]$	Screw in $[100]$	0.35
Mixed in $[0\bar{1}1]$	Mixed in $[100]$	0.17

The stressing system during indentation is rather complex and presumably dislocations of all the above types could be formed. It is only upon a subsequent stress application along $[112]$ that the dislocations that have moved away from the rosette can be identified.

The identification is still not unequivocal where the planes of lower resolved shear stress are concerned i.e. the mixed dislocations could be giving the observed motion, despite the small orientation factor. For absolutely unambiguous results, the movement of dislocations on both $\{111\}$ and $\{110\}$, on the plane of maximum resolved stress should be looked at.

The ideal method of determining the velocities is that adopted by Gilman and Johnston (1962). They introduced the dislocations by indentation and subsequently chemically polished to isolate individual loops. The motion of these individual loops was then studied. Unfortunately, this method is not applicable in this case for the following reason:-

Chemical polishing is conducted using a perchloric acid, aluminium chloride mixture maintained at 250°C. The period of polishing is about 30 minutes and quite severe pinning of the dislocations occurs. The pinning varies from one dislocation to another so extremely erratic movements are observed on stressing.

Thus, an alternative method, often used for this sort of investigation in b.c.c. metals (e.g. Stein and Low, 1960; Erikson, 1962) is adopted. Here, a scratch is scribed along the proposed stress axis using a diamond tipped scriber pressed against the surface of the specimen with a small constant load. This produces a uniform distribution of dislocations around the scratch (fig. 3.1). The specimen is subsequently stressed in a four point bending jig and the average movement of the dislocations away from the scratch observed. The method is not entirely satisfactory because intersections between dislocations moving on inclined planes is required to occur, in certain instances, near the scratch. Thus, it is found more satisfactory to introduce a

series of indents along the length of the specimen (the indentations made using a specific load) and to observe the extension of the individual arms.

In both the scratch and indentation experiments the effect of local stresses, other than the applied stress, are required to be eliminated.

2.2. Effect of Local Stresses

There are two distinct sources of localised stress.

1. The presence of the scratch (or indent) gives rise to a stress concentration in its vicinity; this is a relatively short range effect.
2. The long range stress field of the dislocations behind the leading dislocation. These usually compliment the applied stress and diminish the further dislocation moves from the source.

These local stresses are allowed for quite satisfactorily by defining a distance Xc as the distance moved by the dislocations under the action of the local stresses only (Erikson, 1962, Schadler, 1964).

Thus, $U = \frac{X - Xc}{t}$ - 3.3

Where X is the total distance moved by the dislocation

t is the time of application of the load.

Values of X are always determined in the uniform stress region between the inner knife edges of the bending jig (see fig. 3.2 in this section).

The magnitude of the quantity Xc cannot be estimated by direct experiment but has been considered to be within the range 10 - 30μ (Stein and Low, 1960; Schadler, 1964). However, relatively

accurate estimates of Xc may be obtained theoretically; the two above effects are considered separately.

1. The stress concentration around a circular hole in a stressed body is given by (Dieter, 1961).

$$\tau = -\frac{\sigma a}{2}\left(1 - \frac{3a}{X^4} + \frac{2a^2}{X^2}\right) \sin 2\theta \qquad - 3.4$$

Where a is the radius of the hole

θ is the angle between the applied stress(σa) and the direction considered (X).

A maximum value of Xc_1 is given by substituting $\tau = \sigma a$ at $\theta = 45°$ into equation 3.4.

The diameter of a typical indent is 10 microns, this gives:-

$Xc_1 max = 8$ microns

2. The stress exerted by a dislocation on another dislocation in the same slip plane is (Cottrell, 1953)

$$\sigma xy = \frac{\mu b}{2\pi(1-\nu)} \frac{1}{X} \qquad - 3.5$$

Where ν is poisson's ratio

Thus, the stress associated with a row of similar dislocations is

$$\sigma xy = \frac{\mu b}{2\pi(1-\nu)} \sum \frac{1}{X} \qquad - 3.6$$

Substituting the values of μ, b and ν gives:-

$$\sum \sigma xy = 0.3 \sum \frac{1}{X} \text{ kg.mm}^{-2} \qquad - 3.7$$

(for X measured in microns)

Thus, using the values of X obtained from typical distributions of dislocations observed it is possible to find values of the local stress at the leading dislocation and subsequently a value of Xc_2.

3. Experimental

3.1 Specimen Preparation

Specimens for $\{110\}$ observations are produced by cutting along $\{110\}$, using a wire saw described in the following chapter and subsequently cleaving along $\{111\}$ to produce beams of approximately 18 x 3 x 2 mm^3. They are then chemically polished. This mixture only polishes $\{110\}$ so, for observations on $\{111\}$, the specimens are chemically polished prior to cleavage and the as-cleaved faces used.

3.2 Introduction of Dislocations

3.2.1 Indentation

The indentations are produced using a standard Reichart microhardness indentor. The load used is the minimum required to separate the individual arms so that the local stresses are minimised; thus, a load of 5 gm applied for 10 seconds is found to be suitable. The dislocation rosette dimensions produced are perfectly reproduceable.

3.2.2 Scribing

Scratches are scribed using a diamond tipped scriber of the appropriate shape (e.g. Stein and Low, 1960) loaded at 5 gm. The technique has been described by Das (1967).

3.3 The Stress System

Stresses are applied using a four point bending jig (Bruneau, 1962) in conjunction with an Instron testing machine. This technique provides a region of uniform stress, at the surface of the crystal, between the inner knife edges, given by:-

$$\sigma = \frac{W}{2}\frac{(B-A)}{bh^2}\,6 \qquad -3.8$$

W = applied load

(B-A) is the spacing between the inner and outer knife edges, b and h are the breadth and thickness of the beam respectively.

For the jig used; $\sigma = \frac{12W}{bh^2}$ $\qquad -3.9$

The stress distribution along the stress axis in four point bending is such that the profile created by the movement of the dislocations away from the scratch is of the form shown in fig. 3.2. (after Erikson, 1962).

Unfortunately, this stressing system could not be used under all conditions; when working at high stresses the beams almost invariably fractured before any significant dislocation motion could be observed. To extend the measurements to higher stresses a number of compression tests are performed. Specimen preparation is conducted most carefully to avoid introducing extraneous sources and, to ensure uniform stress application, a hemispherical ball is inserted between the end of the specimen and the compression plate. A further complication arose because the ends of the specimens were slightly rounded during chemical polishing; this provided an erroneous stress at the surface of the specimen. This problem is averted by mechanically polishing the ends of the specimen after the chemical polish, the dislocations introduced during this process are aged at about 300°C prior to indentation (scratching), thereby pinning them and preventing them from interfering with the subsequent experiments.

3.4 Etching

1. {111}

This is achieved using concentrated sulphuric acid maintained at 45°C; etching time 10 - 90 secs.

2. {110}

Aluminium Chloride maintained at 55°C for 90 - 300 seconds.

4. Results and Discussion

4.1 Determination of Xc

The applied stress range used in this investigation is 0.8 - 2 $Kgmm^{-2}$. Thus, from equation 3.7 values of $1/X$ greater than about $1/10$ could provide values of the local stress that are significant in comparison with the applied stress. The distribution of dislocations behind the leading dislocation in a profile of the type in fig. 3.2 gives an indication of the distance that the leading dislocation is required to move away from the indent before the local stresses are effectively zero. For the indentations, this distance is seen to be about 80 microns (40 microns for a scratch). Now, Xc is given by the distance moved by the dislocations under the influence of the local stresses only.

$$\text{Thus, } Xc, = Xc_1 + 80\sqrt{\frac{X(\tau_\mu)}{X(\tau_\mu + \tau_a)}} \qquad - \quad 3.10$$

Where τ_μ is the local stress and varies from about $\tau_a/3$ at the indent to approximately zero at 80 microns.

This gives a maximum possible value of Xc of 30 microns for the indentation experiments (20 microns for the scratch). These are still only approximate values so, to minimise errors due to the selection of Xc, most measurements are made for values

of X greater than 200 microns.

4.2 Dislocation Velocities

The values of edge and screw dislocation velocities have been obtained at 25°C and 75°C; these are plotted against the applied stress, on logarithmic axes, in figs. 3.3, 3.4 and 3.5.

The values obtained from the indentation and scratching experiments on both $\{111\}$ and $\{110\}$ are combined in these graphs. The dislocations moving on the planes of lower resolved stress must be edge on $\{111\}$ and screw on $\{110\}$; if they were mixed they would be required to have a considerably larger velocity than both the edge and screw dislocations, at a particular stress, to provide the observed movements - this is unlikely. This is confirmed by the good agreement between these velocities and those obtained along the plane of maximum resolved stress.

The room temperature edge dislocation velocities obtained are most consistent and independent of the surface, the system and the method by which they are determined. The results fit the relationship given in equation 3.1 quite closely whilst deviating from the exponential relationship, over the relatively small stress range used. The results give a value of $n^{*} = 7 \pm 0.7$ and $\tau_o = 6.2$ Kgmm^{-2}. ($\tau_\mu = 0$, in these high purity single crystals)

The consistency of the velocity measurements is verified by applying a given load to the same specimen for different time intervals and measuring the respective distances moved by the dislocations. The results obtained lie within the error bars indicated on the diagrams; the range of velocities never exceeds a factor of two, so considerable confidence is placed

in the above relationships.

It has already been mentioned that dislocations do not move from all parts of the scratch (fig. 3.6) so all velocities obtained from these experiments are derived from the maximum value of X observed. It is of interest to understand why this occurs. Similar observations in b.c.c metals (Stein and Low, 1960; Erikson, 1962) have been attributed to the pinning of some of the dislocations around the scratch by the impurities present. This explanation is not acceptable in this case because, once the dislocations have initially been moved from the scratch, subsequent ageing for long periods does not inhibit their motion. It is more likely that dislocations of various burgers vectors are produced during scribing and certain of these could combine to form attractive junctions (see Chapter 2). Where junctions form, they cannot be dissociated by the applied stress, so the dislocations do not move; it is only in regions where no interactions occur that the dislocations are free to move. This would also explain why the effect is not observed in the indentation experiments.

The screw dislocation velocities are not quite as consistent, particularly for movement along the plane of maximum stress. Here, for dislocation motion up to about 100 microns from the indent, increasing values of the velocity are obtained; beyond this the results are consistent and within a range extending over a factor of about two, for a given stress. The velocities obtained on $\{110\}$ are quite consistent throughout. (It is suggested that the stress system associated with indentation on $\{111\}$ produces predominantly edge dislocations on the plane of maximum stress; the screw dislocations

interact with these according to equation 2.6 thereby impeding their initial motion). The screw dislocation velocities also fit the relationship in equation 3.1 most closely with a value of $m^* = 9 \pm 1.5$ and $\tau_o = 5.3$ kg/mm^2.

The edge and screw dislocation velocities are compared in fig. 3.5. It is seen that the screw dislocations almost invariably move faster than the edge for a given stress; there are only a small number of points from the two sets of results that overlap. This is exhibited clearly by comparing the extensions of the edge and screw arms from given indents on $\{110\}$ and $\{111\}$, figs. 3.7,3.8. On $\{111\}$ the screw arm has moved considerably further than the edge but the applied stress on the screw slip plane is greater by a factor of about $9/7$. However, on $\{110\}$, although the applied stress on the screw slip plane is smaller by the above factor than that on the edge plane, the screw arm has extended as far as the edge arm. This conclusively indicates that the screw dislocations move faster than the edge.

Velocities are more difficult to obtain at 75°C because pinning occurs quite rapidly i.e. within a period of about twenty minutes after temperature is attained. Thus, measurements have to be restricted to the higher velocities where tests can be completed within this period. Although the scatter obtained is slightly larger than at room temperature the screw dislocations exhibit consistently larger velocities than the edge dislocations.

The results give:-

$m^*_{edge} = 6.5 \pm 0.6$ $\qquad$ $m^*_{screw} = 8 \pm 2$

τ_o edge $= 4.0$ $\qquad$ τ_o screw $= 2.8$

The importance of the determination of the quantity m^* and the effect of temperature on the velocity, stress curves is discussed in Chapter 5.

5. Conclusions

1. The edge and screw dislocations move with velocities that fit the relationship.

$$v = \left(\frac{\tau^*}{\tau_0}\right)^{m^*}_{\tau_{\mu=0}}$$

Values of m^* and τ_o are given in table 6.

TABLE 6. Values of m^* and τ_o

	25°C		75°C	
	Edge	Screw	Edge	Screw
m^*	7 ± 0.7	9 ± 1.5	6.5 ± 0.6	8 ± 2
τ_o (kg.mm^{-2})	6.2	5.3	4.0	2.8

2. For a given value of the resolved shear stress, the edge dislocations invariably move with a lower velocity than the screw dislocations. Thus, any rate controlling mechanism proposed must apply exclusively to the edge dislocation. This result contrasts with observations made in other ionic crystals (e.g. Gilman and Johnston in LiF, 1962, Gutmanas et al in NaCl, 1963).

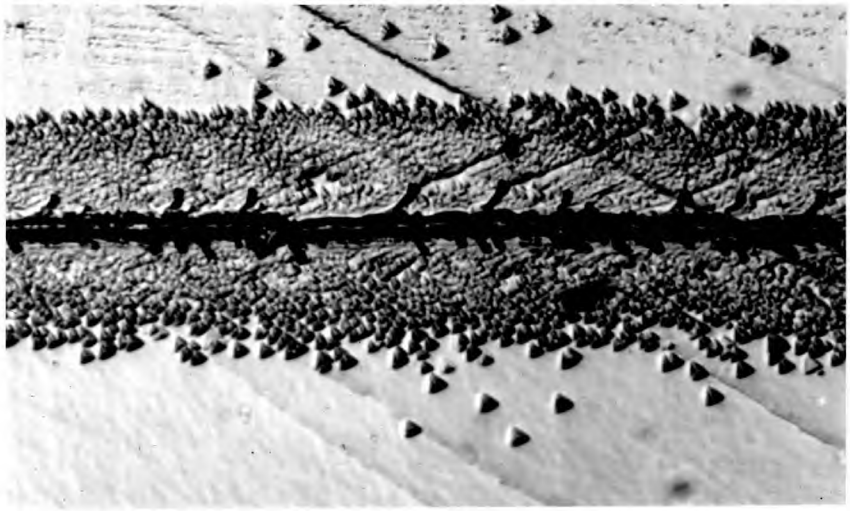

MAGNIFICATION x300

Fig. 3.1. Distribution of dislocations around a scratch on {111}

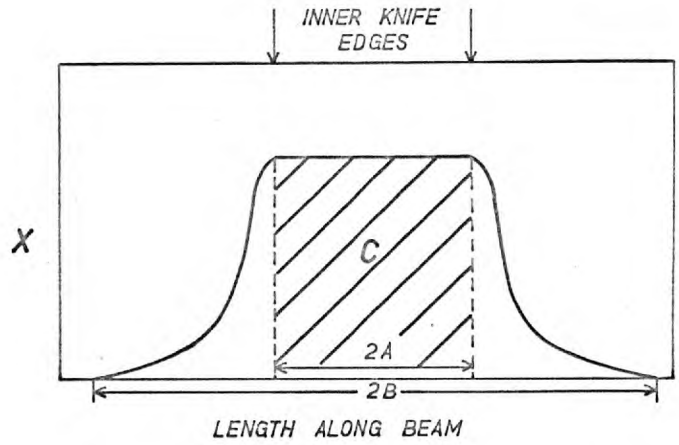

Fig. 3.2. Profile created by the movement of dislocations away from a scratch (or series of indents)

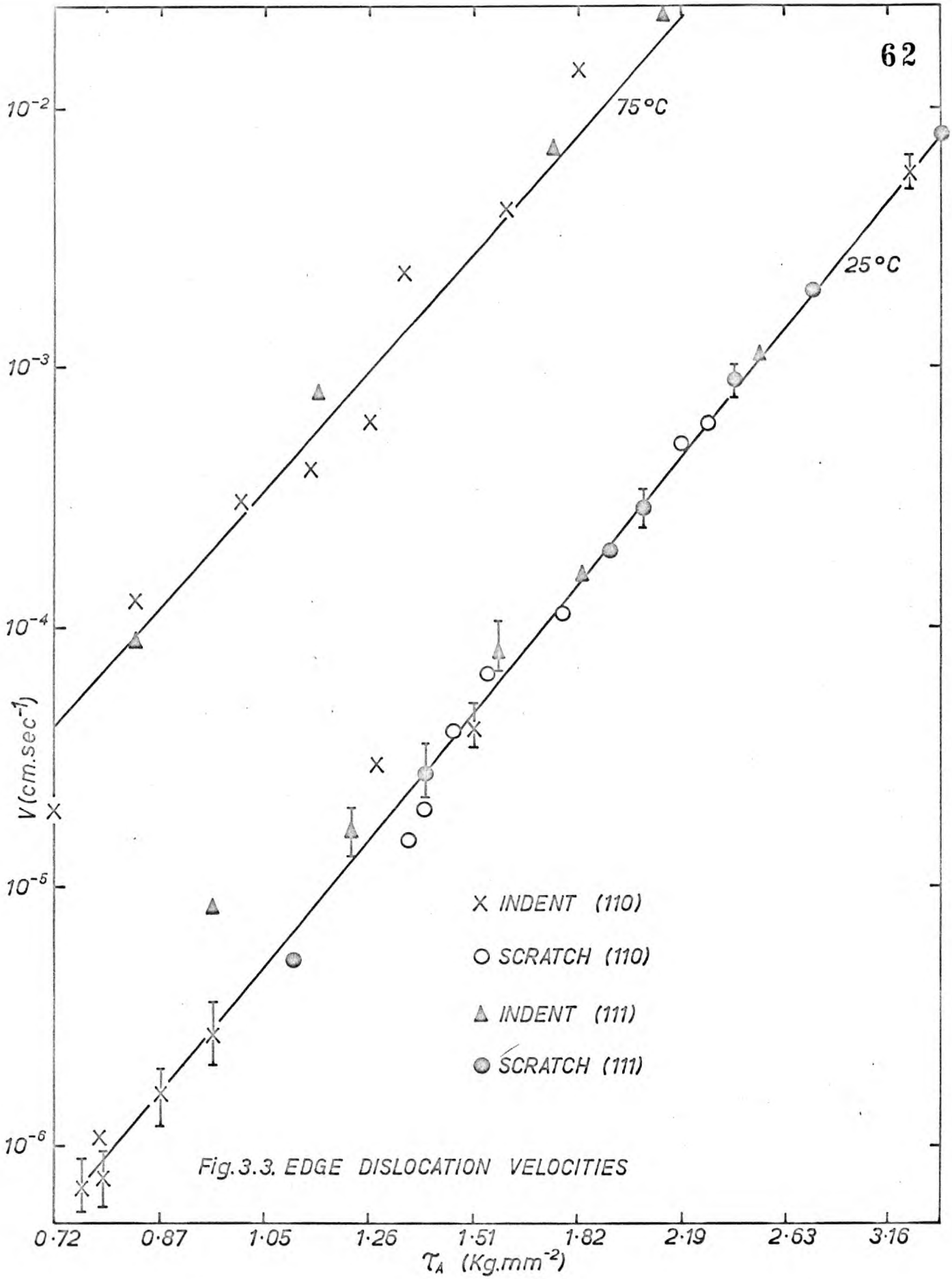

Fig. 3.3. EDGE DISLOCATION VELOCITIES

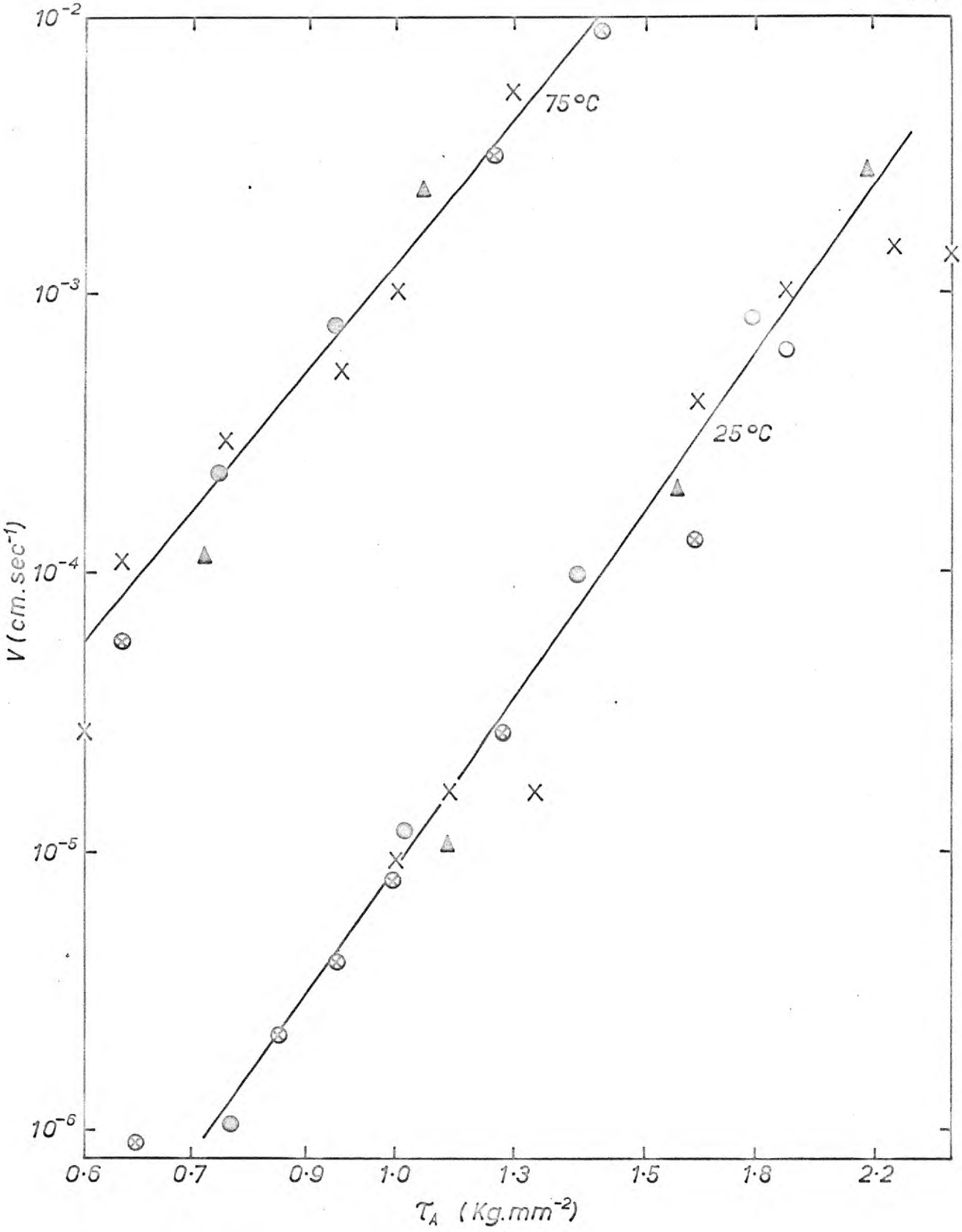

Fig. 3.4. Screw dislocation velocities

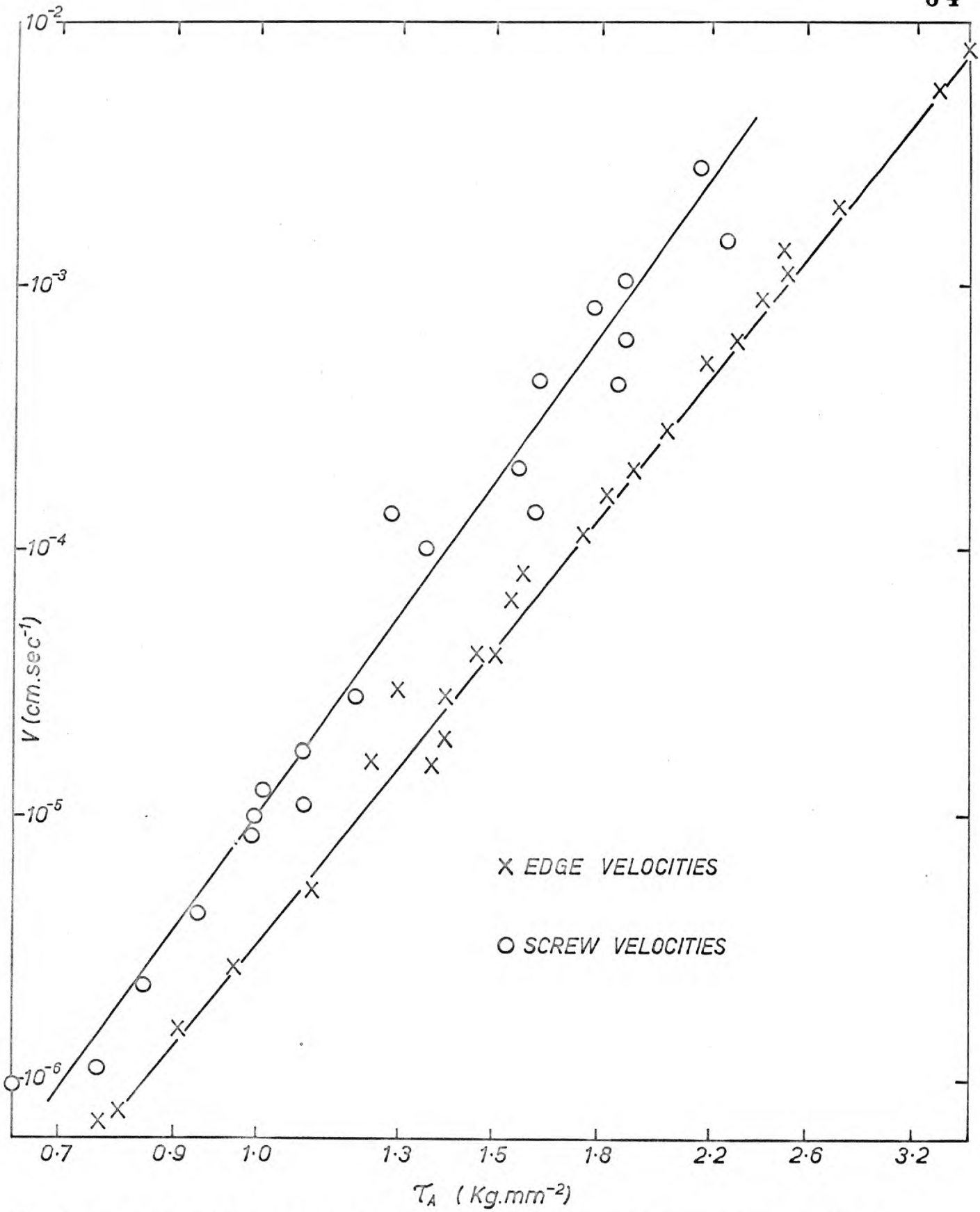

Fig. 3.5. Comparison of edge and screw velocities at room temperature

Fig. 3.6.(a) {111} Mag x 250

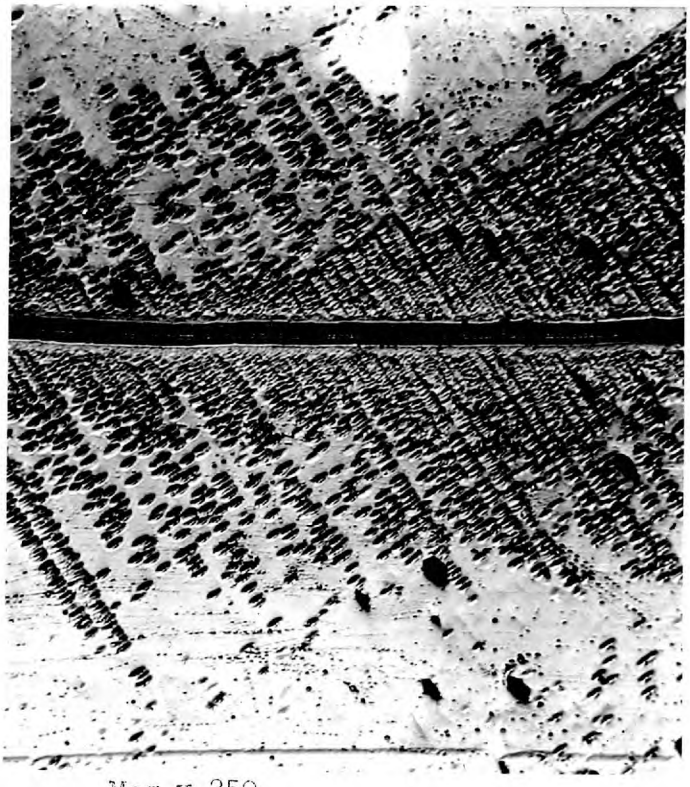

Fig. 3.6 (b) {11C} Mag x 250

The movement of dislocations from a scratch, on type B specimens, stressed at room temperature

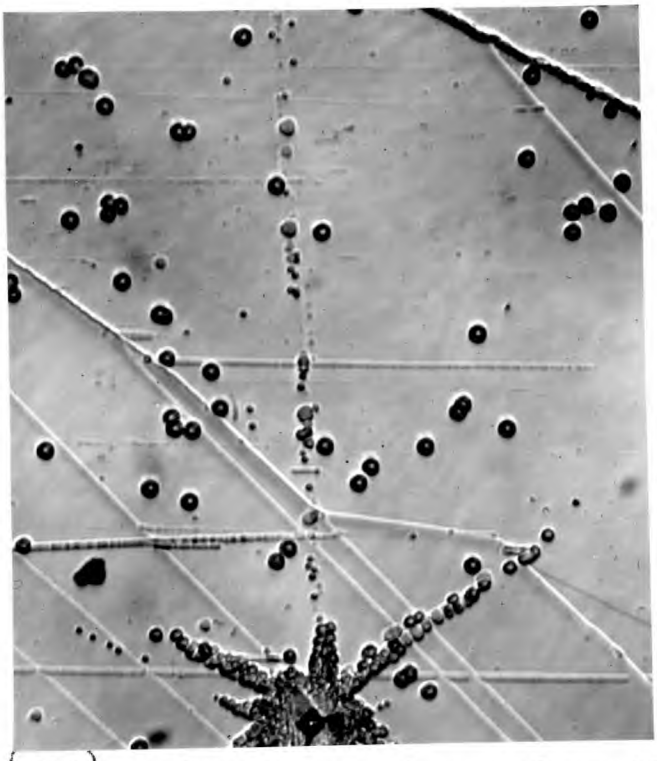

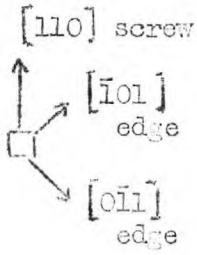

Fig. 3.7 {111} The screw arm has moved considerably further than the edge arm (Mag. x 56)

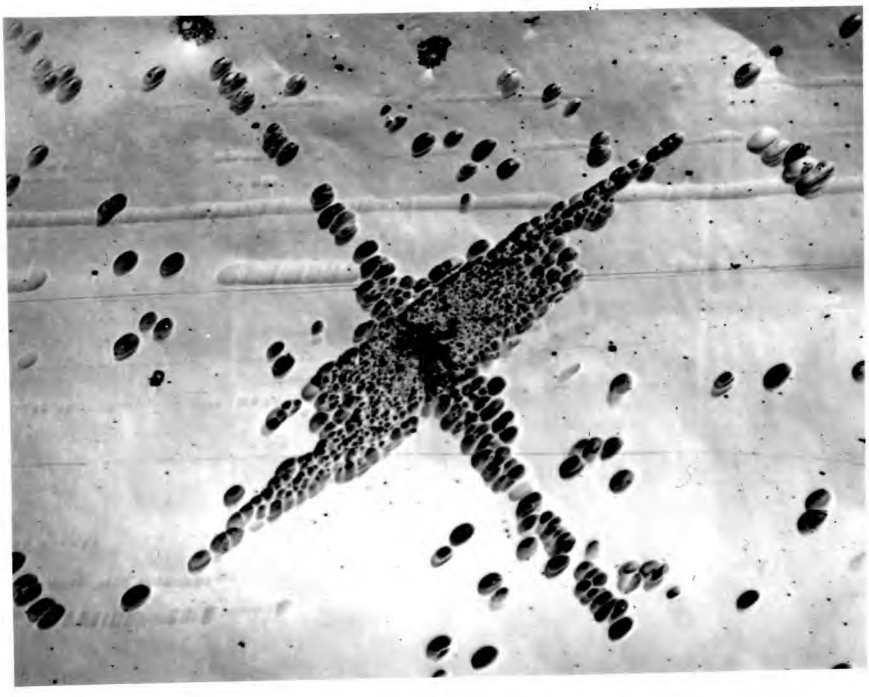

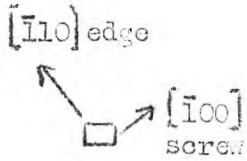

Fig. 3.8 {110} The edge and screw arms have moved similar distances. (Mag. x 150)

The movement of dislocations from indents on type B specimens.

CHAPTER 4

Stress Strain Characteristics

1. Introduction

The characteristics of the plastic deformation associated with primary and secondary slip are established comprehensively in the temperature range where the applied stress contains a thermal component i.e. below about 250°C. The specific characteristics investigated are:-

i) The stress strain curves for various orientations, relative dimensions, temperatures and strain rates.

ii) The development of slip during deformation using the standard techniques of etch pit, slip line and birefringence observations.

2. Experimental

2.1 Specimen Preparation

2.1.a Compression Specimens

The orientation of the crystals supplied is firstly determined using standard X-ray techniques and cut using a wire saw arrangement. This cutting method is used because other available and simpler methods proved inadequate for various reasons.

A cutting machine of the type required was available and has been described by Roy. The arrangement was modified extensively to improve its stability and enable cutting to proceed accurately in the required direction. The modified equipment is shown in fig. 4.1. It consists of a fine nylon wire mounted on six grooved rollers. One of the rollers is eccentrically mounted and acts as a tensioner. The wire is

provided with a sawing motion through the driving rod which, in turn, is driven by an externally mounted electric motor. The specimen is mounted onto an adjustable table which enables it to be aligned in the appropriate orientation. This arrangement can move freely only in the vertical direction, through a series of brass bushes, and is counterweighted to enable the specimen to bear against the wire with an appropriate stress. The actual cutting is achieved by the addition of small quantities of fine corundum powder to the wire. A series of parallel cuts may be obtained by adjusting the position of the specimen with respect to the wire by the operation of the vernier screw arrangement.

The surfaces obtained after cutting are not perfectly flat so a jig was designed capable of grinding the faces flat and square. The jig is shown in fig.4.2. It consists of an arm A constrained to move in a single direction without any transverse motion. The movement takes place on a series of ball bearings sitting in two V-shaped grooves and set in a cage. The position of this arm, with respect to the base B of the brass outer cylinder, can be adjusted finely in a vertical direction by means of a simple screw arrangement. A brass vice C is set in the arm to enable the specimens to be held firmly in two possible positions. Firstly, the specimens can lie horizontally on the region D of the arm to enable the side faces to be ground flat and parallel. Secondly, it can be held vertically in the two carefully ground V-shaped notches to enable the ends of the specimen to be ground flat and absolutely perpendicular to the axis. Grinding is conducted by placing the jig on silicon carbide paper on a glass plate and alternately moving the arm and adjusting the vernier screw to produce the required dimensions.

After the mechanical polish the surface layer contains a relatively high density of dislocations penetrating to a depth of approximately five microns. So this layer is removed by subjecting the specimens to a chemical polish in a 3:1 perchloric acid, aluminium chloride mixture maintained at its boiling temperature. This leaves a perfectly smooth, flat surface. The dislocation structure within the specimens is now the same as in the as-grown crystals so that a high temperature anneal is not required; this is confirmed by comparing the mechanical properties of as-prepared and vacuum annealed, slowly cooled crystals.

b. Tensile Specimens

The type of specimen required is of the form shown in fig.4.3. The crystals are too brittle for the usual grinding methods so the following technique was devised.

Beams of approximately 3 x 6 x 25 mm^3 are cut in the appropriate orientation. The shoulders of the specimen are then cut at 45°C to the surface using the cutting method described previously. Type B orientation specimens are used so the region between the shoulders can be removed by cleavage to produce a specimen of approximately the required shape and size. These specimens are now ground precisely to shape. This is achieved using the polishing jig with the additional components shown in fig. 4.4.a,b. The brass block E and the grips F are the exact shape of the specimen profile required. A nylon cloth impregnated with an abrasive powder is attached to the brass block and the specimen ground to shape with the jig assembled as shown in fig. 4.4.c.

After mechanically polishing to the required shape and size the specimens are subsequently chemically polished to provide smooth, dislocation free surfaces.

2.2. Testing Techniques

a. Compression Specimens

All compression tests are conducted in an Instron testing machine, using the compression jigs described by Harrison (1965) and Pascoe et al (1967). Temperatures between room temperature and 200°C are obtained using an oil bath. Sufficiently accurate temperature control ($\pm$ 1°C) was achieved using a simple coiled heating element, situated in a silica sheath and connected to an Ether controller. The oil is contained in a vacuum container. Temperatures above 200°C are obtained using a simple radiation furnace.

b. Tensile Specimens

The tensile testing arrangement is shown in fig. 4.5. It consists of a universal joint A attached to the crosshead via a framework B and a rod C attached to the universal joint at the load cell, passing through a hole in the crosshead. The specimen is held by the split grips D which contain carefully ground 45° recesses. The grips can be tightened rigidly around the rods E so that the recesses are in the appropriate position to receive the specimen. The shoulders of the specimen can now position themselves accurately on the inserts in the grips. The presence of the universal joints enables perfectly axial loading to be achieved. Heating is attained as described above.

2.3 Birefringence observations

To facilitate the observation of birefringent patterns developed during deformation, the crystals are immersed in n-nonoic acid contained in a quartz cell. This eliminates scattering at surface irregularities.

2.4 Selection of Specimen Orientation

When investigating plastic deformation in compression beyond the yield stress it is important to avoid excessive inhomogeneous deformation. This requires the operation of more than one slip system. It is also important that the resolved stress should be the same on all operating systems (see Chapter 5). So the work hardening on the primary system is studied comprehensively using A orientation crystals.

It also proved important to investigate single slip conditions, so a small number of compression and tension specimens of orientation B are used. Here the resolved shear stress on one primary plane is greater than that on the others.

For the investigation of secondary slip, C orientation crystals (fig. 4.6) are used. Here there can be no interference from slip on the primary system at any stage.

3. Results

3.1 A orientation Crystals

3.1.1 Effect of Specimen Dimensions and Test Conditions

There are two conflicting effects that should be considered when conducting compression tests.

a. Plastic Instability

At relatively large strains, for specimens with a height, diameter ratio greater than 1·5:1 plastic buckling occurs. This is evidently undesirable since it gives rise to a complex stress system and an anomalously low work hardening rate.

b. End Effects

The friction stresses that arise between the compression plates and the ends of the specimen complicate the mode of deformation in that region. The effect of this can be minimised by making the specimens as long as possible and by using a lubricant between the specimen and compression plate.

So the effect of specimen dimensions and surface lubricants is investigated to estimate the most suitable conditions under which the more comprehensive study should be conducted.

i) Surface Lubricants

A number of recognised lubricants have been tested e.g. graphite, P.T.F.E, but equally as effective as these is the silicone oil used as a heating medium, so an additional lubricant is of no advantage i.e. similar curves and deformations are obtained when testing in an oil bath and in air using P.T.F.E. lubricant. To ensure that a layer of oil between the specimen and the compression plates does not produce an anomalous yield point on the Instron Curve, the curves obtained are compared with those from specimens tested in air without any lubricants. The yield points and initial deformation are identical, so this possibility is eliminated.

ii) Effect of Shape of Cross Section

Specimens with three different cross sections are tested.

The relative dimensions are as follows:-

$$\frac{b\ [100]}{d\ [110]} = \frac{3}{1} \quad ; \quad \frac{1}{1} \quad ; \quad \frac{1}{3}$$

The curves obtained are almost identical for all three relative dimensions, a rather surprising result. So the cross section selected is evidently not important but, purely for convenience, specimens with $^{b}/_{d} = {}^{1}/_{1.5}$ are used in all subsequent investigations.

iii) Effect of height, diameter ratio ($^{h}/_{d}$)

Compression Specimens with a wide range of values of $^{h}/_{d}$ are tested. The results are shown in fig. 4.7, d represents the larger dimension of the cross section. The only clearly valid way of determining the stress strain curves is through a series of tensile tests, where the stress system is perfectly homogeneous. So a few tensile specimens of this orientation are laboriously prepared and tested; the results are compared with the compression curves in fig. 4.7. The compression curves with intermediate values of $^{h}/_{d}$ lie closest to the tensile curve, so if compression tests are conducted on specimens with $^{h}/_{d} = 3:1$ the curves obtained should be virtually representitive of the true work hardening. So all subsequent experiments in this orientation are conducted in compression using specimens with dimensions $1.5 \times 2.2 \times 7\ mm^{3}$.

3.1.2 The Effect of Temperature on the Deformation Characteristics

The general variation of the form of the stress-strain curves, over a wide range of temperature, is shown in fig. 4.8. A more detailed study of these curves is facilitated by distinguishing three temperature ranges.

i) Up to 150°C

Three distinct regions of work hardening are discernable within this temperature range, fig. 4.8.

The first region, which is designated Ia, depends very sensitively upon the surface condition of the specimen tested. Thus, a mechanically polished surface produces a curve of the type X whilst a perfect chemically polished surface is accompanied by a large yield drop.

A typical birefringent pattern within this region is shown in fig. 4.10. A close examination of the pattern reveals that slip has started from sources at the edge of the crystal and continued on different systems in different parts of the crystal. There is very little intersection of the dislocations moving on the different systems at this stage.

This region becomes less apparent as the temperature is increased, fig. 4.9.

The subsequent region Ib has an approximately linear work hardening rate which diminishes as the temperature is increased. An average value of the work hardening coefficient is $\mu/60$. The extent of this region again decreases at the higher temperatures.

The development of the birefringent pattern in this region is shown in figs.4.11. In any specific region of the crystal, slip is confined to that one system where slip was initiated in stage Ia. A limited amount of interpenetration of the two systems proceeds in the areas where the two systems meet. The pattern brightens as the strain increases. The slip bands are straight.

The final region prior to fracture Ic is linear with a significantly lower work hardening rate, approximately $\mu/150$. The work hardening rate diminishes slowly as the temperature is increased.

The birefringent pattern is shown in figs.4.12. There is little further interpenetration of the two systems, indicating that only a small proportion of the total dislocation motion proceeds within the intersection areas. Slip continues quite readily in the 'single slip' regions evidently resulting in intensive dislocation pile ups against the relatively inactive intersection areas. Thus, unusually large lattice rotations soon appear there in the form of sharp orientation changes, analagous to Orowan kinks, and are presumably associated with the pile up of dislocations of opposite mechanical sign at opposite ends of the inactive region. This lattice rotation requires a distortion of the lattice in regions beyond the ends of the 'kink'; this is manifested as a gradual curvature.

The investigation is completed by conducting a few slip line observations. Specimens are strained to a certain point, unloaded, the surfaces either chemically or mechanically polished and finally strained again. This enables slip line distributions and lengths to be estimated as a function of strain. The observations on each face are considered separately.

On $\{110\}$ the slip lines are in the same direction throughout. Initially the lines are long and well dispersed but, as the strain increases the length of the lines decreases whilst their density increases. No slip lines other than those due to slip on the primary system can be detected.

On $\{100\}$ slip lines are observed on inclined systems. In any one region the lines are in one direction only whilst in adjacent regions the lines lie in the orthogonal direction with no intersection of the lines between the two systems occurring. No slip lines other than those in the principal direction, in any region, are observed, even at the highest resolution possible in our optical microscope. The length of the lines decreases continuously with strain so that the slip line length is approximately inversely proportional to strain(figs.4.13).

ii) 150°C — 300°C

Here stage Ia is no longer apparent but an additional stage, designated II, can be distinguished. This stage develops at high strains as stage Ic diminishes with temperature. It is a linear region with a consistent work hardening rate of $\mu/100$.

The development of the birefringent pattern with strain at 180°C is shown in fig. 4.14. At this temperature and above slip is more uniformly distributed on both systems in all parts of the crystal so that the areas of lattice rotation are smaller but more numerous. There is no obvious difference between the slip pattern in stage Ic and II, other than the larger degree of lattice rotation in the latter. The occurrence of stage II is evidently not associated with the appearence of this lattice rotation, otherwise a stage II would have been encountered below this temperature, where lattice rotations are also observed.

The slip line observations are more difficult to conduct in stage II because of the associated high strains. However, it appears that the length of the lines does not alter significantly during this stage; this applies to lines on $\{100\}$ and $\{110\}$.

It is still not possible to resolve lines between the lines of the principal system in any specific region, thus slip occurs almost entirely on the original system operating in that region throughout the deformation.

iii) Above 300°C

Here stages Ic, II and an additional stage III are observed. Stage III exhibits a parabolic shape and commences at lower stresses as the temperature is increased.

The development of the birefringent pattern at 350°C is shown in fig. 4.15. Although the birefringence is not particularly informative in stage III, the slip line observations are most significant. At the onset of stage III the slip lines on $\{110\}$ become wavy, fig. 4.16. This can almost certainly be attributed to the macroscopic cross slip of screw dislocations onto the secondary glide planes i.e. $\{110\}$ and perhaps $\{111\}$. The slip lines on $\{100\}$ do not alter in form because the secondary planes intersect this face in the same direction as the primary planes.

3.1.3 Effect of Strain Rate

A series of tests, over a wide range of strain rates, has been conducted at 180°C. The results are shown in fig. 4.17. The effect of an increase in strain rate is somewhat similar to a decrease in temperature i.e. an increase in the extent and the rate of work hardening in stage Ib and a small increase in the work hardening rate in stage Ic. Stage II has a virtually constant work hardening rate, so as the strain rate is increased stages Ic and II are less readily distinguished,

until, at high strain rates the individual stages cannot be identified. There is little, if any, increase in the length of stage Ic as the strain rate is altered. These results contrast with the effect of temperature in that the hardening in stage Ic increases more rapidly as the strain rate is increased, with the length of this stage not simultaneously increasing.

Birefringence observations indicate that slip becomes more homogeneously distributed on both systems throughout the crystal as the strain rate is decreased.

3.2 B orientation crystals

Tests on crystals of this orientation are conducted to determine the work hardening features associated with single slip conditions; this should assist in the interperation of the work hardening characteristics.

Firstly, compression tests are conducted on specimens of various relative dimensions; the results are shown in figs. 4.18. The form of the curves also depends upon the magnitude of $^{b}/_{d}$. One of the interesting things about these results is that the stress range corresponding to stage Ib is independent of these relative dimensions although the work hardening rate varies.

The birefringence observations, fig. 4.19 show that slip is always initiated on the three available systems, in the early stages, near the compression plate. In particular, an intense band of slip on one of the planes of lower resolved stress, always initiates from one corner of the

crystal and spreads across the crystal; this band interferes with slip on the plane of maximum resolved stress. This band is observed even when a hemispherical ball is inserted between the specimen and the compression plate. Thus, the effect of the band is only insignificant when the specimens are long and then plastic buckling obscures the effects under investigation. So it proved essential to prepare tensile specimens.

Tensile tests are conducted over a wide range of temperature; the results are shwon in fig. 4.20. Unfortunately, fracture occurred immediately after yielding at temperatures below 150°C. Above this temperature consistent results are obtained. Stage Ib is still apparent with a stress range similar to that observed in the compression tests on A and B orientation crystals. Stage Ic exhibits a very low work hardening rate virtually independent of the temperature, with a coefficient μ /500, whilst stage II has a hardening coefficient of μ /100, again virtually temperature independent. These results are almost independent of the $^{h}/_{d}$ and $^{b}/_{d}$ ratios.

The development of the birefringent pattern is shown in fig. 4.21. Yielding is accompanied by the propagation of a luders band from the vicinity of the shoulders of the specimen. Slip appears to be confined entirely to a single system in stages I i.e. it is not possible to detect slip traces on intersecting systems. In stage II relatively large amounts of slip are observed to occur on the intersecting systems between the bands of the original system.

Slip line observations are made on $\{111\}$ and $\{110\}$ The lines on $\{111\}$ are straight throughout and decrease only slightly in length as the strain increases (fig. 4.22); the lines are confined to a single system only, even in stage II. It is not possible to detect any lines on $\{110\}$ at the highest resolution of the microscope.

3.3 C orientation crystals

Stress strain curves are obtained in compression as a function of temperature. These represent slip on intersecting $\{110\}\langle 1\bar{1}0\rangle$ systems without any interference from slip on the primary system; the results are shwon in fig. 4.23. After a small yielding region the curves are approximately parabolic with the yield stresses and flow stresses varying somewhat similarly with temperature; there is a small decrease in work hardening rate as the temperature increases. The curves resemble those obtained in many b.c.c. metals.

The birefringence patterns are interesting. At the lower temperatures, slip is initiated on a set of two orthogonal planes in any region with intersection of these systems occurring quite readily. However, in adjacent regions slip is initiated on the other two orthogonal systems and little interpenetration of the slip in adjacent regions proceeds. This gives rise to the 'block slip' situation observed by Roy i.e. on any one face birefringence reveals alternate blank and slip areas. This indicates that the intersection of oblique systems proceeds only with great difficulty (c.f. NaCl, Davidge and Pratt). At higher temperatures, as in type A crystals, intersections occur more readily during the early stages so the slip pattern

becomes more homogeneous. There is no obvious variation of the form of the pattern with strain at any temperature investigated.

The slip lines at the lower temperatures are very short and wavy, fig. 4.24. and, on a particular face, there are alternate regions of slip and no slip, fig. 4.25 indicative of the 'block' slip already described.

4. Discussion and Conclusions

The results, even at this stage, have elucidated certain features of the work hardening and these are looked at briefly.

Stage Ib is a rapid work hardening stage, observed immediately after yield, with a work hardening rate that depends upon temperature and strain rate (and in certain cases specimen dimensions). More important, this stage is observed under all test conditions i.e. single, double and multiple slip, for all specimen dimensions, and extends over a similar stress range for a given temperature and strain rate.

Stage Ic exhibits a low work hardening rate under single slip conditions. However, the hardening rate is increased significantly when slip can occur on an intersecting system and is dependent upon the test conditions i.e. temperature, strain rate and specimen dimensions (for B orientation crystals).

The development of the birefringent pattern provides useful information concerning the deformation of type A crystals in stages I. During the initial stages, slip is initiated on one of the two available systems in any specific region of the crystal , the system selected depends upon the nature of the sources in that region. Slip propagates from these sources

through the crystal and since intersection occurs only with great difficulty the crystal is, at this stage, subdivided into regions where slip has occurred on different systems in adjacent regions. At low temperatures or high strain rates the density of dislocations within a slip band is high (Roy) so the probability of intersection of slip bands propagated from different sources is low and the above described regions are large. At higher temperatures (lower strain rates) the density of dislocations within a slip band is lower; this allied with the larger thermal energy available enables intersections of the slip bands to occur, during the early stages, resulting in a relatively homogeneous distribution of slip throughout the crystal i.e. the above regions are small. At higher strains slip continues predominantly on one system in any region with dislocations of the other system now unable to traverse this region, even at the higher temperatures. This situation results in the observed lattice rotations. It is possible that the different work hardening rates in Ic at different temperatures and strain rates might be associated with the different distributions of slip bands obtained under the different test conditions.

Stage II has a most consistent work hardening rate, almost independent of orientation, temperature etc. The reason for the appearance of this stage could not be elucidated from the birefringence observations on type A crystals. However, the tensile tests on type B crystals indicate unequivocally that stage II is due to slip on an intersecting system in the region between slip bands of the original system. This also probably occurs in type A crystals but could not be unambiguously distinguished from slip that had already occurred on

this system in the early stages of deformation (stage II only occurs at temperatures where slip in stages I is relatively homogeneous). Similar 'fine slip' on intersecting systems is observed in stage II in f.c.c. metals and the hardening could perhaps be explained similarly.

Stage III is due to macroscopic cross slip and can be interperated in the usual manner.

Deformation on the secondary system is similar to that observed in b.c.c. metals. There are four available slip systems, all with identical resolved stresses, so the dislocation structures developed as a function of strain are somewhat complex. There are no individual work hardening stages to be distinguished. The slip lines are wavy, so cross slip can occur, yet they are short, so impenetrable barriers are also formed. No attempt is made to interperet the work hardening on this system in this thesis.

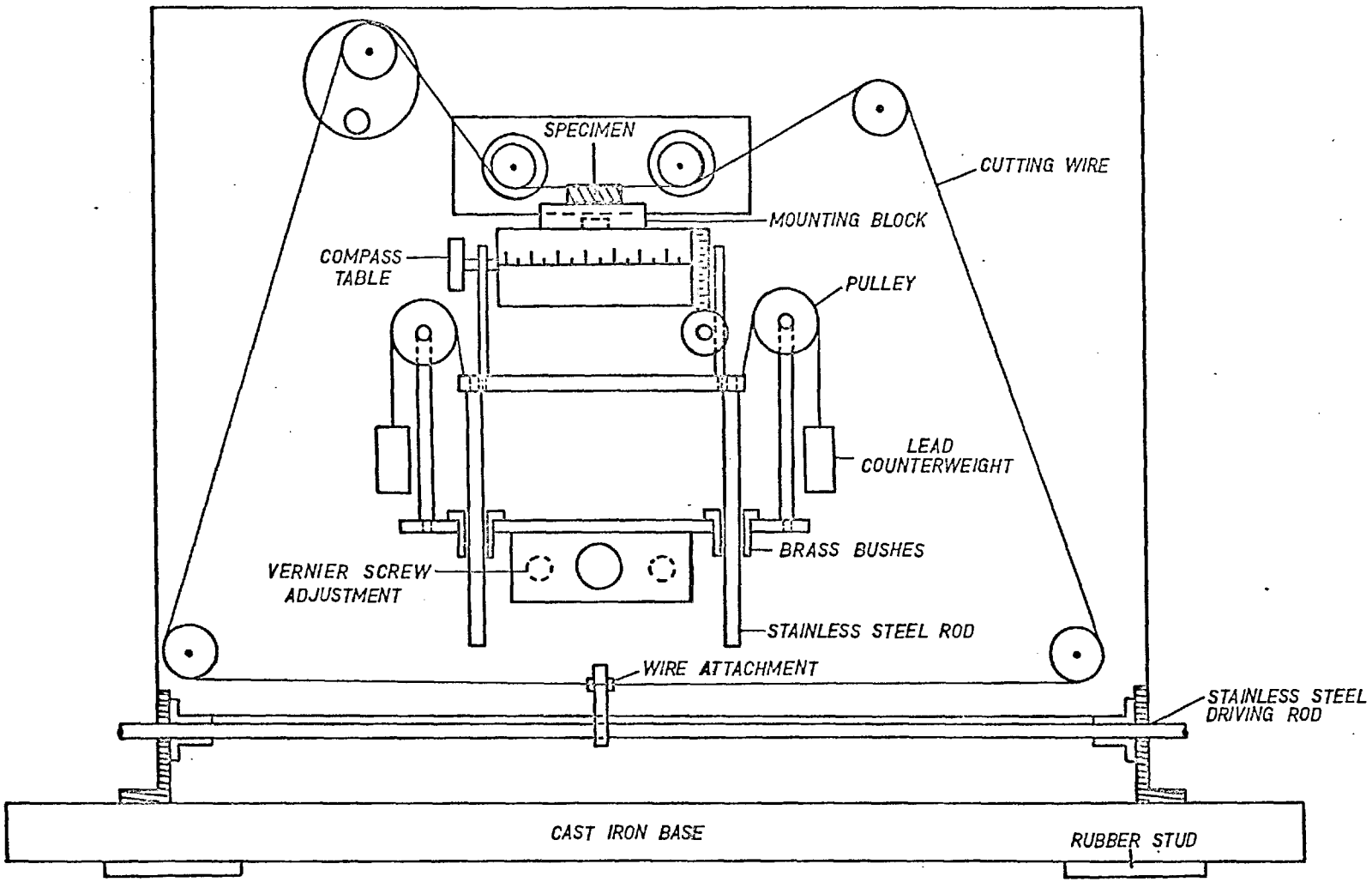

Fig. 4.1. CRYSTAL CUTTING APPARATUS

Fig 4.2(a) The Jig

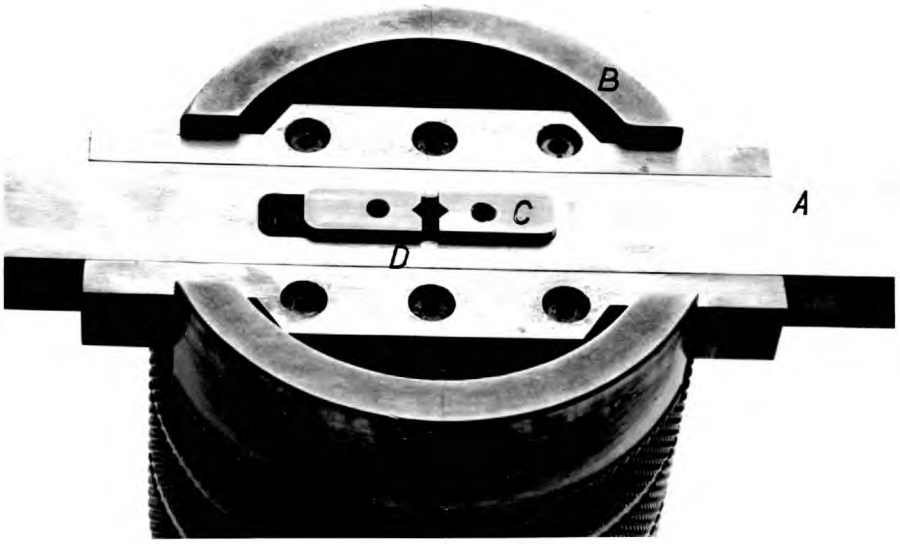

Fig 4.2 (b) The Specimen Grips

The Polishing Jig; for Compression Specimens

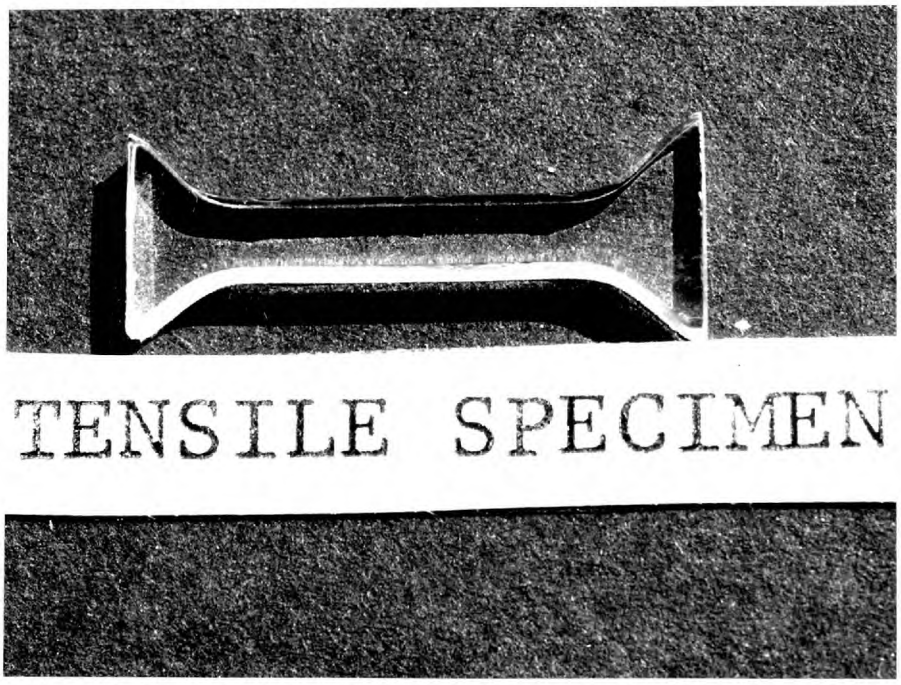

Mag. x 4

Fig. 4.3. A Tensile Specimen

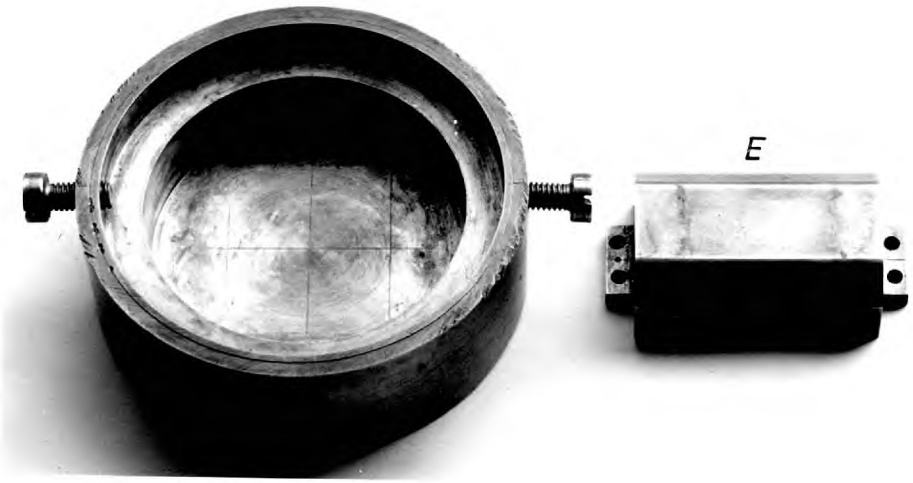

Fig 4.4 (a)
The polishing block and base

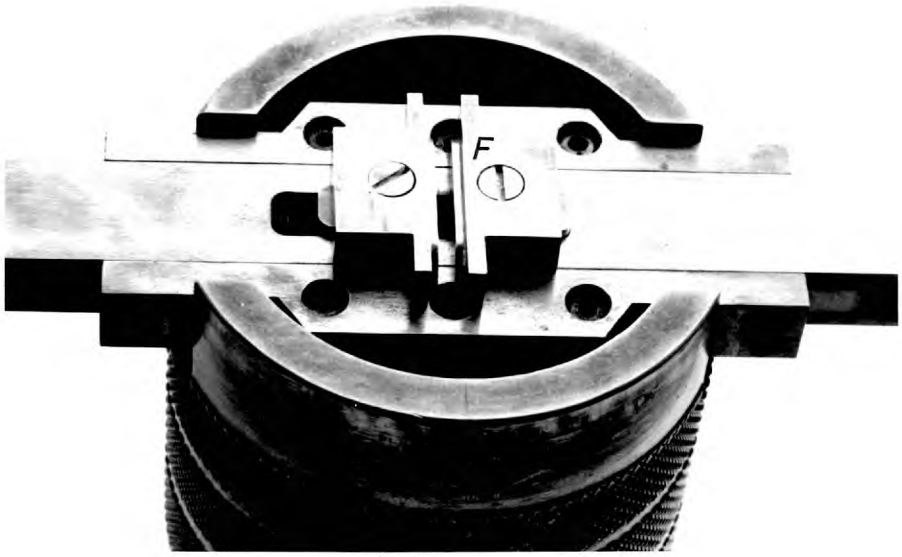

Fig 4.4 (b)
The specimen grips

Fig 4.4 (c)
The jig assembled

The polishing jig; for tensile specimens

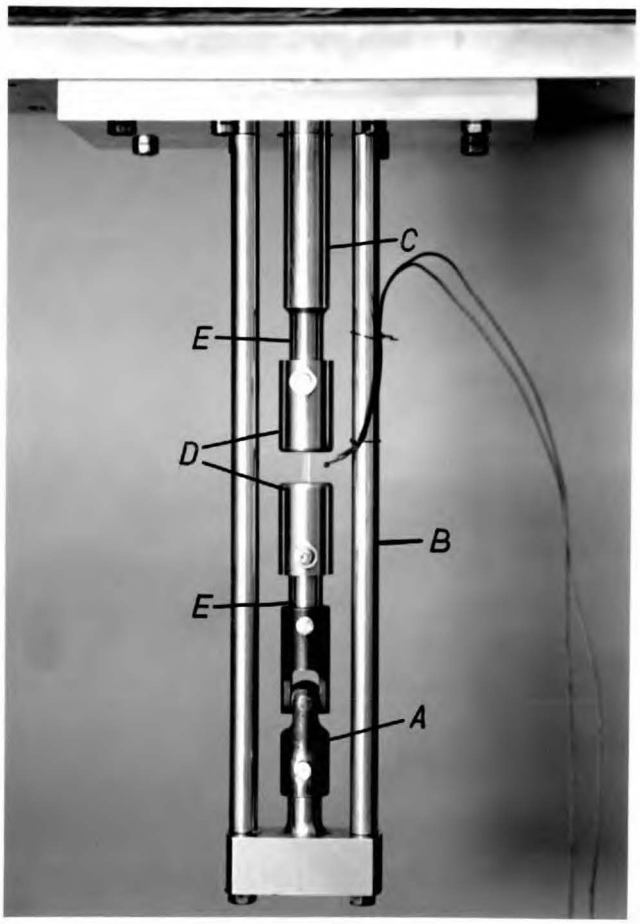

Fig. 4.5. The tensile testing jig with specimen inserted.

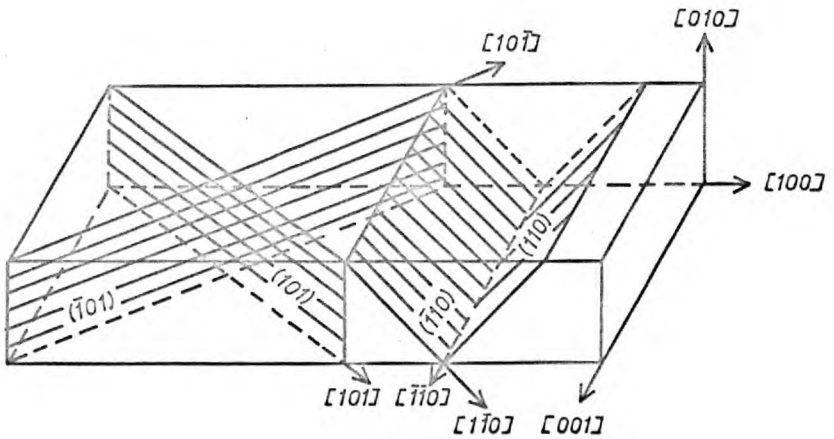

Fig. 4.6. "C" orientation crystal

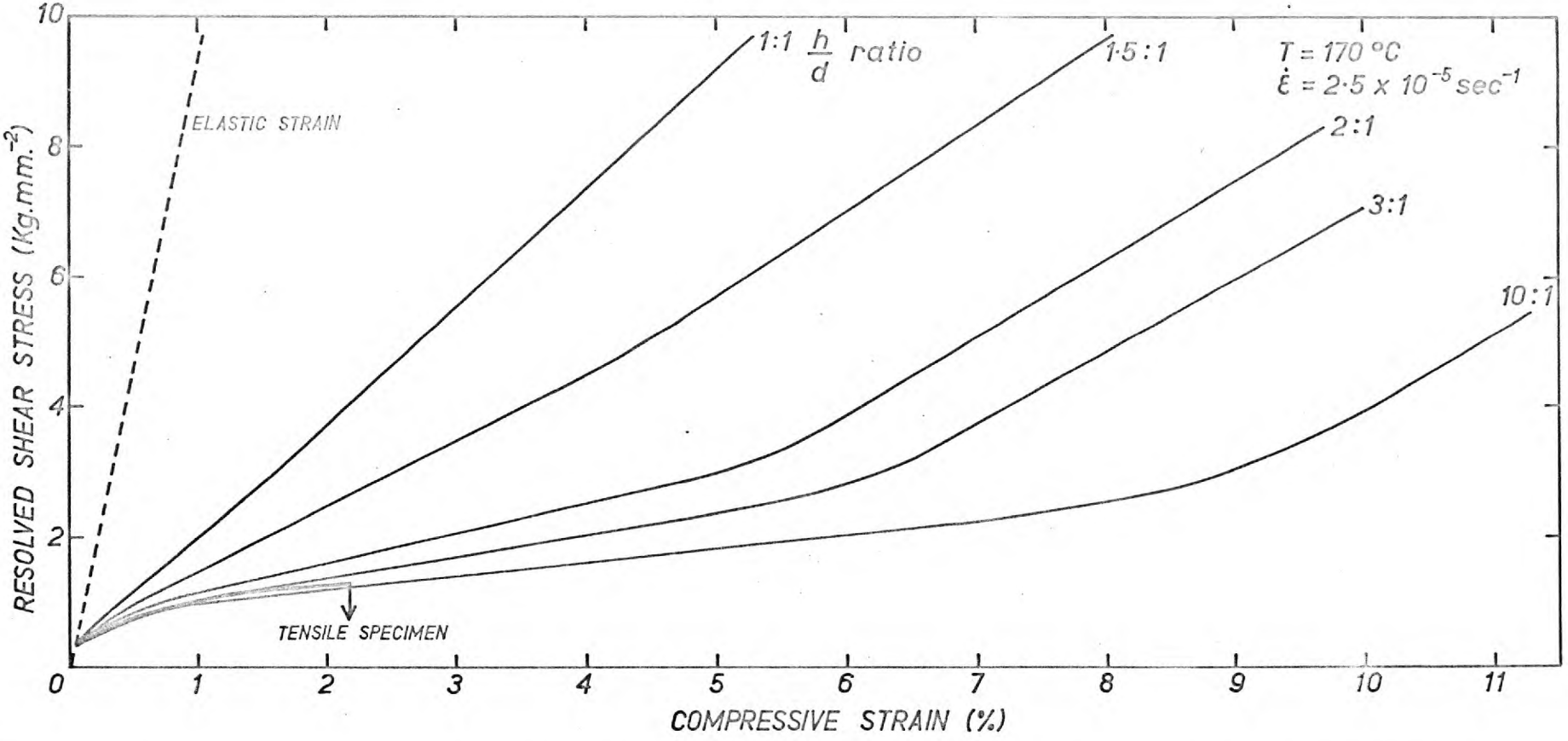

Fig. 4.7. Effect of specimen shape on the stress strain curves of type A crystals in compression

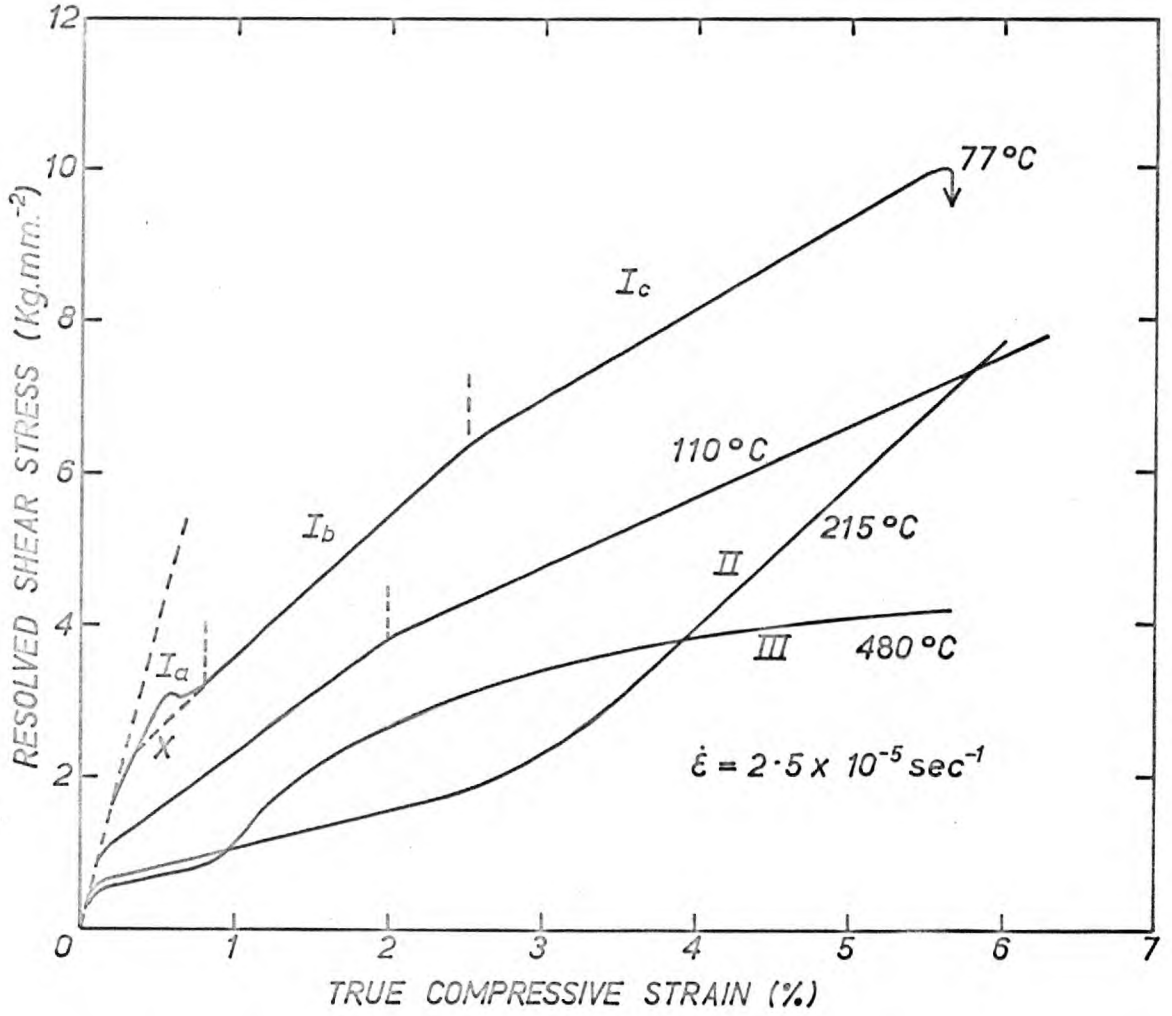

Fig. 4.8. Effect of temperature on the stress strain curves of type A crystals

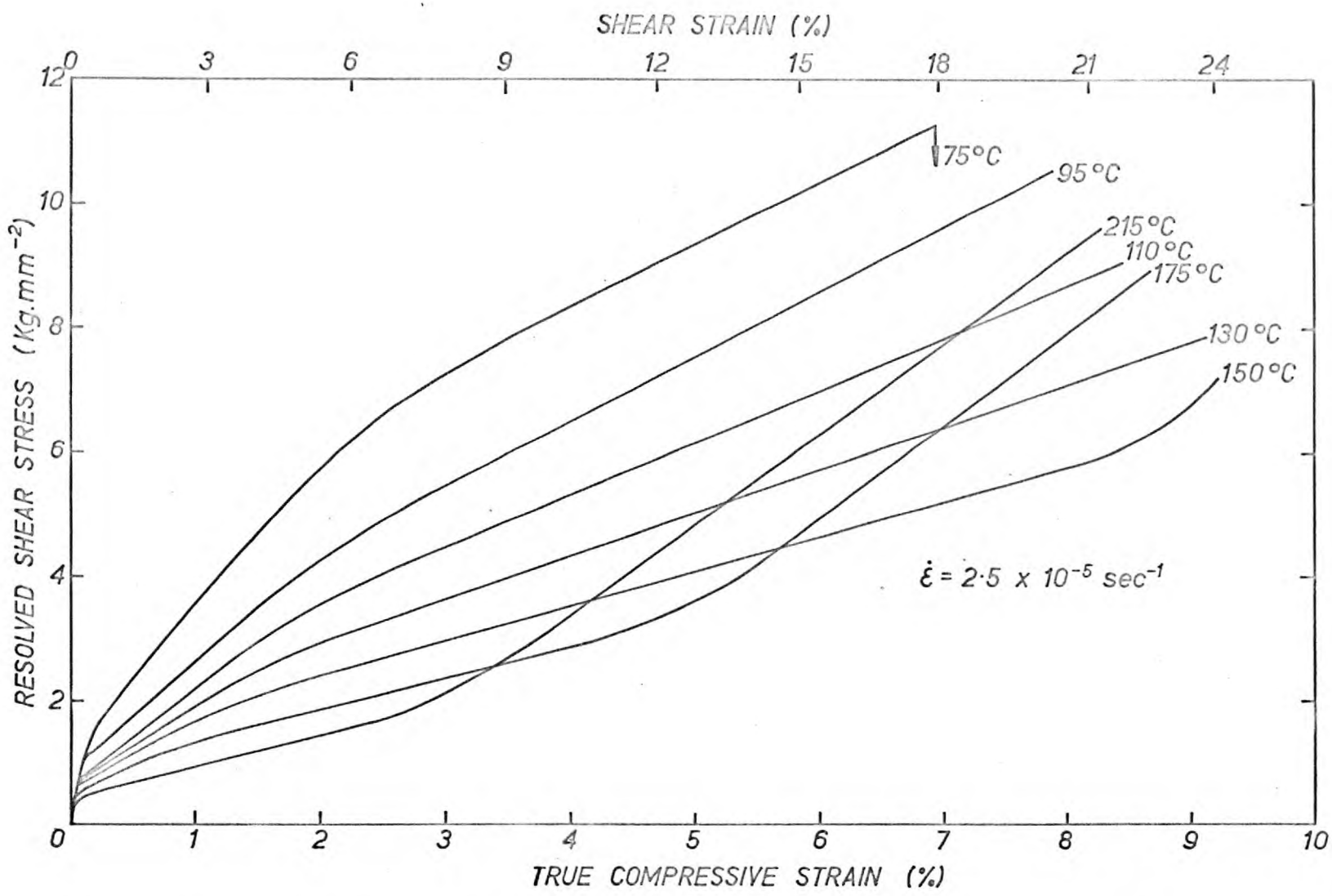

Fig. 4.9. Effect of temperature on low temperature stress-strain curves of type A crystals.

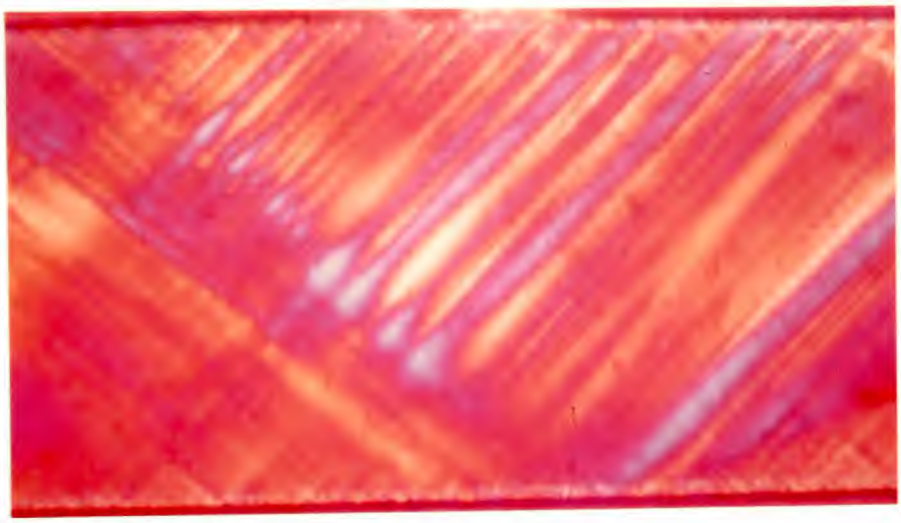

Fig. 4.10
Stage Ia
(ε = 0.1%)
Mag x 30

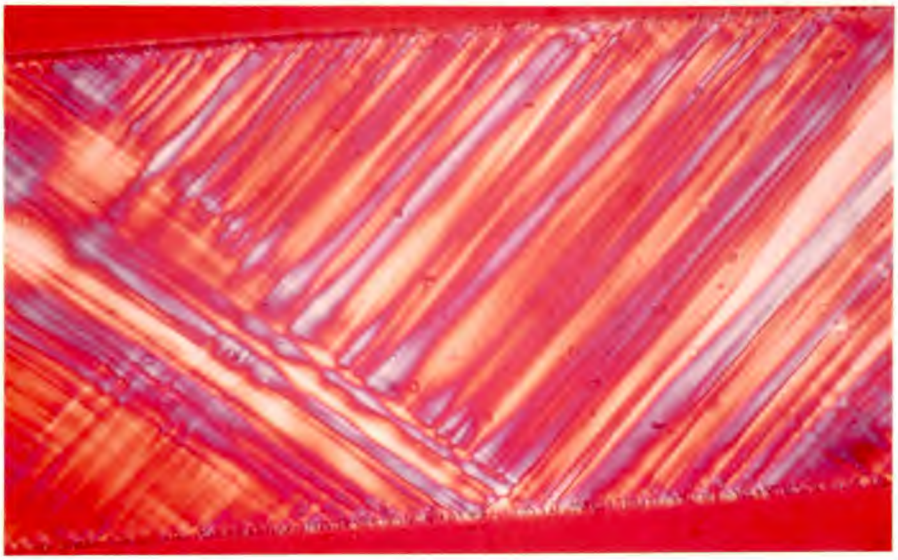

Fig. 4.11
Stage Ib
ε = 1%
Mag x 30

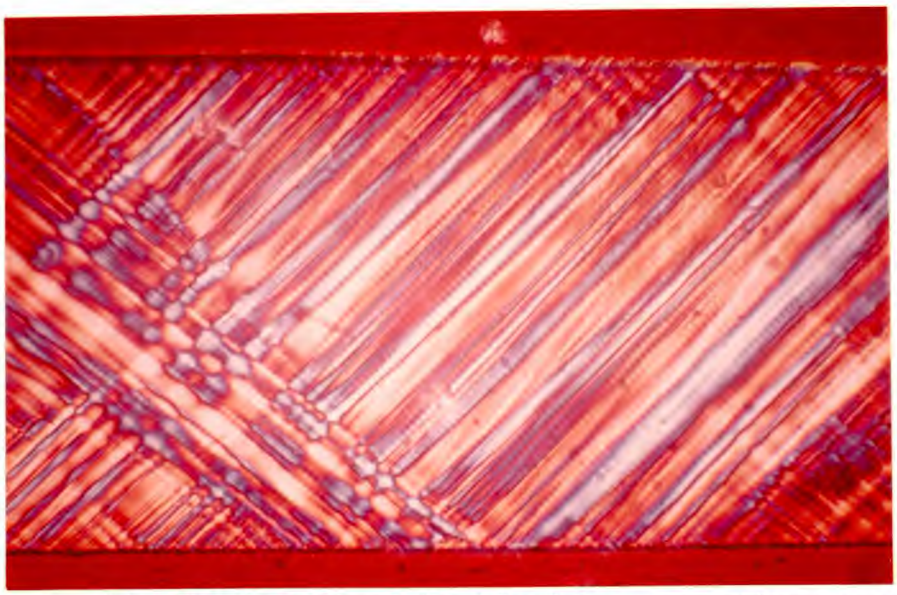

Fig. 4.12 (a)
Stage Ic
ε = 3%
Mag x 30

The development of the birefringence pattern in a type A specimen tested at 110°C, viewed in [100]

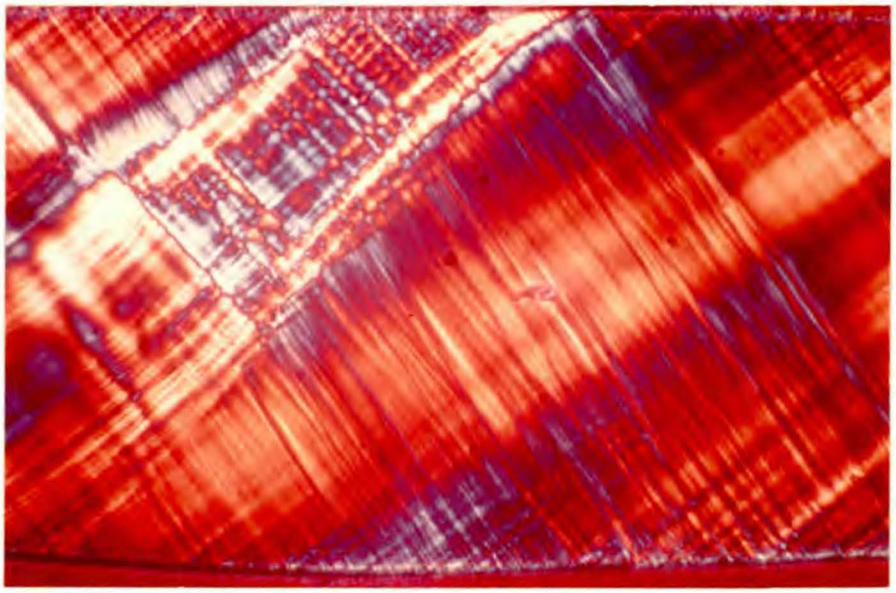

Mag x 30

Fig. 4.12b A kink formed in the same specimen strained 7% at 110°C

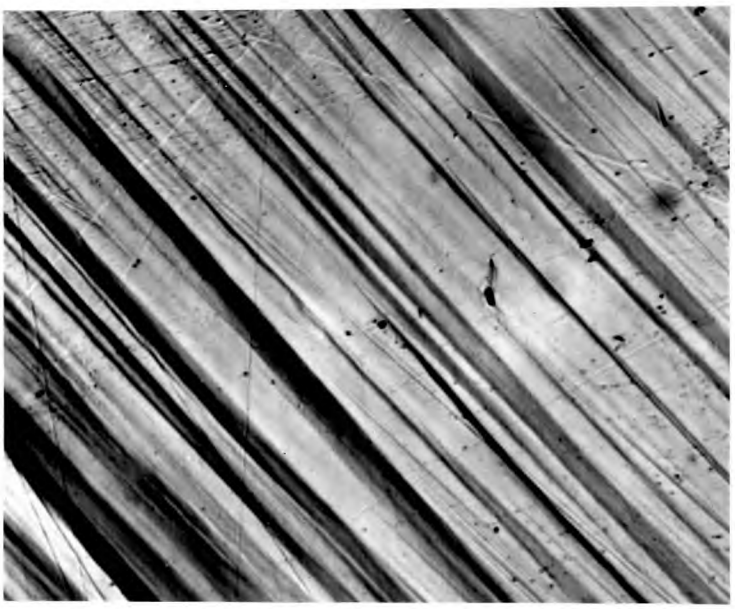

Fig. 4.13 (a) The slip lines after 5% strain Mag x 128

Fig. 4.12 (b) The slip lines after 10% strain; specimen mechanically polished after 5% strain and restrained. Mag x 540

The Slip lines observed on $\{100\}$ in a type A specimen tested at 110°C

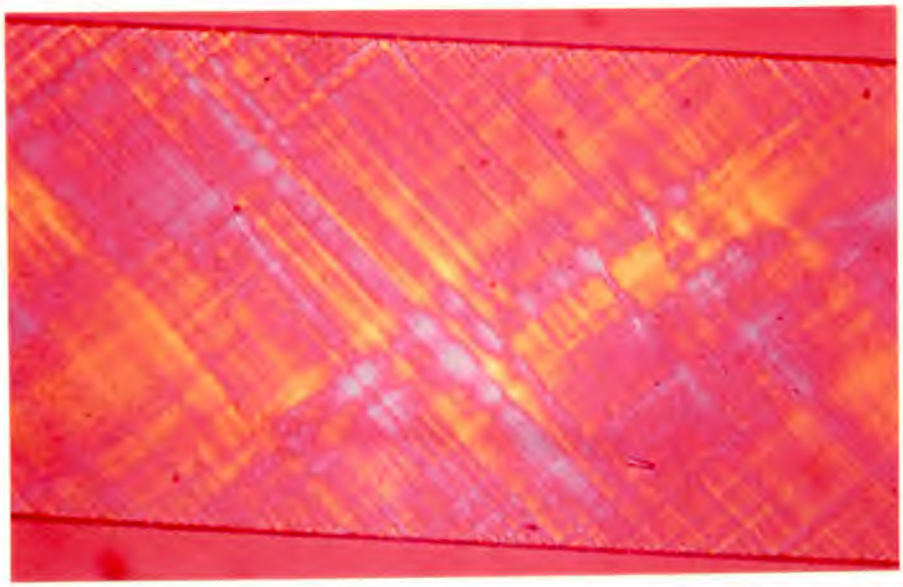

Fig.4.14(a)
Stage Ib
(ε = 0.5%)
Mag x 30

Fig. 4.14(b)
Stage Ic
(ε = 2.5%)
Mag x 30

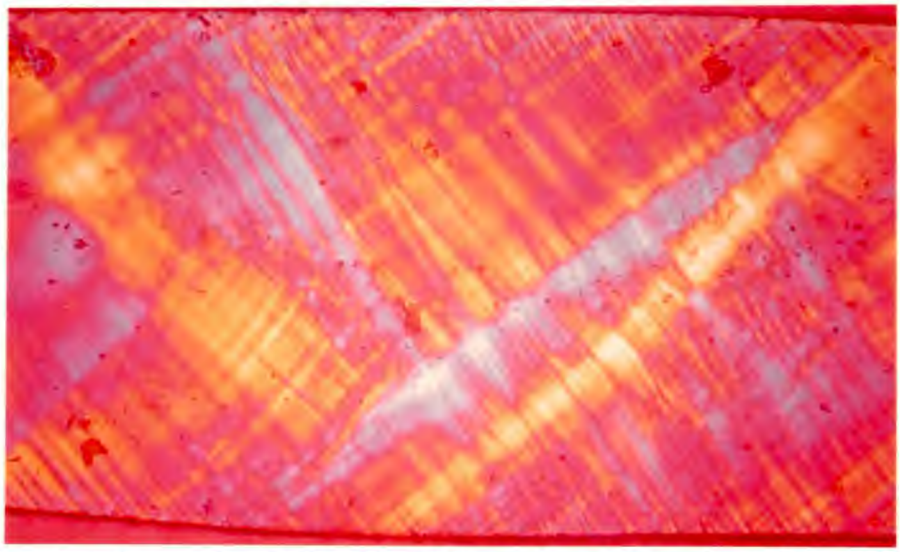

Fig. 4.14 (c)
Stage II
(ε = 7.5%)
Mag x 30

The development of the birefringent pattern in a type A specimen tested at 100°C, viewed in [100]

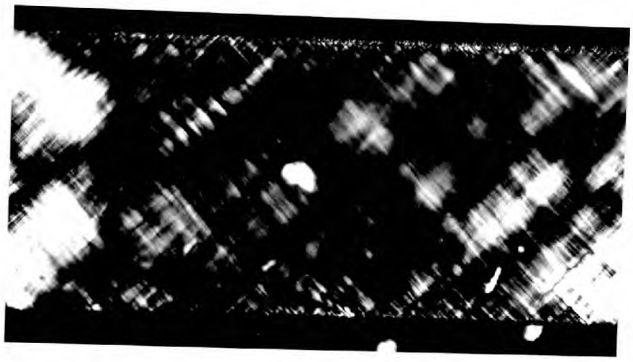

Stage Ic

(ε = 0.5%)

Fig. 4.15 (a) x 35

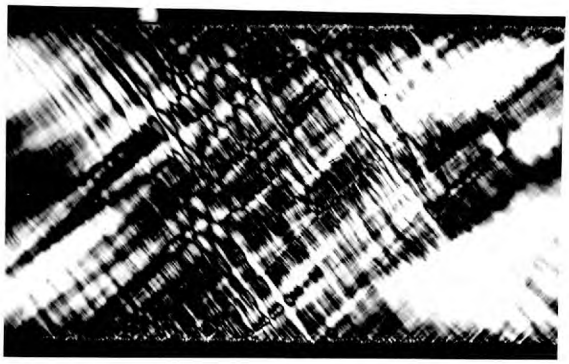

Stage II

(ε = 1.5%)

Fig. 4.15 (b) x 35

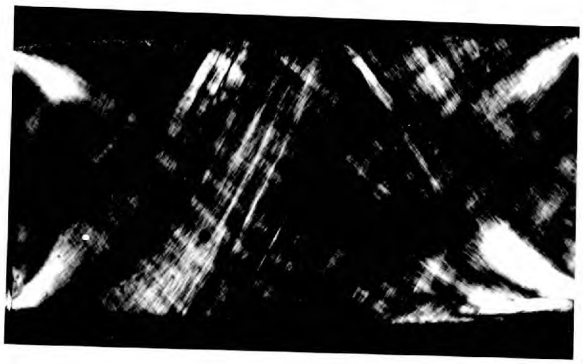

Stage III

(ε = 4%)

Fig. 4.15. (c) x 35

The variation of the birefringence pattern in a specimen compressed at 350°C.

Mag x 360

Fig. 4.16 The wavy slip lines observed in stage III; specimen strained 4% at 350°C

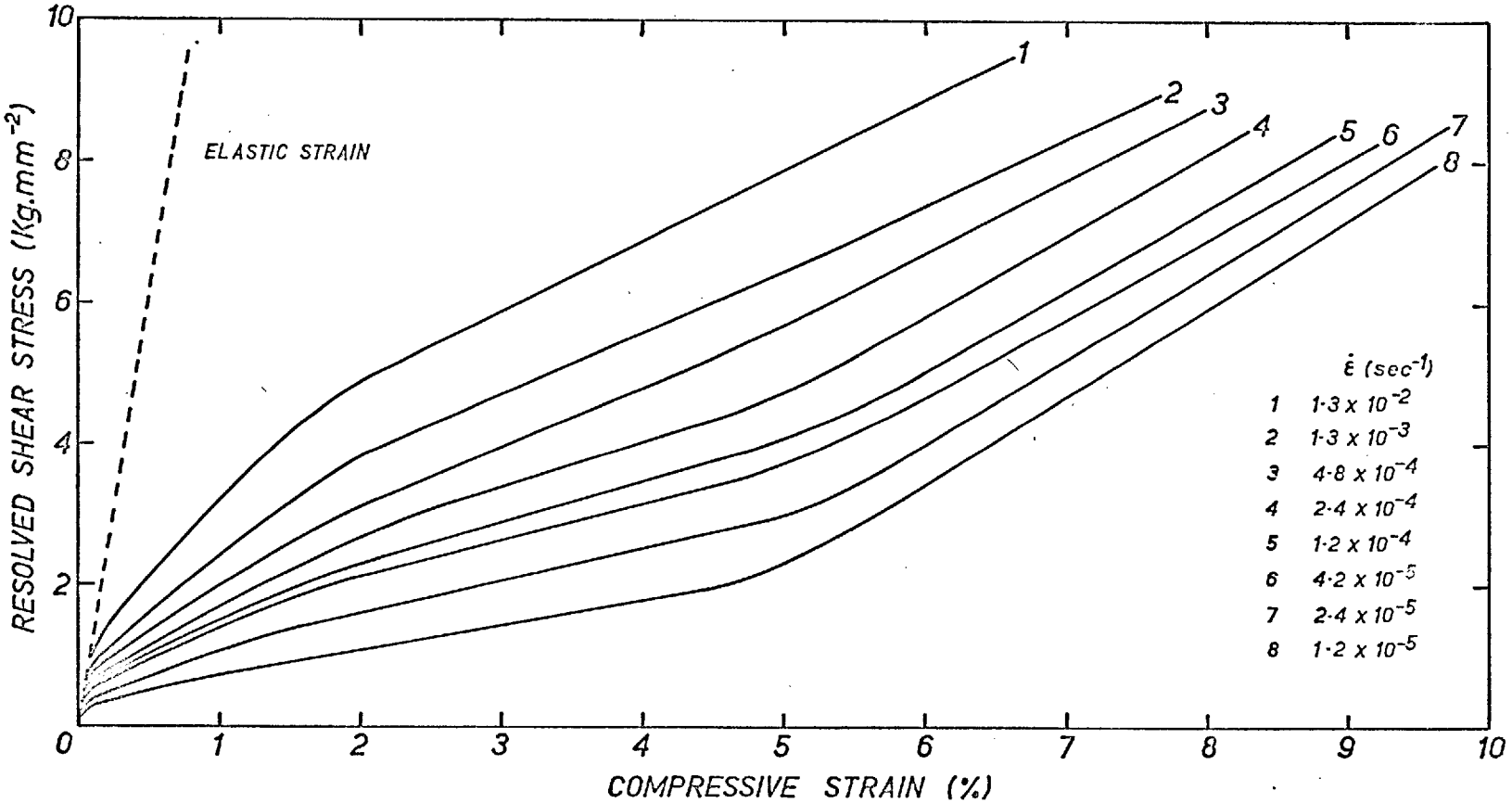

Fig. 4.17 Effect of strain rate on the stress strain curves of type A crystals at 180 °C

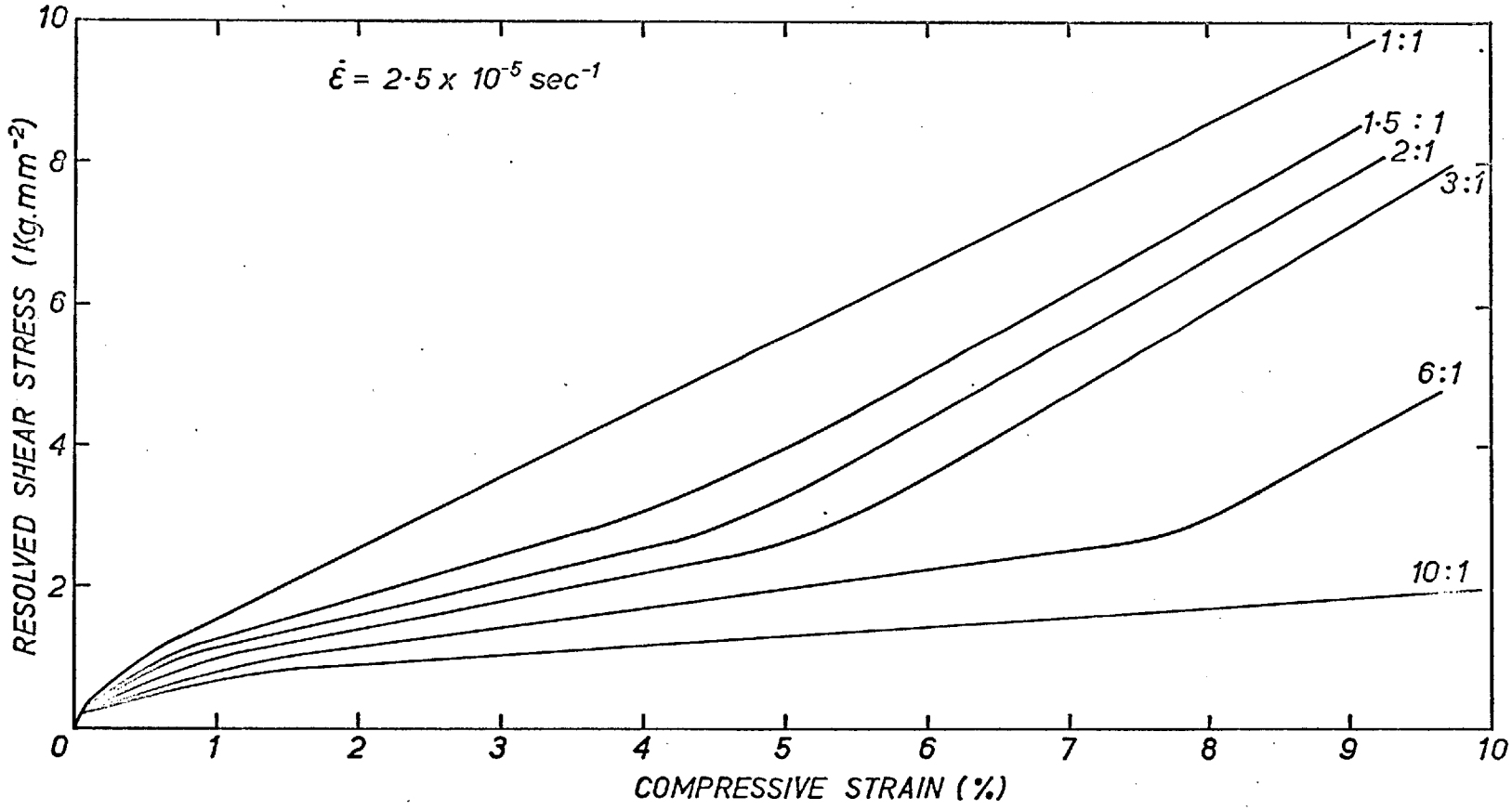

Fig. 4.18. Effect of specimen shape on stress strain curves of type B crystals at 170°C

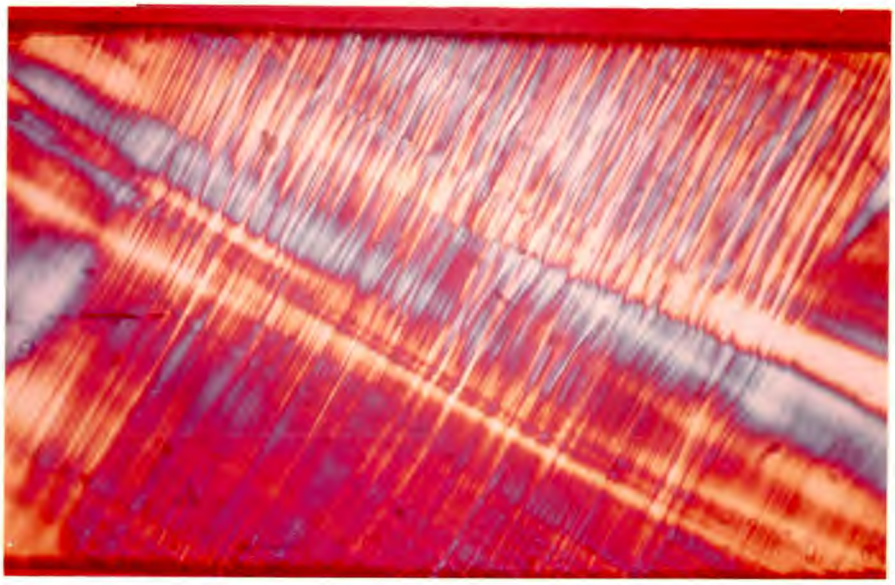

Mag x 30

Fig. 4.19 The birefringent pattern observed in a type B compression specimen strained 3% at 150°C

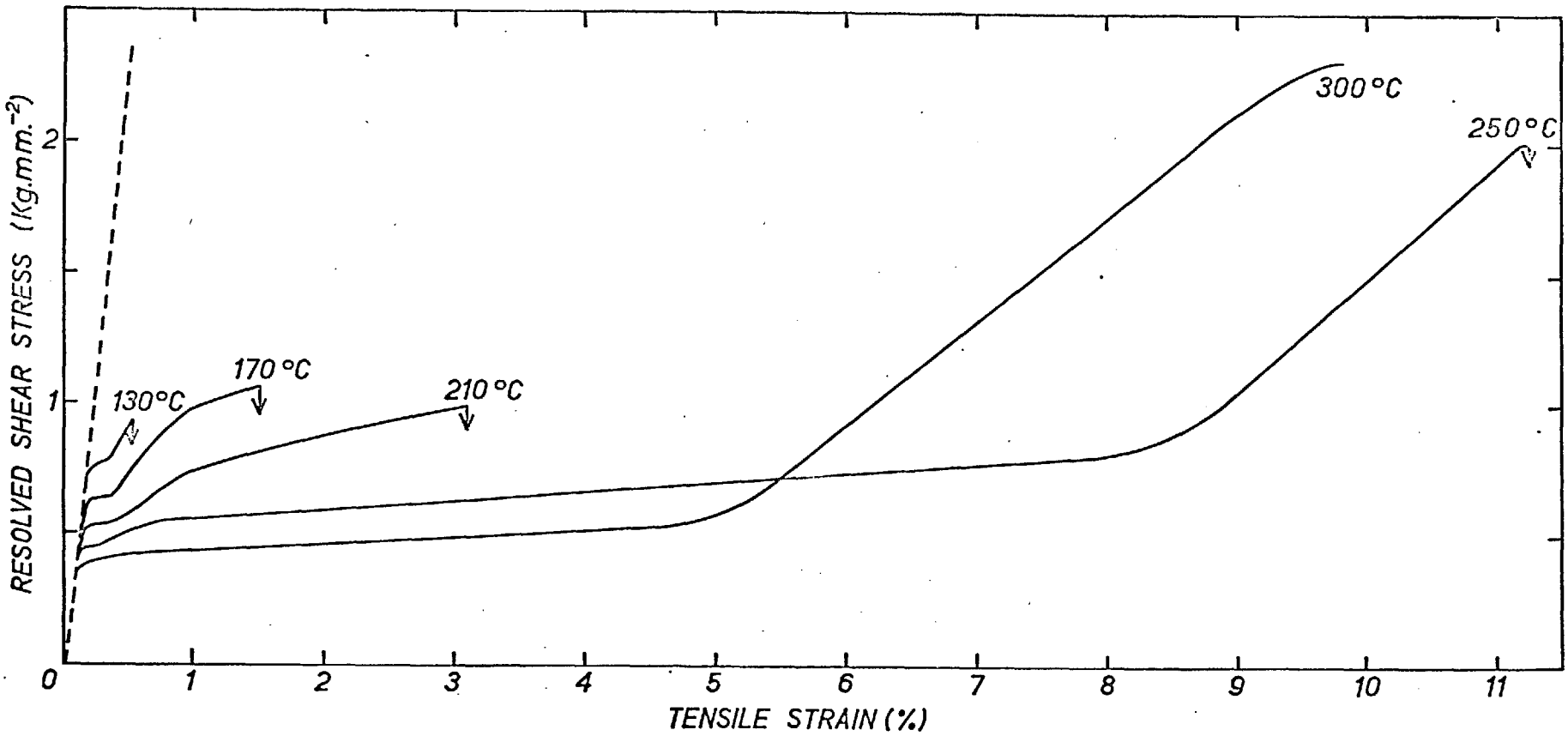

Fig. 4.20. Stress strain curves for type B tensile specimens

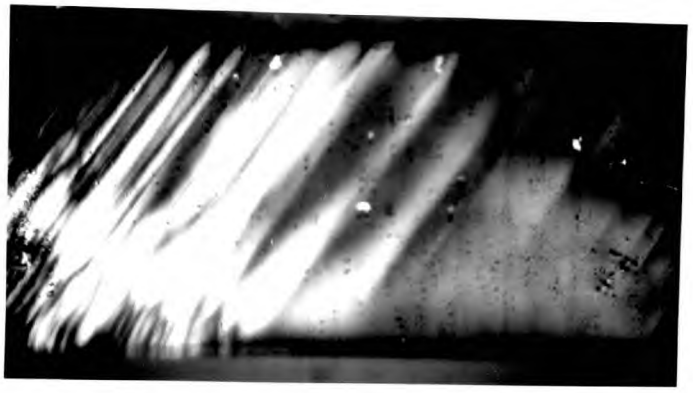

Stage Ia; propagation of a luders band (ε = 0.1%)

Fig 4.21 (a) x 35

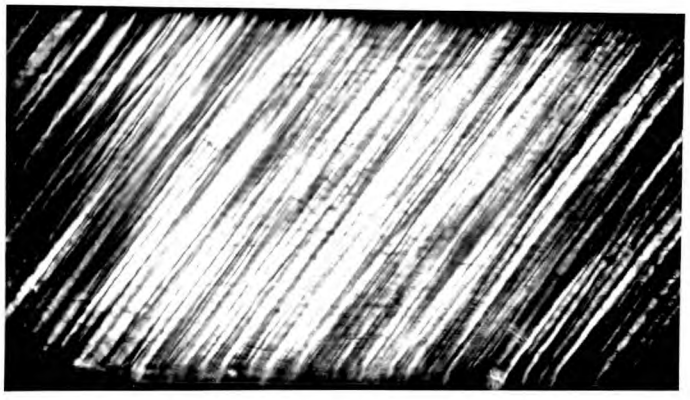

Stage Ic; slip occurring predominantly on one syste (ε = 1.5%)

Fig 4.21(b) x 35

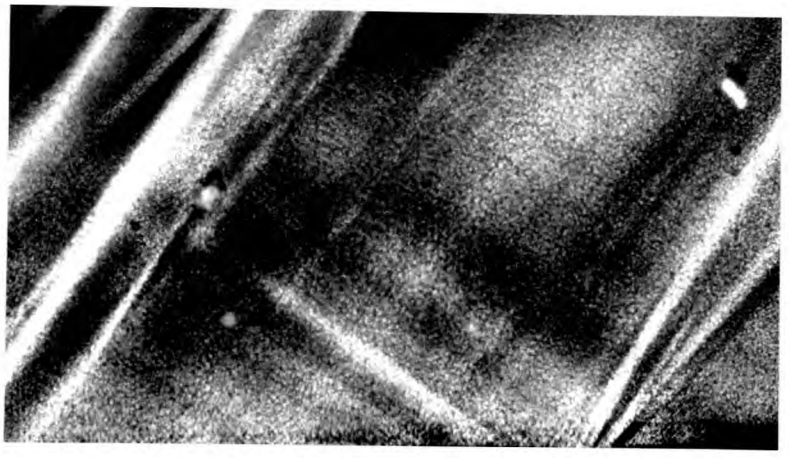

Stage II; the appearance of slip bands on the plane of lower resolved shear stress (ε = 7.5%)

Fig 4.21(c) x 350

The development of the birefringent pattern in tensile specimens; (a) and (b) at 170°C, (c) at 300°C.

Magnification x 96

Fig. 4.22. Slip lines observed on {111} of type B tensile specimen tested at 170°C (ε = 1·5%)

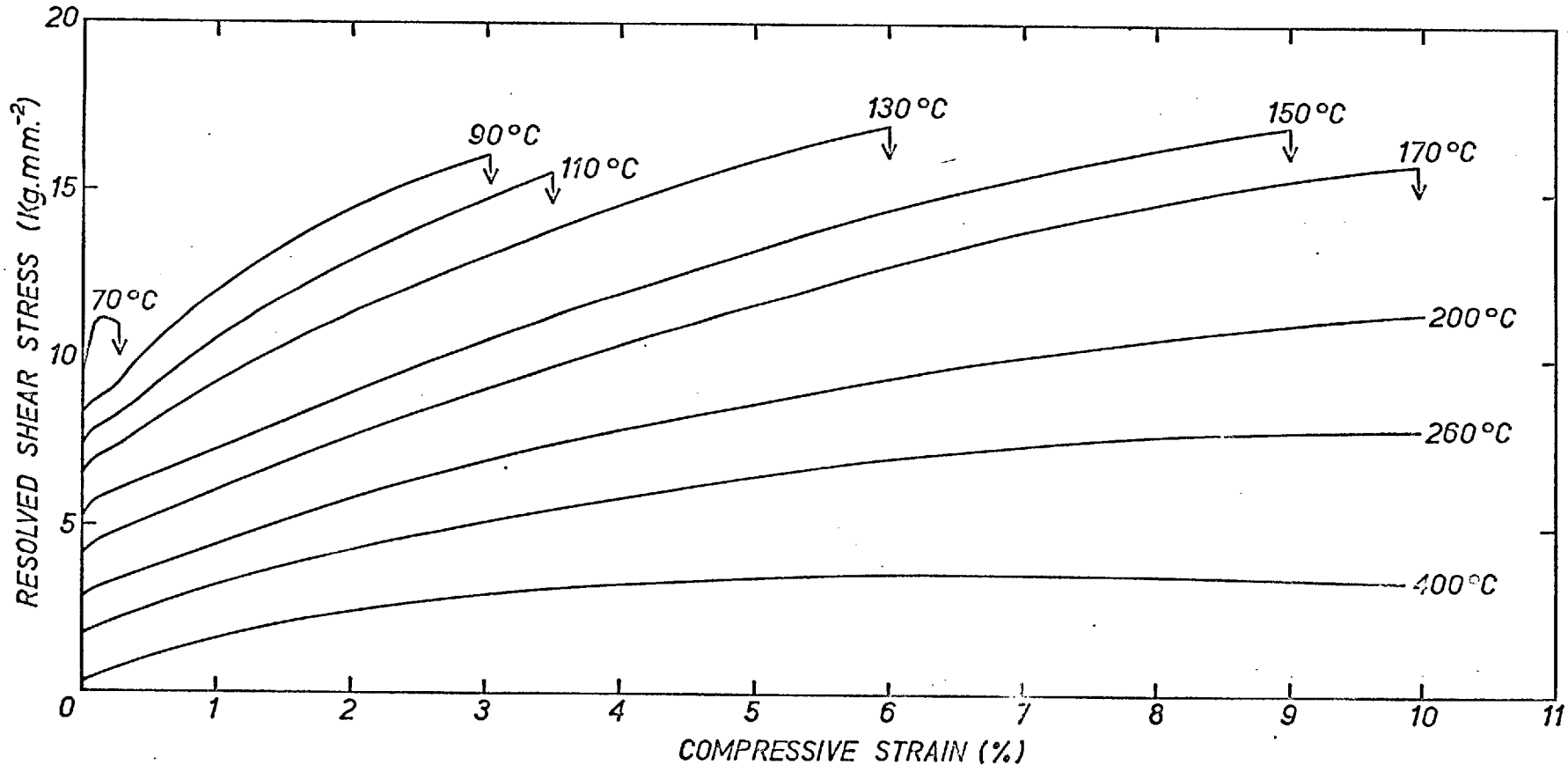

Fig. 4.23. Effect of temperature on stress strain curves for slip on {110} <110> (Type C crystals)

Fig 4.24 (a) x 192

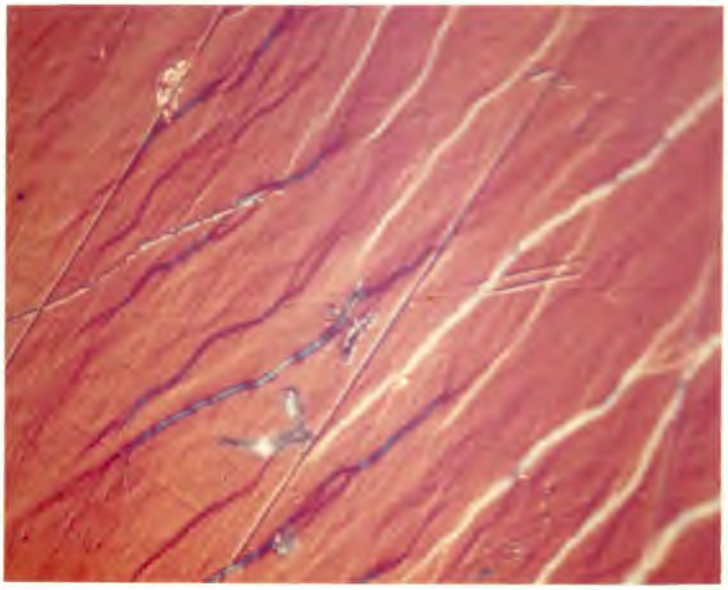

Fig. 4.24 (b) x 360

Slip Lines in C orientation crystals deformed at 170°C ($\xi = 4\sqrt{}$)

Photographed under interference contrast conditions.

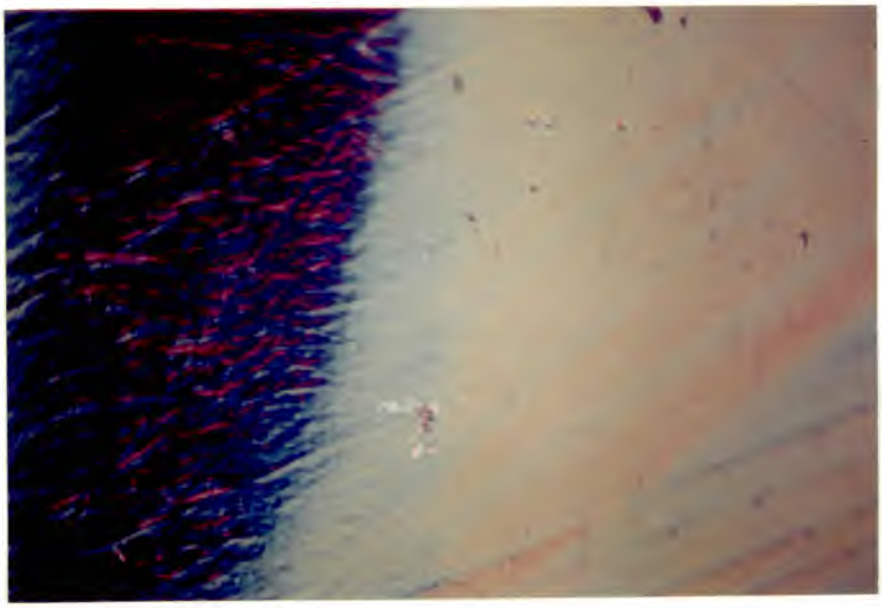

Mag x 128

Fig 4.25 Block slip in a C orientation crystal deformed at 170°C (ξ = 4)

CHAPTER 5

Identification of the Thermal Stress Component

1. Introduction

This section is devoted to the study of thermally activated deformation with the following aims.

(a) To determine the validity of the theory of thermal activation in the case of calcium fluoride.

(b) If the theory is found to be applicable, to use it to study the thermal activation parameters and to attempt to identify the mechanisms controlling the deformation rate.

Before deciding upon an appropriate sequence of experiments, it is important to study the theory of thermally activated flow to determine its limitations and the situations under which it might not be applicable.

2. Theory

The theory has been discussed in great detail by a number of authors (e.g. Conrad, 1964; Basinski 1959; Christian and Masters 1964; Schoeck 1965). A logical summary of the theory with certain important additions, is presented here and the limitations emphasised at each stage.

2.1 The Force on a Dislocation

When a dislocation moves through a crystal lattice, a force is exerted upon it by a variety of obstacles in the vicinity of the slip plane. This force can be separated into two extreme components.

a. Long range forces where the force on the dislocation varies only slowly with the position of the dislocation on the slip plane.

b. Short range forces acting only over a few atomic dimensions.

So, in general, the forces exerted on the dislocation, in its passage across a slip plane, vary in a manner similar to that shown in fig. 5.1 (e.g. Conrad 1964; Kronmuller, 1967). The maximum force required to be exerted on the dislocation to enable it to overcome the obstacles occurs at position A and is given by $(F_l + Fs)$. The physical nature of the defects that interact with the moving dislocations, giving rise to these forces, is considered in the discussion.

2.2. Thermal Activation

To enable the dislocation to move through the lattice an external shear stress must be applied along the slip plane. At $0^{\circ}K$ this stress must be sufficiently large to provide the maximum force $(F_l + Fs)$ at each relevant obstacle. In practice, a value of the stress is provided by considering the average movement of a large number of dislocations through a random array of obstacles and is given by:-

$$\tau = \frac{(F_l + Fs)}{bl} \qquad - 5.1$$

Where l is the average length of dislocation line available at each obstacle (equivalent to the spacing between obstacles).

At any finite temperature T, the thermal energy (manifested as coherent atomic fluctuations, Friedel, 1964) can assist the applied stress in enabling the dislocations to overcome the obstacles. The total energy required to be supplied, for a given applied stress, is essentially equivalent to the area under the force - distance curve (Basinski 1959). So, where long range obstacles only are involved, the relatively small amount of

thermal energy available does not reduce significantly the energy required to be supplied mechanically (fig. 5.1) and the long range stress is virtually independent of temperature. However, the magnitudes of the short range obstacles lie within the thermal energy range so the energy that has to be supplied mechanically to overcome these obstacles can be reduced significantly by the probability of thermal fluctuations; this gives rise to a temperature dependent short range stress.

A study of thermal activation can provide useful information concerning the nature of the short range obstacles and, in particular, the magnitude of the stress required to surmount these obstacles (τ^*) can be obtained and distinguished from the athermal component (τ_μ) of the applied stress (τ_A). The significant activation parameters are now defined and the connection between them derived using basic thermodynamic principles.

2.3 Activation Energies

As a dislocation moves across a slip plane, under the action of an applied stress, and encounters obstacles in its path the Gibbs free energy of the system varies in a manner similar to that shown in fig. 5.2. (c.f.Seeger 1957); short range obstacles only are considered here.

The amount of thermal energy that has to be supplied to overcome a given obstacle when a local stress τ^* is available has been determined by Schoeck (1965) and Gibbs (1967). Consider the work done when a linear segment of dislocation of length l moves from its equilibrium position, under the action of the local stress, to the saddle point of the obstacle.

If the motion occurs reversibly and isothermally, the application of the second law of thermodynamics shows that the minimum Gibbs free energy required to surmount the obstacle is given by (Schoeck):-

$$\Delta G = \Delta g - (\tau_A - \tau_\mu) lb \Delta R \quad - 5.2$$

ΔR is the activation distance.

The term $lb \Delta R$ has the dimensions of volume and is usually referred to as the 'activation volume'.

Δg represents the change in Gibbs free energy associated with the localised atomic interactions (fig. 5.2). At zero stress this is evidently equivalent to ΔG_o, the 'activation energy of the obstacle'.

Gibbs separates Δg into a number of components, showing:-

$$\Delta g = \Delta U^* - T \Delta S^* - T \Delta S_v \quad - 5.3$$

where ΔU^* and ΔS^* are the changes in internal energy and entropy, respectively, associated with the activation and ΔS_v is the entropy change associated with the change in vibrational modes at the saddle point (Granatoetal 1964).

Δg, l and ΔR may depend upon the value of the locally acting stress. The significance of this is discussed in section 2.9.

The only restrictions placed upon the subsequent application of this equation are that the fluctuation should occur reversibly and isothermally. Eshelby and Pratt (1956) have shown that there is no significant temperature change during deformation, so the assumptions are probably valid for most dislocation processes.

It is now required to discover how these parameters can be determined experimentally. Firstly, the relevant rate equations are defined.

2.4. The Rate of Movement of Dislocations

The average velocity of a dislocation line, which depends upon the frequency with which the local obstacles are surmounted with the assistance of thermal fluctuations, is assumed to be given by the usual Arhenius relationship (Zener 1952).

$$U = p\nu \exp\ (-\Delta G/kT) \qquad - 5.4$$

Where p is the distance moved after a successful fluctuation, ν is the frequency of vibration of the dislocation at the obstacle concerned.

This equation assumes that no back fluctuations occur and that the system is 'closed'. This is reasonable for many types of obstacle; the situations under which it is not applicable are considered in Section 2.7.

For a typical compression or tension test, where the applied stress is σ_A , the shear stress acting on the slip plane (τ_A) is given by:-

$$\tau_A = \sigma_A \cos\theta \cdot \cos\phi \qquad - 5.5$$

Where θ and ϕ are the angles between the applied stress axis and the slip direction and the normal to the slip plane respectively.

The total strain rate provided by ρ dislocations of type i moving with an average velocity Ui is given by (Li 1965):-

$$\dot{\varepsilon} = \sum_i \rho_i b U_i \cos\theta_i \cos\phi_i \qquad - 5.6$$

$$\dot{\varepsilon} = \sum_i \rho_i A_i b \nu_i \cos\theta_i \cos\phi_i \exp(-\Delta G_i/kT) \qquad - 5.7$$

Where Ai is the area swept out after a successful fluctuation.

Combining equation 5.7 and 5.2 gives:-

$$\dot{\varepsilon} = \sum_i \rho_i A_i b \nu_i \cos\theta_i \cos\phi_i \exp\left(\frac{-\Delta g_i + V_i \tau^*_i}{kT}\right) \qquad - 5.8$$

If all obstacles have identical shapes and energies this expression reduces to:-

$$\dot{\varepsilon} = \rho A b \nu \cos\theta \cos\phi \exp\left(\frac{-\Delta g + V\tau^*}{kT}\right) \qquad - 5.9$$

In general, Δg, l, ΔR, V, ν and τ^* are the average values for all rate controlling obstacles. The situation that arises when two different types of obstacle could influence the observed strain rate is considered in Section 2.8.

2.5. Experimental Determination of the Activation Parameters

i) Activation Enthalpy

From equation 5.7

$$\Delta G_i = -kT \ln \frac{\dot{\varepsilon}}{\sum_i \rho_i A_i b \nu_i \cos\theta_i \cos\phi_i} = -kT \ln\left(\frac{\dot{\varepsilon}}{\dot{\varepsilon}_0}\right) \qquad - 5.10$$

Differentiating with respect to T gives:-

$$\left(\frac{\partial \Delta G_i}{\partial T}\right)_{\sigma_A} = -k \ln\left(\frac{\dot{\varepsilon}}{\dot{\varepsilon}_0}\right) + kT\left(\frac{\partial \ln \dot{\varepsilon}/\dot{\varepsilon}_0}{\partial T}\right)_{\sigma_A} \qquad - 5.11$$

But, by definition, $$\left(\frac{\partial \Delta G_i}{\partial T}\right)_{\sigma_A} = \Delta S_i \qquad - 5.11$$

Also, $$\Delta H_i = \Delta G_i + T\Delta S_i \qquad - 5.12$$

Thus, $$\Delta H_i = kT^2 \left(\frac{\partial \ln \dot{\varepsilon}/\dot{\varepsilon}_0}{\partial T}\right)_{\sigma_A} \qquad - 5.13$$

Provided ρ_i, A_i, ν_i, θ_i, ϕ_i, b_i remain constant during an increment of temperature, this gives:-

$$\left(\frac{\partial \ln \dot{\varepsilon}}{\partial T}\right)_{\sigma_A} = \frac{\sum_i \Delta H_i \rho_i U_i b \cos\theta_i \cos\phi_i}{kT^2 \sum_i \rho_i U_i b \cos\theta_i \cos\phi_i} \qquad - 5.14$$

So, if only dislocations of one type are moving,

$$\left(\frac{\partial \ln \dot{\varepsilon}}{\partial T}\right)_{\sigma_A} = \frac{\Delta H}{kT^2} \qquad - 5.15$$

The term on the left hand side can be determined experimentally through creep experiments and hence a value of the activation enthalpy obtained.

If equation 5.15. is modified it gives:-

$$\frac{\Delta H}{kT^2} = \left(\frac{\partial \ln \dot{\varepsilon}}{\partial \sigma_A}\right)_T \left(\frac{\partial \sigma_A}{\partial T}\right)_{\dot{\varepsilon}} \qquad - 5.16$$

So the enthalpy may also be obtained from constant strain rate tests. This equation is only valid if the applied stress is a unique function of temperature and strain rate for a given structure. This may be tested by comparing the results obtained from creep and constant strain rate experiments.

Thus, the restriction upon the determination of the enthalpy is that the structure remains unaltered during the increment of temperature (strain rate). The enthalpy obtained is significant only if one specific type of obstacle is rate controlling.

ii) Activation Volume

Differentiation of equation 5.2 with respect to stress gives (Gibbs, 1967, Hirth and Lothe, 1967):-

$$-\left(\frac{\partial \Delta G}{\partial \tau^*}\right)_T = V + \tau^* \left(\frac{\partial V}{\partial \tau^*}\right)_T - \left(\frac{\partial \Delta g}{\partial \tau^*}\right)_T \qquad - 5.17$$

But, since the crystal adopts its lowest free energy in the excited state (Gibbs, 1964; Schoeck, 1965):-

$$(\partial \Delta G)_{T,\tau} = 0 \qquad - 5.18$$

This gives; (Schoeck)

$$\left(\frac{\partial \Delta G}{\partial \tau^*}\right)_T = - V \qquad - 5.19$$

Gibbs (1967) arrives at a slightly different solution

$$-\left(\frac{\partial \Delta G}{\partial \tau^*}\right)_T = V + \tau^* \Delta Rb \left(\frac{\partial l}{\partial \tau^*}\right)_T \qquad - 5.20$$

However, over quite a wide range of τ^* values, 1 is virtually independent of τ^* (Kocks,1967), so under most test conditions, even if the Gibbs solution is correct, equation 5.19 can be regarded as almost exact.

Differentiation of equation 5.10 gives:

$$\left(\frac{\partial \Delta G_i}{\partial \tau^*}\right)_T = -kT \left(\frac{\partial \ell_n \dot{\varepsilon}/\dot{\varepsilon}_0}{\partial \tau^*}\right)_T \qquad - 5.21$$

Thus, $$\frac{V}{kT} = \left(\frac{\partial \ell_n \dot{\varepsilon}/\dot{\varepsilon}_0}{\partial \tau^*}\right)_T \qquad - 5.22$$

and, $$\left(\frac{\partial \ell_n \dot{\varepsilon}}{\partial \sigma_A}\right)_T = \left(\frac{\partial \ell_n \dot{\varepsilon}}{\partial \sigma^*}\right)_T = \frac{\Sigma V_i \rho_i u_i b (\cos\theta_i \cos\phi_i)^2}{kT \Sigma \rho_i u_i b \cos\theta_i \cos\phi_i}$$

$$= \frac{V \cos\theta \cos\phi}{kT} \qquad - 5.23$$

This equation is valid provided all slip planes are similarly inclined to the stress axis and no structural changes occur during the alteration in test conditions.

So V can be obtained from either creep or constant strain rate experiments using equation 5.23. provided the above conditions are satisfied.

iii) Gibbs Free Energy

Schoeck shows that this is given by:-

$$\Delta G_T = \frac{\Delta H + T \, d\mu/dT \, \tau_w/\mu \, V}{1 - T/\mu \, d\mu/dT} \qquad - 5.24$$

$\frac{d\mu}{dT}$ is given by Huffman and Norwood (1960)

iv) The Thermal Stress

There are three principal methods of distinguishing this component of the applied stress from the athermal components.

a. The first method has been widely used for investigations in b.c.c. metals (e.g. Conrad 1961; Arsenault 1966; Ono 1966). It entails plotting the critical resolved shear stress, obtained from constant strain rate experiments, against temperature (e.g. fig.1.1). If the high temperature region is linear, independent of strain rate and has a slope determined by the temperature dependence of the shear modulus only, it may be taken that the deformation here is purely athermal (see equation 6,9). A value of the thermal stress at yield may be obtained by extrapolating the athermal region to low temperatures and subtracting this value from the applied stress. Significant values are obtained only if the structure at yield is independent of temperature. The method could be extended to higher strains but the assumption of constant structure becomes less valid as shown in the previous chapter.

b. In a stress relaxation experiment the dislocations held up at the short range obstacles relax into metastable positions where they lie in the long range stress field only. It has been suggested that the relaxed flow stress is approximately equivalent to the long range stress (Guiu 1964). The principal difficulty with this method is that relaxation is never complete within a finite period of time, so only a maximum value of can be obtained. This difficulty is enhanced if impurities or point defects are present that can pin the dislocations in positions other than the required metastable ones. In addition, the configuration of dislocations in the relaxed condition cannot be the same as that during deformation, so the relaxed flow stress

could only approximate to the athermal stress during deformation.

c. The third method, recently proposed by Michelak (1965), enables τ^* to be obtained directly from strain rate cycling experiments.

Combining equations 5.6 and 3.1b gives:-

$$\dot{\varepsilon} = \rho b \left(\frac{\tau^*}{\tau_a}\right)^{m^*} \quad - 5.25$$

Differentiation of equation 5.6 gives:-

$$\frac{d\ln\dot{\varepsilon}}{d\ln\tau^*} = \frac{d\ln\rho}{d\ln\tau^*} + \frac{d\ln v}{d\ln\tau^*} \quad - 5.26$$

Thus, $$\frac{d\ln\dot{\varepsilon}}{d\ln\tau^*} = m^* \quad - 5.27$$

provided ρ remains constant during the increment of stress (strain rate).

For small changes of strain rate,

$$\frac{\Delta\ln\dot{\varepsilon}}{\Delta\ln\tau^*} = m^* \quad - 5.28$$

Thus, $$\ln\left(\frac{\tau_2^*}{\tau_1^*}\right) = \ln\left(\frac{\tau_1^* + \Delta\tau^*}{\tau_1^*}\right) = \frac{1}{m^*}\ln\dot{\varepsilon}_1/\dot{\varepsilon}_2 \quad - 5.29$$

So, $$\tau_1^* = \frac{\Delta\tau^*}{\left[\left(\dot{\varepsilon}_2/\dot{\varepsilon}_1\right)^{1/m^*} - 1\right]} \quad - 5.30$$

Provided m^* and $\Delta\tau$ values are known, for a given structure, equivalent values of τ_1^* may be obtained. Methods of finding m^*, other than that given in Chapter 3, are considered in Section 2.9. There are no restrictions on the determination of τ^* other than ρ remaining constant during a change in strain rate.

2.6. The Validity of the Experimental Parameters

The limitations of the experimental determinations listed in the relevant sections can be dealt with quite simply apart from the criterion that the pre-exponential term in equation 5.9 remains constant during an increment of temperature or strain rate (stress).

So it is worth considering this aspect in some detail. An indication of the validity of this criterion is obtained by comparing the values of the parameters obtained from completely independent experiments. For instance, if values of V obtained directly using equation 5.23 and those obtained from the slope of a ΔG, τ^* plot (equation 5.19) are comparable it indicates the validity of the criterion.(Schoeck,1965)

Fortunately, there is an unambiguous method of determining whether the factor ρ alters. It entails comparing values of the activation parameters obtained from cycling experiments and direct etch pitting methods. Thus, for instance, from equation 5.6 (Guard, 1961; Christian 1964)

$$\frac{\Delta \ln \dot{\varepsilon}}{\Delta \ln \tau_A} = \frac{\Delta \ln \rho}{\Delta \ln \tau_A} + \frac{\Delta \ln u}{\Delta \ln \tau_A} \qquad - 5.31$$

Thus, from equation 3.1a

$$\frac{\Delta \ln \dot{\varepsilon}}{\Delta \ln \tau_A} = m + \frac{\Delta \ln \rho}{\Delta \ln \tau_A} \qquad - 5.32$$

Thus, a comparison of values of m obtained from etch pitting (c.f. Chapter 3) with values of $\Delta \ln \dot{\varepsilon} / \Delta \ln \tau_A$ unequivocally determines whether ρ alters during a change of stress (strain rate). A similar sort of analysis can be used to determine whether ρ alters with a change in temperature.

The only factor other than ρ, in the pre-exponential term that might conceivably alter significantly with stress(temperature) for a given structure, is the area swept out after a successful fluctuation. This has been looked at theoretically by Kocks (1967) for a random fixed obstacle situation. He shows that, over a wide range of stress i.e. $0.2\tau^*_o \rightarrow \tau^*_o (\tau^*_o = \tau^*$ at $0^oK)$, this quantity varies by a maximum of a factor of two. So during an incremental test where the stress does not alter by more than $0.05\tau^*_o$, it can be taken that this area is essentially constant. In non-fixed obstacle situations e.g. non-conservative jog motion, point defect drag, this areavaries slowly with stress but should be essentially constant provided $\Delta\tau$ is small.

So if it is shown that ρ is constant during the increments of strain rate(temperature), provided relatively small values of $\Delta\tau$ are used, the experiments may be regarded as valid.

There are a number of situations where the above analysis does not apply; these have been mentioned already and are now discussed in more detail.

2.7 Back Fluctuations

Schoeck was the first to realise that back fluctuations can only occur if the distance moved by the dislocation after it surmounts an obstacle is less than the distance over which the dislocation oscillates under the action of thermal fluctuations. The distance moved by a dislocation after a successful fluctuation, for a random fixed obstacle situation, is within the range $l - 4l$(Kocks 1967; Foreman and Makin, 1967) even at relatively low stresses (l is the obstacle spacing).

The amplitude of oscillation of a dislocation under coherent thermal fluctuations is limited by the line tension of the dislocation and certain lattice friction effects (Friedel,1964). If the latter effect is ignored it is possible to obtain an approximate magnitude of the maximum amplitude. This is determined by Schoeck for a free length of dislocation $2l$. For calcium fluoride, at temperatures below 250°C, this amplitude is of the order of $10^{-1} - 10^{-3}$ l, so there is no probability of back fluctuations.

However, there are situations other than the random fixed obstacle case where the possibility of back fluctuations must be considered e.g. non-conservative jog motion, point defect drag. A general treatment of back fluctuations has been conducted by Alefeld (1962). The probability of back fluctuations modifies the rate equation (Christian and Masters, 1964).

$$U = \rho \nu \exp\left(\frac{-\Delta G}{kT}\right) \exp\left(\frac{\Delta G_b}{kT}\right) \qquad - 5.33$$

Where ΔG_b is the activation energy for the reverse fluctuation.

This gives (Alefeld);

$$V = \frac{V \text{ expl.}}{\text{Coth}\left(\nu\tau^*/kT\right)} \qquad - 5.34$$

Thus, the correction only becomes noticeable when $\nu\tau^* < 4kT$

This treatment is not, however, generally applicable to all cases e.g. non-conservative jog motion where the total energy of the system alters after an activation. So each process should be considered separately.

2.8. More than one Rate Controlling Obstacle

In general, several types of obstacle are in existence in a lattice. Whether these obstacles contribute to the observed flow stress depends upon the relative physical positions of the obstacles (c.f. Kronmuller, 1964, 1967).

There are a number of distinct possibilities, two of these are considered briefly.

a. Alternative Processes

A possible situation is represented in fig. 5.3. where the two obstacle types are similar in width and coincide physically in the lattice; the average athermal stress is taken to be similar at all obstacles. There is a single point of activation where the two processes coincide and, in general, the value of τ^* required to be supplied (equation 5.9.) is greater for one type of obstacle than another, so only one process is rate controlling; the other contributes in no way to the observed thermal stress.

An example of this could be impurity dragging and impurity interaction.

b. Series Processes

This is a more frequently encountered situation and an example represented in fig. 5.4. The flexibility of the dislocation must be considered when the observed thermal stress is estimated. Foreman and Makin (1967) have briefly investigated the situation where two obstacles of different "strengths" are randomly distributed in the lattice. They conclude that the observed stress is intermediate between that associated with the individual obstacles and depends upon the relative strength and concentration

of obstacles. The obstacles are not always randomly distributed and in general the deformation is represented by the following equation.

$$\dot{\varepsilon} = \sum_n \dot{\varepsilon}_n = \rho_1 A_1 b v_1 \exp\left(\frac{-\Delta g_1 + V_1 \tau^*_1}{kT}\right) + \rho_2 A_2 b v_2 \exp\left(\frac{-\Delta g_2 + V_2 \tau^*_2}{kT}\right) + \ldots \quad - 5.35$$

If two or more of these terms are approximately equal the experimentally determined parameters do not apply to either process.

An example of this sort of process might be non-conservative jog motion and the interaction with tetragonal defects.

There are evidently numerous other situations and each combination should be considered separately.

2.9 The Application of the Measured Parameters

Having obtained experimental values of the activation parameters, and their validity has been established, their application to the understanding of the plastic deformation must be resolved. Each parameter is considered in turn.

i. The Thermal Stress

As already mentioned τ^* values can be obtained quite readily at yield (method a) and zero strain (assuming $\tau_\mu = 0$ in the etch pit experiments and using equation 5.30). However, if the contribution of τ^* to the work hardening is to be estimated, values must be found as a function of strain. There are a number of methods of achieving this other than the rather dubious relaxed flow stress method. Two such methods are considered here.

a. The first was developed by Michelak(1966)

From equations 3.1b and 5.27, provided the mobile dislocation density does not alter during an increment of strain rate,

$$m^* = \frac{\Delta \ln \varepsilon}{\Delta \ln \tau^*} = \frac{\Delta \ln \dot{\varepsilon}}{\Delta \ln (1 + \Delta\tau/\tau^*_1)}$$

$$= \frac{\Delta \ln \dot{\varepsilon}}{\Delta \tau} \left(\tau^*_1 + \frac{\Delta \tau}{2} \right) \qquad - 5.36$$

provided, $\Delta\tau << \tau^*_1$

Thus, $m^* \frac{\Delta \tau}{\Delta \ln \dot{\varepsilon}} = \tau^*_1 + \frac{\Delta \tau}{2}$ - 5.37

So a plot of $\Delta\tau/2$ against $\Delta\tau / \Delta \ln \dot{\varepsilon}$, obtained at a specific strain, has a slope m^* and an intercept τ^*_1. A further value of τ^*_1 may be obtained by substituting m^* into equation 5.30.

b. The second method, outlined by Li(1967) enables m^*, and hence τ^*_1 to be determined from stress relaxation experiments.

Provided the density of mobile dislocations and the athermal stress do not alter during the relaxation, the curves are shown to fit a relationship of the form;-

$$\tau_A - \tau_\mu = K(t + a)^{-n} \qquad - 5.38$$

which is an alternative way of expressing equation 3.16, with $n = 1/(m^* - 1)$.

Differentiating equation 5.38 with respect to time gives

$$\log \left(\frac{-d\tau_A}{dt} \right) = \log nK + (n + 1) \log (t + a) \qquad - 5.39$$

So, a plot of $\log \left(\frac{-d\tau_A}{dt} \right)$ against logt has a slope of $\frac{m^*}{1 - m^*}$

when $t >> a$ i.e. at long times.

So values of m^* can be found, and hence τ^*

ii. Activation Volume

The experimental activation volumes are usually converted into the dimensionless quantity V/b^3 for the purposes of comparison.

By definition, $\tau^* = \frac{F_s(\Delta R)}{lb}$ - 5.40

$$V\tau^* = F_s(\Delta R)\Delta R \qquad - 5.41$$

When V and τ^* are determined for a given structure (c.f.Basinski 1959).

So a plot of V against τ^* must have a specific shape and magnitude that depends solely upon the dimensions of the rate controlling obstacle i.e. if a single process is rate controlling throughout a universal, monotonic curve is obtained.

The actual magnitude of the activation volume term can also provide valuable information e.g. if large values are obtained, obstacle types with suitably large l and ΔR values must be invoked and certain mechanisms can be eliminated immediately. However, great care must be exercised because both l and ΔR are stress dependent and this has to be taken into consideration when comparing experimental values of V with expectedvalues for a specific obstacle type. ΔR depends upon stress only through the shape of the obstacle and can be accounted for. The variation of l with stress has been determined theoretically, as already considered; it can vary from three times the obstacle spacing at low stresses to 0.3 times this spacing at high stresses. Use of the curves obtained by Kocks and Foreman and Makin enables this variation to be allowed for.

iii. Activation Enthalpy

It is important that the enthalpy of the obstacle should be found so that it can be compared with the theoretical enthalpy values of the possible obstacles; this assists in identifying the actual rate controlling mechanism.

It can be shown that (Gibbs 1967)

$$\Delta G = \Delta U^* - V\tau_a - T\Delta S + V\tau_{\mu_0} \qquad - 5.42$$

τ_{μ_0} is the athermal stress at $0^\circ K$

Therefore,

$$\Delta H = \Delta U^* + V(\tau_{\mu_0} - \tau_a) \qquad - 5.43$$

But, for calcium fluoride (Huffman and Norwood, 1960)

$$\tau_\mu = \tau_{\mu_0}(1 + \beta T) \qquad - 5.44$$

Where β is a constant

So, $$\Delta H = \Delta U^* - V\left[\frac{\tau^* - \beta T\tau_a}{1 - \beta T}\right] \approx \Delta U^* - V\tau^* \qquad - 5.45$$

For relatively low temperatures.

So, for a single rate controlling mechanism, a univerral $\Delta H, \tau^*$ plot should be obtained with a slope equivalent to V, provided the temperature is low.

A value of ΔH_o ($\doteq \Delta U_o$), the actual enthalpy of the barrier (independent of stress) may be obtained by extrapolating values of ΔH and ΔU ($\doteq \Delta H$) to zero effective stress (c.f. method for finding ΔG_o).

There is an alternative, and probably more satisfactory way of finding ΔH_o(Arsenault 1966).

From equation 5.19 $\quad V = -\left(\frac{\partial \Delta G}{\partial \tau^*}\right)_T$

$$\therefore \int_{\Delta G_{\tau^*=0}}^{\Delta G_{\tau^*}} \partial \Delta G = -\int_0^{\tau^*} V \, d\tau^* \qquad - 5.46$$

$$\therefore \Delta G - \Delta Go = -\int_0^{\tau^*} V \, d\tau^* \qquad - 5.47$$

$$\therefore \Delta H - T\Delta S = \Delta Ho - T\Delta So - \int_0^{\tau^*} V \, d\tau^* \qquad - 5.48$$

For low temperatures, or if ΔS is independent of τ^*, this becomes

$$\Delta H = \Delta Ho - \int_0^{\tau^*} V \, d\tau^* \qquad - 5.49$$

This is the relationship derived less rigorously by Arsenault. It is probably not true that ΔS is independent of τ^* (Gibbs 1967) but the magnitude of the term $T(\Delta So - \Delta S)$ is small particularly at low temperatures.

Equation 5.49 can be used to find values of ΔHo over a range of τ^* values and hence to see if the obstacle type changes.

3. Experimental

Tests at strain rates of about 10^{-5} sec $^{-1}$ and above are all conducted on an Instron testing machine where change in strain rate tests can be performed instantaneously. All temperatures are attained as described in the previous chapter. The temperature change tests are conducted using two oil baths maintained at the required temperatures and merely alternated in position around the jig. This technique enables rapid, controlled temperature changes to be achieved.

It is shown in the previous section that tests are required to be conducted under constant stress conditions. It is also desirable that results should be obtained at strain rates lower than 10^{-5} sec $^{-1}$, so suitable creep equipment has been constructed.

The arrangement is shown in fig. 5.5. It consists of two interpenetrating frameworks that can move relative to one another on a series of adjustable ball races. One framework is attached to a cast iron base through a set of rigid supports. The rams are constructed of pyrophylite and aligned by suitable adjustments of the ball races. The load is applied by the addition of lead shots to an Xlon container (up to a maximum of 100 kg); the addition of a constant stress device was not required since only small strains ($< 0.1\%$) are necessary in each experiment. The strain is measured using a transducer arrangement which is attached to the rigid supports and can be moved over and inserted into a recess in the mobile framework, when the specimen is in position. The transducer is connected through a multimeter to a Honeywell recorder to enable a continuous displacement -time plot to be recorded; this is imperative for the sort of incremental test required to be conducted, where, the instantaneous change in strain rate is to be measured.

The temperature is required to be controlled most accurately ($\pm$ 0.5°C) otherwise the expansion and contraction of the specimen and rams superimposes an undesirable waveform, of long wave length, upon the displacement-time recording. So the oil bath arrangement is inadequate and a suitable radiation furnace is designed; this is shown in fig. 5.6. It consists of two concentric nichrome windings attached to separate voltage supplies. The brass ends of the furnace are water cooled and the region between the windings and the steel outer cylinder is filled with vermiculite insulator. The spacing between adjacent windings is adjusted to provide a uniform temperature within the enclosure; this is facilitated by the use of

the rams of low thermal conductivity. Accurate temperature control can be achieved by passing a fixed current through the outer windings and attaching an anticipatory Ether controller to the inner windings. Temperature changes of up to 50°C can be achieved within 15 minutes by adjusting the current in the outer windings, by a predetermined amount, coupled with a suitable alteration on the controller. This is adequate for the temperature change experiments envisaged; the load is partially removed during the temperature change period.

4. Results

4.1 A Orientation Crystals

4.1.1 Effect of Specimen Dimensions

Before a systematic investigation of the activation parameters is conducted the effect of specimen dimensions upon these parameters is established. So specimens with a range of relative dimensions, similar to those used in the previous chapter are tested. Values of $\Delta\tau$, for a given strain rate increment, are determined. It is found that all results fit an identical $\Delta\tau$, τ_A plot (even for type B crystals) at a specific temperature, although there is no universal $\Delta\tau$, ξ plot. So the dimensions of specimen used are evidently unimportant but, again for convenience, dimensions similar to those used in the previous investigations are employed.

4.1.2. The Determination of m^*

The first objective is to discover whether the density of mobile dislocations changes during an increment of strain rate. This requires the determination of m^* from strain rate cycling experiments to compare with those values obtained directly in Chapter 3.

1. Extrapolation Technique

Values of m (given by equation 5.32) have been obtained as a function of strain for a series of temperatures and strain rates. The results are shown in figs. 5.7:5.8: 5.9a - f. If it is again assumed that at zero strain (dislocation density $< 10^5$ cm^{-2}) the long range stress is approximately zero (probably valid for these high purity single crystals), then m extrapolates to m^* at zero strain.

The results reveal that m^* is independent of both strain rate increment and base strain rate (figs. 5.7; 5.8) but decreases as the temperature is increased.(fig. 5.10).

In fig. 5.10 these values of m^* are compared with those obtained directly in Chapter 3. The agreement is almost exact at 75°C. m^* decreases linearly with T such that $m^* T$ is virtually constant and if the plot is extrapolated to lower temperatures it passes through the etch pit value obtained at 25°C. Thus, it may be concluded unambiguously that the density of mobile dislocations does not alter during an increment of strain rate at temperatures below 75°C, at small strains. Unfortunately, no etch pit experiments have been conducted at finite strain but there is no reason for

presuming that the density of mobile dislocations should alter simply because the athermal stress is larger; the validity of this statement is tested indirectly in section 4.1.3. There is no direct comparison at the higher temperatures. However, if the mobile density altered during an increment of strain rate, this method would give values of m^* larger than the correct value, for an increase in strain rate, and smaller for a decrease in strain rate and dependent upon the strain rate increment used. Even at 170°C, consistent values of m^* are obtained under all conditions (fig. 5.8), so the mobile density presumably does not alter significantly up to this temperature; this too is confirmed in Section 4.1.3. Kommik et al (1967) show that this criterion is not valid at temperatures close to the athermal stress region for NaCl and LiF, so the validity of tests conducted above 200°C is questionable and tests are confined to lower temperatures.

The variation of m with strain is interesting. In stage Ib it remains approximately constant and equal to m^*. In stage Ic it increases approximately linearly with strain; similarly in stage II it increases linearly, but more rapidly, with strain.

A combination of equations 3.1a and 3.1b gives:-

$$m = \frac{\tau_A \, m^*}{\tau^*} \qquad - 5.50$$

So the variation of m depends upon the relative variations of τ_μ and τ^* and is considered when more information concerning these stresses is available.

A further interesting feature of the results is the anomalously low values of m obtained at low strains and temperatures in specimens tested in the mechanically polished condition. This effect is discussed in Section 5.1.1.

ii. Strain Rate Cycling Method

Firstly values of the stress increment ($\Delta\tau$) are obtained as a function of strain by cycling from a specific base strain rate to a series of higher strain rates. The results are shown in fig. 5.11. Values of $\Delta\tau$, corresponding to each strain rate increment, obtained at a specific strain, are plotted against the quantity $2\Delta\tau/\ln(\dot{\varepsilon}_1/\dot{\varepsilon}_2)$ for the same strain; the slope gives a value of m^*. The plots are constructed for a series of strains, figs. 5.12: 5.13. They show that m^* is independent of strain throughout, the values of m^* are in good agreement with those already obtained at zero strain.

iii. Stress Relaxation Method

The validity of this method requires that both the mobile dislocation density and the long range stress remain constant throughout the test. This is probably not valid for long times, as shown by subsequent strain ageing experiments, particularly at high temperatures. However, the method only applies at relatively long times, so it is not ideal and has to be restricted to a small range of times; typical logt, $\log(-d\tau_a/dt)$ plots are shown in fig. 5.14. The associated values of m^* are shown in fig. 5.15. The results at 110°C are most consistent and show that m^* is independent of strain; they are also in good agreement with other values obtained already. However, values at

170°C are erratic; a consequence of the small time period over which the linear relationship is obeyed.

These results indicate two important things.

1. The density of mobile dislocations does not alter significantly during an increment of strain rate between room temperature and about 170°C in the strain rate range $10^{-5} - 10^{-2}$ sec^{-1}.

So it is now possible to continue with the determination of the activation parameters within this range of temperature and strain rate.

2. The value of m^* is independent of strain. These values of m^* are used to determine the variation of the thermal stress with strain.

4.1.3. The Estimation of the Activation Parameters

4.1.3.1 Thermal Stress

The three methods outlined in the theory are used.

a. Extrapolation from the Flow Stress, Temperature Curve

Values of yield stress are obtained as a function of temperature for both type A and B specimens. The results are almost identical to those obtained by Roy (fig.1.1); the only significant difference appears above 350°C i.e. no strain rate dependence is encountered in this investigation. The values of τ^* obtained are useful for comparison with values given by the other methods.

b. Stress Relaxation

After the crosshead is arrested during a constant strain rate experiment, the stress is allowed to relax for a period of twenty four hours. The relaxed flow stress is

subtracted from the applied stress to give a possible value of the thermal stress (τ^*_R). The values of τ^*_R increase with strain in stage Ib but remain virtually constant in all subsequent stages, certain of the results are shown in fig.5.16.

c. Strain Rate Cycling

Values of τ^*, at the base strain rate, are obtained using the above values of $\Delta\tau$ and m^* in equation 5.30 and from the intercepts of the plots in figs. 5.12: 5.13. The values obtained are identical for both methods and shown in fig. 5.16. The magnitude of the athermal stress is now obtained by subtracting τ^* from the applied stress (fig. 5.16); it varies approximately linearly with strain and almost independent of temperature.

The values of τ^* obtained at yield are in good agreement with those given by the first method. Their variation with strain is similar to τ^*_R, although the magnitude of the latter is considerably smaller (this is readily explained as shown in Section 2.5). Although these values of τ^* are not entirely unequivocal, because it is not unambiguously established that the mobile dislocation density does not alter during a strain rate change at large strains, considerable confidence is placed in them and these are the τ^* values used subsequently. It is now possible to understand the variation of m with strain. The almost horizontal region corresponding to stage Ib arises because τ^* increases almost as rapidly as τ_A. However, in stages Ic and II, τ^* does not alter so the increases in m are directly related to increases in the athermal stress.

4.1.3.2. Activation Volumes

Values of the activation volume are obtained by strain rate cycling experiments over a wide range of temperatures and strain rates. Typical variations of the activation volume with applied stress are shown in fig. 5.17; after a rapid decrease in the activation volume with strain in stage Ib, it remains virtually constant in all subsequent stages. There is no obvious relationship between the values at different temperatures when plotted against the applied stress.

It was shown in Section 2.9 that the activation volume should be uniquely related to the thermal stress for a specific obstacle type. So corresponding values of the activation volume and the short range stress, obtained by several independent methods, are plotted in fig. 5.18. All results fit a single curve. The agreement between the values determined from the velocity measurements obtained in Chapter 3 and all strain rate cycling values tends to confirm the previous statement that the density of mobile dislocations does not alter during an increment of strain rate, at strains greater than zero. In addition the same obstacle appears to be rate controlling throughout; this is confirmed by the enthalpy measurements (Section 4.1.3.3.).

A further interesting feature of the results is the low values of activation volume obtained for a given applied stress in stage Ia, in mechanically polished specimens. The results are rather erratic but it is possible to obtain approximate values of τ^*, assuming that m extrapolates to m^* at zero strain; the values determined, plotted in

fig. 5.18: fit a different curve. Thus, it seems possible that a different mechanism controls yield and flow in these crystals.

4.1.3.3. Activation Enthalpies

Values of the activation enthalpy can be obtained from temperature cycling experiments using equations 5.15: and 5.16. Before commencing these tests it must be established that there is no significant change in structure (recovery or pinning) during the time interval that the temperature change is occurring. So specimens are unloaded, after straining to a certain stress, and reloaded, after a certain period, to see if the stress has altered from its unloading value. If not this would indicate that the mobile density does not alter significantly during this period.

Below 110°C there is no change, other than the usual metarecovery, for periods of less than about forty minutes. However, for periods in excess of a few hours unusually large and extensive yield regions (similar to those in stage Ia in mechanically polished specimens) are observed. The regions diminish in stage Ic and beyond. Above 110°C, the yield regions decrease in magnitude but appear more rapidly but there is still no significant effect in less than twenty minutes. Between 150°C and 220°C (the maximum test temperature used) there are no significant yield drops but at the latter temperature permanent recovery is first observed.

Since the experimental temperature changes can be effected within twenty minutes, these tests should be valid but least accurate within the temperature range 110°C — 150°C.

A systematic study of enthalpies, as a function of stress, is best achieved from constant strain rate experiments using equation 5.16; this requires values of the quantity $(\Delta\tau/\Delta T)_{\dot{\varepsilon}}$ to be determined. This is conducted at various temperatures at a strain rate of $2 \times 10^{-4} sec^{-1}$; the results are plotted in fig. 5.19, as a function of the applied stress (the values are independent of the temperature increment and are similar for both increase and decrease in temperature experiments). This quantity increases with stress in stage Ib but remains virtually constant in all subsequent stages. It is now required to relate $(\Delta\tau/\Delta T)_{\dot{\varepsilon}}$ with τ^*, this is done in fig.5.20; $(\Delta\tau/\Delta T)_{\dot{\varepsilon}}$ increases as τ^* increases and is generally lower, for a given τ^*, the higher the temperature.

Now, values of the activation enthalpy can be estimated for various τ^*, the results are shown in fig. 5.21. There is quite a scatter at a particular τ^* but it is possible to detect a general decrease in the enthalpy as τ^* increases; the variation becomes more apparent at lower stresses. The enthalpies do not depend systematically upon temperature i.e. all results can be approximated to a single curve.

Values of the quantity ΔH^* (or ΔU^*) (equation 5.45) are also determined (the error bars give maximum and minimum possible values). However, the important quantity is ΔH_o (equation 5.49), the enthalpy of the barrier. This is computed and also plotted in fig. 5.21. Within the limited accuracy of the results, ΔH_o appears to be independent of τ^*, with a magnitude 1 ± 0.1 eV. Also, the ΔH and ΔH^* plots can be reasonably extrapolated to this value at zero stress, tending to confirm the magnitude of ΔH_o.

These results are compared with values obtained from etch pit and creep experiments. The constant strain rate results, when extrapolated to low stresses, pass through the creep values; this confirms the validity of equation 5.16 and hence the applicability of the constant strain rate method (see Section 2.5). The direct values are slightly larger, at a given τ^*, the difference is not large and can be accounted for by a slight change in the mobile dislocation density in the temperature change tests. The results provide a value of ΔH_0 within the error range quoted above, thus giving confidence in the magnitude of the enthalpies obtained from the constant strain rate experiments.

The slope of the ΔH, τ^* plot should, according to equation 5.45 give a value of the activation volume. The values of V obtained this way are indeed of similar magnitude to those in fig. 5.18; this provides indirect confirmation that the mobile dislocation density is approximately constant for all the constant strain rate experiments.

The experiments provide the important result that the obstacle type is the same for all strains, temperatures and strain rates used.

For the mechanically polished specimens in stage Ia, the results are most erratic and give a value of $\Delta H_0 = 0.6 \pm 0.4$ ev.

4.2 B Orientation Crystals (Single Slip)

A similar series of experiments are conducted on tensile specimens of this orientation. All activation parameters fit identical thermal stress relationships, even giving similar values of τ^*_{max} at a specific temperature and strain rate. The only difference in the deformation characteristics lies in the variation of the athermal stress with strain.

4.3. Secondary Slip

The same experiments are repeated for specimens of type C orientation. The results are summarised below.

1. Determination of m^*

Values of m increase approximately linearly with strain at all temperatures, fig. 5.22. m^* is independent of strain and decreases approximately linearly as the temperature is increased, fig. 5.23.

2. The thermal stress

Values computed using equation 5.30 are independent of strain fig. 5.24, and compare well with those values obtained by the extrapolation technique (Section 2.5).

3. Activation Volumes

These too are independent of strain for a given temperature and strain rate. Values are plotted against τ^* in fig. 5.25.

Activation Enthalpies

Enthalpies, obtained as before, are plotted in fig. 5.26; $(\Delta\tau/\Delta T)_\epsilon$ is independent of strain. The results give a value of $\Delta H_o = 1.4 \pm 0.1$ ev, independent of τ^*. Thus, the same mechanism is rate controlling throughout and differs from that controlling primary slip.

5. Discussion

5.1 Primary Slip

5.1.1. Yielding

In chemically polished specimens the activation parameters are identical for yield and flow whilst in mechanically polished specimens they are different. The difference is probably

associated with the observation that a layer of dislocations is introduced at the surface on mechanical polishing, whilst it is removed by the chemical polish (Chapter 4). The yield drop in the chemically polished specimens (fig. 4.8) is typical of the situation where the initial mobile dislocation density is low and yielding is controlled by the rate of multiplication of dislocations, with the obstacle type identical for generation and propagation of dislocations. In the mechanically polished specimens, the operation of the initial sources possibly involves a different mechanism than subsequent propagation. Here, the density of obstacles at the sources is higher than in the lattice; this suggests that the dislocations introduced during polishing are lightly pinned by point defects before testing commences (this is confirmed by experiments on strain aged crystals where the activation parameters obtained on yielding obey similar relationships to those in mechanically polished specimens in stage Ia). Thus, the mobile dislocation density required to comply with the applied strain rate on yielding is provided by the unpinning of these dislocations from thin impurity atmospheres (or by dragging the atmospheres with the existing dislocations); this evidently occurs at lower stresses than the operation of sources in 'as-grown' crystals (fig. 4.8) where the grown in dislocations are heavily pinned.

At low temperatures unpinning (dragging) controls yield but, since the 'propagation' stress increases with strain, a transition occurs as a function of strain so that in stage Ib

deformation is controlled entirely by this 'propagation' mechanism. As the temperature is raised the stress to operate the 'as grown' sources reduces rapidly so that, at 150°C, they can operate equally as readily as the unpinning sources and deformation is controlled throughout by the same 'propagation' mechanism. The situation is more readily comprehended after the 'propagation' mechanism is identified.

5.1.2. Work Hardening

The work hardening in stage Ib is primarily due to an increase in the short range stress whilst that in stages Ic and II is due solely to increases in the long range stress. The athermal effects are considered in the following chapter, now the activation parameters are analysed to try to understand this variation in the thermal stress.

The activation volume decreases with strain in region Ib (c.f. Tungsten, Schadler, 1964; Iron, Stein, 1966) whilst the thermal stress increases. This decrease in the activation volume must correspond either to a decrease in the activation distance (ΔR) or the obstacle spacing (l) or both. Any change in ΔR evidently corresponds to a change in the form of the force - distance curve i.e. the obstacle type changes, so this would be accompanied by a change in ΔH_o and the V, τ^* curve. Since these do not alter during the deformation it may be reasonably concluded that ΔR does alter (apart from that due to any change of the equilibrium position of the dislocation at the obstacle as the thermal stress increases). Thus, the decrease in activation volume in stage Ib must be due to an increase in the density of obstacles of a specific type as the strain(stress)

increases. (It should be noted here that it is not possible to explain the decrease in activation volume by invoking different equilibrium positions of the dislocation at the obstacles, for this cannot change simply through an increase in the athermal stress i.e. without a change in obstacle density occurring first). The next step is identification of the obstacle type that increases in density during stage Ib.

There are a number of features of the deformation, other than those mentioned above, that can assist in identification of the obstacle type; these are listed below.

a. The magnitudes of V and ΔH_o.

b. Edge dislocations are rate controlling.

c. The activation parameters are identical for single and multiple slip.

d. τ^* attains a maximum value during deformation, the magnitude depends upon temperature and strain rate.

The identification procedure takes the form of an elimination process. All possible mechanisms are listed, table 7, and the clearly inapplicable processes are eliminated so that the remainder can be considered in more detail.

Non-conservative jog motion and climb are eliminated because of the high enthalpies involved.

The dislocation forest density in the tensile experiments is low (Chapter 4) and cannot account for the small obstacle spacings required by the activation volume measurements. A similar argument eliminates intersection of dislocation dipoles (see also Chapter 6, II).

TABLE 7 Possible Rate Controlling obstacles in Calcium Fluoride

Mechanism	Expected Activation Parameters			References	Possible range of obstacle spacings(based on experimental values of V/b^3 and allowing for variation of l with stress)
	$\Delta R(b)$	Obstacle spacing(b)	ΔH_o(ev)		
. Peierls-Nabarro	~ 1	1 - 10	?	e.g. Dorn and Rajnak(1964)	1 - 20
. Point Defect Drag	~ 1	1 - 10^3	?	Whitworth(1967)	1 - 2 x 10^2
. Point Defect Interactions	< 10	1 - 10^2 X_1	?	Fleischer(1962) Friedel (1964)	1 - 20
. Dislocation Forest Intersection	< 10	$> 10^3$ X_2	?	Dorn (1963) Basinski (1959)	$\sim$ 1 - 20
. Conservative Jog Motion	~ 1	10 - 10^3	?	Hirsch (1962)	1 - 2 x 10^2
. Non-conservative Jog Motion	~ 1	10 - 10^3	> 2 ev	Mott (1952) Weertman (1965)	1 - 2 x 10^2
. Cross slip	~ 1	10 - 10^3	?	Brown and Ekvall (1962)	1 - 2 x 10^2
. Climb	~ 1	10 - 10^3	> 2 ev	Weertman(1957)	1 - 2 x 10^2
. Intersection of Dislocation Dipoles	$1 \rightarrow 10$	$> 10^3$ X_3	?	Davidge (1966)	$\sim$ 1 - 20

X_1 Based on a point defect concentration $>$ 1 p.p.m.

X_2 For a forest density of $< 10^9 cm^{-2}$

X_3 For a dipole density of $< 10^9 cm^{-2}$

A short range interaction with dislocation dipoles is eliminated primarily because a sufficiently high density of these dipoles is unlikely and secondly because it is not possible to explain a maximum value of dipole spacing that does not alter in Stage II (Davidge et al, 1964, observes a marked increase in this density in stage II in NaCl).

The fact that edge dislocations control the deformation eliminates conservative jog motion and cross slip.

Thus, three possible rate controlling processes remain; these are considered in more detail.

Peierls -Nabarro Mechanism

A considerable amount of literature has been devoted, in recent years, to the study of this mechanism (e.g. Seeger et al,1957; Celli et al, 1963). This is not reviewed here because an excellent review article by Guyot and Dorn (1967) has recently appeared. They summarise the criteria required for the operation of this mechanism. These are as follows:-

i) The activation volume is independent of strain (Wynblatt and Dorn,1965 Conrad et al, 1962).

ii) The energy required to nucleate a pair of kinks (at zero stress) is evidently related to the line energy of the dislocation comprising the kinks. The theory relates these quantities as follows (Seeger 1956)

$$Uk = \frac{2\Gamma_o a}{\pi}\left(\frac{2\tau_{pl} b \Delta R}{\pi \Gamma_o}\right)^{\frac{1}{2}} \qquad - 5.51$$

Uk is the kink energy, Γ_o is the line energy, τ_{pl} is the thermal stress at $0^{\circ}K$.

Thus, if the mechanism operates, substitution of the experimentally determined values of U_K and τ_{pl} should give a value of Γ_o similar to that determined in Chapter 2.

iii) The activation volume, given by equation 5.19, is shown to fit the relationship in fig. 5.27 if this mechanism applies, (Dorn and Rajnak, 1964). This plot can be compared with experimental values.

The first criterion is not established unequivocally and there is no fundamental reason why the activation volume should not vary with strain, so this is not sufficient reason for discarding this mechanism.

Substitution of the experimental values of τ_{pl} and U_K into equation give a value of Γ_o of 2 ± 1 ev for a length b of dislocation. This is considerably lower than even the minimum expected value of 7 ev given in Chapter 2.

Values of the experimental activation volume are normalised to give values of $V_{exp.} \tau_p / 2U_K$ and these are plotted against τ^*/τ_{pl} in fig. 5.27. The agreement with the theoretical curve is quite good at high stresses but at low stresses there is a large discrepancy (c.f. Fleischer, 1967). Fleischer argues that discrepancies at low stresses discount the operation of the Peierls process.

Thus, it seems most unlikely that this mechanism controls the deformation. Where the Peierls mechanism is quite likely to control the thermal stress, a much closer fit to theoretical predictions is encountered. (see Section 5.2).

Point Defect Interactions

There are a number of possible interactions; these are listed below.

a. The interaction with the tetragonal strain field of impurity-vacancy (interstial) complexes (e.g. Fleischer 1962).

b. The cutting of small precipitates (e.g. Byrne, Fine and Kelly, 1961).

c. The interaction of the charged core of the edge dislocation with isolated point defects; this is short range because the alternating sign of the charge at the dislocation eliminates any long range effects (Freidel, 1964).

d. The rotation of impurity complexes in the vicinity of the dislocation core; this could be short range if the rotation is controlled by electrostatic rather than elastic considerations (c.f. Pratt et al, 1963)

Each process is considered in turn.

a. The interaction energy between the dislocations and the tetragonal strain field of the complex is given by Fleischer(1962). The magnitude depends upon the degree of tetragonality and is usually within the range 0.5 - 0.9 ev, so the mechanism is possible. It is required that, for a specific slip plane, there should be complexes within a few burgers vector distances of this plane and spaced about 10 - 100b apart (given by the experimental activation volume). This necessitates an aliovalent impurity content, in the required complex form, of at least 40 p.p.m. Tests on high purity crystals (Chapter 7) show that this mechanism is unlikely.

b. The experimental value of the activation volume requires the precipitates to be spaced about 20b apart on the slip plane. This requires a concentration of impurity in excess of 10^3 p.p.m. which is well in excess of the impurity revealed by analysis; so this mechanism is eliminated.

c. A charged, isolated point defect could interact electrostatically (as well as elastically) with the charged core of the edge dislocation. The magnitude of the interaction energy depends upon the exact nature of the core of the dislocation. An approximate value can be obtained from simple electrostatic considerations. Thus if, for instance, there are three adjacent charges of a certain sign a value of 1 ev is obtained; this rises to 1.4 ev for twelve adjacent charges. This magnitude is reasonable and the mechanism possible.

d. This process gives an interaction energy of less than 0.6 ev so is immediately eliminated.

Thus, only mechanisms (a) and (c) are possible.

It is now required to explain how the obstacle density can increase as the applied stress increases until a certain maximum value is obtained. In the case of the impurity complex mechanism this could be achieved by small aggregates being cut by passing dislocations (c.f. Newey et al 1966) leaving an increased density of complexes on the slip plane (the cutting mechanism always being able to operate at lower stresses than the interaction mechanism). The efficiency of dispersion of the aggregates is required to increase as the stress increases; the maximum value of τ^* being achieved when all aggregates on the slip plane can be dissociated into

complexes.

The isolated point defects situation is more realistic. If the point defects are vacancies or interstitials these can be produced by the non-conservative motion of jogs on screw dislocations; the jogs are formed even under single slip conditions by multiple cross glide(Johnston and Gilman, 1960). If the stress required to move the jogs is lower than that to move the edge dislocations at a similar velocity, the non-conservative motion is not observed as a rate controlling obstacle nor can it contribute to the athermal stress at the edge dislocation. The formation of point defects by this process has been considered recently by a number of investigators e.g. Weertman, 1965; Barrett and Nix, 1966; Hirth and Lothe,1967. They conclude that, except at very high stresses, the defect with the lowest formation energy is created at one type of jog whilst the other type of jog moves by absorption of certain of these defects; the situation is evidently more complex in ionic crystals where more defect types are involved. As the concentration of defects on the slip plane increases larger stresses are required to create further point defects; this is purely a 'chemical' effect. Thus the concentration of defects of the predominant type in excess of the equilibrium concentration (Co) in the vicinity of the jog, is related to stress according to the expression (Weertman, 1965)

$$\frac{C}{Co} = \exp\left(\frac{\tau_j b \ell_j \Delta R_j}{kT}\right) \qquad - 5.52$$

Where C is the total concentration of point defects of the type considered; $\tau_j = \tau_A \pm \tau_\mu$ at the jog.

The value of τ_μ at the jog is unlikely to be the same as the measured value at the edge dislocation so it is not possible to find exact values of τ_j to fit this relationship. The sequence of events during deformation is as follows; at yield the edge dislocation can interact with the equilibrium defects providing a specific value of τ^* and a certain positive value of τ_j, at the jogs; thus a non-equilibrium concentration of defects can be produced. The subsequent edge dislocations are required to interact with the increased density of defects giving a larger value of τ^* and so on.

The difficulty arises in explaining the maximum value of τ^* reached at a certain applied stress in each test. The only way in which it could be explained is by assumingthat, at a certain defect density, as many defects that are created can be absorbed by jogs and other sinks so that a dynamic equilibrium is reached and maintained.

It is of interest to determine the order of magnitude of the point defect concentration required for this mechanism. Thus, using the experimental value of the activation volume, a density of defects close to the slip plane of 10^{21} cm^{-3} is required. However, defects are only produced on the slip planes so, for a dislocation density of 10^{9} cm^{-2} (the maximum value encountered, Chapter 6), an average defect density throughout the crystal of 10^{16}--10^{17} cm^{-3} is required. This is not greatly in excess of the equilibrium concentration of 10^{15}cm^{-3}(Ure,1957) but it should be possible to detect in ionic conductivity measurements, if the measurements are made immediately after deformation is arrested.

The situation would not be as simple as this, for isolated aliovalent impurity ions have a similar interaction energy and could contribute to the observed obstacle density; their density could even

increase with stress through the dispersion of aggregates as already shown. However, a density of aliovalent impurity of more than 40 p.p.m. is required for impurities alone to control deformation and this is unlikely (Chapter 7).

Point Defect Dragging

When a length of charged edge dislocation of a specific sign encounters an isolated point defect of opposite sign the two associate with a release of energy (a reduction of electrostatic and elastic energy is involved). If the association energy is large, dissociation does not occur and the point defect is required to migrate along with the dislocation. This mechanism is evidently the alternative to the interaction mechanism just considered; the process that occurs is that with the lower activation energy.

Whitworth (1967) has considered the migration of point defects with edge dislocations in NaCl. He uses the ionic configurations of the edge dislocation in its various translation positions as determined by Huntingdon et al (1955); he concludes that the migration energy is relatively low and considerably lower than the bulk migration energy, when the point defect always lies close to the dislocation.

It is possible to obtain an expression for the population of available sites from simple thermodynamic considerations (Read 1954, Whitworth 1967).

$$\Delta g_B = kT \ln f/(1-f) - kT \ln C_\infty \qquad - 5.53$$

Where Δg_B is the binding energy between the point defect and the dislocation.

f is the fraction of sites occupied.

C_∞ is the fraction of ion sites occupied by vacancies (interstitials, impurities).

In this case Δg_B is large because it involves a reduction in electrostatic as well as elastic energy (see Chapter 7). As described previously, C_∞ can increase during deformation so a detailed analysis of this equation would enable f to be determined for the various test conditions and to be compared with experimental values of f; this is not possible at this stage because Δg_B and C_∞ are not known accurately.

The distinct advantage of this mechanism is that it can readily explain the appearance of a maximum value of τ^* in a given test. Thus, once C_∞ readhes a specific value (that depends upon temperature) f becomes approximately unity and these can be no further significant increase in f, and hence τ^*. It has already been shown how C_∞ on the slip plane can increase as the stress increases, so f can increase during deformation and attain the maximum value at a specific stress

If this situation applies, the difference in values of τ^*_{max} at different temperatures and strain rates is required to be explained by varying values of the activation distance as ΔG in equation 5.2. varies with temperature (or strain rate) i.e. a consequence of the shape of the force-distance curve. Thus, at relatively low values of τ^*_{max}, ΔR is required to be large (e.g. at least [illegible]^{4}b at 220°C) and the situation does not correspond to Whitworth's where the point defect always lies close to the dislocation core. So, in fact, the activation enthalpy for this migration process might approach the bulk migration energy of the defect involved.

It is interesting to consider the activation process involved because it differs from the usual fixed obstacle type. The initial activation involves the 'unpinning' of the dislocation from the defect.

It cannot move completely away from the influence of this defect because the thermal stress available is not sufficiently large. Now, thermal fluctuations can occur either to move the dislocation further away from the point defect (this increases the energy of the system) or to move the point defect towards the dislocation(reducing the energy of the system). The latter evidently occurs in preference to the former so that the activation enthalpy is given by the migration enthalpy of the defect in the vicinity of the dislocation. The situation is a complex one especially at higher temperatures where fluctuations of the dislocation away from the defect might occur prior to the migration of the defect to the dislocation. The definition of the activation distance is not clear nor is the variation of the activation enthalpy with the thermal stress readily predicted.

The above activation process occurs when the point defect at the dislocation can still be identified as such (c.f. Brown, 1960). This is possible for an aliovalent impurity ion but not so for vacancies or interstitials. Thus, when the latter associate with the edge dislocation half jogs are created similar to those already in existence (Chapter 2), so the association merely reduces the half jog spacing on the dislocation. (Chapter 7) The motion of the dislocation corresponds to the migration of these jogs. Again, the definition of ΔR and the variation of ΔH with τ^* are not clear.

An approximate magnitude of aliovalent impurity required for impurity migration to control the deformation is determined to see if this process is possible. There must be, initially, adequate impurity available in the vicinity of the slip planes to saturate all the dislocations that pass through a specific area of slip plane.

Consider the passage of a single dislocation across a slip plane in a specimen of typical dimensions. At low temperatures where little diffusion occurs all defects must lie within a few burgers vector distances of the slip plane. So the concentration of defects required to saturate this dislocation in its passage through the crystal is approximately $10^{17} cm^{-3}$. A typical slip step height at yield requires 500 dislocations to have traversed a given slip plane (Pratt 1953), so an impurity concentration of 50 p.p.m. is required to saturate all dislocations. Although the dislocations are not saturated at yield, it is expected that more dislocations would traverse this same plane during deformation, so this impurity level is regarded as a minimum requirement; the mechanism is thus possible but unlikely (See Chapter 7).

The situation is probably not a straight forward one and certain other features might be required to be considered.

i. The motion of the dislocation might be controlled by the combined effect of impurities, vacancies and interstitials associated with it.

ii. The concentration of 'free' defects increases as the temperature increases so fewer defects are required to be created during deformation.

iii. A limited amount of diffusion might occur that modifies the point defect distribution on the slip planes.

iv. Sufficient defects to saturate the dislocations may not be created so that τ^*_{max} corresponds to a maximum rate of

production of defects on the slip plane.

At this stage, it is not possible to decide which of the three mechanisms outlined above controls the deformation because all can be adjusted to fit the experimental results. It is also possible that another mechanism which has not been considered might be involved.

5.2. Secondary Slip

Unfortunately, there is not sufficient information available to perform such a thorough analysis of rate controlling processes in this case. In particular, the relative velocity of edge and screw dislocations is not known. Thus a number of mechanisms are possible. (table 7); these are as follows

1. Peierls-Nabarro
2. Conservative Jog Motion
3. Cross slip
4. Interaction with point defects
5. Point defect dragging

The secondary edge dislocation is uncharged so the energy of association with point defects is low and given approximately by the Cassani-Thompson calculation as 0.4 ± 0.2 ev, for an isolated defect. Thus, the dragging of point defects is unlikely (see Section 5.1).

The interaction with isolated point defects and complexes cannot be the sole source of the thermal stress because these are not orientation dependent effects and it would not be possible to explain the lower thermal stress(activation enthalpy etc.) in the primary orientation if either mechanism should be invoked.

The three remaining processes are all possible and might even operate in conjunction with an impurity mechanism with a similar activation enthalpy (see Section 2.8). It is not possible to differentiate between these processes until the relative velocity of edge and screw dislocations and the effect of impurities on the deformation are known. However, it is of interest to see if the experimental parameters fit the criteria for operation of a Peierls mechanism, listed in section 5.1.2.

The activation volume is independent of strain so the first is satisfied. The line energy of the dislocation given by equation 5.51 is 7 ± 2 ev for a length b of dislocation; this compares with a minimum value of 8ev given in Chapter 2. So this condition is satisfied.

The experimental activation volume is compared with theoretical values in fig. 5.27. The agreement is good even at low stresses.

Thus, it seems quite likely that the Peierls mechanism operates in this case although this cannot be regarded as unequivocal.

6. Conclusions

1. Primary Slip

a. The mobile dislocation density does not alter significantly during an instantaneous change in strain rate between room temperature and 170°C.

b. The mobile dislocation density changes by a small amount during temperature change experiments, even at low temperatures.

c. There appear to be three rate controlling processes that might explain the observed deformation characteristics on this system.

i) The interaction with impurity-point defect complexes.

ii) The interaction with isolated, charged point defects. The difficulty here arises in explaining the requirement that the density of obstacles on the slip planes reaches a maximum possible value. A tentative explanation has been given but not substantiated.

iii) The migration of point defects with the dislocation. The attraction of this mechanism is the ready means of explaining a maximum value of obstacle density attained at a specific applied stress. However, the mechanism is unlike fixed obstacle types and the determination of the force-distance curve and the variation of the enthalpy with stress present rather complex problems. Thus, it is not possible to determine whether the experimental values of activation distance and the enthalpy, stress relationship are reasonable for this model as they are for fixed obstacle processes.

The situation is discussed in more detail in Chapter 7 when tests on very high purity crystals have been conducted.

2. Secondary Slip

The parameters obtained can be explained by invoking a number of mechanisms. However, they fit the Peierls criteria remarkably closely and since the Peierls stress is likely to be high for slip on this system (Chapter 2) it seems quite likely that this process is rate controlling.

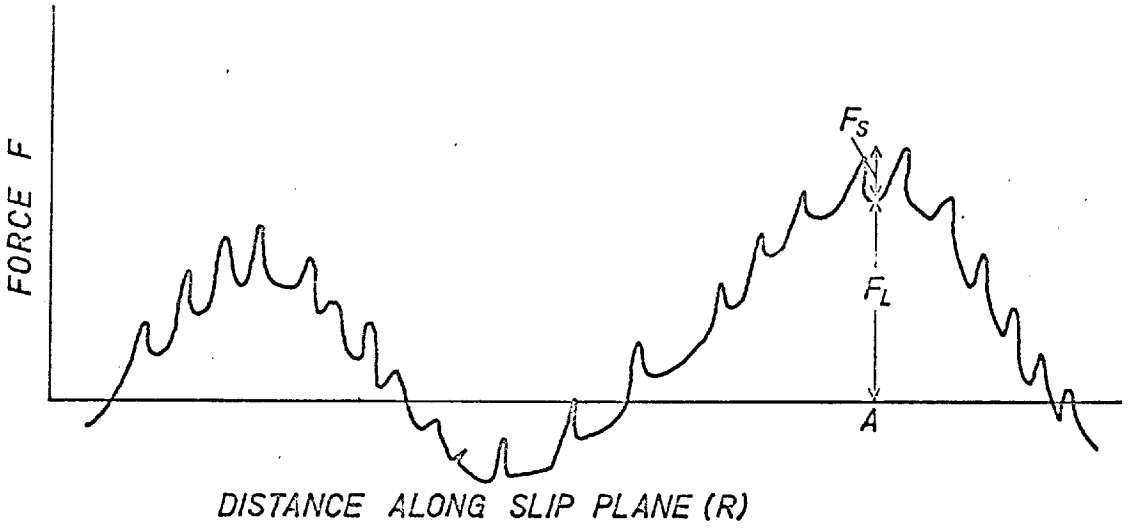

Fig. 5.1. Variation of the forces on a dislocation with distance along the slip plane (After Kronmuller 1967)

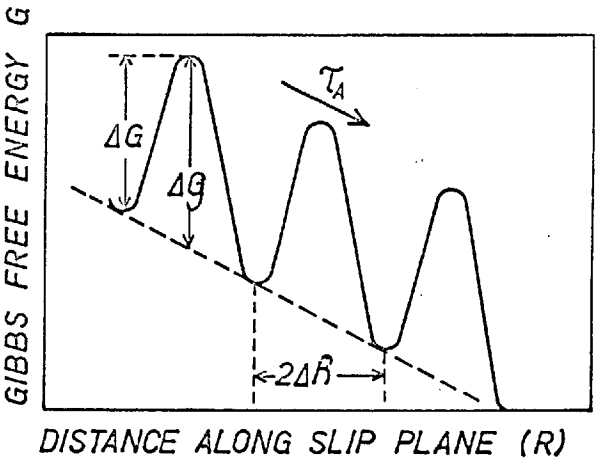

Fig. 5.2. Variation of Gibbs Free Energy along a slip plane

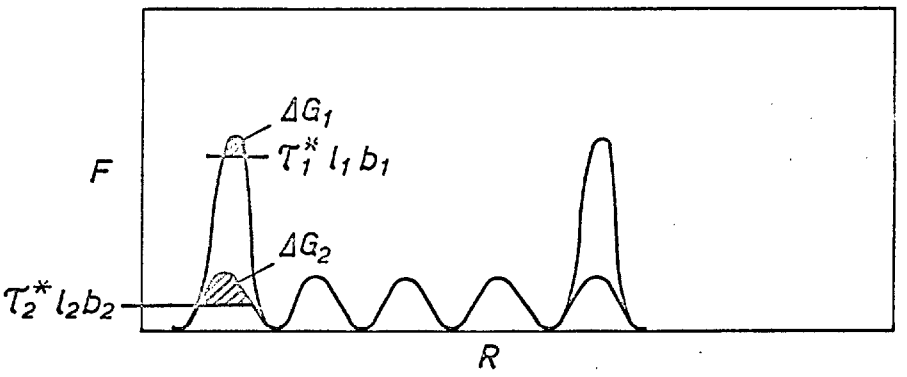

Fig. 5.3. The force - distance curve for the alternative obstacle situation.

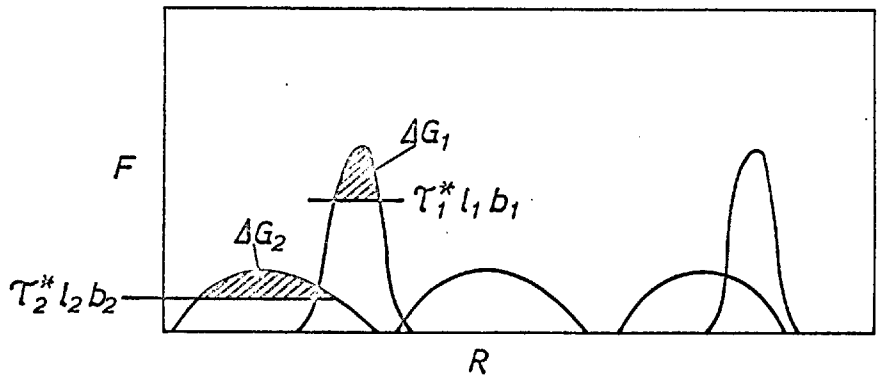

Fig. 5.4. The force - distance curve for the series obstacle situation.

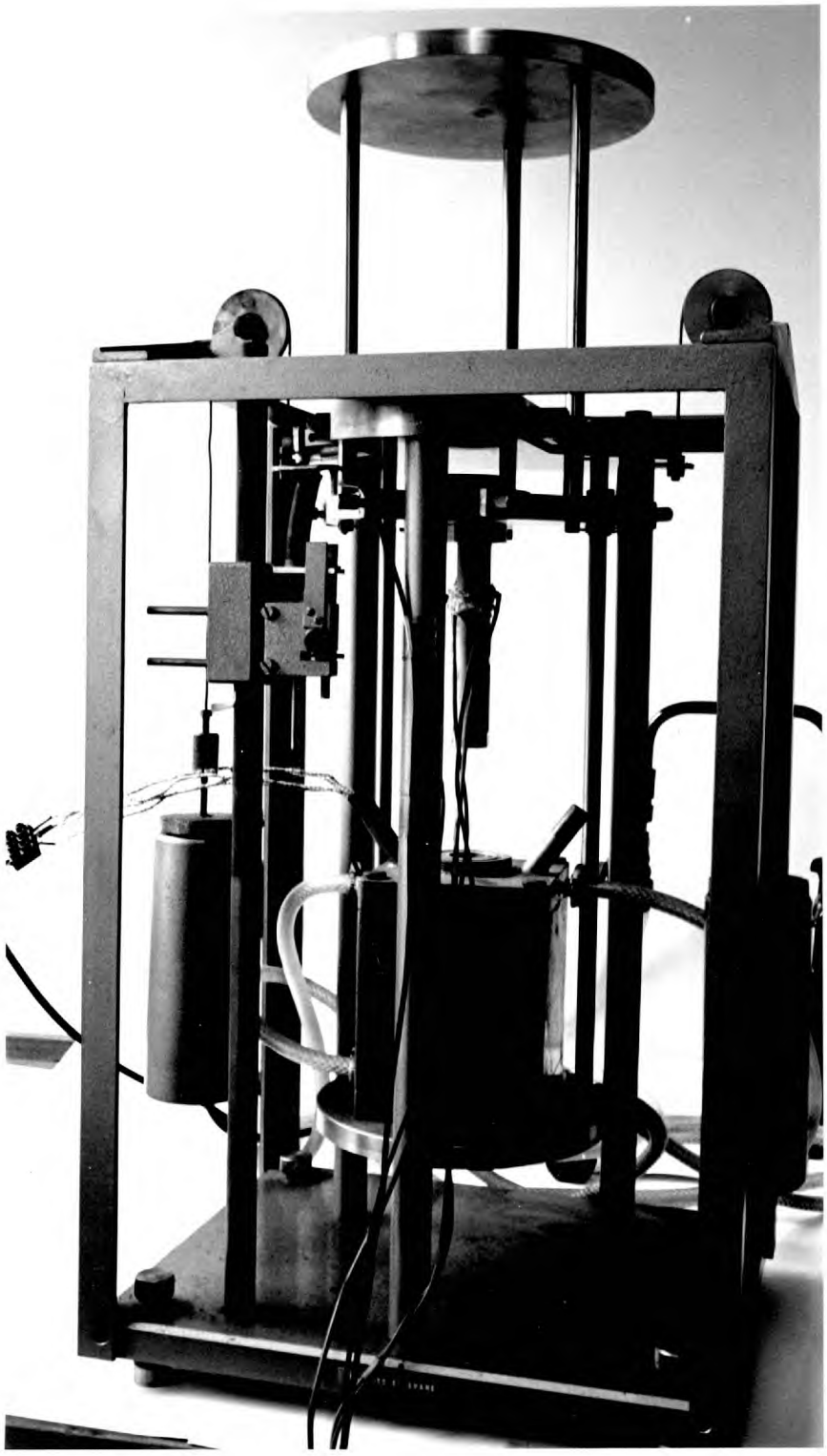

Fig. 5.5 The Creep Jig

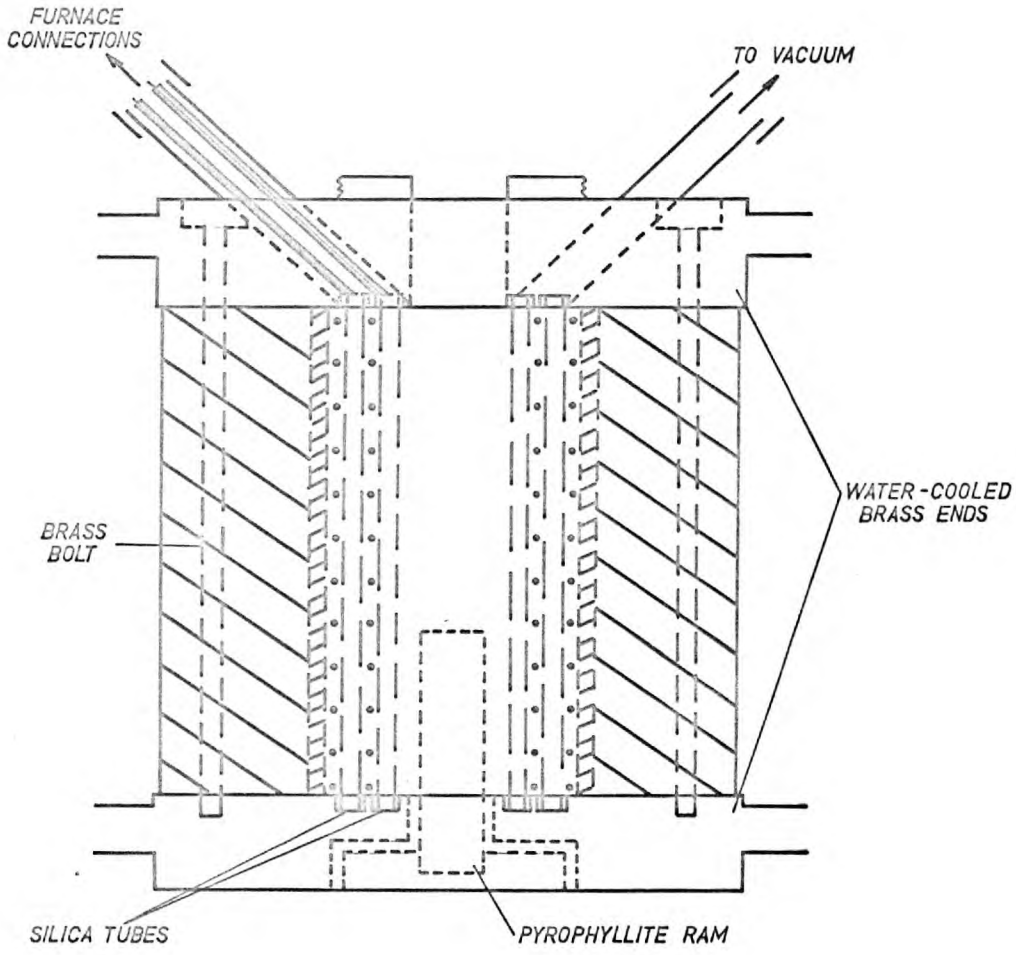

Fig. 5.6. CREEP FURNACE

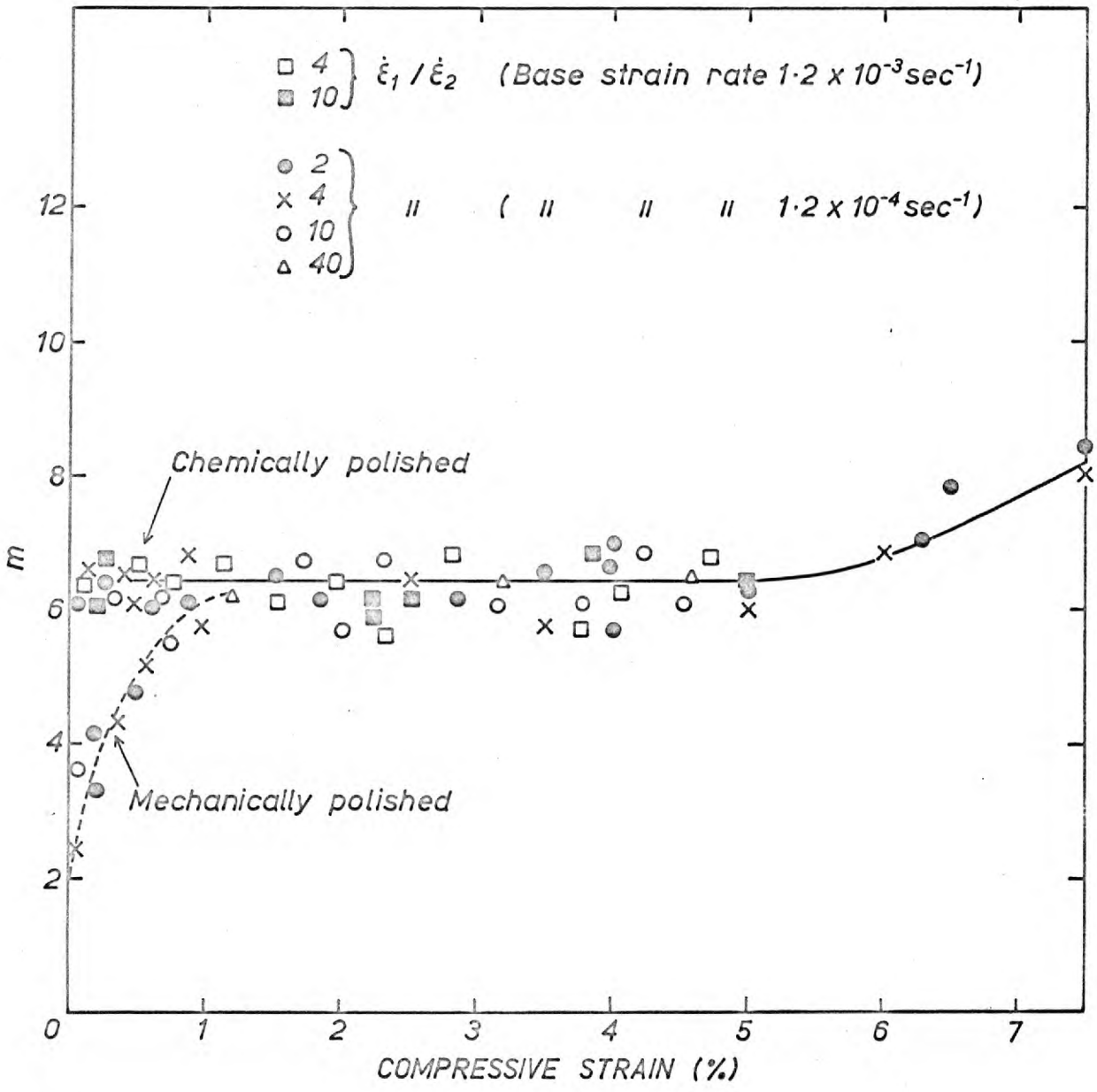

Fig. 5.7. The variation of m with strain at 110 °C

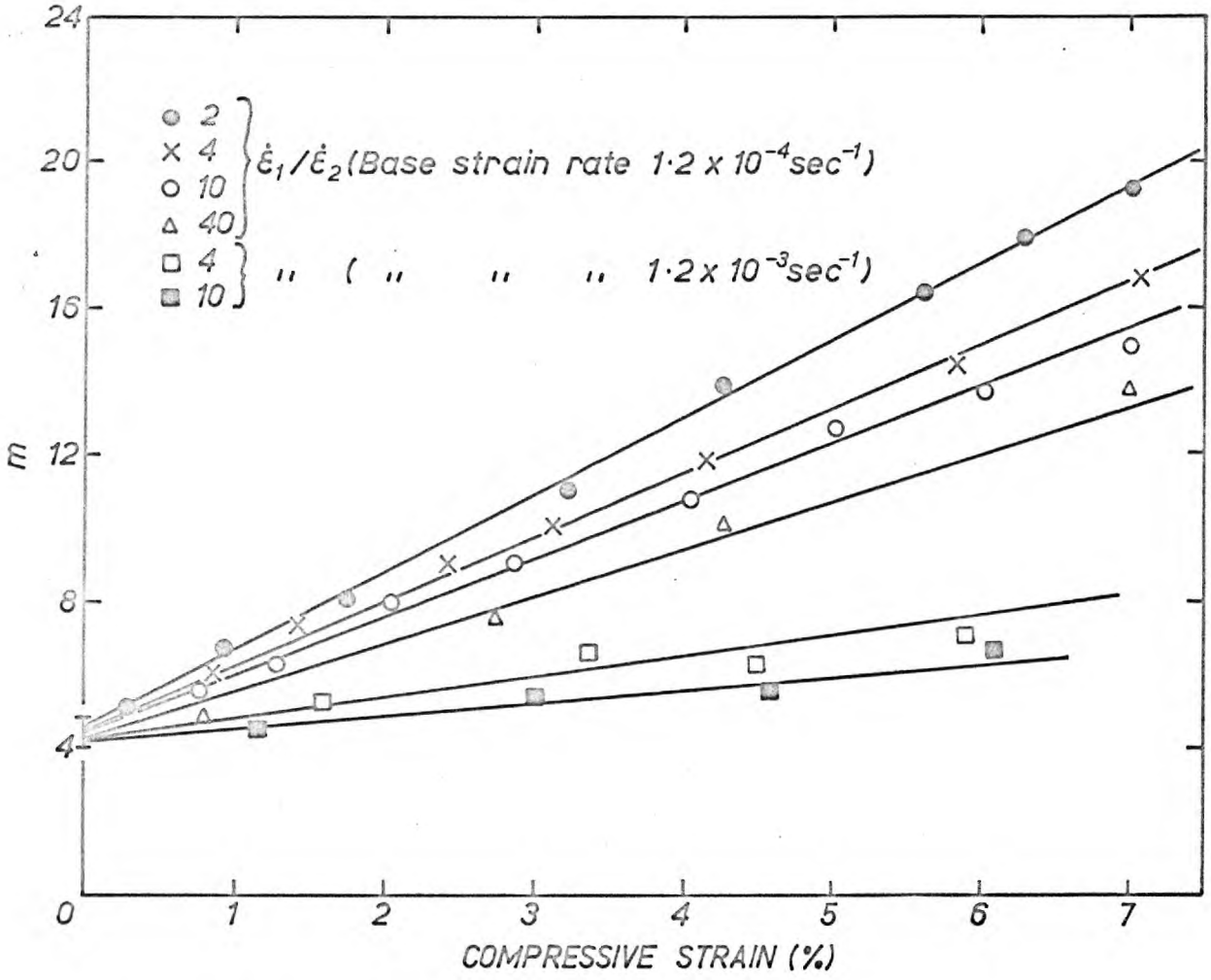

Fig. 5.8. Variation of m with strain at 170 °C

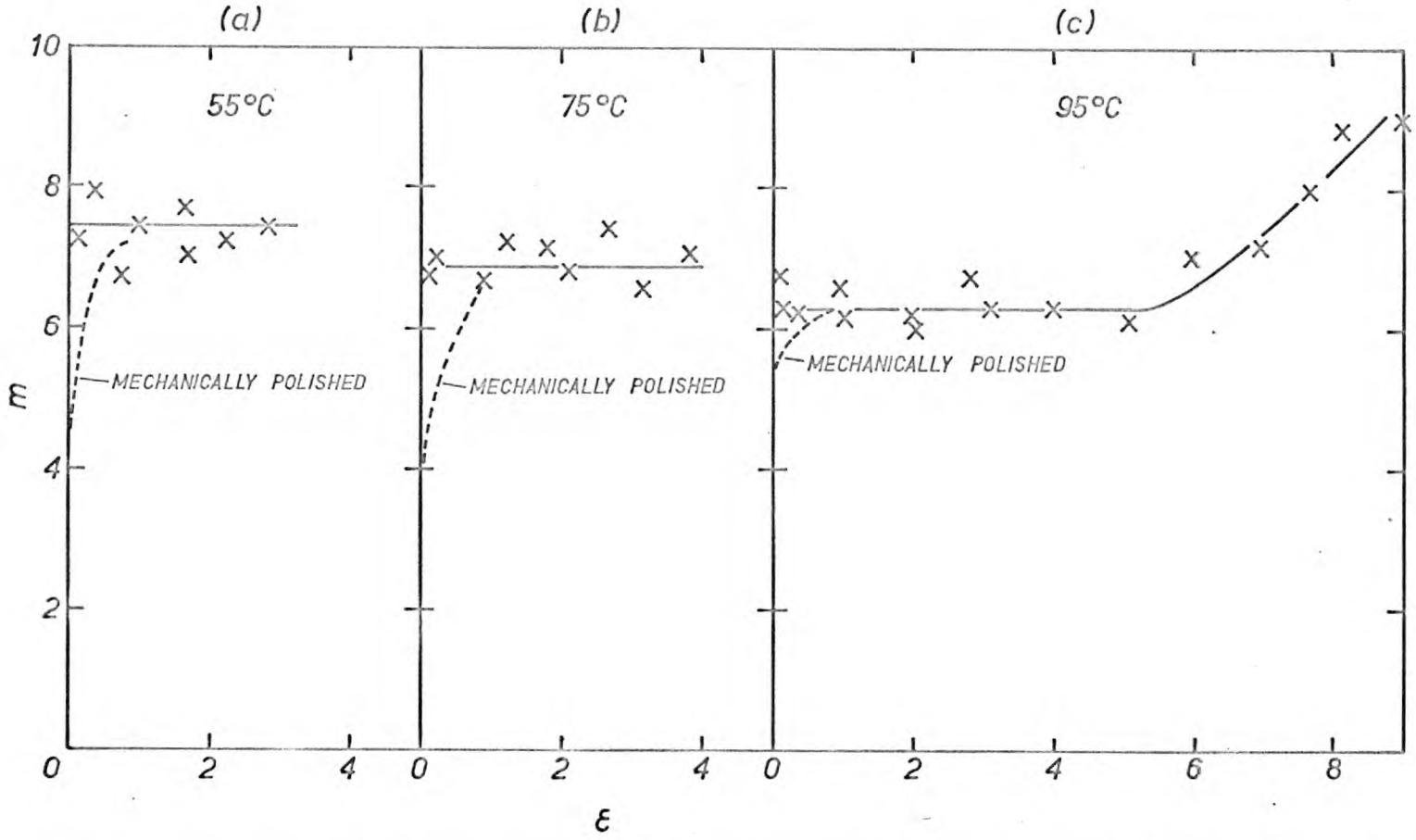

Fig. 5.9. Variation of m with strain at a strain rate ratio 4:1 (Base strain rate $1{\cdot}2 \times 10^{-4} sec^{-1}$)

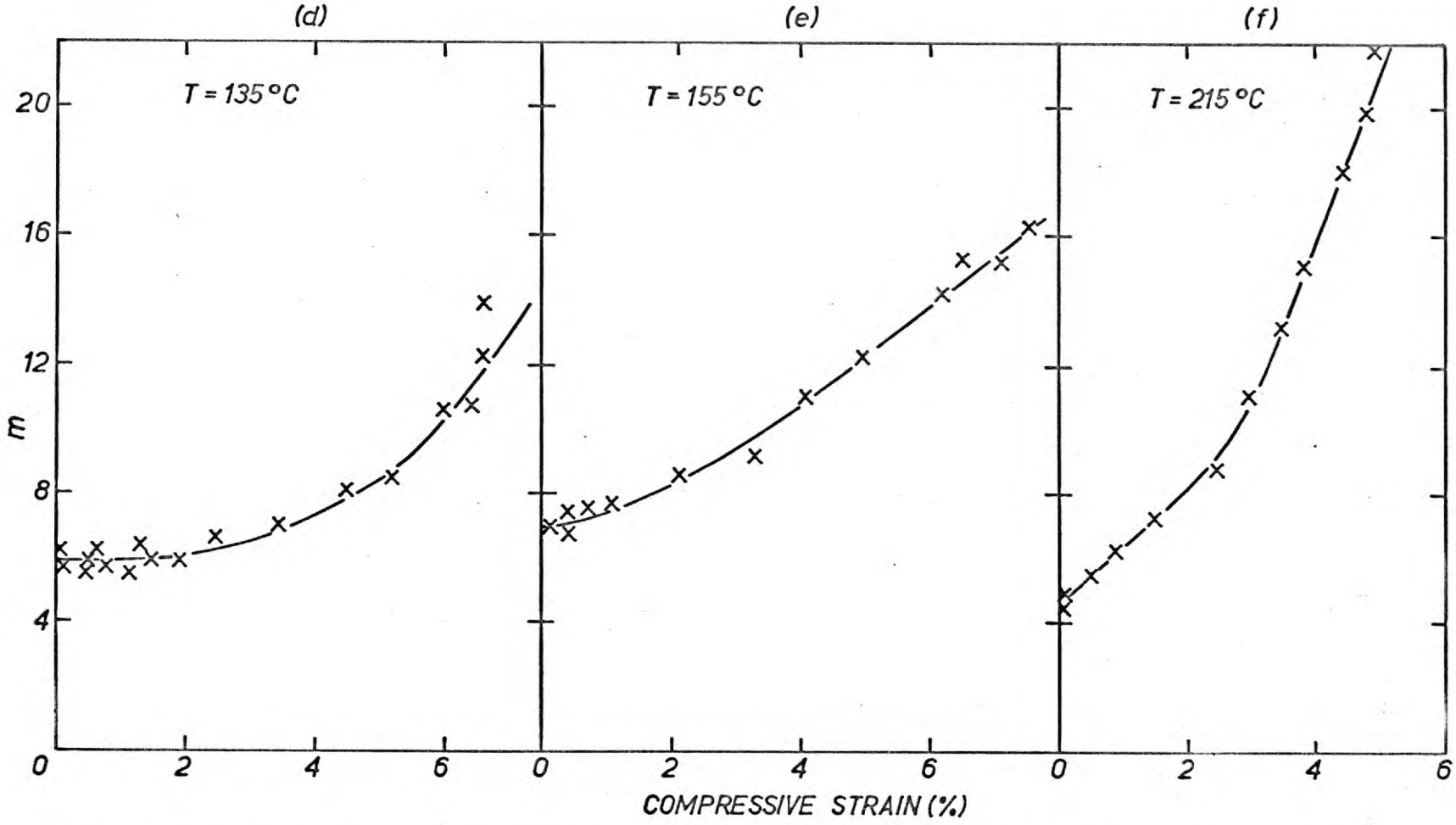

Fig. 5.9. Variation of m with strain at a base strain rate of $1{\cdot}2 \times 10^{-4} sec^{-1}$ and strain rate increment 4:1

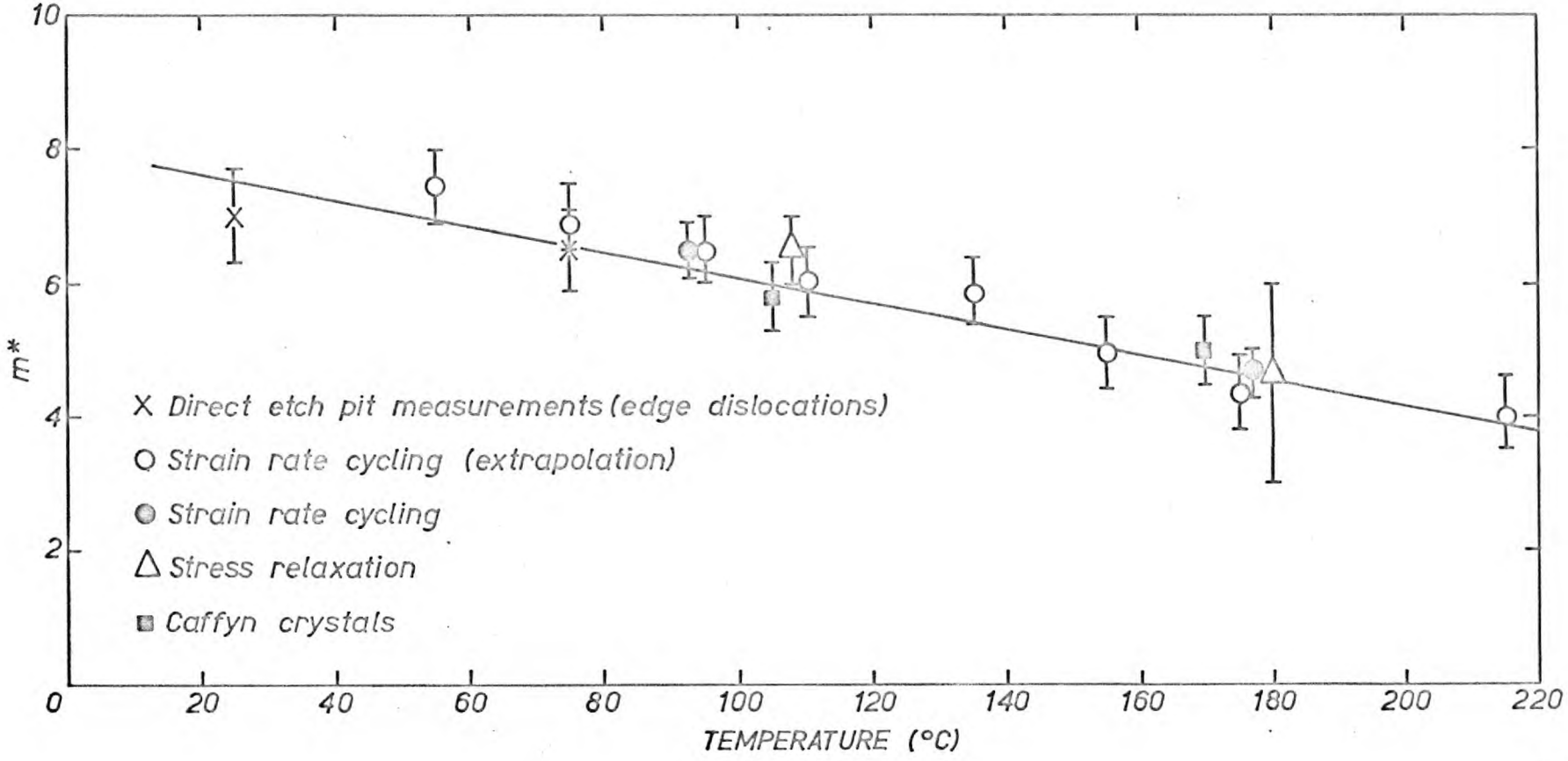

Fig. 5.10. The variation of m* with temperature for primary slip

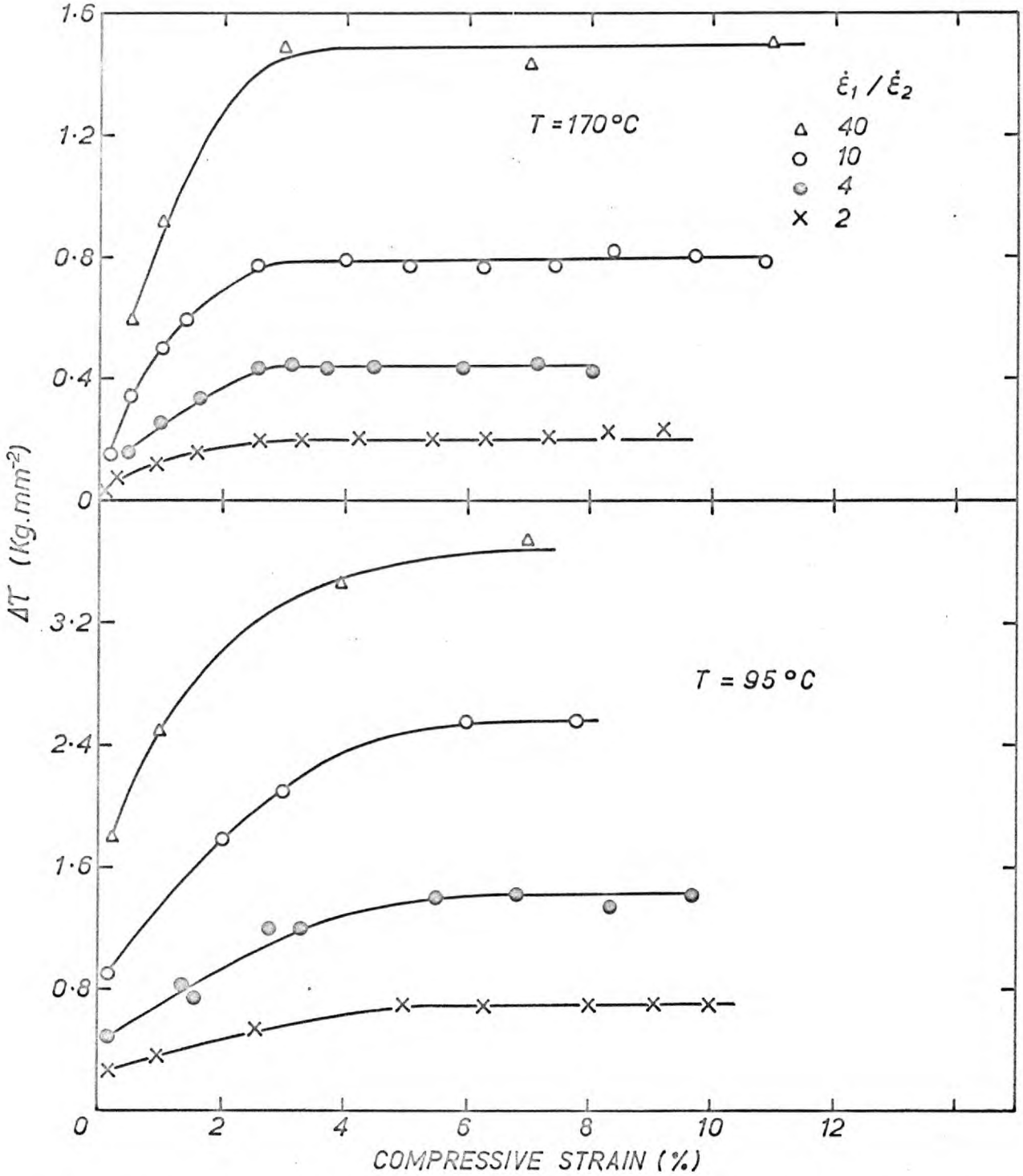

Fig. 5.11. The variation of stress increment (ΔT), obtained for a given strain rate increment, as a function of strain for various strain rate increments at 170 °C and 95 °C

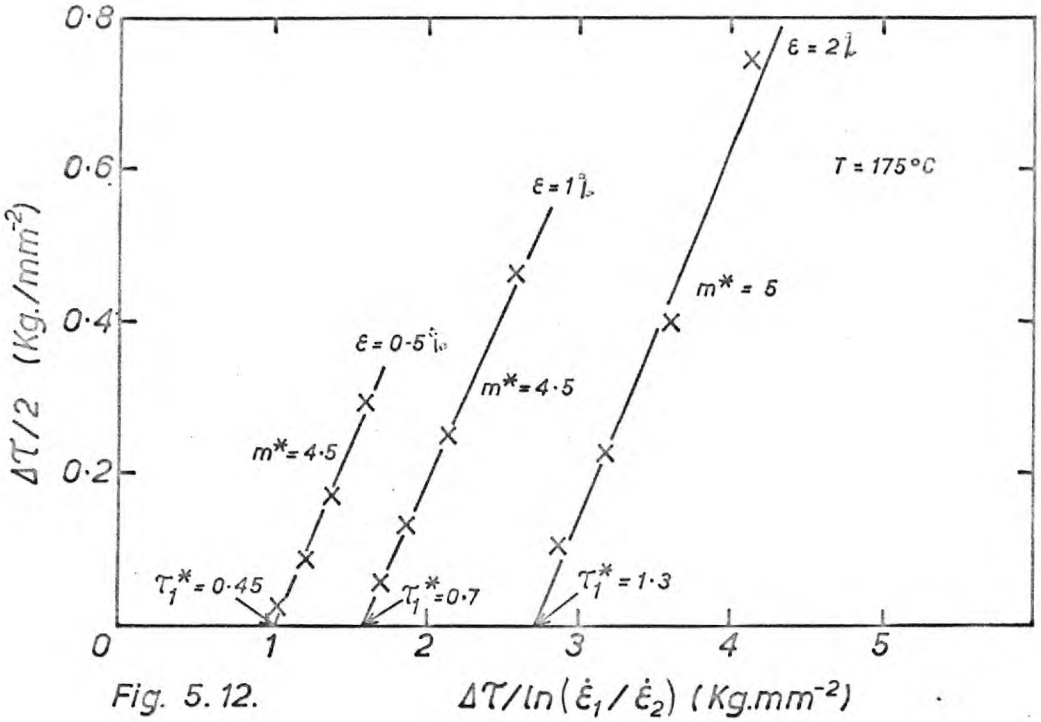

Fig. 5.12.

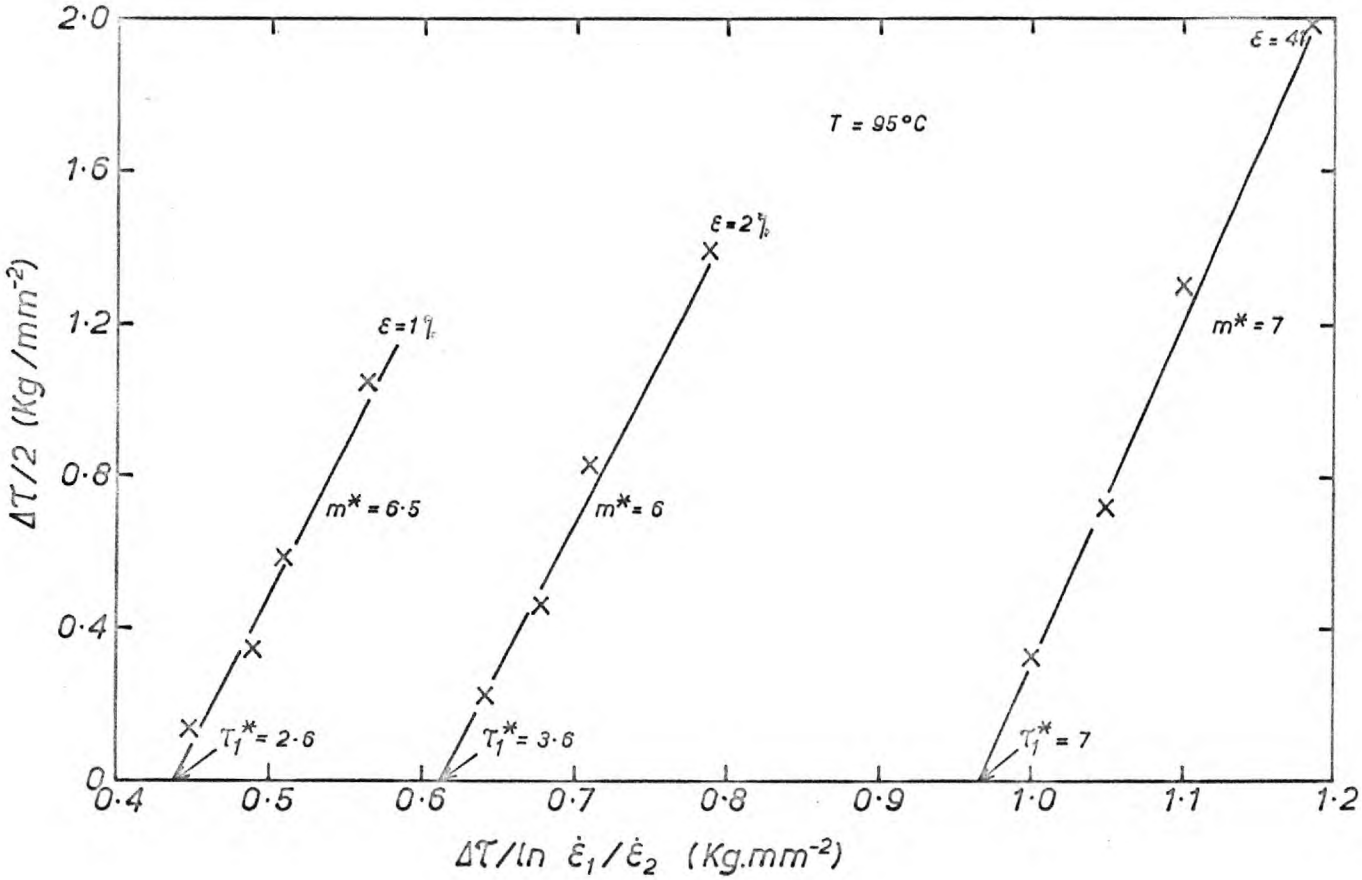

Fig. 5.13. Plots of $\Delta\tau/2$ versus $\Delta\tau/\ln(\dot{\varepsilon}_1/\dot{\varepsilon}_2)$ at various strains for given values of τ_1^* and m^*

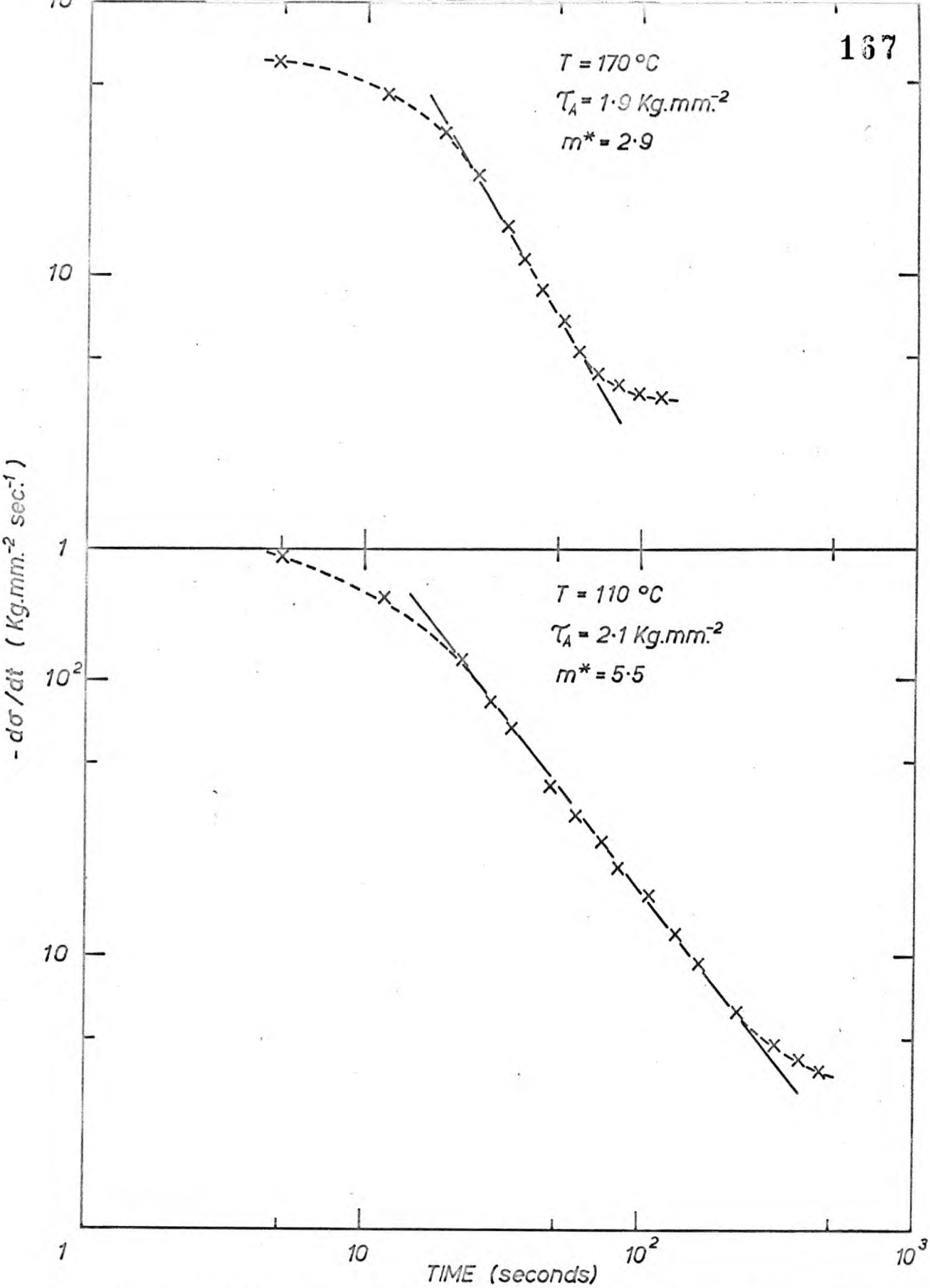

Fig. 5.14. Variation of (- dσ/dt) with time on logarithmic axis, obtained from relaxation experiments at 110 °C and 170 °C

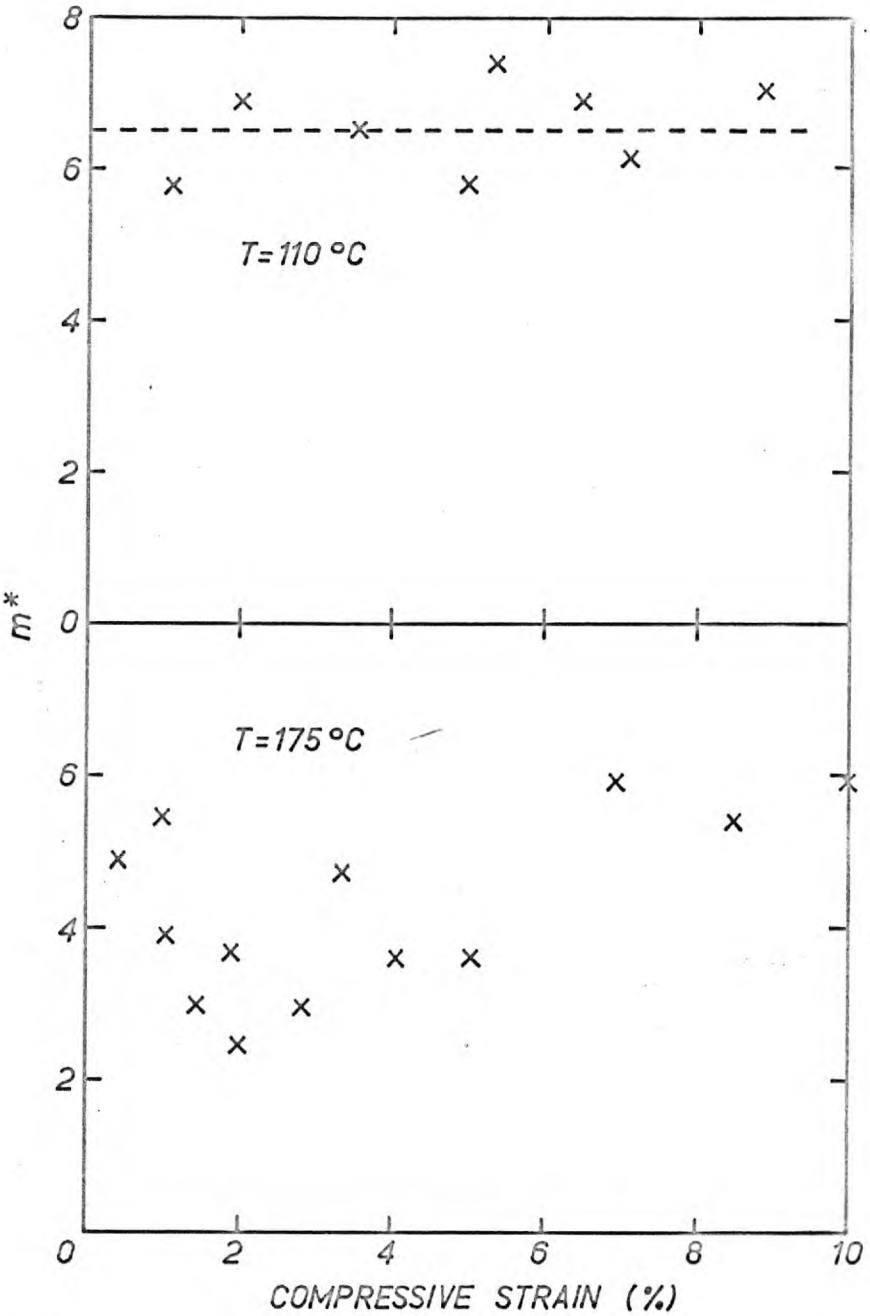

Fig. 5.15. Values of m as a function of strain obtained from stress relaxation experiments at 110 °C and 175 °C.*

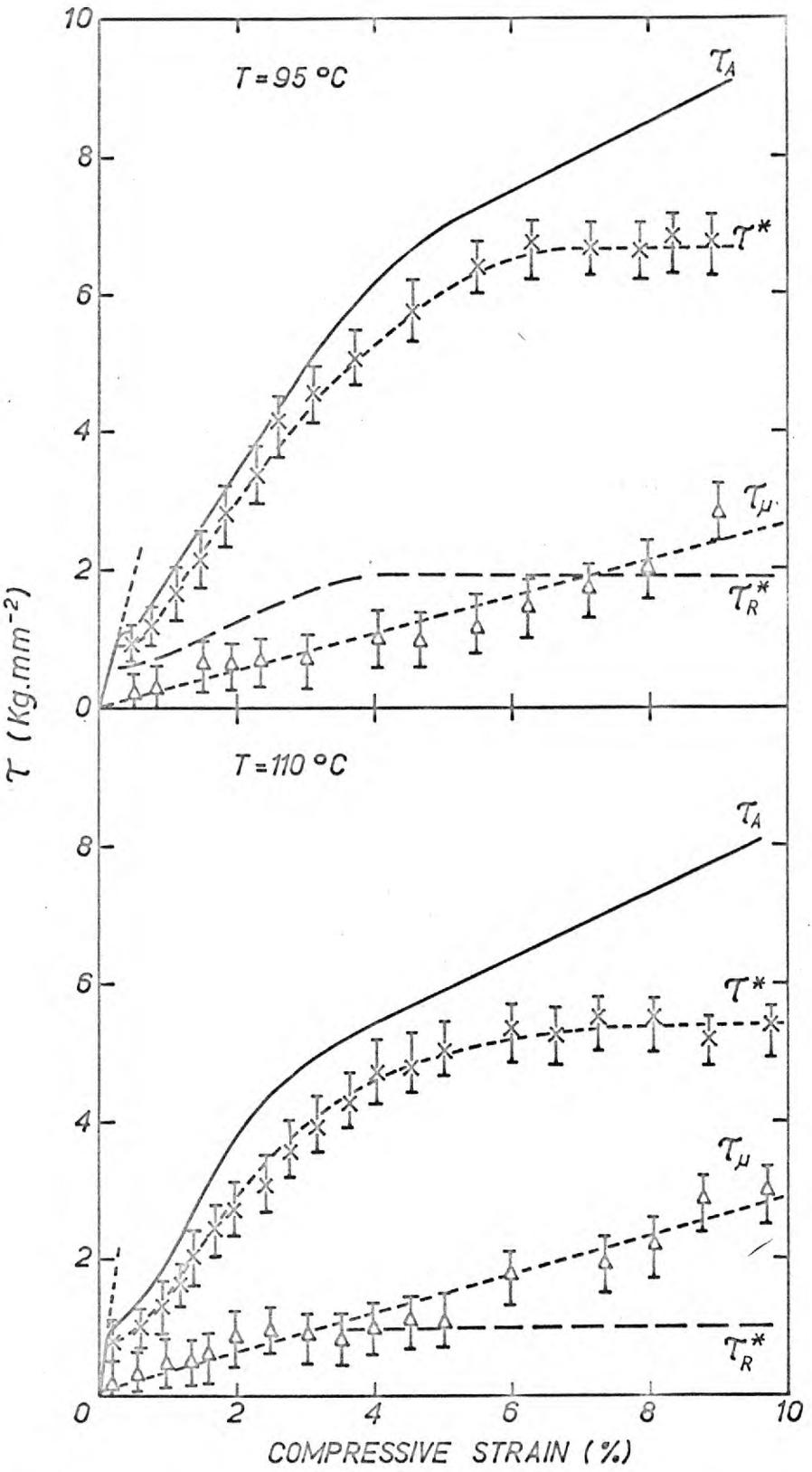

Fig. 5.16a. Variation of τ_A, τ_μ, τ^* and τ_R^* with strain for compression tests on type A crystals

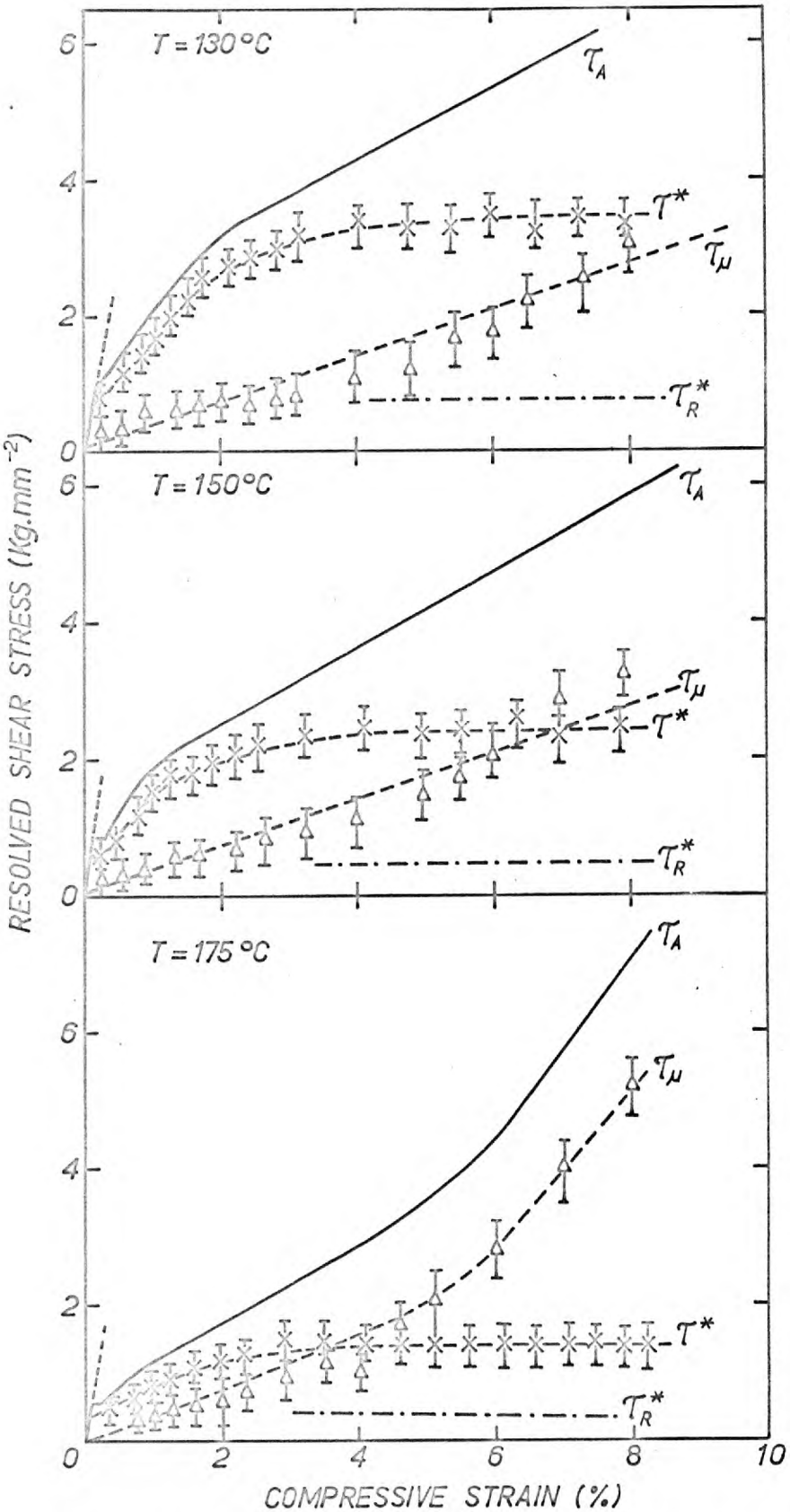

Fig. 5.16b. Variation of τ_A, τ_μ, τ^* and τ_R^* with strain for compression tests on type A specimens

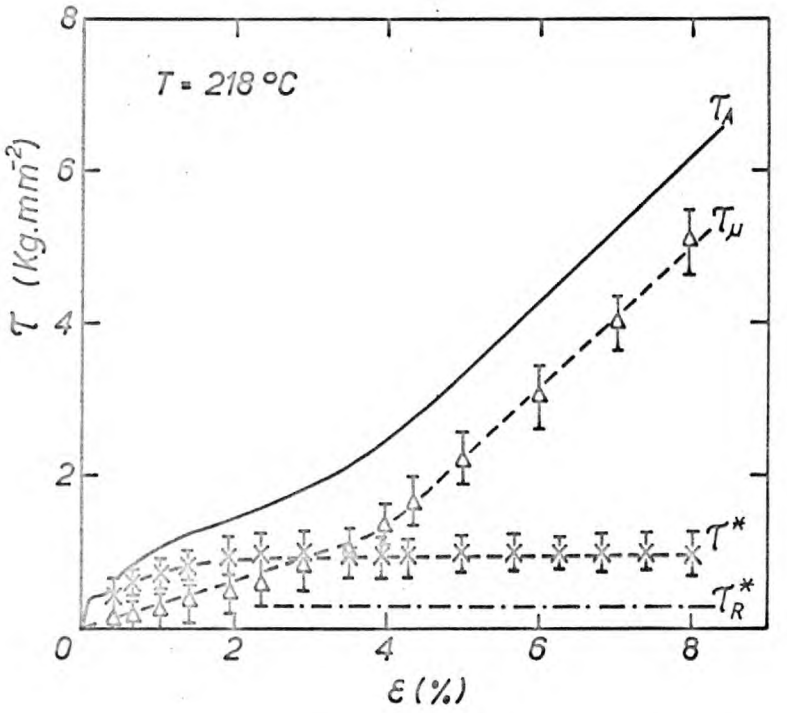

Fig.5.16c. Variation of τ_A, τ_μ, τ^* and τ_R^* with strain for compression tests on type A specimens.

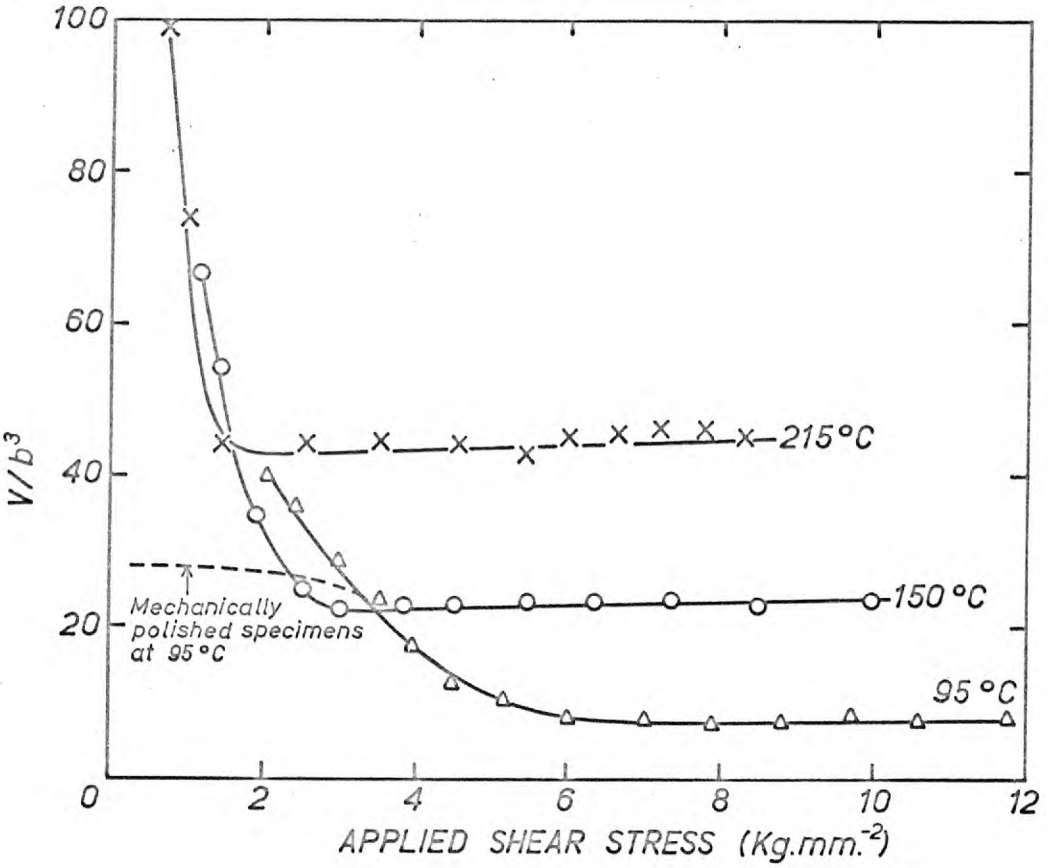

Fig. 5.17. Variation of activation volume with applied stress at a strain rate of $1{\cdot}2 \times 10^{-4}$ sec^{-1}

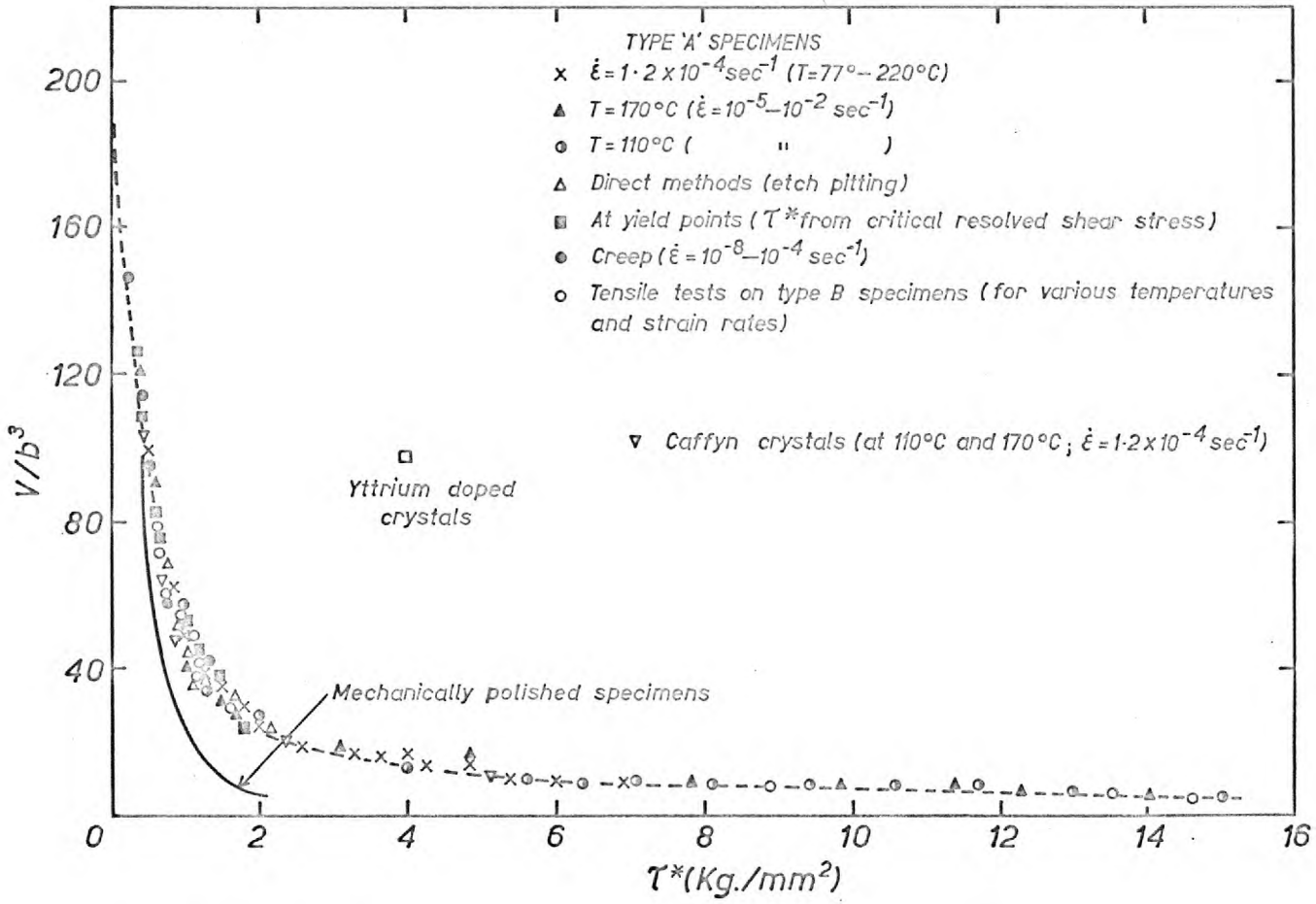

Fig. 5.18. Activation volume versus τ^* for primary slip

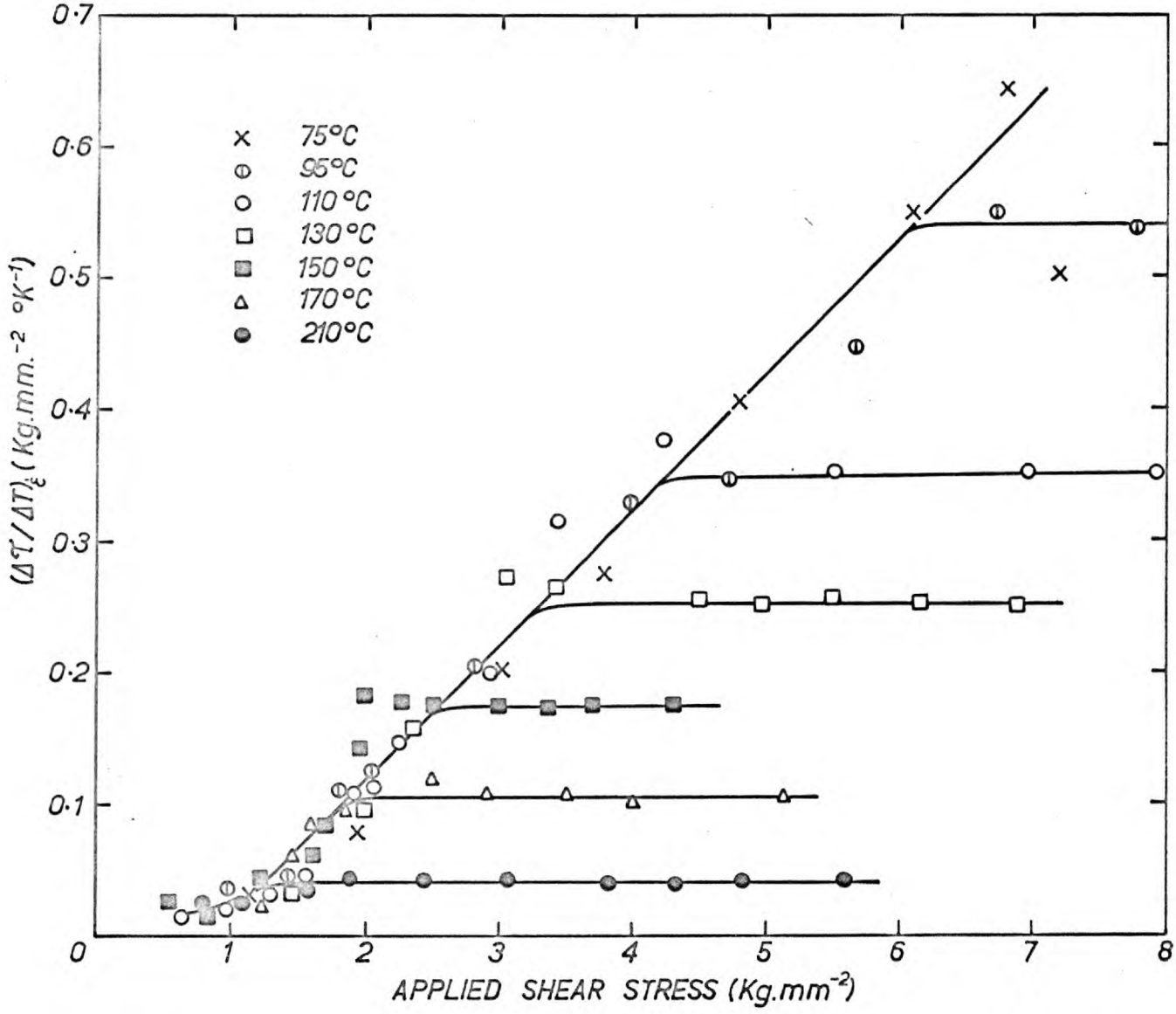

Fig. 5.19. Variation of $(\Delta\tau/\Delta T)_{\dot{\varepsilon}}$ with applied stress, at a strain rate of $1{\cdot}2 \times 10^{-4}$ sec^{-1} for a series of temperatures

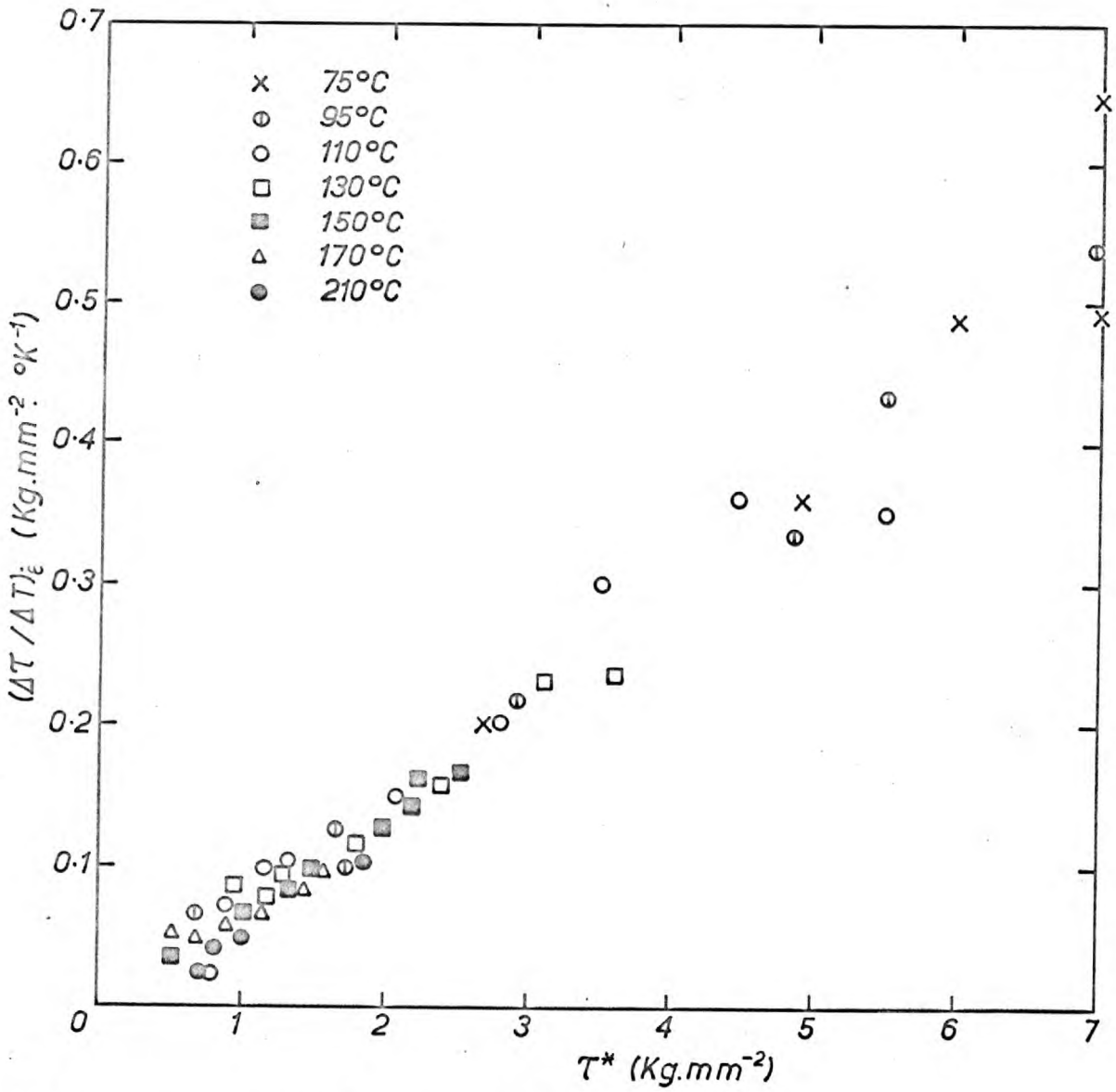

Fig. 5.20. Variation of $(\Delta\tau/\Delta T)_{\dot{\varepsilon}}$ with τ^*

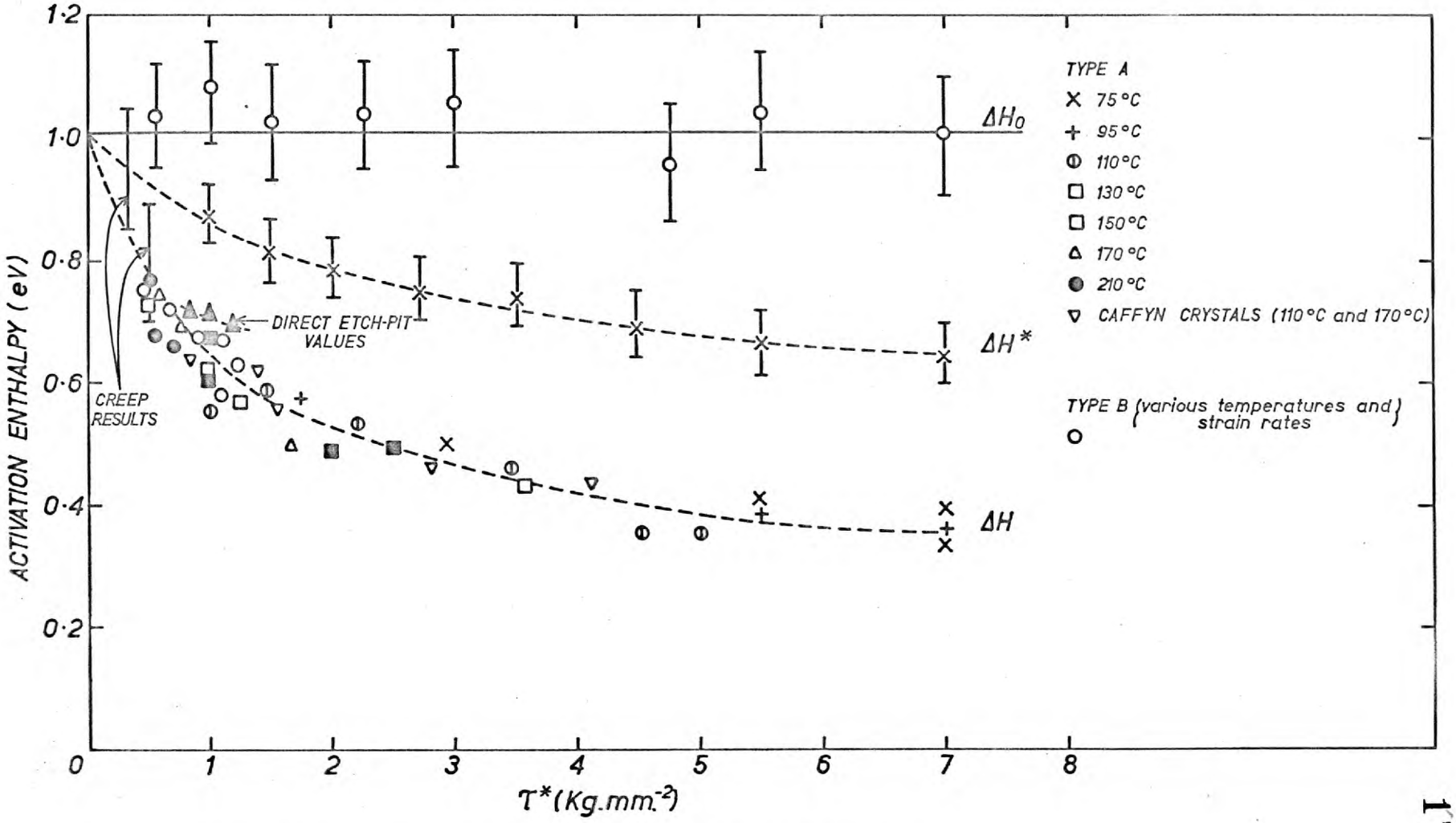

Fig. 5.21. Variation of ΔH, ΔH^* and ΔH_0 with τ^* for primary slip

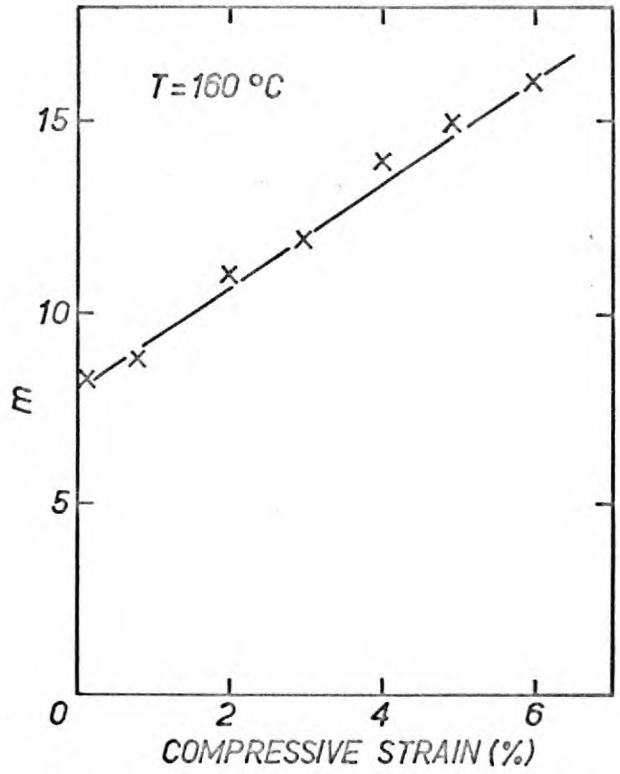

Fig. 5.22. Variation of m with strain for type C crystal at 160 °C and a strain rate of $1{\cdot}2 \times 10^{-4} sec^{-1}$

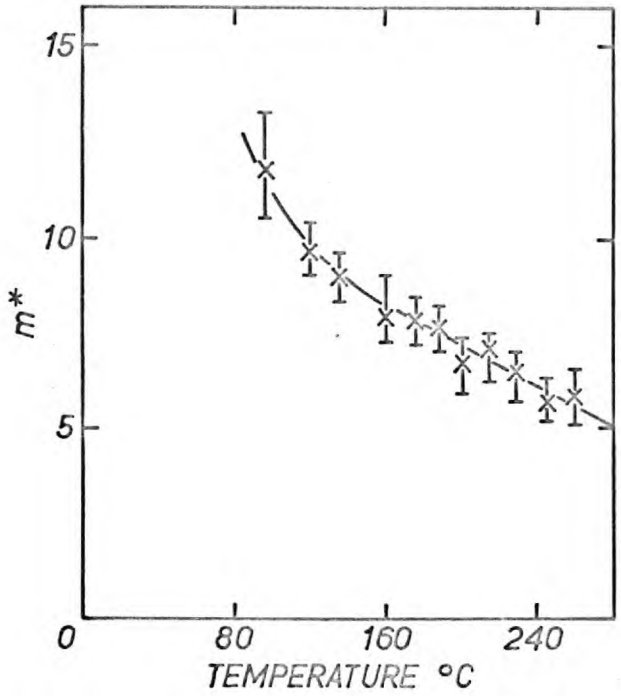

Fig. 5.23. Variation of m* with temperature for secondary slip

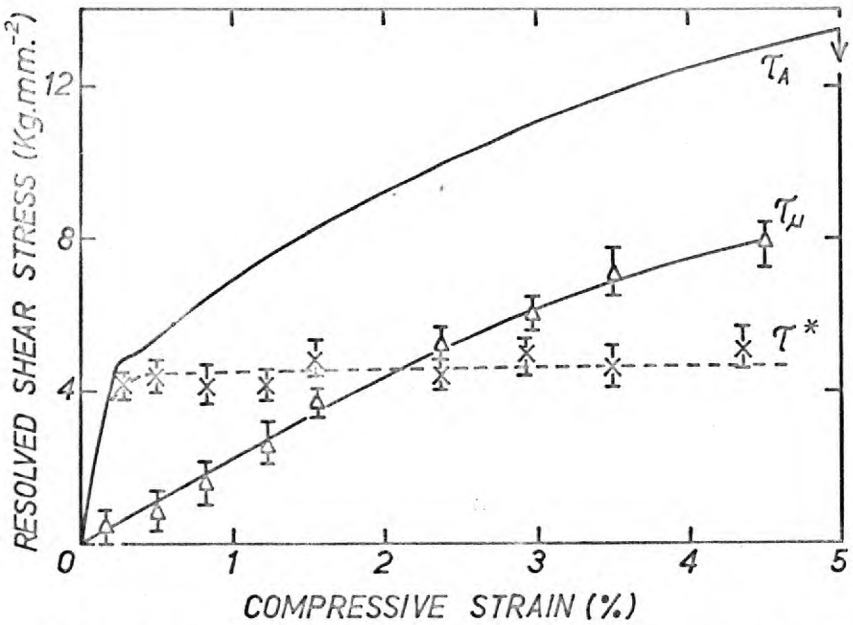

Fig. 5.24. Variations of τ_A, τ^*, and τ_μ with strain for type C crystals at 160 °C

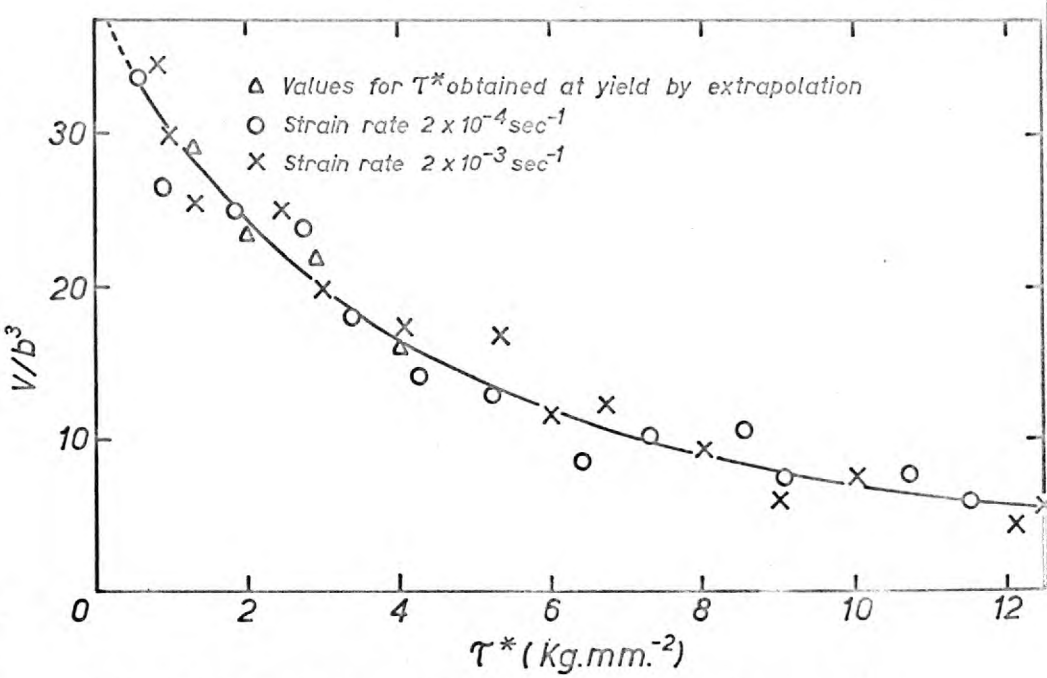

Fig. 5.25. Variation of the activation volume with stress for secondary slip

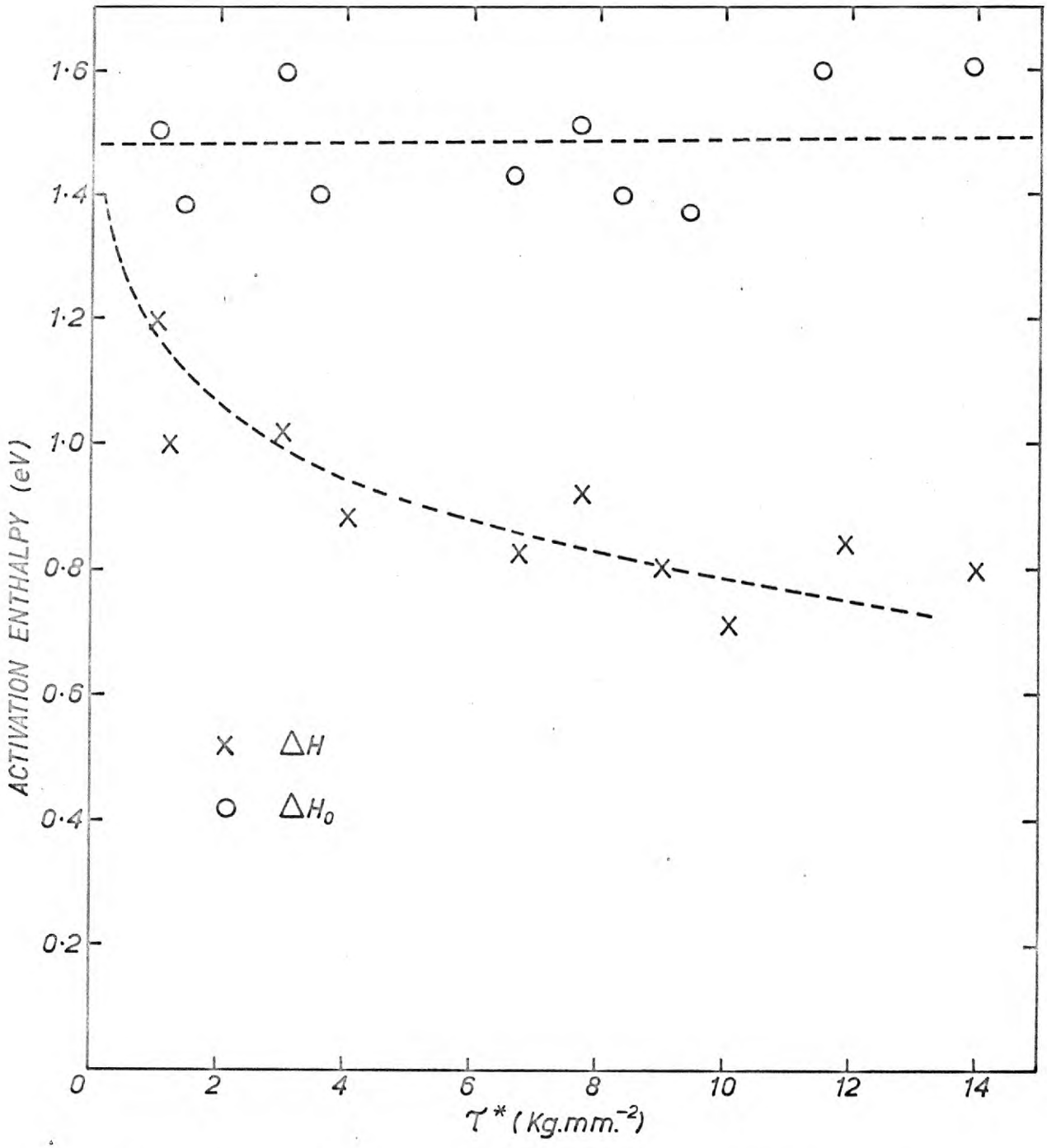

Fig. 5.26. Variation of ΔH and ΔH_0 with τ^* for secondary slip

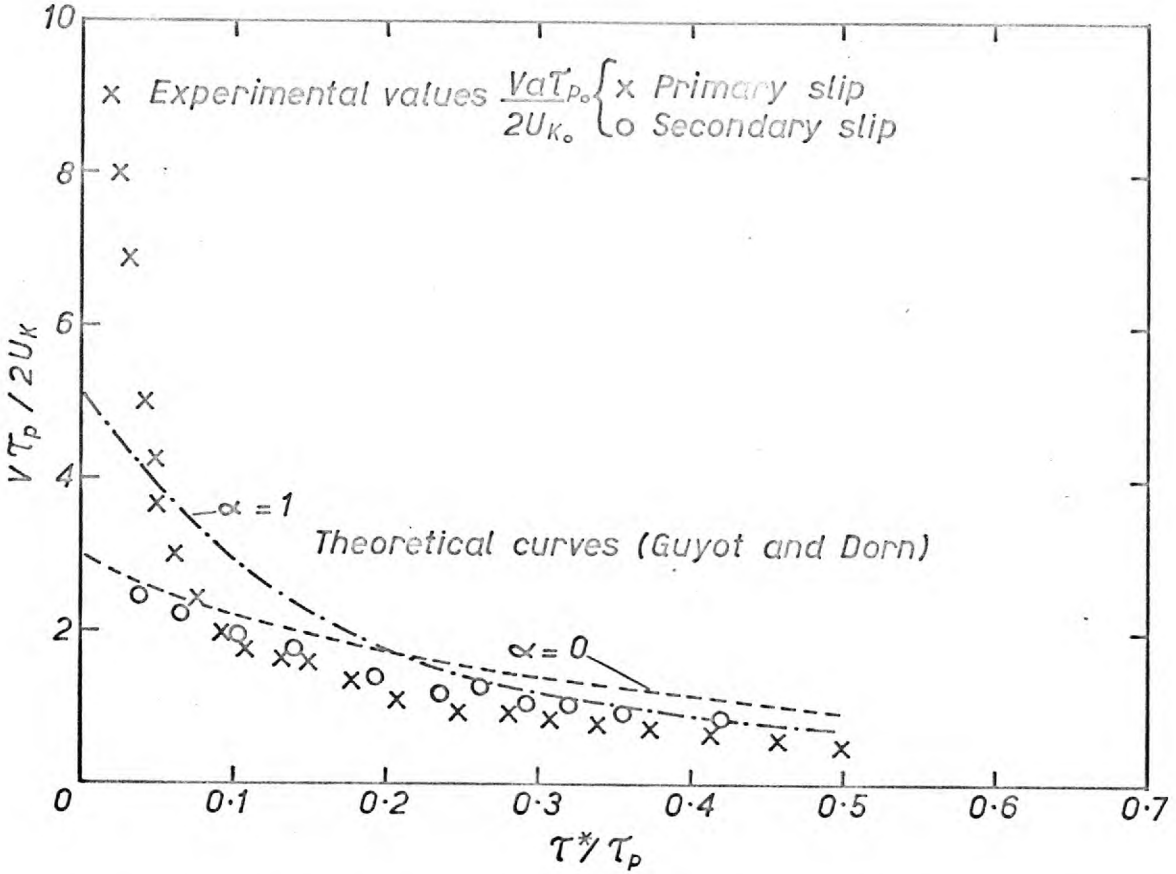

Fig. 5.27. Variation of the activation volume with thermal stress Comparison of experimental values with the theoretical predictions of the Peierls mechanism

CHAPTER 6

The Origin of the Athermal Stress

Part I

Dislocation Densities

6.I.1 Introduction

The magnitudes of the thermal and athermal stress components and their variation with strain have already been determined. In addition, the mechanisms providing the thermal stress have been tentatively identified. It is now required to determine the origin(s) of the long range stress to understand why it varies in the observed manner. In these high purity crystals this stress is provided by the dislocations themselves; its magnitude depends upon the density, distributionand shape of the dislocations. So a detailed investigation of dislocation arrangements should assist in determining the origin of the stress. Two types of investigation are required i.e. etch pit and transmission electron microscope studies. Unfortunately neither a sufficiently high voltage microscope (Evans, 1963) nor a source of in situ radition (Essmann, 1963) are available so the latter study is not possible. Consequently, the investigation is confined to etch pit studies. The method enables densities up to about $10^{8} cm^{-2}$ to be estimated and, in conjunction with the slip line and birefringence observations (Chapter 4) should provide useful information concerning the origin of the athermal stress. Unfortunately, the observed distribution of etch pits is not of great use because the dislocations are in relaxed positions after etching.

2. Theories

The athermal stress is frequently related to the total average

dislocation density (Nt) according to the expression:-

$$\tau_\mu = A\sqrt{N_t} \qquad - 6.1$$

where $A = \alpha \mu b$, α is a constant that depends upon the distribution of the dislocations.

This relationship is an empirical one found invariably in f.c.c. metals (e.g. Hordon, 1962; Livingston,1962; Basinski and Basinski,1964) and occasionally in ionic crystals (Haasen and Hesse, 1963; Davidge and Pratt, 1964). In f.c.c. metals values of α obtained vary from 0.2 to 0.5, similar values are obtained for all orientations and for polycrystals (e.g. Copper, Wiedersich, 1964). In ionic crystal, NaCl has been studied in some detail by Hesse (1966,1967). He finds that A is both temperature and strain rate dependent below 250°C with values of α ranging from 0.4 to 0.8.

This relationship is not observed in stage II in ionic crystals (Hesse, 1967) nor in certain b.c.c. metals (e.g. Mo, Guiu, 1964). In the former a linear relationship between dislocation density and applied stress is observed. Gilman and Johnston (1960) also find a linear variation in LiF throughout the deformation.

All theories are developed to fit these empirical relationships. The theories have been confined almost entirely to the explanation of the parabolic relationship in f.c.c. metals; it is considered expedient to review the theories briefly at this stage.

The first theory was developed by Taylor (1934), he considered the interaction of dislocations with the stress field of random arrays of parallel dislocations. Saada (1960) shows that the theory gives a value of $\alpha = 1/2\pi$. Experimental values of α generally differ from this so alternative theories have been developed using more realistic dislocation distributions e.g. Hazzeldene (1967), Kronmüller (1967), Seeger (1958)

Hirsch and Mitchell (1967), Jackson and Basinski (1967), Hirsch (1960) Kuhlmann-Wilsdorf (1962).

The most satisfactory theories are those of Seeger and Kronmuller and Hirsch and Mitchell, both theories attribute the athermal stress primarily to the interaction of dislocations with the stress field of other dislocations. The theories disagree about the proportion of the stress derived from the dislocations on the slip planes of maximum resolved stress ('primary' planes) and the other slip planes ('secondary' planes). Seeger suggests that the stress is provided almost entirely by the back stress from 'primary' dislocation pile ups whilst Hirsch requires the stress to be derived from complex 'obstacles' consisting of 'primary' and 'secondary' dislocations of various mechanical signs. The other theories e.g. jog theory (Hirsch, 1960) and forest interaction theory (Hirsch 1958) do not provide a suitable means of effectively blocking dislocations as is required by the slip line observations (Hirsch and Mitchell) so are not entirely satisfactory. Thus any athermal stress theory must provide suitable blocking obstacles; this is discussed in more detail in section I.5.

Gilman and associates have developed a theory to explain Gilman and Johnston's observations in LiF. The theory is based upon the interaction of dislocations with dislocation dipoles; this is also considered in Section I.5.

It is now required to establish density stress relationships for calcium fluoride and, hence, to determine whether the observed athermal stress variations can be explained using existing theories or whether new theories have to be developed.

II.3 Experimental

Before starting an etch pit density investigation of this sort it must be established that there is a 1 : 1 correspondence between dislocations and etch pits.

I.3.1 Correspondence between Etch its and Dislocations

Firstly, the correspondence between etch pit and birefringence bands indicates that the pits are associated with dislocations. Successive polishing and etching of the surface enables the pits to be identified with line defects only i.e. no point defects, this is shown clearly by comparing the etch pits on opposite faces of a cleaved surface. Similar observations were made by Gilman and Johnston (1962) in LiF. An exact correspondence between pits and dislocations has been shown in LiF by Newkirk (1959) and Yoshimatsu and Kohra (1960); they detected dislocations using X-rays and found that each dislocation intersecting the surface was associated with an etch pit (and there were no additional pits). Thus, by analogy, it can be assumed that there is a 1 : 1 correspondence in calcium fluoride.

I.3.2 Specimen Preparation and Testing techniques

Most tests are conducted in compression, so B orientation compression specimens with dimensions 8 x 2.5 x 1.5 mm^3 are prepared as described in Chapter 4.

The crystals are compressed to a certain stress at the test temperature; good alignment is ensured by superimposing a hemispherical ball between the specimen and upper compression plate. It is unloaded and cooled slowly to room temperature to avoid inducing quenching stresses that might alter the density and distribution of the dislocations. The specimen is then cleaved along $\{111\}$

containing the stress axis; this does not introduce a significant quantity of additional dislocations. The cleaved faces are etched in concentrated sulphuric acid maintained at 45°C (the etching time varies from 5 to 30 seconds).

Etch pit counts are conducted over the central region of the crystal so that any effects associated with the inhomogeneous deformation region near the compression plates are eliminated. Provided the strain is not large i.e. less than about 10%, the shape of the crystals does not alter significantly during the deformation so shear stresses along the slip planes can be determined directly from the applied stress. The general tendencies of the results are confirmed by conducting a few tensile experiments where the stress system is perfectly homogeneous throughout.

I.3.3 The Relation between Etch Pit and Dislocation Densities

Reference to fig. 2.13 reveals that the dislocations intersecting $\{111\}$ are the screw dislocations lying on the 'primary' plane (density NSp) and edge dislocations (NEs) and dislocation dipoles (NDs) on the 'secondary' planes. The existing theories relate the athermal stress either to the total dislocation density on the 'primary' plane (Np = NEp + NSp) or the total dislocation density (Nt = Np + Ns). So approximate values of Nt are required in terms of the etch pit density (N). This may be achieved as follows.

a. In tensile experiments slip occurs almost exclusively on the 'primary' system and the density of dislocations lying on the 'secondary' planes may be quite low. Thus, etch pit counts on these crystals give approximate values of NSp (on $\{111\}$) and NEp + NDp (on $\{110\}$).

b. If it is assumed that the shape of a dislocation loop depends upon the relative velocities of edge and screw dislocations (this requires that the athermal stress should be the same at edge and screw dislocations) then the ratio of the length of edge to screw dislocation is given by Us/Uc. Thus, (Chapter 3)

$$NE_{P,S} \approx 2NS_{P,S} \qquad - 6.2$$

This also assumes that annihilation of screw dislocations by cross glide does not occur.

c. Etch pit densities are also measured on $\{110\}$ of the compression specimens to give a value of (NEp + NDp + NSs)

Now, let,

$$NSp + NEs + NDs = N_1 \qquad - 6.3$$

it must be remembered to include the appropriate orientation factors for each slip plane with respect to the plane of measurement.

Also, let,

$$NEp + NDp + NSs = N_2 \qquad - 6.4$$

From tensile tests, $\frac{NDs}{NEs} = \frac{NDp}{NEp} = \frac{N^1Ep + N^1Dp - N^1Sp}{2N^1Sp} = N_3 \qquad - 6.5$

These give; $$N_t = 3(N_3 - 2N_2 - 1)\ \frac{N_1 - 2N_3(1+N_2)}{1-4(1+N_2)} \qquad 6.6$$

Thus, an approximate value of Nt may be found in terms of the etch pit densities.

I.4 Results

Etch pit densities are measured as a function of strain at two temperatures (110°C and 170°C). At the higher temperature, almost immediately after yield, a random distribution of dislocations is observed throughout the specimen, with a density variation of less that 20% over different parts of the central region. At the lower

temperature a banded structure is observed up to strains of about 0.8% whilst at higher strains the distribution is almost perfectly random again with density variations of up to 25% encountered over the central region of a crystal; the results quoted at low strains are average values taken over a large number of banded and dislocation free areas.

The etch pit densities are plotted against strain on logarithmic axes in figs. 6.1a,b. There are two distinct regions, one corresponds to all stages up to the start of stage II whilst the other corresponds to stage II itself. The former has a slope of 0.6 ± 0.1 whilst that of the latter is 0.9 ± 0.2.

The stress dependence is of a more interest, so plots of etch pit density against applied stress, on logarithmic axes, are shown in figs.6.2a,b. There is no obvious relationship, However, as shown in Section I.2 the dislocation density need only be related to the athermal stress, so values of τ_μ (obtained in the last Chapter) are plotted against the etch pit density, also in figs. 6.2a,b. A linear relationship is observed in stages I, at both temperatures, with a slope of 0.5 ± 0.1. In stage II another relationship is observed, it is approximately linear with a slope of 0.9 ± 0.2. Thus, in stages I, the athermal stress is related to the dislocation density according to equation 6.1 whilst in stage II they are related approximately linearly.

Having established these relationships, stages I are looked at in more detail. The next objective is the determination of the constant α, so values of Nt are required; These are determined as described in the previous section.

Firstly etch pit counts on $\{110\}$ are made. It is found that N_1/N_2

is virtually constant in stages I (c.f. NaCl, Hesse, 1966) and equal to 1.8 ± 0.2; in stage II it increases slightly with strain.

From the tensile tests conducted at 170°C, counts are made on $\{111\}$ and $\{110\}$ faces; the ratio of etch pit densities is again independent of strain with, $\frac{N^1Ep + N^1Dp}{N^1Sp} = 2.1 \pm 0.2$ (e.g. figs. 6.3.a,b)

Thus, very few of the dislocation dipoles formed actually etch, an indication that only narrow dipoles are formed (c.f. Davidge and Pratt) It does not indicate that dislocation dipoles are not created, see Appendix I.

So for the purposes of this investigation $ND \approx 0$

Thus, from equation

$$Nt \approx 3.3 \blacksquare_1 N_1 - 6.7$$

for all strains used

These are evidently only very approximate because a number of the assumptions are not strictly valid but still give an indication of the appropriate factors.

Now plots of τ_μ against $\sqrt{Nt}$ are constructed, figs. 6.4a,b. The slopes in stages I give a value of α; within the quite considerable range of error, similar values are obtained at both temperatures, giving

$$\alpha = 0.32 \pm 0.06$$

The validity of the experiments is confirmed by plotting values of τ_μ against $\sqrt{Nt}$ obtained from tensile experiments at 170°C. Slightly smaller values of Nt are obtained for a given $\tau_A (\tau_\mu)$ but the general tendencies are similar. The results give a value of α within the range 0.2 to 0.3 (fig. 6.4b)

It is not possible to obtain sufficient results in stage II to establish a more precise relationship.

A.5 Discussion

It is established that the applied shear stress in Stages I hardening in calcium fluoride is given by:-

$$\tau_A = \tau^* + 0.32\mu b\sqrt{Nt} \qquad - 6.9$$

The hardening in stage II is not so well established but is given approximately by:-

$$\tau_A = \tau^* + KNt + C \qquad - 6.10$$

where K and C are constants.

Hesse (1967) has found the following relationship applies for NaCl, under all conditions:-

$$\tau_A = A\sqrt{Nt} + BNt \qquad - 6.11$$

where A and B are constants

If the thermal stresses are taken into consideration this relationship also fits approximately the results obtained in calcium fluoride.

The problem in the identification of the origin of the athermal stresses is the additive nature of these stresses, so that the contributions from a number of separate sources often have to be considered. Also of importance is the relative physical positions of the obstacles contributing to this stress; for instance, possible line tension contributions might only be apparent in regions where pile up stresses can assist the applied stress, so they do not contribute to the observed athermal stress (e.g. dislocation sources, Nabarro, 1964). Without knowing in detail the actual relative positions of all possible obstacles it is not possible to determine

the origin of the athermal stress unequivocally. However, a consideration of the results obtained this far enables certain possibilities to be eliminated, thereby narrowing the field of interest.

Each stage is now considered in turn.

1. Stage I

As already mentioned there are numerous processes capable of giving the observed parabolic relationship. It is expedient to look firstly at the tensile experiments. Although slip is occurring predominantly on a single system the value of α is larger than that required by Taylor's theory. Yet the athermal stress arises largely from interactions between dislocations on parallel systems and perhaps certain line tension effects. A similar situation in f.c.c. metals has been considered by Hazzeldene (1967). His theory requires that edge dislocations of opposite mechanical sign, initiated from different sources, should interact to form multipoles. The athermal stress is derived from the interaction of groups of dislocations of opposite sign trapped behind the multipole. The theory, in its present form, gives a value of α of about 0.1 for calcium fluoride, so cannot be the sole source of athermal stress

There are other possible obstacles. Thus, Chen et al (1964) have shown that single dislocations can interact with dislocation dipoles to form complexes; these could then act as relatively immobile barriers to edge dislocations on the slip plane, with small pile ups forming behind. The dipoles must be of suitable density and distribution to block the entire length of edge dislocation, if they are to be effective. Deformation proceeds with slip occurring predominantly on planes between existing slip bands; the dipoles created on these adjacent bands are too far

from the moving dislocations for the interaction stress to be significant (see later in this section). Thus, only dipoles created on or near the operative slip plane are effective and the blocking condition is not likely to be satisfied unless the first screw dislocation to traverse the slip plane produces a sufficient density of dipoles. This situation is then similar to one discussed in Chapter 7, where the first dislocation to move across a slip plane can do so at a significantly lower stress than all subsequent dislocations. The dipoles must be produced predominantly through multiple cross glide. (Washburn, 1963).

Alternatively, as considered in Chapter 2, dislocations with orthogonal burgers vectors, moving on the same slip plane, could interact to form dislocation junctions, which could impede the passage of other dislocations. However, even if these junctions can form they are not very stable and would not be capable of holding up many edge dislocation...

Finally, since the orientation factors for the 'primary' and 'secondary' slip planes do not differ greatly, the small pile ups on the 'primary' plane could initiate slip on the 'secondary' planes (c.f. Hirsch, 1964). The extent of 'secondary' glide can only be small (see Chapter 4) but could be sufficient to enable interactions with 'primary' dislocations to occur to form junctions (equation 2.5). The junctions form in the mixed ($\theta = \pi/4$) orientation and could quite effectively block these dislocations. Although the junctions are stable they are not strictly sessile like the Lomer-Cottrell barrier formed between extended dislocations; so they cannot be regarded as impenetrable barriers capable of holding up dislocations under all conditions but can effectively impede slip (Carrington et al 1960)

The athermal stress in all above situations is derived from the interactions between piled up groups of dislocations formed on the 'primary' planes. It is not possible to determine, at this stage, whether these stresses are of the appropriate magnitude to provide the observed work hardening. If not, more complex obstacles might be created as discussed later.

The slip line observations on the tensile specimens refer to screw dislocation slip distances only. Thus, they do not provide any useful information about the obstacles to edge dislocations, they simply indicate that no effective blocking obstacles for screw dislocations are created during deformation. So the obstacles created are not able to block the expansion of dislocation loops all around; whichever obstacle type is selected is required to account for this. Evidently the typical Hirsch obstacle does not apply; the multipole and dipole mechanisms are possible because they do not impede screw dislocations; stable junction can form in two orthogonal (mixed) orientations in type B crystals and could possibly block slip all around so may not be applicable. It is not possible to be more specific than this at this stage. The explanation of the work hardening here is probably also complicated by the movement of a large number of dislocations out of the crystal.

Additional line tension contributions might arise from the shape of the dislocation loops (Hirsch and Mitchell) and from the bowing out between dipoles if their density is not sufficient to block the dislocations.

Compression Specimens

The development of deformation in the compression specimens is obscured through slip occurring on all available primary systems in the

early stages. However, it is observed that, in any specific region, slip occurs principally on one system so that intensive pile ups occur against adjacent regions; this is particularly apparent in type A crystals. The slip line observations on these crystals refer to mixed ($\theta = \pi/4$) dislocation slip distances; these decrease continuously with strain. The slip line length variations in other orientations have not been determined but it is assumed that similar variations occur for edge dislocation slip distances and perhaps screw dislocations. So, with blocking obstacles being created within each region during deformation, the athermal stress is not provided solely by the back stress from the pile ups at the end of each region.

The rate of work hardening (μ /150) is similar to the larger values observed in stage II in f.c.c. metals (μ /150 - μ / 500). Similar observations are made in other ionic crystals e.g. NaCl (μ /1000, Davidge and Pratt), LiF (μ /500, Washburn, 1963), MgO (μ /120, Stokes, 1965). The dislocation density, athermal stress relationship is also similar, even the magnitude of the constant α, and the length of the slip lines is approximately inversely proportional to strain in both cases. The only difference concerns the specimen size and strain rate dependence of the work hardening; such large variations are not observed in f.c.c. metals. Thus, there is good reason for presuming that stage I hardening here is similar to stage II in f.c.c. metals; the specimen size and strain rate effects need not rule out this possibility (see Section II4). There is a wealth of literature devoted to the theories of work hardening in f.c.c. metals and it is not considered in any great detail here. The slip line observations indicate that the athermal stress is derived predominantly

from interactions between dislocations held up at blocking obstacles rather than from interactions with the elastic field of forest dislocations during intersection (Hirsch and Mitchell), the jog mechanism (Mott, 1960) does not apply to edge dislocations. The form of the blocking obstacles could be simply those already described in connection with the tensile experiments (analagous to Seeger's theory) or the pile ups behind these obstacles could initiate slip on the 'secondary' systems in their vicinity so that complex obstacles are created (analagous to the Hirsch theory). The latter is favoured in this case because the simple obstacles are not particularly effective i.e. the junctions are glissile and form in a single orientation in type A crystals and the dipoles incapable of holding up more than a few single dislocations of the same sign (Chen et al). The birefringence observations (e.g. at 110°C) and slip line observations indicate that there are no distinct slip bands created on the 'secondary' planes during this stage, so whichever theory is adopted is required to account for this. The Hirsch theory requires a relatively large 'secondary' dislocation density but only a small proportion of the dislocation motion need occur on these systems so the experimental observations do not discount the theory (c.f. Nabarro et al, 1964). It is not really possible to positively identify the form of the obstacle without, at least, extensive electron microscope studies.

2. Stage II

The theory adopted for stages I must also be able to provide a logical transition into stage II. The tensile experiments showed that stage II corresponds to the onset of slip, in the form of bands, on the 'secondary' planes. The theories adopted to explain Stage I

require a certain amount of slip to have proceeded on the 'secondary' systems; this cannot have occurred in the form of distinct bands (as already described). Thus, the transition to stage II might occur at a stress where definite slip bands can be formed on the 'secondary' planes or perhaps might correspond to a certain density of 'secondary' dislocations and dipoles.

The other significant features of stage II are firstly that the slip line length (i.e. the slip distance) does not alter although the forest density is increasing and secondly the onset of the stage corresponds to a rapid increase in the total dislocation dipole density (Davidge and Pratt). The formation of dislocation dipoles in calcium fluoride is considered in Appendix I; the term dipole is used throughout but might equally refer to dislocation loops and point defect clusters.

Thus, some form of dissociation at the available obstacle sites might be occurring, to account for the slip line effect, and this results in the formation of dislocation dipoles. The most logical explanation of these effects is that extensive intersection of the dislocations comprising the obstacles can commence, with the resultant formation of sessile, long jogs on screw dislocations and hence dislocation dipoles. If the obstacles are of the simple Seeger type, the above situation could arise when the stress at the obstacle (applied plus internal stress) is sufficiently large to dissociate certain of the junctions that are created (or cause them to become glissile). Blocking is then only achieved where the density of obstacles ('secondary' dislocations) is suitably high i.e. depends upon the inhomogeniety of the distribution of the 'secondary' dislocations. The dipoles

produced in this case would form predominantly on the 'primary' planes. Alternatively, if Hirsch type obstacles are required, intersection might commence at the obstacles to reduce their complexity so that their trapping radius decreases more rapidly with stress than in stage I. This releases both 'primary' and 'secondary' dislocations that can glide away and produce dipoles on both sets of planes. This could account for the distinct 'secondary' slip bands observed during this stage. Thus, both the approximate invariance of the slip distance and the increased dipole density can be adequately accounted for, so the above explanation is reasonable. The Hirsch obstacle is again favoured because it accounts more satisfactorily for blocking and for the formation of 'secondary' slip bands during this stage. There does not appear to be any alternative explanation of the slip line effect, especially since the forest density is increasing with strain. [Intersection commences at a certain magnitude of the total stress at the head of a pile up. Thus, as the applied stress increases, the obstacles are able to support fewer dislocations before intersection occurs (where the spacing between dislocations comprising an obstacle does not increase). Thus, the athermal stress component associated with the long range stress field of the dislocations at these obstacles cannot increase more rapidly with strain than in stage I because this would require the number of dislocations at the obstacle to increase with strain according to the expression (Hirsch and Mitchell, Kronmuller):-

$$L \propto \frac{f(n)}{\varepsilon} \qquad - 6.12$$

Where L is the slip line length (independent of strain in this case) and n the number of dislocations held up at the obstacle.]

Thus, some additional contribution to the athermal stress is required. This is possibly the interaction of the dislocations with the dislocation dipoles produced, in large quantities, at the onset of this stage (Kear et al,1966). There appears to be three mechanisms that might give the required linear athermal stress, dislocation density relationship, when these are the sole contribution to the athermal stress.

i) The first mechanism, proposed by Gilman (1962), requires dislocation dipoles to be formed on the 'secondary' planes; they can then be regarded as analagous to coherent precipitates. If the spacing between the dipoles is of the appropriate magnitude and the strain field around them suitable it might be possible to invoke a Mott-Nabarro solute hardening mechanism i.e. the dislocation is required to adopt a curvature to conform with the strain field of the dipoles. The stress is derived from the line tension associated with the imposed curvature. The mechanism provides an athermal stress proportional to the dipole density. The dipole density increases approximately linearly with strain in Stage II (Davidge and Pratt), and since the dislocation density itself is observed to increase approximately linearly with strain, then the required linear dislocation density, stress relationship is obtained.

ii) The second mechanism, proposed by Stokes (1965) requires a high density of dipoles to be formed on the 'primary' plane. The dislocations can interact with the stress field of these dipoles according to the relationship (Kroupa, 1962), $\tau \propto 1/l^2$, where l is the distance of the dislocation from the dipole. If l is proportional to the spacing between dislocations this gives the required relationship. This mechanism is essentially a short range interaction and hence can only contribute to the

athermal stress if the dipoles are sufficiently long and dense on the slip planes to impede the dislocations along their entire length. Presumably, the role of 'secondary' slip in this process is to provide the required high density of dipoles on the 'primary' plane through the formation of intersection jogs. This mechanisms is only effective for edge dislocations; the screw dislocations are impeded by the increased density of jogs that are either sessile or required to move non-conservatively.

iii) The Mott-Nabarro mechanism was originally developed for defects with a spacing of a few tens of angstroms only and might not apply in the case of dislocation dipoles. If it does not apply the dislocation is required either to bow out between the dipoles or to interact with the dipole stress field during intersection. The latter can only provide a component of athermal stress if dipole intersection determines the thermal stress; this is not so (see Chapter 5). Thus, the bowing out between dipoles, according to the Orowan process, might be a third possible mechanism (Nabarro et al, 1964). The Orowan process gives;

$$\tau_p \propto 1/l \qquad - 6.13$$

Where l is the spacing between impenetrable obstacles (dipoles, in this case).

If the spacing between dipoles on the 'secondary' planes is proportional to the average spacing between dislocations, this gives a parabolic stress, dislocation density relationship. This does not necessarily apply; even if it should, each time a dislocation passes a dipole, a loop of dislocation remains surrounding the dipole, so, in fact, l might decrease more rapidly than the spacing between dipoles, so this mechanism could give the relationship observed in stage II.

The thermally assisted intersection of debris proposed by Kear et al (1966) as a stage II hardening mechanism cannot apply because the work hardening is strictly athermal; this is shown more clearly in the latent hardening experiments where the thermal stress is the same for dislocations requiring to intersect debris and for approximate single slip conditions in relatively dislocation free crystal.(See Section III).

If dislocation loops (point defect clusters) are created rather than dislocation dipoles (especially at the higher temperatures) a similar situation exists for loops formed on the 'primary' planes. The elastic stress fields of these defects have been analysed by Kroupa (1962) and Makin (1964). They derive a relationship of the form;

$$\tau = \frac{0.14\, ba\mu}{l^2 \pi(1-\nu)} \qquad - 6.14$$

Where a is the radium of the loop and l is the distance of the dislocation from the loop.

So these too could contribute to the athermal stress if their distribution and density should be suitable.

In addition, if they are formed on 'secondary' planes they might act as impenetrable obstacles with dislocations bowing out between them.

These individual interactions are clearly not the only contributions to the athermal stress so the more general cases are now considered.

If the density of dipoles on the 'primary' planes is sufficiently large and the distribution suitable, then the stress required for individual dislocations to pass through their strain field might provide the major proportion of the athermal stress. The total athermal stress is then given by

$$\tau_\mu = \tau_0 + (\tau_K - \tau_p) \qquad - 6.15$$

Where τ_D is the stress due to the interaction with the dislocations associated with the blocking obstacles.

τ_K is the dipole passing stress = $\frac{\mu b}{8\pi l(1-\nu)}$ (Chen etal)

Where l is the distance of the dislocation from the dipole.

τ_P, is the internal stress, associated with the blocking obstacles, at the dipole and depends upon the position of the dipoles with respect to the blocking obstacles.

For τ_K to provide a significant contribution, l is required to be within the range 10^2--10^3Å . This is an order of magnitude lower than the spacing between dislocations observed under these conditions, so, if dipoles are formed only on the slip planes containing the dislocations this cannot have a significant effect. However, a detailed study of dipole distribution is required before any quantitative estimates can be made.

The dipoles formed on the 'secondary' planes can also contribute to the athermal stress as already described. So the overall athermal stress might be;

$$\tau_\mu = \tau_o + (\tau_K - \tau_{P_1}) + (\tau_F - \tau_{P_2}) \quad - 6.16$$

Where τ_F is either a Mott-Nabarro or an Orowan term. $\tau_{P_{12}}$ depends upon the relative physical position of the dipoles with respect to the blocking obstacles and 'primary' dipoles.

For an Orowan mechanism, $\tau_F \approx {}^2\mu^b/l$; this is about an order of magnitude greater than τ_K and could provide the major proportion of the athermal stress, if the spacing between 'secondary' dipoles is similar to the spacing between dislocations (although it must decrease more rapidly than the dislocation spacing, as already described).

There is not sufficient information available concerning the dipole misfit terms to enable the alternative Mott-Nabarro contribution to be estimated.

Thus, the possible contributions to the athermal stress in stage II are listed but it is not possible to make any quantitative estimates of their relative magnitudes without a detailed knowledge of the dipole (and loop) density and distribution.

II. Latent Hardening Experiments

1. Introduction

Basically the experiment involves deforming a specimen such that slip proceeds on a certain slip plane, then reorienting the crystal so that slip cannot occur on this system but is required to take place on another intersecting system (c.f. Alden, 1963 Kocks, 1964; Jackson and Basinski, 1967). The experiment enables intersections to be investigated in a relatively controlled manner and should be able to provide useful information about the athermal stress.

2. Experimental

A B orientation specimen is compressed to a specific strain so that slip occurs largely on single system in the central region of the specimen. Then, a type A specimen is cut from the central region such that the original slip plane contains the new stress axis. Subsequent deformation of this specimen requires that slip should proceed on the other two primary systems, necessitating the

intersection of the original slip bands. A number of additional dislocations are presumably produced during the cutting of the second specimen but these are confined to the surface layers and should not influence the subsequent deformation significantly.

3. Results

Firstly a few simple birefringence observations are made to confirm the mode of deformation. The birefringent pattern after the original deformation is shown in fig. 6.5a; after the second deformation, this pattern is completely broken up, fig. 6.5b. This indicates that extensive intersection of the original slip bands has proceeded.

Secondly, the stress strain characteristics are established. A typical result is shown in fig. 6.6, for a specimen prestrained into stage Ic at 170°C. The significant features of the latent hardening are as follows,

a. The stress required to move a dislocation through an existing slip band is considerably larger than that required to propagate slip within that band. The stress increment increases as the prestrain increases (sufficient results to establish a definite relationship have not been obtained).

b. Whatever the magnitude of the prestrain in stage Ic, the rate of work hardening in the second deformation is almost identical to that in a type A specimen that has not been prestrained. (c.f. Alden, 1964), this applies at both 170°C and 110°C.

The situation is slightly different for specimens prestrained into stage Ib; a typical experiment is shown in fig. 6.7. During the second deformation, the curve has an identical form to that of a

type A specimen of similar dimensions that has not been prestrained, when the curves are superimposed at similar stresses. Thus, a specimen prestrained sufficiently into stage Ib will adopt a stage Ic hardening rate immediately, during the second deformation.

It is now evidently important to distinguish the contributions to latent hardening due to thermal and athermal stresses. So typical change in strain rate and temperature tests are conducted on prestrained specimens. Firstly, specimens prestrained into stage Ic are tested. All activation parameters obtained i.e. $V(\tau^*)$, $\Delta H(\tau^*)$, $\tau^*(\tau_A)$, $m^*(T)$, are identical to those determined in Chapter 5 for as prepared specimens. Thus, the thermal stress is identical for dislocations moving through low and high densities of forest dislocations and dislocation dipoles, fig. 6.6; this confirms a previous observation that forest intersection and dislocation dipole intersection cannot contribute in any way to the observed thermal stress. The latent hardening is, therefore, entirely athermal in origin.

The experiments are repeated for specimens prestrained into stage Ib at 110°C. The results are interesting. The magnitude of the parameters obtained immediately upon reloading differ from those obtained during prestraining, immediately prior to unloading. However, on plotting these activation parameters (V, τ^*, ΔH, ΔHo) against the applied stress, apart from a few initial values, the curves obtained are identical to those determined previously for as-prepared crystals (Chapter 5). The variation of τ^* is shown in fig. 6.7; the latent hardening is partly athermal and partly thermal in origin. In addition, the magnitude of the thermal stress, at a given temperature and strain rate, depends only upon the applied stress and not upon structure or

strain etc., this also confirms the conclusions, drawn in Chapter 5, concerning the likely thermal mechanisms.

II.4 Discussion

The results provide useful information not only about the origin of the athermal stress, as was originally intended, but also upon the thermal stress. The athermal stress is considered first.

The work hardening in stage Ic is not affected by the density and distribution of static dislocations on an intersecting system. This confirms previous slip line observations that the distribution of initial pile up positions cannot influence the work hardening significantly i.e. some alternative blocking obstacle is generated during deformation. Thus the effect of temperature, specimen size and strain rate on the work hardening cannot be associated with the differing homogeniety of the original deformation as suggested in Chapter 4.

More realistic, qualitative explanations of these effects are attempted here; the specimen size effect is considered first. This must evidently be associated with the inhomogeneous stress system around the compression plates. No specimen size effects are observed in Stage II in f.c.c. metals (Kocks et al, 1964) and since stage I hardening here has been regarded as similar to stage II in f.c.c. metals,

the discrepancy must be accounted for. The onset of stage II commences at an approximately similar applied stress in all cases. Thus, beyond a certain magnitude of the applied stress there must be a constant rate of production of obstacles (dipoles) under all conditions to provide the relatively constant stage II hardening observed (this has to be explained by any stage II theory developed quantitatively). Stage Ic hardening presumably cannot be solely due to interactions with blocking obstacles, except for large values of $^{h}/d$, otherwise a constant hardening rate would be observed as in f.c.c. metals. The most reasonable explanation is that the friction stresses, in specimens with small values of $^{h}/d$, alter the resolved shear stresses on the 'secondary' and 'primary' slip planes such that a relatively high dipole density is produced before intersection at the obstacles provides the required stage II rate of production. The total athermal stress is then given by equation 6.16 with small contributions from τ_F and/or τ_K. It is not attempted to provide any worthwhile explanations of how these additional dipoles are produced at this stage. Whether this argument is correct can be tested by dislocation density and bulk density measurements on squat specimens. Thus, the dislocation density, stress relationship should be intermediate between the parabolic and linear relationship in stages I for these crystals. In addition, the bulk density should increase more rapidly with strain in this stage indicating a more rapid increase in dipole density. Unfortunately, these effects have not yet been investigated.

In NaCl (Davidge and Pratt) and LiF (Gilman and Johnston) dipoles are produced during 'easy glide' so there must always be a contribution to the athermal stress from these interactions.

In a material like LiF where a high density of dipoles appears to be produced without intersection it is possible that these interactions provide the major contribution throughout, as suggested by Gilman, so that only one work hardening stage is encountered. Thus, the above size effect explanation appears possible with the work hardening depending upon the relative variations of τ_p and τ_K and perhaps τ_F with strain in equation 6.16. It is only at relatively high dipole densities that τ_K and τ_F can produce a significant effect, so presumably in specimens with relatively large values of h/d the parabolic relationship is obeyed quite closely in stage I.

The effect of temperature is entirely different for, as the temperature decreases, both the length of and the rate of work hardening in stage Ic increase. Now, the lower the temperature, the larger the stress required for intersection to proceed at a given strain rate; this explains how the onset of stage II might occur at higher stresses at lower temperatures. The rate of work hardening in stage Ic varies slowly with temperature, although the variation is more rapid than a simple shear modulus effect.

This might also be associated with a variable production of dipoles during this stage i.e. the lower the temperature the higher the rate of production of dipoles. If this is correct, at the lower temperatures, the stress dislocation density relationship would deviate slightly from the parabolic relationship. Unfortunately, the results at 110°C are not sufficiently accurate to test this.

The strain rate effect is an intermediate case with a relatively rapid increase in work hardening in stage Ic, as the strain rate is increased, and a corresponding increase in the stress associated with

the onset of stage II. It is expected that the effects of temperature and strain rate upon the stage II starting stress should be similar but the increase in hardening rate in stage Ic is contrary to expectations and an explanation is not readily apparent.

The actual origin of the athermal latent hardening is not of great importance since the structure is not equivalent to that developed during deformation. It is presumably either associated with the formation of obstacles through the interaction of the static dislocations with the mobile ones, as already described, or with the interaction with forest dislocations and/or dislocation dipoles on an intersecting system. It is not intended to differentiate between these possibilities.

The significance of the thermal stress measurements are now considered. The thermal stress, activation volume etc. depend only upon the magnitude of the applied stress at a particular temperature and strain rate; this confirms the previous observations made on specimens of various relative dimensions. This indicates that the rate of production of obstacles on the slip planes depends only upon the applied stress and not upon strain, structure etc. This essentially means that the obstacles are created on the slip planes only and not generally throughout the lattice; this is consistent with the mechanisms proposed in the previous Chapter.

Conclusions

1. The applied stress in stage I deformation is given by:-

$$\tau_A = \tau^* + 0{\cdot}32\mu b\sqrt{N_t}$$

The athermal work hardening is most likely to be associated predominantly with the interactions between the stress

field of dislocations comprising obstacles on the slip planes. These obstacles are formed by the interactions between dislocations on the planes of maximum resolved stress and the other primary planes. The actual physical nature of these obstacles is not clear.

2. The applied stress in stage II deformation is given approximately by:-

$$\tau_A = \tau^* + K N_t + C$$

There are a number of contributions to the athermal stress in this stage. The principal contribution is possibly associated with the interaction of the dislocations with dislocation dipoles created during deformation. If this is so, the onset of stage II is associated with the stress required for copious intersection to proceed at the stage I obstacles, with the resultant rapid increase in dipole density.

3. The temperature, strain rate and specimen size dependence of the work hardening are not satisfactorily explained. The variation of the work hardening rates in stage Ic might be associated with the variable formation rates of dislocation dipoles in each case. The stress corresponding to the onset of stage II is explained logically by assuming that it is the stress associated with a thermally activated process i.e. intersection of dislocations at the stage I obstacle.

Appendix I

The Formation of Dislocation Dipoles During Deformation

The bulk density measurements of Roy show that point defects and/or dislocation depoles are produced during deformation; the density of defects is greater, for a given strain, in type A than in type B specimens. His measurements are made after an ageing period of many hours at room temperature and the results are independent of time. Similar observations are made in NaCl(Davidge and Pratt; Kear et al,1966). If the density change is due to vacancies or interstitials they could be detected from ionic conductivity measurements (Ure). So the ionic conductivity of compression specimens is measured before and after deformation (the conductivity arrangement is described by Phillips,1967); there is no significant change. This indicates that the density change is due predominantly to dislocation dipoles (and loops) and perhaps isolated impurities and point defect clusters. The fact that the density is independent of time eliminates isolated impurities as a major contribution. So it is established that dislocation dipoles and/or loops and/or point defect clusters are generated during deformation in calcium fluoride.

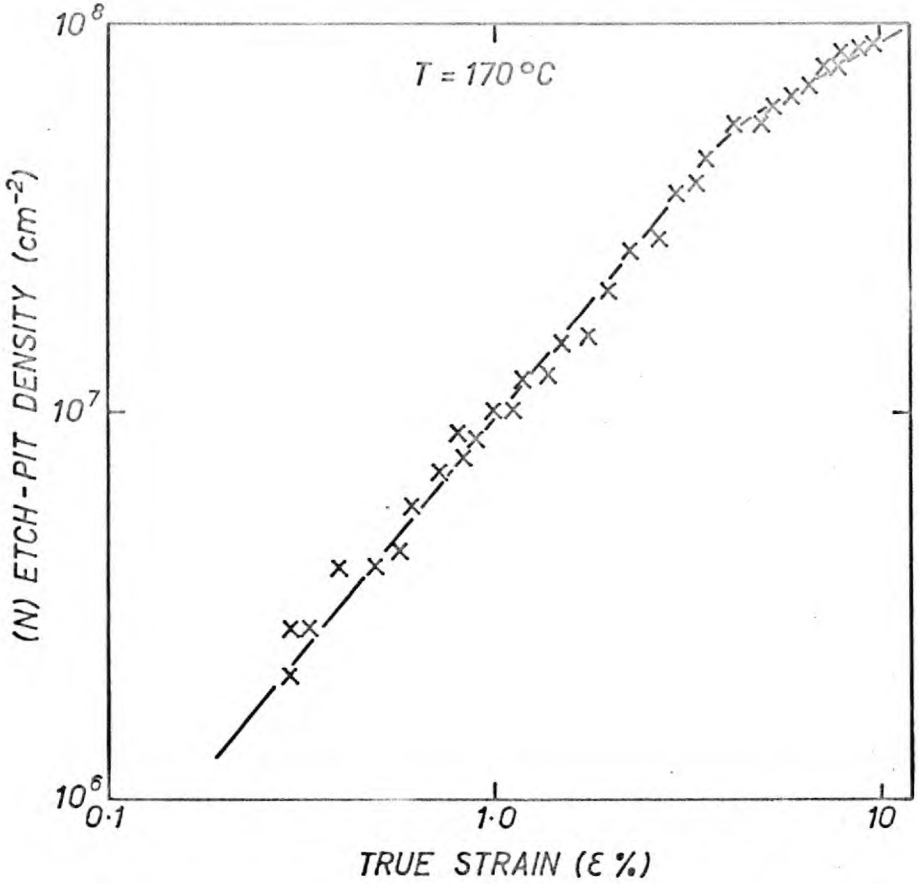

Fig. 6.1a. Variation of etch-pit density with ε at 170°C

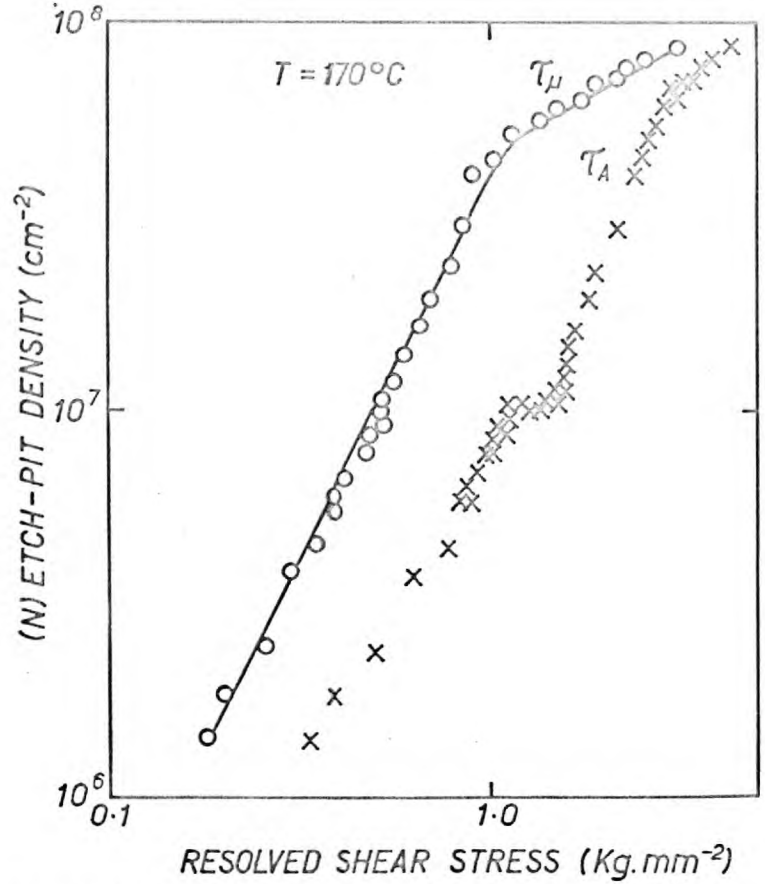

Fig. 6.2a. Variation of etch-pit density with τ_μ and τ_A at 170°C

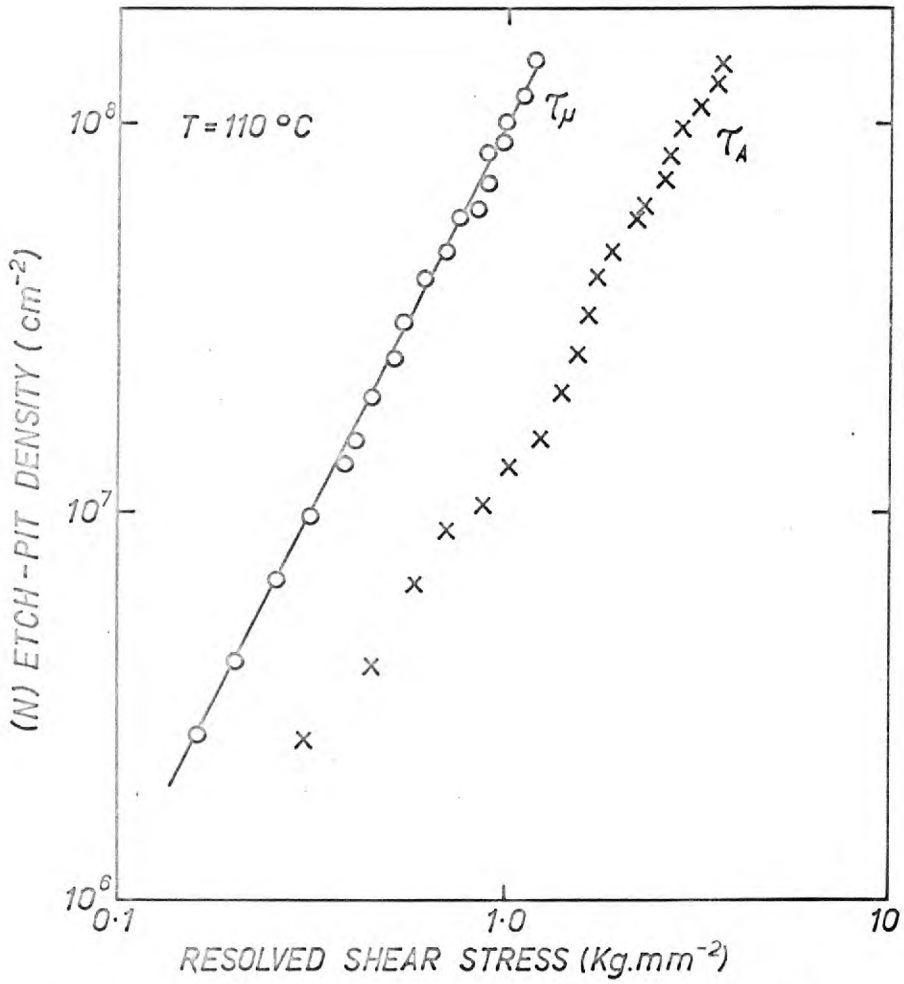

Fig. 6.2b. Variation of etch-pit density with τ_μ and τ_A at 110 °C

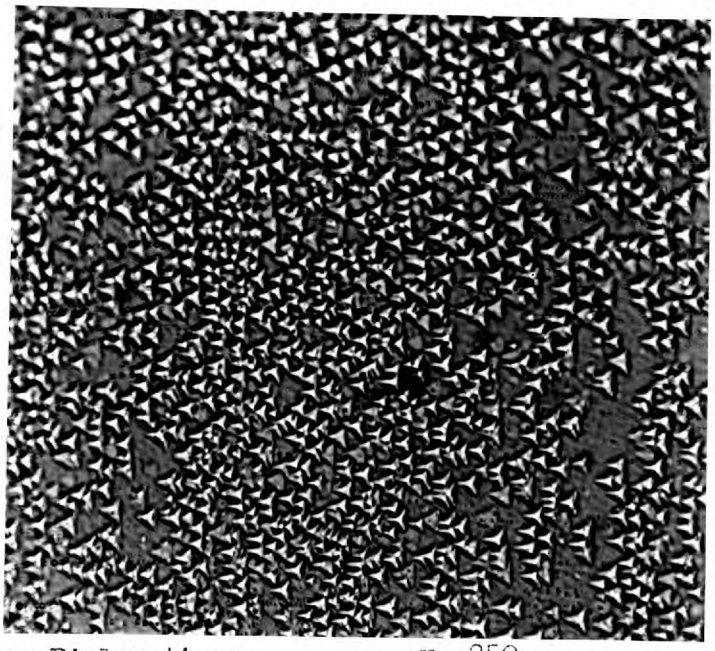

Fig. 6.3(a)

{111} Screw Dislocations x 250

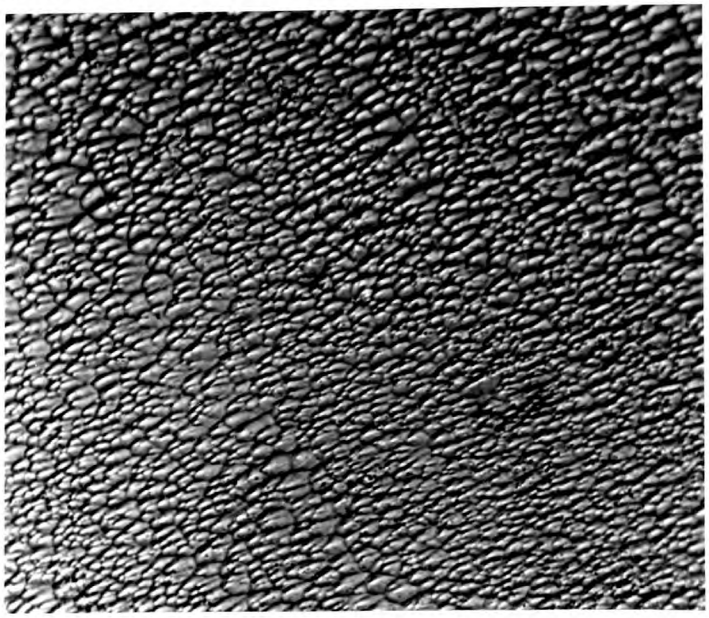

Fig. 6.3(b)

{110} Edge Dislocations x 250

The Relationship between Edge and Screw dislocation densities in a tensile specimen tested at 170°C (ξ= 0.8%)

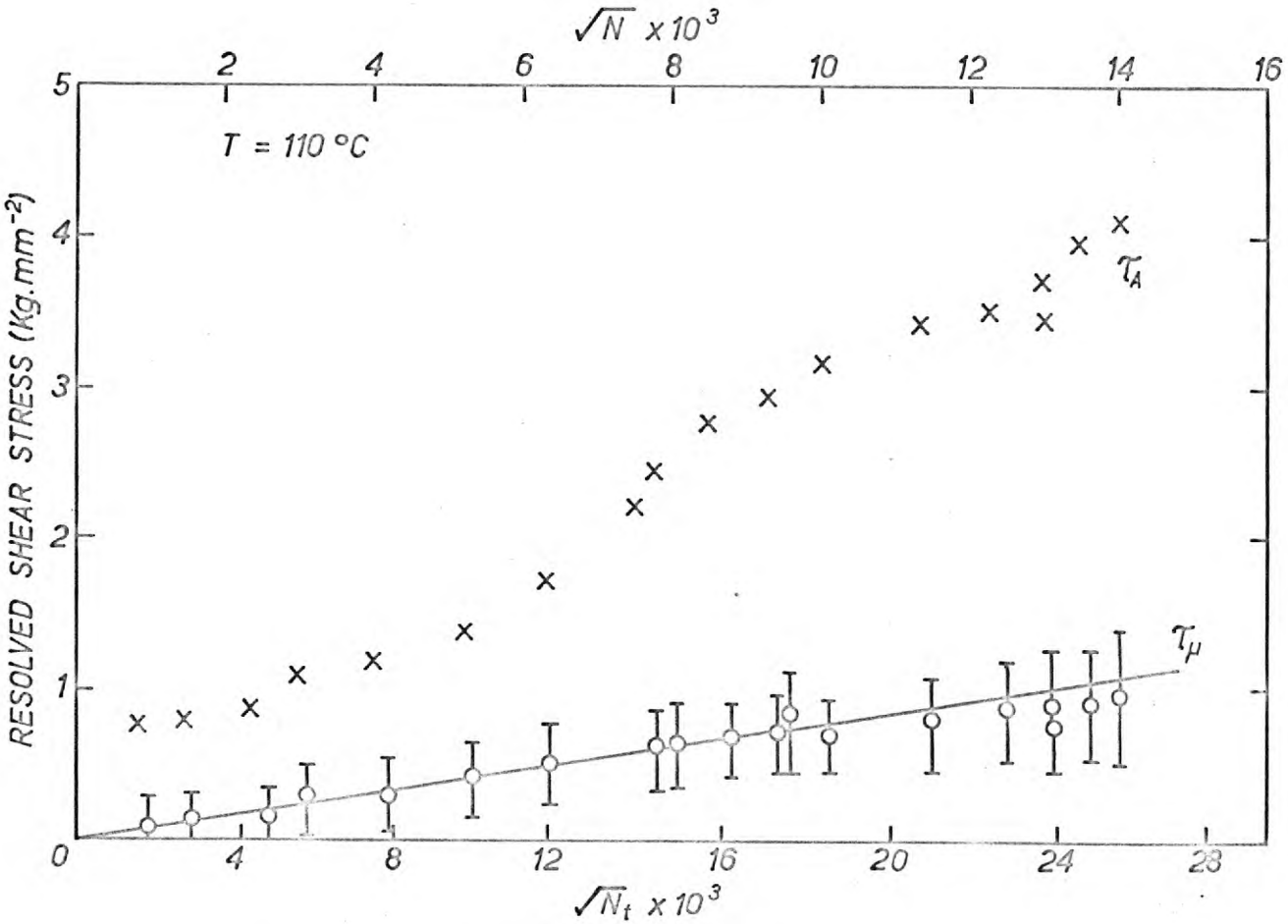

Fig. 6.4a. Variation of τ_A and τ_μ with $\sqrt{N}$ and $\sqrt{N_t}$ at 110 °C

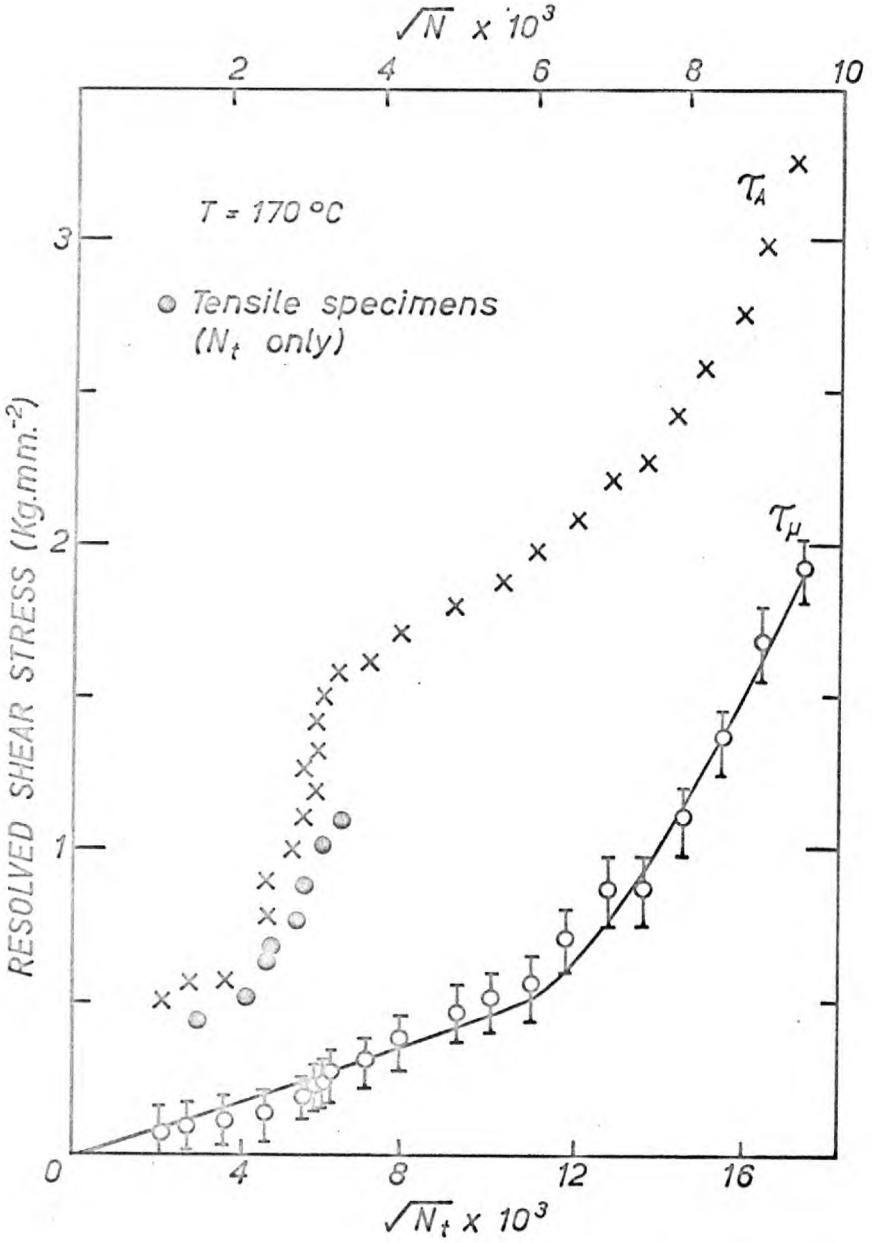

Fig. 6.4b. Variation τ_A and τ_μ with $\sqrt{N}$ and $\sqrt{N_t}$ at 170°C

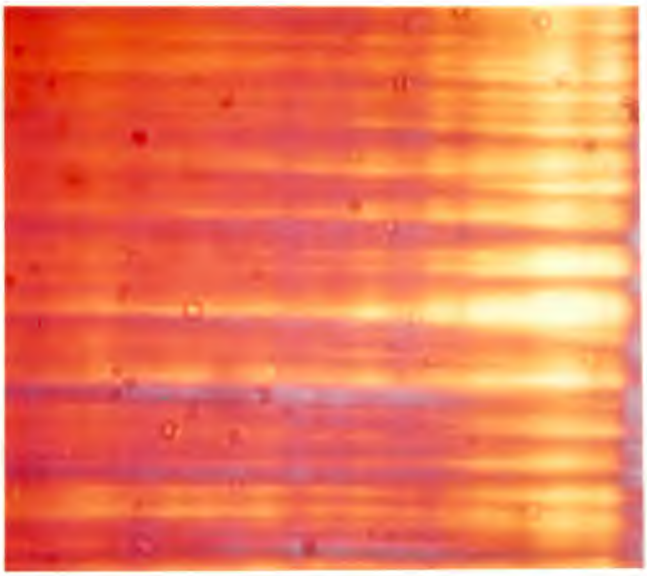

Fig. 6.5 (a) Prestrained 1% x 30

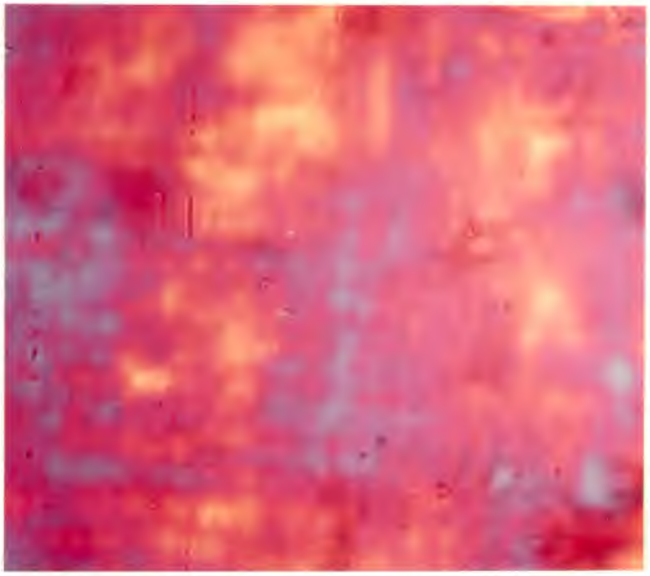

Fig. 6.5 (b) After the second deformation x 30

The variation of the birefringence pattern in the latent hardening experiments at 110°C.

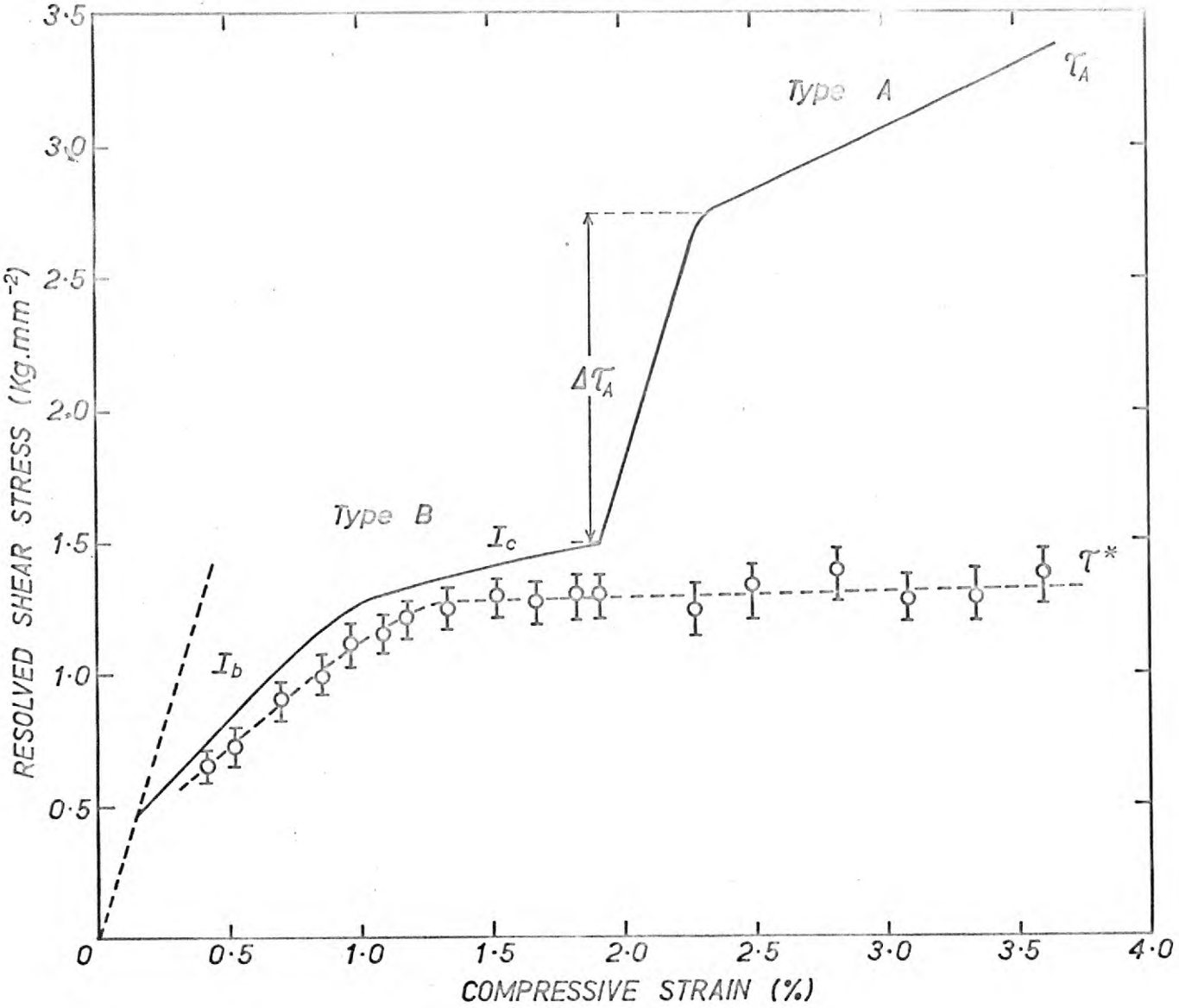

Fig. 6.6. Latent hardening in stage I_c at 175 °C

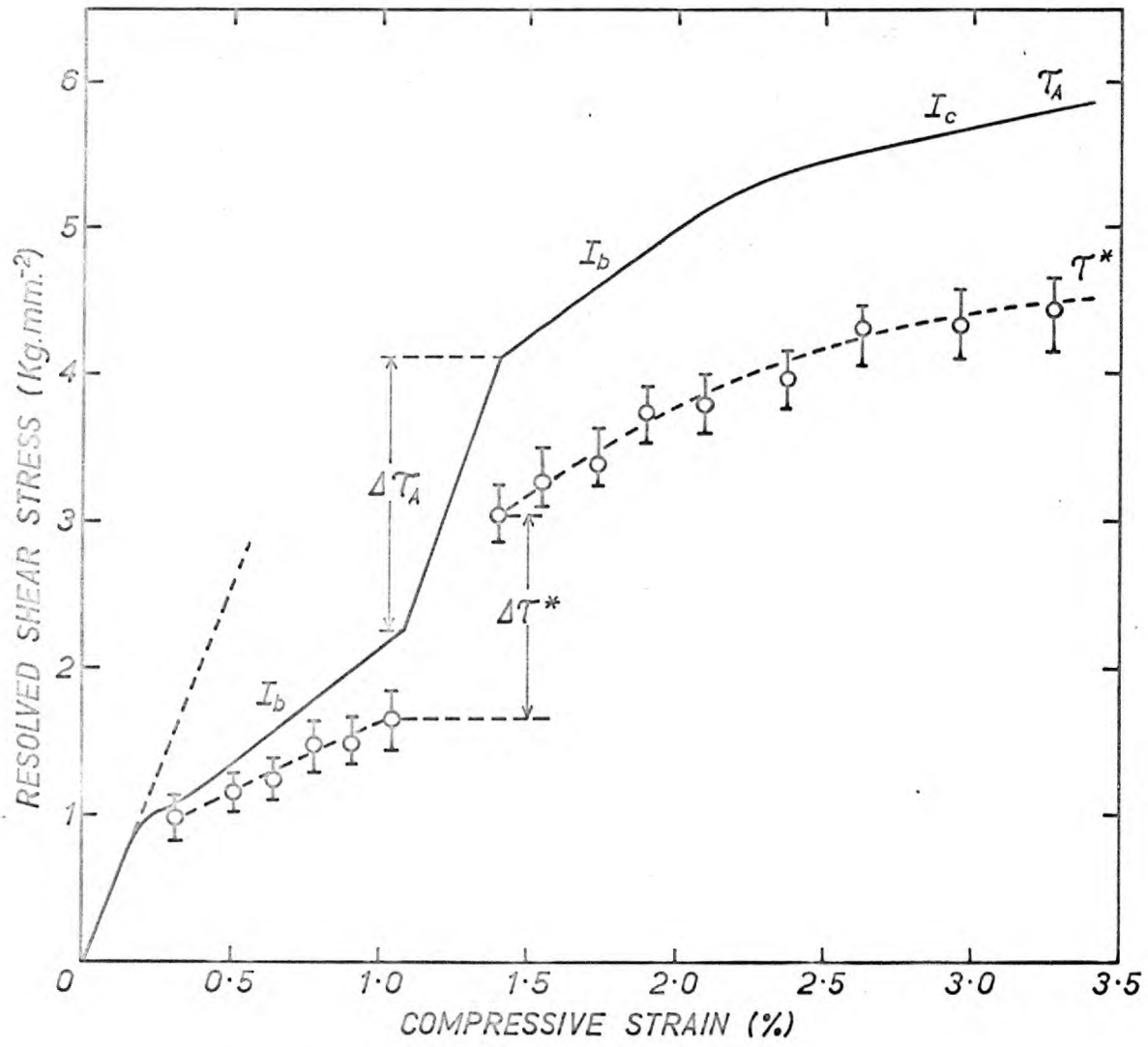

Fig.6.7. Latent hardening in stage I_b at 110 °C

CHAPTER 7

The Deformation of Very High Purity and Yttrium Doped Crystals

1. Introduction

It has been concluded in the previous sections that the thermal stress might be dependent upon interactions with impurity ions or complexes. So the effect of differing quantities of impurity upon the deformation characteristics is studied briefly to determine whether these impurity mechanisms are possible. Thus, as described in Chapter 1, very high purity and yttrium doped crystals have been obtained and these are studied.

2. Experimental

A orientation specimens, prepared as described in Chapter 4 are tested over a series of temperatures, using the techniques outlined already.

3. Results

High Purity Crystals

Stress strain curves have been obtained for these crystals at 110°C and 170°C. The results are shown in fig. 7.1. There is little difference from the Harshaw crystals apart from a lower work hardening rate in stage Ic with the transition from Ic to II occurring at higher stresses. (This differs from observations made in NaCl by Hesse , 1967).

The activation parameters i.e. $m^*(T)$, $V(\tau^*)$, $\Delta H(\tau^*)$, $\tau^*(\tau_A)$ are identical to those obtained in Harshaw crystals (figs. 5.19, 5.18, 5.21). Thus, for relatively small quantities of impurity, the rate controlling obstacle is independent of the impurity content. This is a most important result and its relevance is seen in Section 4.

Yttrium Doped Crystals

Firstly, specimens are tested in the fully aged condition i.e. they are left at the test temperature for a few hours prior to testing.

The stress strain curves obtained are shown in fig. 7.2c. There is no significant deformation below 150°C. Above this temperature, yield is followed immediately by a horizontal region up to about 1% strain and then a transition to a region of linear work hardening (c.f. LiF stress-strain curves obtained by Gilman and Johnston, 1960)

The activation parameters that can be obtained from change in strain rate experiments are also determined. Unfortunately, it is not possible to conduct valid temperature change experiments because rapid and severe dislocation pinning is encountered. The results obtained are shown in fig. 7.2,a,b,d. The activation volume and the thermal stress are independent of strain. For a strain rate of $1.2 \times 10^{-5} sec^{-1}$, the activation volume lies within the range $1--3 \times 10^{2} b^{3}$ between 180°C and 300°C; the results are not sufficiently numerous to warrant plotting a V, τ^{*} diagram. This activation volume is well in excess of that obtained in the pure crystals for a similar value of the thermal stress e.g. an order of magnitude higher at $4 kgmm^{-2}$ (fig. 5.18). Values of m^{*}, obtained by the extrapolation of m to zero strain, increase as the temperature increases. This might be an anomalous result either because the density of mobile dislocations alters during the increment of strain rate at the higher temperatures (see Chapter 5) or because zero strain does not correspond to the condition of zero athermal stress, so it is not m^{*} that is being measured.

The experiments are repeated on crystals that have been heated in vacuo at 1000°C and cooled to the test temperature as rapidly as possible, in an attempt to produce a different aggregation state for the yttrium impurity. However, there is no difference in the deformation characteristics. This means that either the heat treatment does not alter the distribution of impurities, or that the form of the impurity does not significantly influence the mechanical properties.

4. Discussion

The results reveal that for given test conditions, the thermal stress (and other activation parameters) is independent of the impurity content, for small quantities of impurity, and differs from that obtained in crystals containing a relatively large quantity of aliovalent impurity. It is not intended to identify the impurity mechanism, it merely suffices at this stage to note that, in crystals with an aliovalent impurity content of more than 200 p.p.m., the deformation is controlled in some way by the impurity, and this mechanism differs from that encountered in pure crystals.

The aliovalent impurity content (anion plus cation) in the high purity crystals is less than 20 p.p.m. For the Fleischer interaction mechanism to be able to provide the observed activation volumes a concentration of aliovalent impurity greater than 40 p.p.m. is required (see Chapter 5). Even if 40 p.p.m. of aliovalent impurity should be present, it is unlikely that it is all manifested as the appropriate individual complexes required for this mechanism (c.f. Quin, 1967), so it is regarded as a

most unlikely mechanism in this case. Similarly, for the interaction and migration mechanisms to be controlled entirely by aliovalent impurities, at least 40 and 50 p.p.m. respectively of the impurity in the appropriate form is required, so these are also regarded as most unlikely.

Thus, the interaction and migration mechanisms, requiring at least a proportion of the obstacles to be vacancies or interstitials, remain as the most likely mechanisms; these are considered further.

The particular mechanism that operates is determined by the relative values of the binding energies and migration energies (Chapter 5) at the specific thermal stress concerned. An approximate value of the former may be obtained from a relatively simple calculation.

Consider the association of a positively charged defect (e.g. a fluorine vacancy) with an edge dislocation consisting of three adjacent negative charges, with half jogs on both sides. If the vacancy associates with the dislocation at the central position of this configuration, there is a decrease in electrostatic energy of about 1 ev (see Chapter 2); the association energy in any other position is smaller. There is also a reduction in strain energy (largely electrostatic and core repulsive in origin). Bassani and Thomson have calculated the association energy between a vacancy and an uncharged dislocation in NaCl and obtain a value of 0.4 ± 0.2 ev. The calculation will not be significantly different in calcium fluoride, so a total association energy of about 1.4 ev is involved. (It should be noted that this situation differs from the formation case considered in Chapter 2, because there the displacement energy at the half jog had to be created whereas here it is already available in the form of the vacancy).

Unfortunately, it is not possible to estimate the migration energies of the half jogs and no values for the migration of aliovalent impurities are available, so it is still not possible to decide which is the most likely to operate. However, it might be possible to differentiate between them by indirect means.

It has already been determined that a point defect concentration of the order of 10^{16} to 10^{17} cm^{-3} is required for the interaction mechanism to provide the observed activation volumes. The migration mechanism evidently requires a smaller concentration to be available at any instant during deformation.

An order of magnitude is obtained here. The maximum expected value of the mobile dislocation density is $10^{6}cm^{-2}$. Then, the density of point defects required to saturate all available edge sites on these dislocations is $10^{14}cm^{-3}$ (assuming the loop expands to a diameter of $10^{5}A^{o}$ before being arrested). The creation and absorption of these defects is a dynamic effect so this is probably a maximum possible value, especially in stage Ib where most defects on the slip plane are absorbed by the moving edge dislocations. Thus, a higher concentration of free point defects is expected if the former mechanism applies. In addition, the variation of this concentration with strain is different in both cases. For the interaction mechanism, the concentration increases in stage Ib but remains constant in all subsequent stages; for the alternative mechanism the concentration increases in all stages and probably more rapidly in stages Ic and II. It has already been established that a proportion of those defects must be vacancies or interstitials, so it might be possible to detect them using ionic conductivity measurements (Ure, 1957). The conductivity should be measured immediately after deformation is arrested (c.f. Taylor, 1958; Gamagni et al, 1965).

A particular problem presents itself where mechanisms requiring an increased density of obstacles to be produced on the slip plane are involved. Thus, after the first dislocation has traversed an area of slip plane, the thermal stress on this plane is higher than on adjacent planes, so the following dislocation would prefer to move on the adjacent planes at every stage; this would encourage dislocations to move individually with only a slow increase in obstacle density on the

operative slip planes as the strain increases. However, for this situation to arise, dislocation sources must be available on the planes of lowest thermal stress (obstacle density). In addition, the respective magnitudes of the athermal stress on the possible slip planes must be considered i.e. dislocations prefer to move mid way between existing slip bands and sources operate only where the internal stress is favourable (Chapter 6). So the problem is a complex one with a detailed knowledge of dislocation sources and dislocation distributions required. The slip line observations (Chapter 4) show that dislocations move in bands, as in other crystals, but this does not necessarily rule out the above mechanisms.

One of the important criteria used in elimination of possible rate controlling processes is that the screw dislocations move faster than the edge dislocations. This is determined experimentally at zero strain and assumed to apply under all test conditions; the assumption may not be valid. The application of the criterion requires two conditions to be satisfied. The first is that the athermal stress component at the screw dislocations is not significantly in excess of that at the edge dislocations. If this should not be so and $(\tau_\mu + \tau^*)$ at the screw dislocation is larger than the corresponding value at the edge dislocation then it is the screw dislocation motion that determines the magnitude of the thermal stress measured. There is clearly a difference between the blocking obstacles for edge and screw dislocations in stage I (c.f. Hirsch and Mitchell). However, it is not expected that the athermal stress at the screw dislocation should be significantly larger than that at the edge.

Secondly, in a typical constant strain rate experiment, the thermal stress is related to the applied strain rate rather than the velocity according to equation 5.9.Thus, if the density of mobile edge dislocations is greater than the corresponding screw density, the thermal stress at both could be similar in magnitude, or even larger for the screw dislocations. If dislocation motion can always be regarded simply as the expansion of individual loops, from a source, this density is evidently the same for both components and the above possibility does not arise. However, the actual deformation process might be more complex than this, in which case this possibility must be considered.

This uncertainty raises the interesting possibility that the edge dislocation controls the deformation at yield (as shown by the etching experiments) with a gradual transition to the screw dislocation process occurring in stage Ib until, in stage Ic, it depends entirely upon the motion of the screw dislocations. This is most unlikely because it requires both edge and screw activation enthalpies to be very similar and m^* to be the same for edge and screw dislocations (the etch pit measurements in Chapter 3 show that this is probably not so).

Finally, there is the possibility that more complex processes are involved; two interesting possibilities are considered. Firstly, the presence of point defects (or complexes) could influence the nucleation and/or lateral motion of Peierls kinks (Cottrell, 1963; Guyot and Dorn)so that a modified Peierls process applies. Secondly, if the impurity complex intersection energy and the point defect interaction energy are similar, the former could apply at the start of deformation, with stage Ib representing a transition to the

latter, as intersection produces a higher density of isolated point defects, then in stage Ic the latter applies exclusively with no more point defects capable of being produced.

There are probably further possibilities. The identification of the actual rate controlling mechanism is not possible until more precise theoretical and experimental enthalpies are determined, for the various processes.

Conclusions

The most likely rate controlling deformation processes in calcium fluoride appear to be either the interaction of the edge dislocation with isolated charged point defects (vacancies or interstials and perhaps aliovalent impurities) or the migration of point defects with the dislocation. However, there are a number of more complex possibilities that cannot be eliminated so it is not possible to unequivocally identify the rate controlling obstacles at this stage.

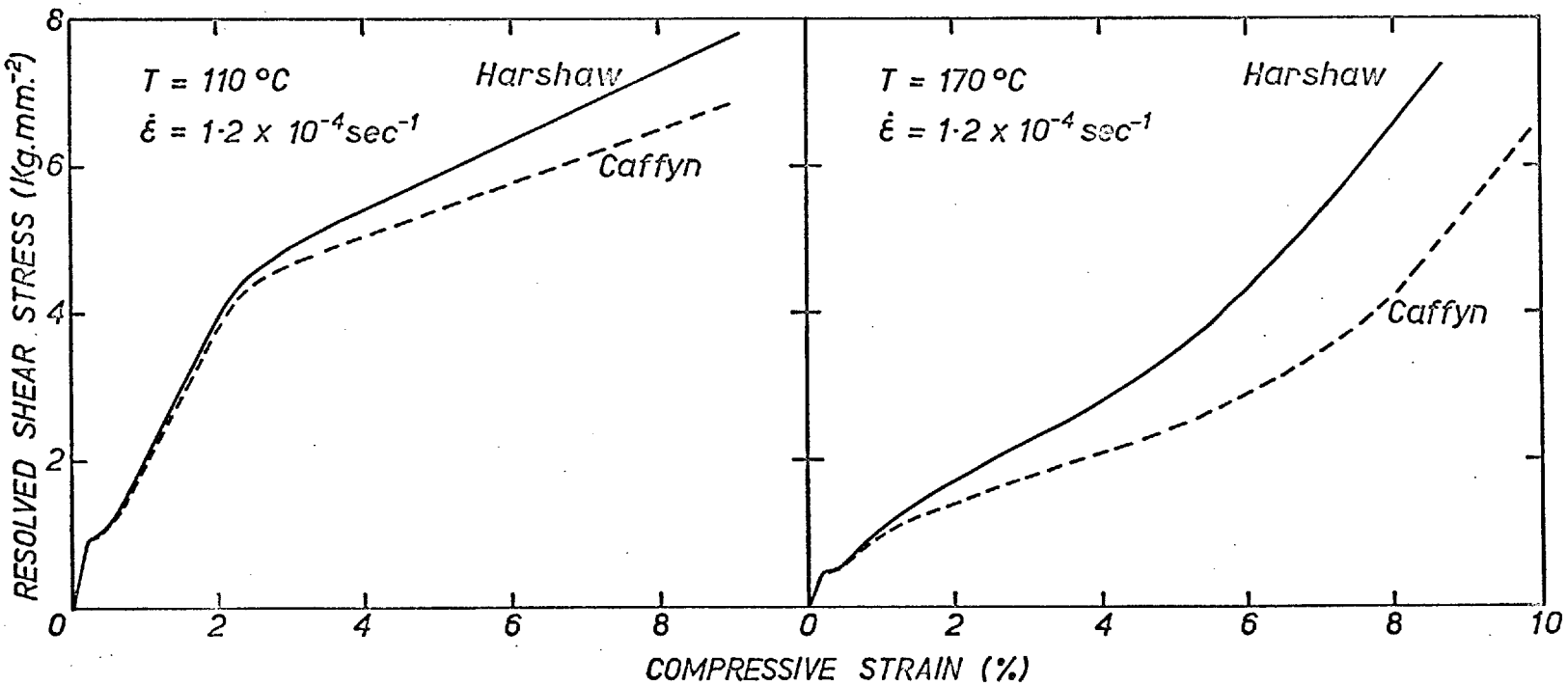

Fig. 7. 1. Stress strain curves for high purity (Caffyn) crystals

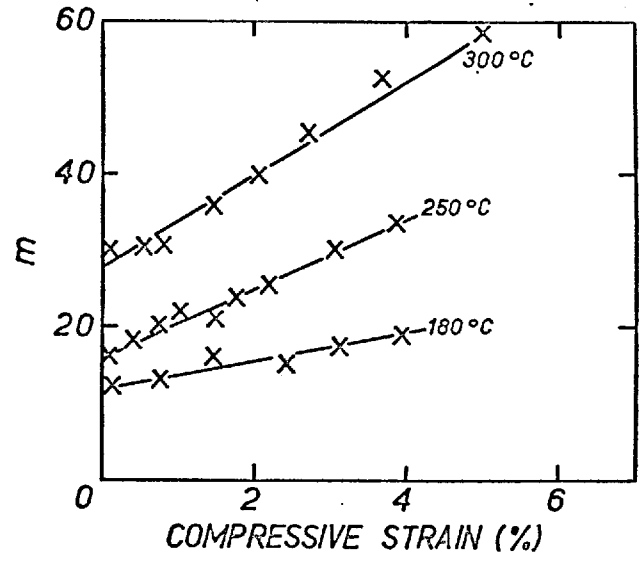

(a) Variation of m with strain

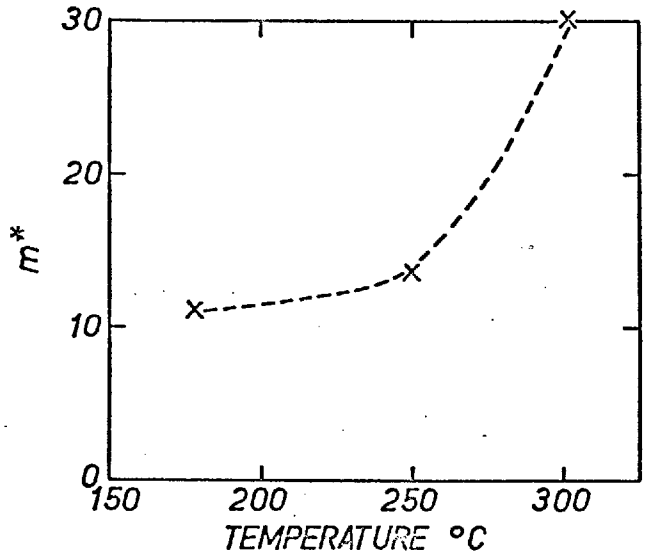

(b) Variation of m* with temperature

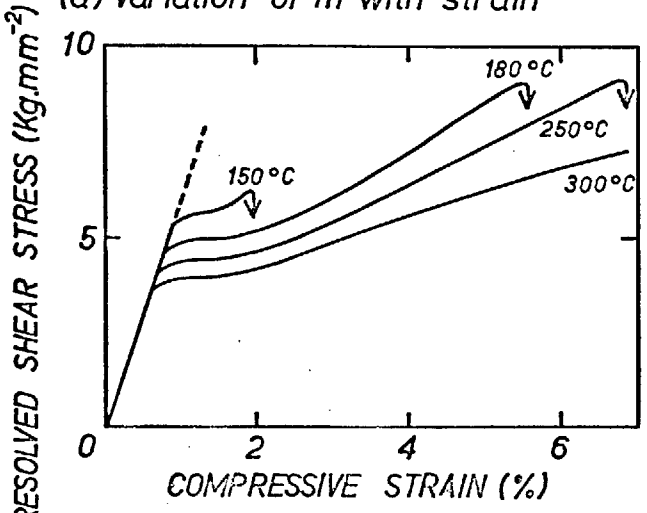

(c) Stress strain curves at strain rate $1{\cdot}2 \times 10^{-4} sec^{-1}$. Yttrium doped crystals

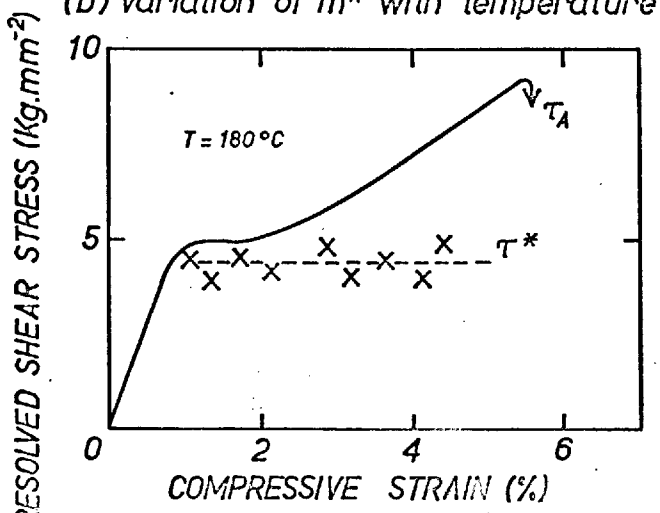

(d) Variation of τ_A and τ^* with strain at 180 °C

YTTRIUM DOPED CRYSTALS

Fi~. 7.2.

CHAPTER 8

General Conclusions and Suggestions for Further Work

1. Conclusions

This study has provided a certain amount of information concerning the deformation of calcium fluoride crystals. The principal conclusions derived from this work are presented here.

1. The edge dislocation on the $\{100\}\langle 110\rangle$ system, although macroscopically neutral, consists of regions of relatively high local charge, the sign of the charge alternating along the length of the dislocation. The presence of these charges appears to influence the deformation on the primary slip planes.
2. The edge dislocations on the primary system move at a lower velocity than the screw dislocations, for a given value of the thermal stress. This is the inverse of the situation observed in other ionic crystals (e.g. LiF, Gilman and Johnston, 1962; NaCl, Gutmanas et al, 1963); it indicates that it is the movement of the edge dislocations that controls the rate at which deformation proceeds for a given applied stress. This is possibly associated with the unusual configuration of the edge dislocation on this system.
3. Over the range of temperature investigated, the stress-strain curves show five separate regions. Apart from the rapid work hardening region observed immediately after the yielding stage, the stages are similar to those observed in other ionic crystals (e.g. NaCl, Davidge and Pratt; Hosse) with a typical three stage curve, plus a yield region. The curves also depend upon the mode of deformation i.e. tension or compression and upon temperature, strain rate and specimen size (for compression specimens).

4. The agreement between the stress dependence of the dislocation velocity obtained from etch pit experiments (for edge dislocations) and from change in strain rate experiments indicates the validity of the latter, macroscopic, method for the determination of the activation parameters in calcium fluoride e.g. τ^*, V. The temperature dependence shows that the macroscopic incremental temperature method provides a close approximation to the activation enthalpy of the rate controlling deformation process. Application of the analysis of thermally activated deformation to the results obtained shows:-

a. The rapid work hardening stage, Ib, is due largely to an increase in the thermal stress with strain.

b. The increase in the thermal stress probably arises from an increase in the density of thermal obstacles of a given type on the slip planes, during deformation.

c. The thermal obstacle involved is most likely to be associated either with the interaction of the charged regions of the edge dislocation with isolated charged point defects, generated during deformation, or with the migration of point defects (or half jogs), picked up during deformation, with the dislocation.

5. The variation of the athermal stress with strain is similar to that observed in other ionic crystals, in particular NaCl, and can probably be explained similarly. The stage I hardening features are adequately explained by invoking a theory similar to that developed to explain stage II hardening in f.c.c. metals, with the athermal stress derived predominantly from the interactions between the stress fields of dislocations held up at impenetrable

obstacles developed during deformation. The form of the obstacles could either be simple dislocation junctions (and dislocation dipoles) or complex arrangements of 'primary' and 'secondary' dislocations of various mechanical signs. The stage II athermal stress is possibly derived principally from interactions with dislocation dipoles generated during deformation.

6. The characteristics of secondary deformation have not been studied in such detail. The only significant conclusions are that the thermal stress is larger than that required for primary slip at a given temperature and strain rate (it is also independent of strain) and that the experimental activation parameters fit a Peierls process analysis quite closely. Thus, the Peierls process might be the important thermal mechanism but the cross slip of screw dislocations and conservative jog motion cannot be ruled out as alternative mechanisms. The athermal stress origin has not been investigated.

2. Further Work

Through the course of this study various additional fields of study have been apparent, these have generally been mentioned in the appropriate sections. The most significant and interesting of these are considered briefly below.

1. A detailed study of the core configuration of the primary edge dislocation, in particular, rigorous lattice calculations. This should enable the most favourable configuration to be estimated and hence the interaction energy of this dislocation with various defects to be calculated. This would assist in the identification of the rate controlling thermal mechanism.

2. The measurement of the dislocation velocity as a function of stress on deformed crystals (c.f. Gilman and Johnston, LiF, 1960). This is experimentally extremely difficult and requires fresh dislocations to etch differently than old dislocations, as in LiF. However, if this sort of measurement could be performed it would be able to confirm the important assumption that the mobile dislocation density does not alter during an increment of strain rate even at relatively large strains.
3. The measurement of ionic conductivity during and after deformation. This would provide information about the concentrations of free vacancies and interstitials produced during deformation. These concentrations are of great importance in the identification of the thermal obstacle, as already described.
4. Transmission electron microscope studies; these should be conducted on crystals irradiated in situ, immediately after deformation is arrested, so that all line defects are pinned in the positions they occupy during deformation. This would enable the distribution of dislocations and dislocation dipoles to be studied to provide valuable information about the athermal stresses. These should be conducted in conjunction with comprehensive etch pit and slip line observations (the latter conducted to find the slip distances of edge, mixed and screw dislocations).
5. A comprehensive study of the effect of aliovalent impurities upon the deformation characteristics to determine the role of these, if any, upon the thermal stress of the high purity crystals and their effect upon the athermal stress.

References

V.G. Alefeld (1962)	Z.Natur for schng	17a	899
T.H. Alden (1963)	Acta. Met.	11	1103
T.H. Alden (1964)	Trans. Met. Soc. A.I.M.E.	230	649
S. Amelinckx (1958)	Il Nuovo Cim., Supp.	7	569
R.J. Arsenault (1966)	Acta. Met.	14	831
C.R. Barrett and W.D. Mix (1965)	Acta. Met	13	1247
Z.S. Basinski (1959)	Phil. Mag.	4	343
Z.S. Basinski and S.J.Basinski(1964)	Phil. Mag.	9	51
F.Bassani and R.Thomson (1956)	Phys. Rev	102	1264
W. Bontinck and W.Dekeyser (1956)	Physica	22	595
L.M.Brown (1960)	Ph.D thesis -University of Birmingham		
H.Brown and R.A. Ekrall (1962)	Acta.Met	10	1101
A.Bruneau (1962)	Ph.D thesis - University of London		
J.Byrne, M.E. Fine and A. Kelly(1961)	Phil. Mag	6	1119
J.E. Caffyn(1966)	Private Communication		
P.Camagni and A.Manara(1965)	J.Phys. Chem Solids	26	449
W.Carrington;K.F.Hale, and D.McLean (1960)	Proc.Roy,Soc	A259	203
V.Celli; M.Kabler; T.Ninomiya and R.Thompson(1963)	Phys. Rev	131	58
H.S. Chen; J.J.Gilman and A.K. Head (1964)	J. Appl Phys	35	2502
J.W. Christian (1964)	Acta.Met	12	99

J.W.Christian and B.C.Masters (1964)	Proc.Roy,Soc	281	240
H.Conrad (1961)	J.I.S.I.	198	364
H. Conrad (1964)	Journal of Metals	16	582
H.Conrad and S.Fredrick (1962)	Acta. Met.	10	1013
A.H.Cottrell (1953)	Dislocations and Plastic Flow in crystals (Wiley, London)		
A.H. Cottrell (1963)	The Relation between the structure and mechanical Properties of Metals H.M.S.O.p.3566		
G.C. Das (1967)	Ph.D thesis - University of London		
R.W. Davidge (1966)	Proc. Brit Ceram. Soc	6	295
R.W. Davidge and P.L.Pratt(1964)	Phys. Stat. Sol	6	759
J.E. Dorn (1963)	U.C.R.L. 10455		
J.E. Dorn and S.Rajnak (1964)	Trans. A.I.M.E.	230	1052
G.E. Dieter jnr.(1961)	Mechanical Metallurgy (McGraw Hill, New York)		
J.F. Duke (1964)	N.P.L. Mtl Report	29M	3136
J.S. Erickson (1962)	Journal of Applied Physics	33	2499
J.D. Eshelby (1949)	Phil Mag	40	903
J.D. Eshelby and P.L.Pratt (1956)	Acta. Met.	4	560
U.Essman (1963)	Phys. Stat. Sol	3	932
A.G. Evans, C. Roy; P.L.Pratt (1966)	Proc. Brit.Ceram.Soc	6	173
T. Evans (1963)	Phil. Mag	8	1235
R.L. Fleischer (1962a)	Acta Met	10	835
R.L. Fleischer (1962b)	Journal applied physics	13	3504
R.L. Fleischer (1967)	Acta Met	15	1513

A.J.E. Foreman (1955)	Acta Met	3	322
A.J.E. Foreman and M.J.Makin (1967)	Canad. Journ. Phys.	45	511
A.D. Franklin (1964a)	J.Phys. Chem. Solids	26	933
A.D. Franklin (1964b)	Unpublished results		
A.D.Franklin (1966)	Private Communication		
J. Friedel (1964)	Dislocations (Pergamon Press, London)		
G.B. Gibbs (1964)	Phys. Stat. Sol	5	693
G.B.Gibbs (1967)	Phil. Mag	16	97
J.J. Gilman (1959)	Acta Met	7	608
J.J. Gilman (1962)	J.A.P.	33	2703
J.J. Gilman and W.G.Johnson(1960)	J.A.P.	31	687
J.J. Gilman and W.G. Johnson (1962)	Solid state physics. Vol.13		
A.V. Granato; K.Lucke; J.Schlipf and L.J.Teutonico (1964)	J.A.P.	35	2732
G.W. Groves and A.Kelly(1963)	Phil Mag	8	777
R.W. Guard (1961)	Acta Met	9	163
F. Guiu (1964)	Ph.D.Thesis -University of London		
E.U.Gutmanas; E.Nadgornyi and A.V. Stepanov (1963)	Soviet Physics-Solid state	5	743
P.Guyot and J.E.Dorn(1967)	Canad.J.Phys.	45	983
P.Haasen and J.Hesse(1963)	The Relation between the structure and mechanical properties of metals, H.M.S.O.		
R.P. Harrison (1965)	Ph.D.thesis - University of London		
P.M.Hazzeldine (1967)	Canad. J.Phys	45	765
J. Hesse (1965)	Phys. Stat. Sol	9	209
J. Hesse (1967)	ibid	21	495

J.P.Hirth and J.Lothe (1967)	Canad J.Phys	45	809
P.B. Hirsch (1958)	Internal Stresses and fatigue in Metals (Elsevier, Amsterdam)		p.139
P.B. Hirsch (1962)	Phil Mag	7	67
P.B. Hirsch (1960)	Acta Cryst.	13	1114
P.B. Hirsch (1964)	Discussions, Farad.Soc	38	111
P.B.Hirsch and T.E. Mitchell (1967)	Canad. J.Phys	45	663
M.J.Hordon(1962)	Acta. Met	10	999
T.R. Huffman and N.H.Norwood (1960)	Phys. Rev	117	709
H.B.Huntingdon; J.Dickey and R. Thomson (1955)	Phys. Rev	100	1117
P.J. Jackson and Z.S.Basinski (1967)	Canad. J.Phys.	45	707
H.B.Johnston; N.J.Tolar; G.R. Miller and I.B.Cutler (1966)	J.Amer.Ceram Soc.	49	458
W.G. Johnston and J.J. Gilman (1960)	J.Appl. Phys.	31	632
B.H.Kear; P.L.Pratt and A. Taylor (1959)	Phil. Mag	4	665
B.H.Kear;C.E. Silverstone and P.L. Pratt (1966)	Proc. Brit. Ceram.Soc	6	269
E. Koch and C.Wagner (1937)	Z.Physik Chem	B38	295
U.F. Kocks (1964)	Trans. Met.Soc. A.I.M.E.	230	1160
U.F. Kocks (1967)	Canad. J. Phys.	45	737
U.F. Kocks; Y.Nakada and B.Ramaswami (1964)	Trans. Met. Soc. A.I.M.E.	230	1005
S.N.Komnik; V.Z.Bengus; E.D. Lyak (1967)	Phys. Stat. Sol	19	533
H.Kronmuller (1964)	Disc. Farad.Soc	38	174

E. Kronmuller (1967)	Canad. J. Phys.	45	631
F. Kroupa (1962)	Phil. Mag	7	783
D.Kuhlmann-Wilsdorf(1962)	Trans. Met. Soc. A.I.M.E.	224	1047
J.C.M.Li (1965)	Trans. Met. Soc. A.I.M.E.	233	219
J.C.M. Li (1967)	Canad. J. Phys	45	493
E. Madelung (1918)	Physik Z	19	524
M.J. Makin (1964)	Phil. Mag	10	695
D. McLean (1962)	Mechanical Properties of metals (J.Wiley,London)		
J.T. Michelak (1965)	Acta Met	13	213
J.T. Michelak (1966)	ibid	14	1364
N.F. Mott (1952)	Phil. Mag	43	1151
F.R.N. Nabarro (1964)	Disc. Farad. Soc.	38	137
F.R.N. Nabarro; Z.S. Basinski and D.B. Holt (1964)	Advances in Physics	13	193
C.J.A. Newey; R.P.Harrison and P.L. Pratt (1966)	Proc.Brit. Ceram.Soc	6	305
J.B. Newkirk (1959)	Trans. A.I.M.E.	215	483
J.R. O'Connor and J.H.Chen (1963)	Phys. Rev	130	1790
K. Ono (1966)	Acta Met	14	1863
E. Orowan (1954)	Dislocations in metals (A.I.M.M.E. New York p.103		
R.T. Pascoe; K.C. Radford R.D. Rawlings and C.J.A. Newey (1967)	J.Scien. Inst.	44	366
D.C. Phillips (1967)	Ph.D.thesis - University of London (to be published.		
W.L. Phillips Jnr(1961)	Journ.Amer.Ceram.Soc	44	499
P.L.Pratt (1953)	Acta Met	1	103
P.L.Pratt; R.Chang and C.J.A. Newey(1963)	J.Appl. Phys. Let	3	83
J.Quin (1967)	Ph.D.thesis - University of London		

W.T. Read (1953)	Dislocations in crystals (McGraw Hill, New York)		
W.T. Read (1954)	Phil. Mag	45	775
C. Roy (1962)	Ph.D. thesis - University of London		
G. Saada (1960)	Acta. Met	8	200
G. Saada (1961)	Acta. Met	9	166
H.W. Schadler (1964)	Acta. Met	12	861
G. Schoeck (1965)	Phys. Stat. Sol	8	499
A. Seeger (1956)	Phil. Mag	1	651
A. Seeger (1957)	Dislocations and Mechanical Properties of crystals (Wiley - New York)		
A. Seeger (1958)	Handbuch der Physik - vol. VII/2		
A. Seeger; H.Donth: F. Pfaff(1957)	Discussions of the Faraday Society	23	9
R. Srinivasan (1958)	Proc. Roy. Soc	72	566
D.F. Stein (1966)	Acta. Met	14	99
D.F. Stein and J.Low(1967)	J.A.P.	31	362
R.J.Stokes (1965)	Basic mechanisms of strain Hardening in Ceramics N.R.-65-274		
G.I. Taylor (1934)	Proc. Roy. Soc	A145	362
A. Taylor (1958)	Ph.D thesis - University of Birmingham		
R.W. Ure (1957)	J.Chemical Physics	26	1363
A.A. Urosovskaya and V.G. Govorkov(1966)	Soviet Physics - Crystallography	10	437
J. Washburn (1963)	Electron Microscopy and strength of crystals (Wiley, New York)		
J.Weertman (1965)	Trans. Met Soc. A.I.M.E.	233	2069
J. Weertman (1957)	J.A.P.	28	1185
R. Whitworth (1967)	Phil. Mag	15	205

H. Wiedersich (1964)	A.I.M.E. Jnl. Met	16	425
P.Wynblatt and J.E. Dorn(1966)	Trans. Met Soc.A.I.M.E.	236	1431
C. Zener (1952)	Imperfections in nearly perfect crystals (Wiley, New York) p.289		

Acknowledgements

The author wishes to thank his supervisor, Prof. P.L.Pratt, for his continued interest and encouragement and the members of the ionic crystals research group, in particular Dr. J.Quin, for many enlightening discussions.

I am greatly indebted to the workshop staff for their skill and patience in the construction of my apparatus; Mr. B. Dalgleish for his invaluable assistance with the experimental aspects of this work and Mr. H. Haddow and Miss P.R. Martins for their technical advice.

Finally, I acknowledge the Student Research Council for financial support and Prof. J.G. Ball for providing the research facilities.

Reprinted from
"PROCEEDINGS OF THE BRITISH CERAMIC SOCIETY"
No. 6, June, 1966

16.—The Role of Grain Boundaries in the Plastic Deformation of Calcium Fluoride

By A. G. EVANS, C. ROY, and P. L. PRATT
Imperial College of Science and Technology, London.

ABSTRACT

Single crystals of CaF_2 begin to glide on $\{100\}<1\bar{1}0>$ at temperatures above 60°C and on $\{110\}<1\bar{1}0>$ above 200°C. The critical resolved shear stress for slip on these two systems becomes comparable above 300°C. According to von Mises's criterion a general strain should be possible if both systems can operate simultaneously. Hot-pressed pore-free polycrystalline CaF_2 becomes fully ductile in compression above 320°C, in agreement with the single-crystal results. Below this temperature, cracking near grain boundaries leads to fracture.

1. INTRODUCTION

The study of the mechanisms of plastic deformation of CaF_2 is of general interest in the field of ionic crystals, but it has a special interest in view of the similarity in crystal structure of CaF_2 and UO_2, which is used as a nuclear material. The early investigations on the plasticity of ionic crystals were summarized by SCHMID and BOAS[1] where it is reported that CaF_2 deforms by slip on a (100) plane in a $[1\bar{1}0]$ direction (Figure 1). By using a decoration technique, BONTINCK

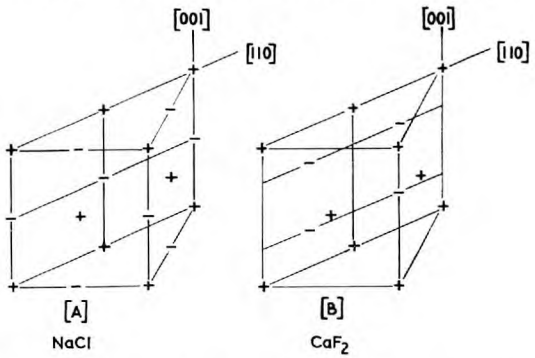

FIGURE 1.—Slip planes and directions in the CaF_2 structure compared with those in the NaCl structure.

and DEKEYSER[2] studied the configuration of dislocations in natural CaF_2, reporting that dislocations with Burgers vectors $a/2$ [110] (a is the side of the unit cell) are the most probable and the expected slip plane should be of {110} type. Recently, PHILLIPS[3] has studied the deformation and fracture processes in CaF_2 single crystals tested in compression. He found no ductility in as-cleaved or in as-cleaved and vacuum-annealed CaF_2 tested below 400°C. Above 400°C the critical resolved shear stress decreased exponentially with increase of temperature, and the glide elements were (100) [1$\bar{1}$0], in agreement with Schmid and Boas.

In our work the plastic properties of CaF_2 single crystals have been studied in compression, in the temperature range 20° to 600°C.[4] It is the first purpose of this paper to emphasize certain important features of the glide elements which were not observed in the work of Phillips. Furthermore, we have studied the plastic properties of polycrystalline CaF_2 over the same temperature range, and the second purpose of this paper is to emphasize the role of grain boundaries in determining the onset of brittleness at low temperatures. Some of the single-crystal results were presented at the meeting of the British Ceramic Society at Hastings in 1962.

2. EXPERIMENTAL PROCEDURE

The single crystals used in this work were purchased from Harshaw Chemical Co., Ohio, and the polycrystalline material was kindly donated by the Worcester Royal Porcelain Co. Ltd, and by Kodak Inc., Rochester, New York. Although the nominal composition has not been checked spectrographically, it is claimed that impurities amount to a few tenths of p.p.m. in the single crystals. The Worcester material, a crucible lid prepared by slip-casting and sintering, contained some 400 p.p.m. of impurities, and about 4% porosity, which made it opaque. The grain size was in the range 10–20μm, with most of the porosity in the form of closed pores along the grain boundaries. The Kodak material, prepared by vacuum hot-pressing, was fully transparent and of very high purity and low porosity. The grain size varied from 15–35μm, with 20μm as the average.

2.1 Preparation of the Single-crystal Specimens

Rectangular specimens with a cross-sectional area of about 3 mm^2 and 8 mm long were used. As CaF_2 cleaves to an octahedral shape, a wire saw was used for cutting the crystals. Single crystals with at least one cleaved surface were oriented by the X-ray back-reflection Laue method and then sawn parallel to the desired planes. The accuracy of cutting was kept within 3° of the plane.

A technique has been developed for polishing CaF_2 by chemical means. The {110} and {211} surfaces are reasonably well polished when agitated for 1 min. in a boiling solution of perchloric acid saturated with aluminium chloride and then washed in water and successively rinsed in absolute alcohol and anhydrous ether. With the same solution the {100} and {111} surfaces became deeply etched, making difficult the interpretation of any surface markings produced by deformation ; therefore the {100} faces were mechanically polished and the {111} were cleaved.

2.1 Preparation of Polycrystalline Specimens

Polycrystalline specimens were cut from larger pieces by means of a diamond wheel and a wire saw. These specimens were ground and polished to a finished size of $3{\cdot}50 \times 1{\cdot}50 \times 1{\cdot}50$ mm^3.

2.2 Examination

The mechanisms of plastic deformation were studied by using photoelastic techniques to examine stress birefringence, by microscope examination of slip band traces on the free surfaces, and by dislocation etching techniques.

All the mechanical tests were carried out on Instron testing machines, and similar strain rates were used for the single-crystal and for polycrystalline specimens.

3. EXPERIMENTAL RESULTS

3.1 Determination of Glide Elements in Single Crystals

In order to determine the glide elements and to study the effect of orientation on the stress/strain behaviour of CaF_2, crystals of four different orientations were deformed in compression. This enabled different combinations of glide elements to become operative and microscope studies to be made on different crystallographic surfaces. Figure 2 gives a schematic illustration of the two different crystal orientations which would involve slip on the {100} planes. Compressed in the [110] direction, the Type A crystal has two systems equally favoured using the {100} planes, while the <110> directions are inclined at 45° and 60° respectively to the stressing axis. Compressed in the $[\bar{1}\bar{1}2]$ direction, the Type B crystal has three available $\{001\}<1\bar{1}0>$ systems, but since the resolved shear stress is greater on one of these systems, single slip should predominate.

All crystals oriented for slip on {100} were brittle at room temperature but, in contrast to the results of Phillips, could be deformed plastically at 60°C and above.

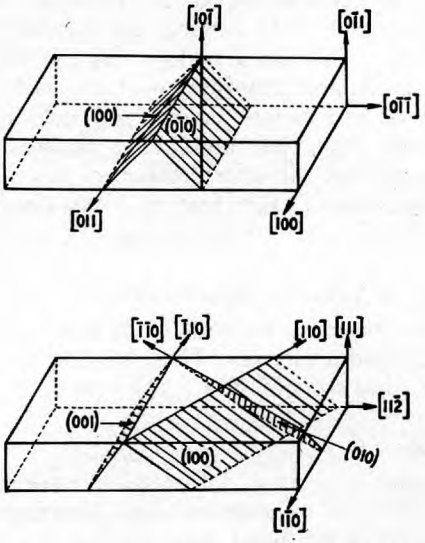

FIGURE 2.—Crystals oriented for slip on $\{110\}<1\bar{1}0>$ systems.

3.11 Type A Crystal

Stressed in the [110] direction, Type A crystals were found to deform by slip on the two {100} planes inclined at 45° to the compression axis. The birefringence pattern observed normally to the [100] of a specimen strained by 1·2% at 104°C is shown in Figure 3. The bands intersecting at 90° and making 45° with the [110] compression axis represent residual stresses after glide on two orthogonal (100) planes. This was accompanied by the formation of corresponding slip lines on both pairs of lateral faces (Figure 4). The slip bands on

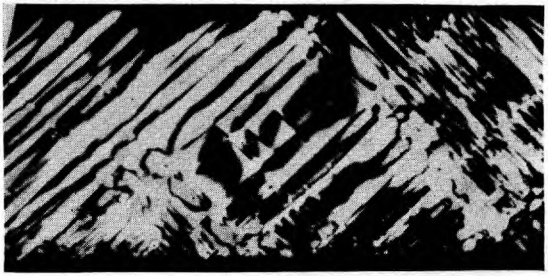

FIGURE 3.—Stress birefringence on Type A specimens strained by 1·2% at 104°C (×20).

the $(0\bar{1}1)$ face were running normal to the [110] compression axis. From these observations it can be deduced that slip occurred on the two available $\{100\}$ planes with a strong indication of the $<1\bar{1}0>$ slip direction.

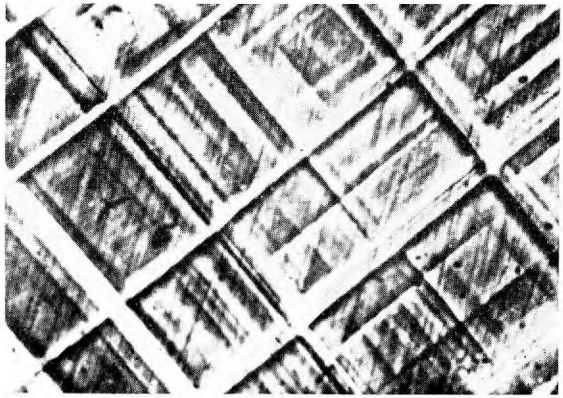

FIGURE 4.—Slip line pattern on the (100) surface of specimen of Figure 3 (× 186).

3.12 Type B Crystal

Stressed in the $[\bar{1}\bar{1}2]$ direction, Type B crystals strained by 1% at 80°C deformed initially by single slip on the (001) plane inclined at about 55° to the compression axis. The birefringence bands observed normal to the (110) face, and shown in Figure 5, make an angle of 55° to the long axis of this specimen and to the $\{111\}$ pair of side faces. The micrographs of Figure 6 show the sharp slip bands developed on the $\{111\}$ faces; no slip markings were revealed on $\{110\}$ crystal surfaces. Figure 7 shows slip bands on a $\{111\}$ surface after etching.

FIGURE 5.—Birefringence pattern on Type B crystal strained by 1% at 80°C (× 18).

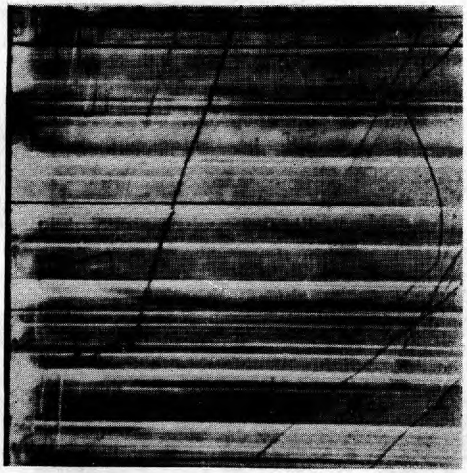

FIGURE 6.—Slip line pattern on (111) surface of the specimen of Figure 5.

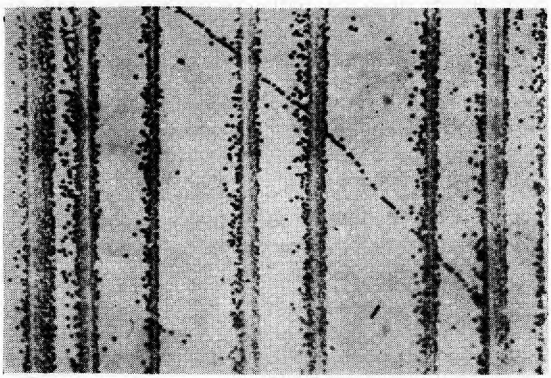

FIGURE 7.—Etch pits formed at slip bands on (111) surface of Type B crystal strained by 0·6% (× 141).

These observations confirm that the primary slip system in CaF_2 is $\{001\}<1\bar{1}0>$.

The two different crystal orientations chosen to activate slip on the $\{110\}<1\bar{1}0>$ system are illustrated in Figure 8. These are defined as Type C and D crystals. The compression axis for both types was the [100] direction, which gives maximum shear stresses on four $\{110\}<1\bar{1}0>$ systems but no resolved shear stress on the

$\{001\}<1\bar{1}0>$ system. Type C and D crystals are essentially equivalent except for the crystallography of their side faces. Type C crystals have the faces of the cube, and Type D crystals side-faces of the $\{110\}$ type, because the chemically polished surfaces are smoother, thereby facilitating microscope examination.

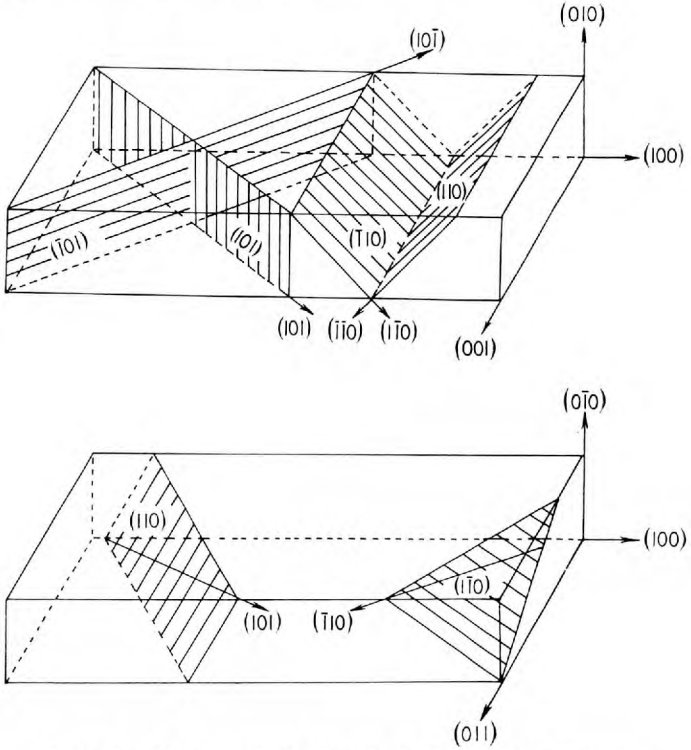

FIGURE 8.—Crystal oriented for slip on $\{110\}<1\bar{1}0>$ systems.

All the crystals oriented for slip on $\{110\}$ were brittle at room temperature, but they could be deformed plastically at temperatures above 200°C.

3.13 Type C Crystal

Slip in this orientation occurred with difficulty at 200°C, but became progressively easier and more homogeneous with increasing temperature. Block slip, on different systems in different parts of the crystal, occurred extensively around 200°C, but was absent at about 400°C. Two intersecting orthogonal systems operated preferentially at high temperature (Figure 9); these systems were generally situated

in such a way that the slip planes intersected the narrow faces in a [110] direction and the wide faces in a [100] direction. This indicates that the slip systems which have the shorter slip distance to reach the surface are more active, as in sodium chloride.

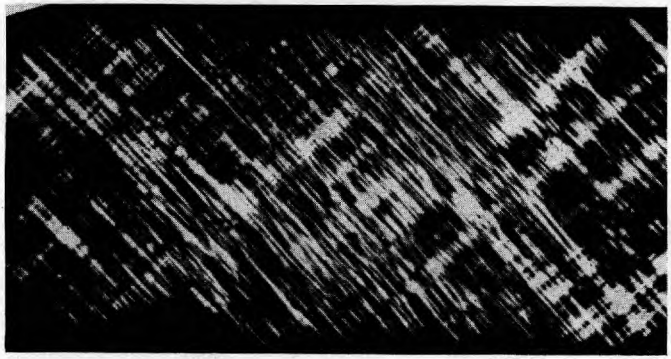

FIGURE 9.—Stress birefringence on Type C crystal compressed by 8% at 393°C (×20).

3.13 Type D Crystal

Compressed in the [100] direction, Type D crystals deformed by slip on the {110} planes. Because the lateral faces are all of the {110} type, the specimens had to be rotated by 45° to see birefringent patterns equivalent to those of a Type C crystal. The stress birefringence of a specimen strained by 6% at 433°C is shown in Figure 10. As shown in Figure 11, sharply defined wavy slip bands have developed during deformation. The slip markings were observed on the four side faces of the specimen and were inclined at about 60° to the compression axis. Slip on the $\{110\}<1\bar{1}0>$ system is in accordance with these observations and those made on Type C

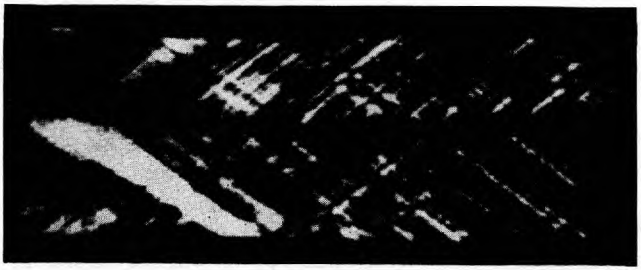

FIGURE 10.—Stress birefringence on Type D crystal compressed by 6% at 433°C (×18).

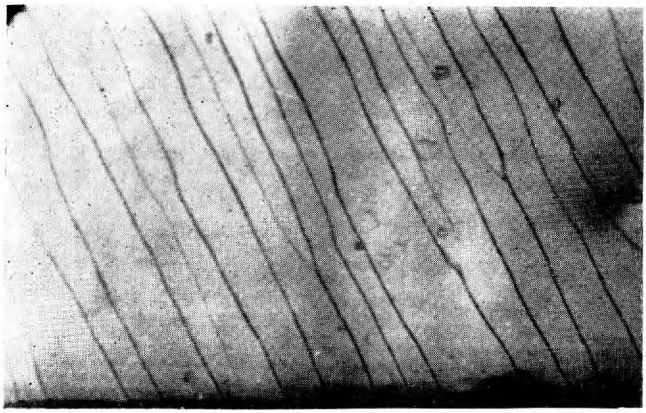

FIGURE 11.—Wavy slip line pattern on (110) face of specimen shown in Figure 10 (×141).

crystals. This permits us to conclude that, above 200°C, CaF_2 can deform by slip on the $\{110\}<1\bar{1}0>$ system.

These slip systems are very reasonable. The common $<1\bar{1}0>$ directions contain the only glide vector for which the Ca and the F sub-lattices are preserved; and this is the shortest lattice vector in the crystal, $a/2$ [110]. As far as the slip planes are concerned, the Chalmers and Martius ratio b/h (where b is the slip distance, or Burgers vector, and h is the interplanar spacing normal to b) should be a minimum for the primary glide plane; for $\{100\}$ in CaF_2, $b/h = 1{\cdot}42$, compared with 2·0 for $\{110\}$. Finally considering anisotropic elasticity, the elastic energy of a dislocation line lying in $\{100\}$ is somewhat less than that of the same length of line lying in the $\{110\}$.

3.2 Temperature Dependence of the Yield Stress for Slip on {100} and {110}

Specimens of the four types of crystal were deformed in compression to study their stress/strain characteristics over a range of temperatures. The temperature dependence of the critical resolved shear stress was determined for slip on both systems at two strain rates. The two lower curves in Figure 12 are for Type B specimens slipping on $\{100\}$, and the two upper for Type D specimens slipping on $\{110\}$. The yield stress varies exponentially with temperature for both specimens at the two strain rates. At the lower strain rate the temperature dependence becomes very large for Type B specimens near 100°C, and for Type D specimens near 300°C.

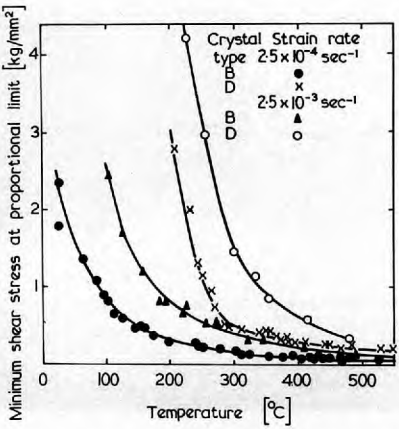

FIGURE 12.—Temperature dependence of the critical resolved shear stress for slip on {100} and {110} planes.

3.3 Deformation of Polycrystalline Specimens

GROVES and KELLY[5] applied the von Mises criterion to the CaF_2 structure, showing that slip on $\{001\}<1\bar{1}0>$ yields three independent slip systems, while slip on $\{110\}<1\bar{1}0>$ yields two further independent systems. Thus a general strain involving five independent slip systems is possible if both families operate simultaneously and independently.

The single-crystal results (Figure 12) show that, for a strain rate of $2{\cdot}5\times10^{-4}$ sec^{-1}, slip should be possible on {100} at all temperatures above 60°C, whereas slip on {110} should not occur, at comparable stresses, below about 300°C. Thus, polycrystalline material would be expected to possess only a limited ductility below 300°C, with a rapid increase to true polycrystalline plasticity above this temperature.

Compression tests performed on fully dense polycrystals of high purity yield results that are in close agreement with predicted behaviour. At low temperatures the yield stress is high (Figure 13) but it decreases between room temperature and 300°C. The ductility is low (Figure 14), only attaining a value of 5% at the higher temperature. Microscope examination of the free surfaces revealed that yielding in this temperature range was accompanied by grain boundary cracking (Figure 15). Straining beyond the yield point enabled these cracks to extend and widen and to initiate other cracks in adjacent grains (Figure 16). Slip occurred on {100},

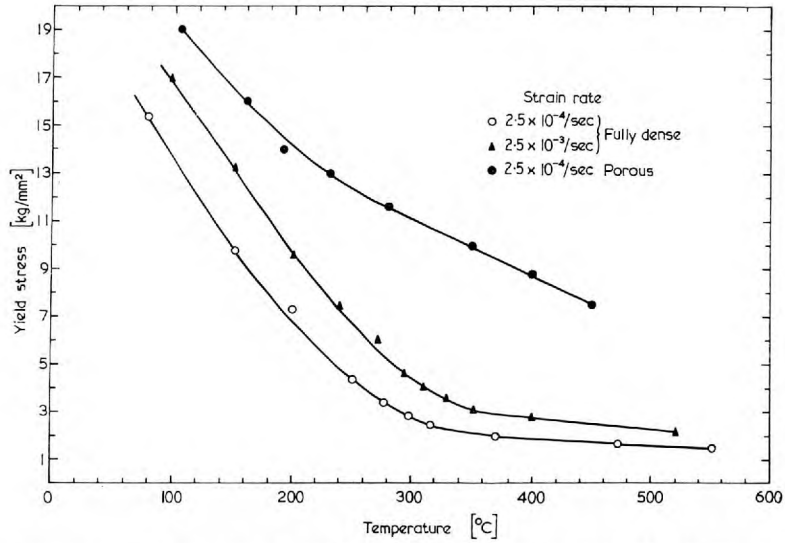

FIGURE 13.—The variation of yield stress with temperature for CaF_2 polycrystals in compression.

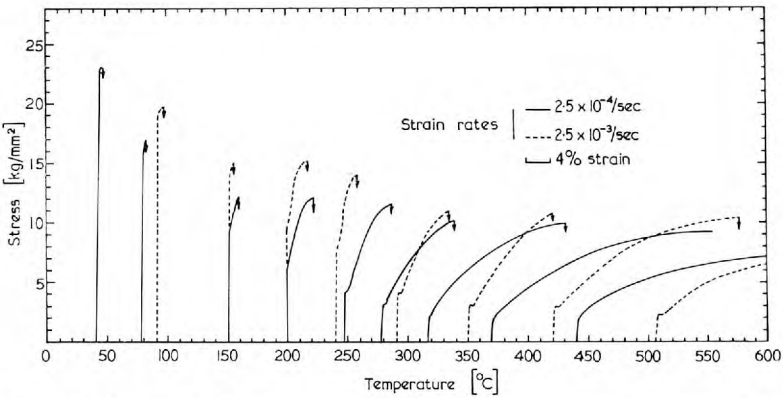

FIGURE 14.—The effect of temperature and strain rate upon the stress/strain curves for polycrystalline CaF_2 in compression.

producing very fine straight slip-lines in certain grains (Figure 17), like those in single crystals (Figure 6). Superposition of single-crystal yield-stress curves for slip on {100} upon the polycrystalline curves of Figure 13 indicates that, prior to yielding, slip should have been possible in grains of a number of orientations. However, the slip step

FIGURE 15.—Cracking of a grain-boundary triple point accompanying yielding at 120°C (× 360).

heights were not sufficiently large to enable slip lines to be distinguished using the optical microscope until the later stages of deformation. As the temperature was raised towards 250°C, {100} slip became more extensive and stress concentrations at grain boundaries were relieved by cracking at lower applied stresses. The number of regions of grain boundary cracking observed immediately after yielding increased as the temperature was increased. This would account for the more distinct yield point encountered at the higher temperatures in this range.

At approximately 250°C, limited numbers of wavy slip lines were first identified. The form of wavy slip is typical of slip on {110} as revealed by single-crystal work. Superposition of single-crystal curves upon the polycrystalline yield stress/temperature diagrams indicates that {110} slip should have been possible below the observed yield stress at temperatures as low as 200°C, but then only in ideally orientated grains. However, slip step heights are only sufficiently large for identification above 250°C. Above this temperature the extent of wavy slip increases rapidly until it is predominant at about 320°C. The ductility increases quite markedly over this temperature range (Figure 14), whilst the yield stress diminishes more slowly than at previous temperatures. Grain-boundary

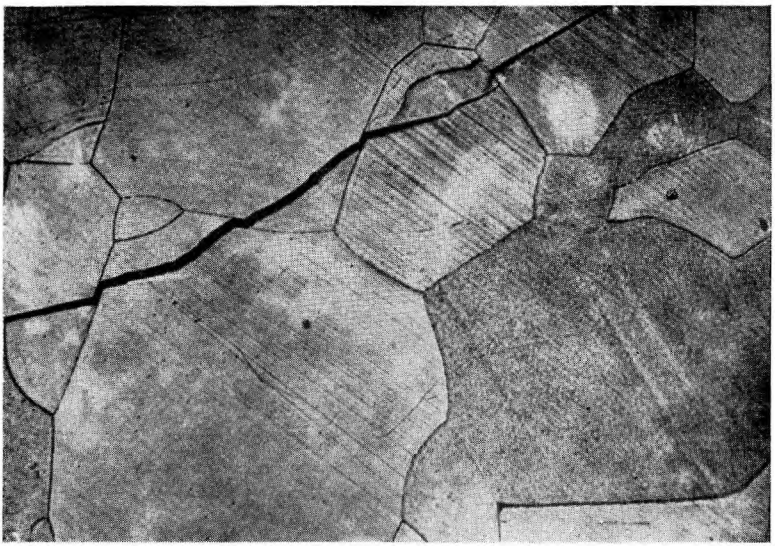

FIGURE 16.—The propagation of a crack through a specimen deformed to fracture at 120°C (Specimen etched prior to deformation; ×55).

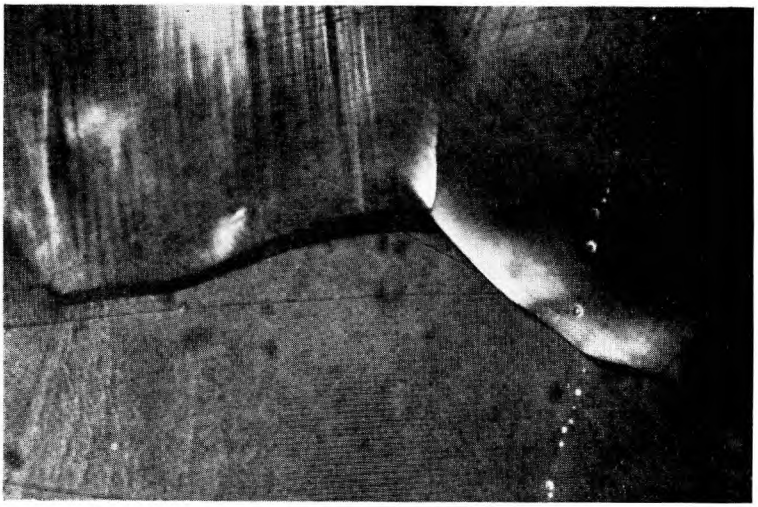

FIGURE 17.—Fine straight slip-lines observed after 2% compressive strain at 150°C (×360).

cracking immediately after yield is less profuse, although it is still observed in the later stages of deformation.

Above 320°C the transition to true polycrystalline ductility is virtually complete, i.e. {110} slip can occur in grains of most orientations at stresses lower than those required to initiate grain boundary fracture. Slip lines are abundant and almost entirely wavy (Figure 18), but remarkably straight slip lines are still observed in a very few grains, even after extensive strain. It is significant that, when cracks do form, they often emanate from boundaries of this type of grain.

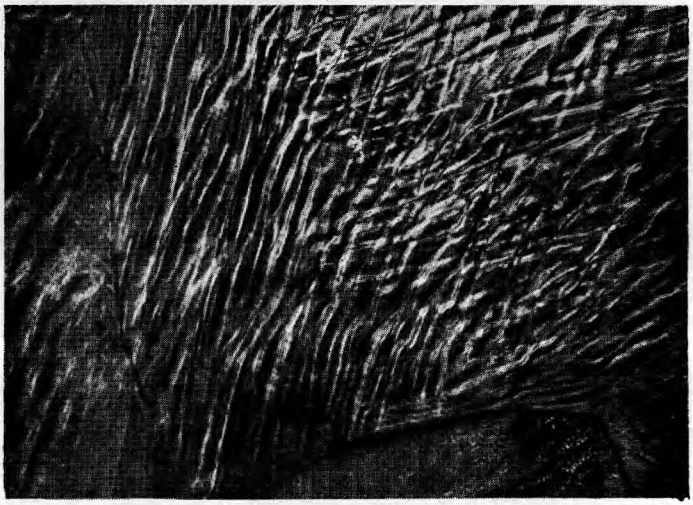

FIGURE 18.—Wavy slip lines observed after 20% compressive strain at 450°C (×360).

There is very little reduction in yield stress above this temperature, which appears reasonable when it is considered that the critical resolved shear stress for {110} slip (Figure 12) diminishes very little above this temperature. The ductility is well in excess of 20%.

Increasing the strain rate by an order of magnitude not only raises the yield stress and results in more distinct yield points but also raises the brittle–ductile transition range. The observed increase agrees very favourably with that expected from the effects observed in the single crystals. Thus, wavy slip was observed first at about 290°C and very little further change in the behaviour of the polycrystals was encountered above 360°C.

It is interesting to compare these results with tests performed on porous polycrystals containing a higher impurity concentration, reported in a previous paper.[6] The effect of temperature upon the deformation characteristics of these crystals is essentially similar to the effect already related for fully dense polycrystals. Thus, observations of yield stresses and ductilities (Figure 19) and of slip lines show that the transition from a brittle to a ductile condition still occurs in the vicinity of 300°C.

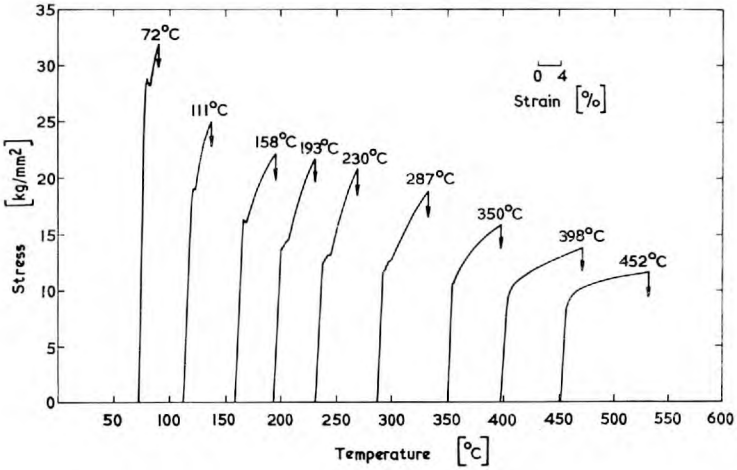

FIGURE 19.—Effect of temperature on the stress/strain curves of polycrystalline CaF_2, in compression

Ductility is very limited below 300°C, whilst slip lines are very fine and straight. Wavy slip lines first appear at about 230°C, and this form of slip is predominant above 350°C. At 400°C the specimens can withstand a compression of 16% before fracture occurs; at this stage, wavy slip is most profuse, with cracks extending across many grains.

At low temperatures sharp drops in yield were encountered; these were attributed to the appearance of microcracks immediately after yielding. The microcracks were almost invariably initiated at the grain-boundary pores. Thus a good criterion for the onset of true polycrystalline ductility would be the disappearance of a yield drop. This occurs in the vicinity of 300°C.

The differences in deformation characteristics of the two types of polycrystal are interesting. The yield stresses of the porous specimens

are higher at all temperatures. The pores, lying at the grain boundaries, could be expected to exert little effect upon dislocation motion and thus upon the high-temperature yield stresses, The effect at high temperature can be attributed to the higher concentration of impurity by virtue of its effect upon the lattice friction. That the pores have little effect upon the high-temperature deformation is confirmed by the similarity of work-hardening rates observed in both types of polycrystal. The overall ductility of the porous material is lower, a consequence of the relative ease of crack formation, at the pores, in the later stages of deformation.

Below the transition temperature the yield stresses are controlled by the size and distribution of pores. Thus, stress concentrations are relieved, at yielding, by crack initiation at these pores. In materials of similar purity, this type of cracking can occur at lower applied stresses than grain-boundary cleavage. Its temperature variation is less pronounced, however, and this contributes to the indistinct change in yield stress encountered during the transition.

4. CONCLUSIONS

The application of the von Mises criterion has proved remarkably successful in explaining the behaviour of polycrystalline CaF_2 in terms of the deformation characteristics of single crystals. A more complete understanding of the plasticity of ceramic polycrystals can only be achieved, however, by determining the precise effect of grain size and impurity content. Work on these aspects is now in progress.

ACKNOWLEDGMENTS

The authors would like to thank: Professor J. G. Ball for providing research facilities in the Department of Metallurgy; the Atomic Energy Research Establishment, Harwell, for continuing financial support and encouragement throughout the whole period of this research; and the Worcester Royal Porcelain Co. Ltd. and Kodak Inc., New York, for providing the polycrystalline material.

REFERENCES

1. SCHMID, E., and BOAS, W., "Plasticity of Crystals" (F. A. Hughes : London, 1950) p. 236.
2. BONTINCK, W., and DEKEYSER, W., *Physica*, **22**, 595, 1956.
3. PHILLIPS, W. L., Jr., *J. Amer. Ceram. Soc.*, **44**, 499, 1961.
4. ROY, C., Ph.D Thesis, London University, 1962.
5. GROVES, G. W., and KELLY, A., *Phil. Mag.* **8**, 777, 1963.
6. PRATT, P. L., ROY, C., and EVANS, A. G., North Carolina Conference on "Role of Grain Boundaries and Surfaces in Ceramics" (1964).